ZANCO Journal of Pure and Applied Sciences
The official scientific journal of Salahaddin University-Erbil
https://zancojournals.su.edu.krd/index.php/JPAS

ISSN (print):2218-0230**, ISSN (online):** 2412-3986**, DOI: http://dx.doi.org/10.21271/zjpas**

RESEARCH PAPER

Material flow analysis for household waste

Sazan M. Ali[1,*], Dana K. Mawlood [2]

[1]Department of civil engineering, college of engineering, Salahaddin University-Erbil, Kurdistan Region-Iraq
[*] Surveying dept. Noble Private Institute (NPI), Erbil. Iraq
[2]Department of civil engineering college of engineering, Salahaddin University-Erbil, Kurdistan Region-Iraq

A B S T R A C T:
Material flow analysis (MFA) is a tool used for a sustainable quantification and assessment of matter and substances during a specific period of time. The MFA system is mathematically controlled by a simple mass balance which defines all inputs, outputs and stocks of a process. Waste management in Erbil city has become the main problem and increased the generation rate per capita per year with economic growth and changing lifestyle. The current study aims to apply MFA for household waste in Erbil city to obtain a better, systematic waste management. The process model includes all input and output flows of household wastes and it provides a better management in household waste in the city. The total import of the household waste is 1.62 ton/year that is divided into four parts which are 1.23 tons/year is for kitchen waste (organic, combustible and incombustible), 0.03 tons/year for garden waste, and 0.03 tons/year for other waste and 0.33 for stocks material.

KEY WORDS: Material flow analysis (MFA), household waste, recycling, Erbil governorate
DOI: http://dx.doi.org/10.21271/ZJPAS.33.5.1
ZJPAS (2021) , 33(5);1-16 .

1.INTRODUCTION :

According to Tran et al., (2018), identified that flow and stock materials can be systematically analyzed by MFA that is based on space and time for the systems. The substance flow analysis is defined based on the MFA which represents substances and goods. The good stands are referring to the waste, sludge cars while, and substance stands are referring to the gas material such as nitrogen and phosphorus. The fundamental principles of MFA are should be the input equal to the output that is retuned in years ago by Greek Philosophers (Vidal, 1985). It means that the input materials have balanced with output materials (Brunner and Ruchberger, 2004).

The quantify stocks and flows substances in the modern system are analyzed through MFA process (Condeixaet al., 2017, Cencic and Rechberger, 2008). It works based on the mass balance of input and output. The mass that came to the MFA system is accumulated and some leave the system (Bureecam, et al., 2018). Urbanization and economic growth are increasing the amount of solid waste generation in Erbil city. All waste production in the city is collected and directly disposed to the landfill site that is without any appropriate treatments and recycling of the waste. The landfill is not referring a sanitary landfill since, all combustible and incombustible wastes are mixed together without any segregation and treatments. The compositions of the solid wastes are mostly consisting of organic waste which is coming from food waste in Erbil city. Therefore waste recycling is giving the problems of waste management in the Erbil city. Composting is an important method for the biodegradable solid wastes (Aziz, et al., 2011). MFA has been widely used for environmental issues, especially in

* **Corresponding Author:**
Sazan Mohammed Ali
E-mail: sazanengs@yahoo.com
Article History:
Received: 22/01/2021
Accepted: 08/05/2021
Published: 20/10 /2021

management of waste material. MFA can be used for policy of the waste management. In this research, MFA used for household waste in Erbil northern Iraq that is to determine both out and input flow material in the household to obtain better organize waste management.

In this paper, MFA was aimed for the quantification and identification of input and output of household waste so as to achieve a better systematic management of household waste. The application of Material Flow Analysis (MFA) in this study is relevant in monitoring waste flows and substances within the model. In addition, MFA is looking for finding the flow waste in the model for management of the household waste and determine input and out flows in household waste of Erbil city. The data is obtained from previous studies and researches.

2. MATERIALS AND METHODS

2.1. Study Area & data collection

Erbil city is the capital of Kurdistan region northern Iraq situated at 36.1901° N, 43.9930° E. It has a population of more than one million citizens (figure 1). The solid waste generation is 0.654 kg per capita per day in 2010 in Erbil city (Aziz et al., 2011). Table 1 shows the data of solid waste components for a single family that is contains 5 persons in Sarbasti quarter in Erbil city for one week duration. Considering one family represent all methodologies that needed to be taken into account in determination of generation rate of household wastes. Samples were collected in plastic bags. Each plastic bag weighed alone for each day during one week. The components of solid waste and its generation rate (GR) determined during one week for a five members of the family. Based on the following equation (Metcalf & Eddy, 2003):

$$\text{Generation rate (GR)} = \frac{Total\ solid\ waste\ (gm)}{No.of\ persons * period(day)} \quad \ldots\ldots\ldots\ldots\ldots\ldots (1)$$

Figure 1 Location of Erbil city map

Table 1 Components and generation rate of solid waste for a household in Erbil city

Period (Day)	No. of person	Food (gm)	Paper(gm)	Metal (gm)	Plastic (gm)	Glass (gm)	Cloths (gm)	Total weight (gm)	GR Kg/cap.day	Combustible (gm)	Incombustible (gm)
	5	5936	413	162	191	304	383	7389	1.4778	987	466
	5	2260	29	…	141	154	354	2938	0.5876	524	154
	5	2648	150	…	57	….	160	3015	0.603	367	0
	5	3522	238	86	52	354	57	4309	0.8618	347	440
	5	4290	581	…	18	84	245	5218	1.0436	844	84
	5	2152	265	459	43	479	27	3425	0.685	335	938
	5	2691	612	…	829	150	500	4782	0.9564	1941	150
Total		23499	2288	707	1331	1525	1726	31076		5345	2232

According to the table 1, the average generation rate is 0.887 kg per capita per one day. It is indicated that each person in Erbil city produces 0.887 kg of solid waste per one day. The household solid waste comes from organic waste (food waste) from kitchen, combustible (plastic, paper and cloth) and incombustible (metal and glass) wastes. The total food waste is 23.499 kg per week. In addition, the total combustible waste (paper, plastic and cloth) is 5.345 kg/week while the total amount of incombustible waste (metal and glass) is 2.232 kg per week. Food waste generates majority of wastes from households which is 23 kg/week (about 75% of total waste. Figure 2 illustrates the amount of wastes generates during one week in kg. Total waste generated from the household family is 31.076 kg per week.

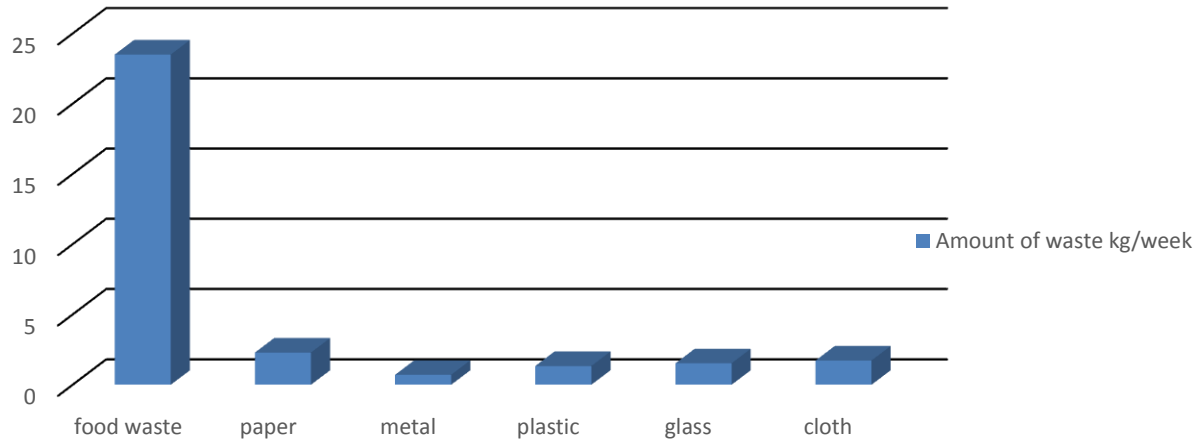

Figure 2 shows the waste generation from household in Erbil city

2.2 Mathematical implementation and calculation algorithm of MFA

During starting calculation to compute unknown of a graphical models created by STAN, it has to be transformed automatically into a mathematical models using four types of equations as follows:
Balance equation: ∑input= ∑output + change in stock
Transfer coefficient equation: output x = transfer coeff. to output x ∑inputs

Stock equation: stock Period i+1 = stock Period i + change in stock Period i
Concentration equation: mass substance = mass good · concentration substance
The above equations contain measured, unknown and exactly known variables
To enhance the accuracy of measurements, at least one equation should be known with one measured variable data reconciliation. To obtain this goal, a Gauss-Jordan elimination method is proposed by (Madron, 1977) for the original linear constraint matrix. Necessary corrections of the measurements are check by statistical tests which can be explained by random errors or gross errors. Consequently, for the unknown quantities, improved values are used to calculate the quantity. The corresponding uncertainties are determined with the method of error propagation.

2.3 MFA for household waste management in Erbil city

The below flow analysis is demonstrated by STAN 2.6.801 software (figure 3). It illustrates the material flow analysis MFA for waste in households. The input and output wastes are illustrates. The majority of solid waste in households in Erbil city is organic waste based on data of this study and other researchers in literature review. The input flow of household waste mainly generated from kitchen, garden, bathroom and others. The output flow is the system is mostly organic, combustible (plastic, paper and cloth), incombustible (metal and glass), and wastewater and methane gas emission.

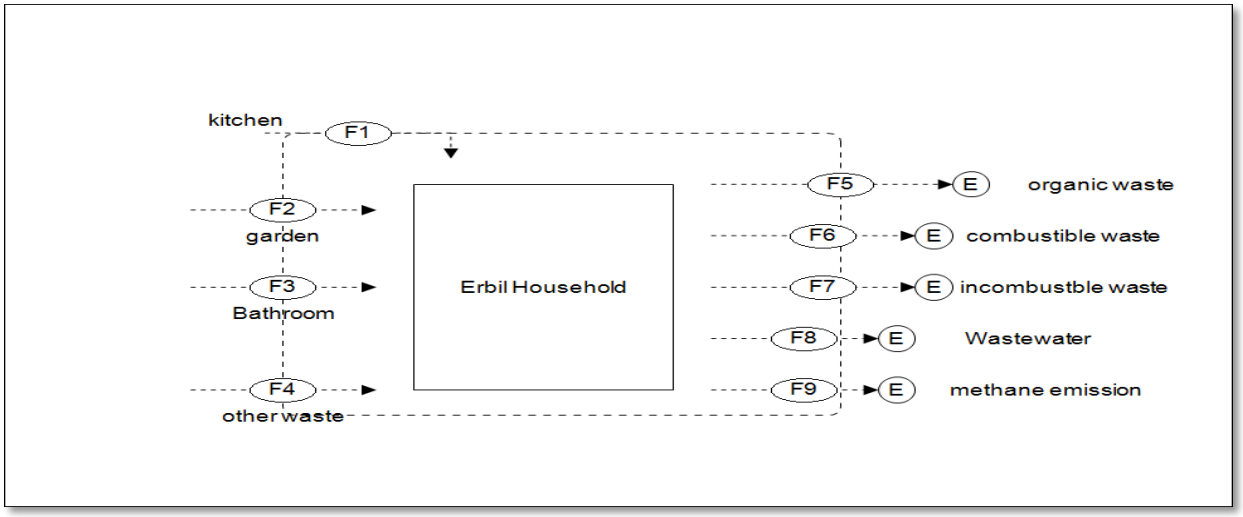

Figure 3 shows the MFA input and output household waste in Erbil city

2.4 MFA processes (input and output data with STAN)

STAN is free software used for material flow analysis. It is based on mass balance principles to input data (Tang and Brunner, 2013, Laner et al., 2014). Figure 4 and 5 show the Material Flow Analysis (MFA) for household system in Erbil for 2020. It illustrates the total input and output of the system and the source of waste contributed from kitchen, bathroom, garden and other wastes, from kitchen, organic waste, combustible and incombustible wastes were generated. The total input of the system is 1.62 tons per year. The organic waste which is food waste contributed the highest amount of waste with 31.076 kg per week i.e. %75 of waste generation is food waste. Followed combustible is about (%17), incombustible (%7.18) and garden waste. It is supported by other studies that major component of municipal solid waste in Erbil city is food waste (%79) (Aziz et al., 2011). Since all activities occurs in the kitchen such as cleaning, cooking and waste generation (organic, combustible and incombustible wastes), so the total input flow for kitchen in the MFA system is 1.23 tons per year. The input flow for organic waste, combustible and incombustible waste are 0.7, 0.3 and 0.23 tons per year. The rest of the wastes refer to garden and other wastes. The output waste of organic waste can generate home composting. A part of home composting (0.3 tons per year) can be used back for gardening and another portion (0.4 tons per year) will disposed to landfill resulting in degradation of organic materials. High concentration of heavy metals inside compost result in harmful compost for

planting and animals (Abdii and Schlosser, 2019) solid waste On the other hand, combustible waste can be treated by thermal treatment such as gasification and incineration treatment (0.3 tons per year), while the final production of the treatment (fly ash) go to landfill. Moreover, the input flow for incombustible waste is 0.23 tons per year. The output of incombustible material can be separated and recycled as a raw material for industrial using (0.76 tons per year) while other part (0.15 tons per year) disposed to landfill site. For the input flow of water supply system, 279 liter per capita per day estimated according to literature review and general directorate of water and sewerage in Erbil city (GDWS and Abdullah et al., 2020). The input water supply is 509.51 m3 per year is used as water consumption use for a household system which is calculated as below. The output flow produced wastewater, which is about 80% of water consumption (406.61 m3 per year). The wastewater generation is discharged into the environment directly. In addition, in the landfill site methane gas is estimated to be emitted into the air which is produced from the waste disposal as a result of waste accumulation (Qayyum & Norahikin, 2017 and Ghani et al., 2019).

After conducting all input and out flow of waste. The software calculates and analysis the system for a given period of time with showing no error in the calculation part of the system as in the bottom box all layers are in blue color with right description of each of them(Yoshida et al., 2009) (figure 6). In this study, MFA is conducted for waste management in household in Erbil city.

Water consumption L capita/day= 279
Water consumption for a family with 5 person/ year= 279*5*365/1000= 509.175 m^3/year

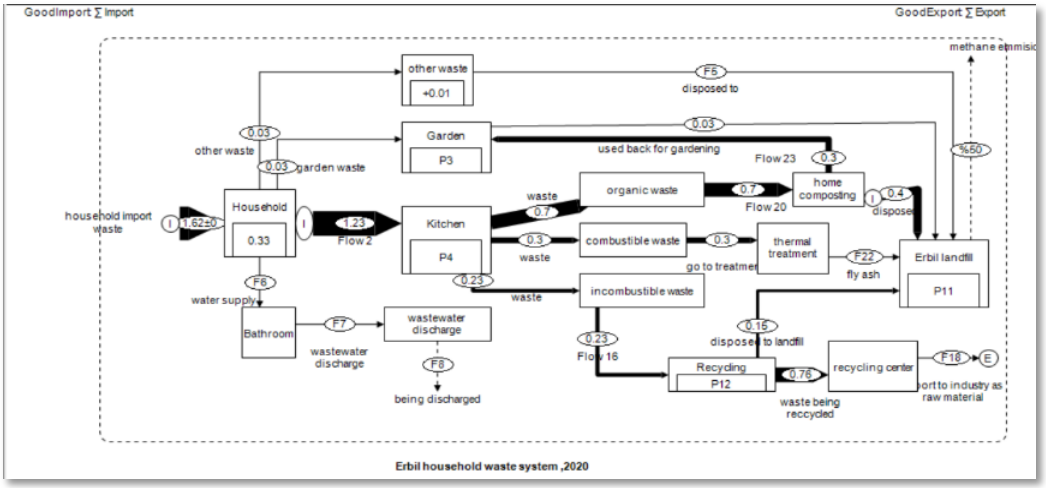

Figure 4 MFA system analysis (mass flow tons/year)

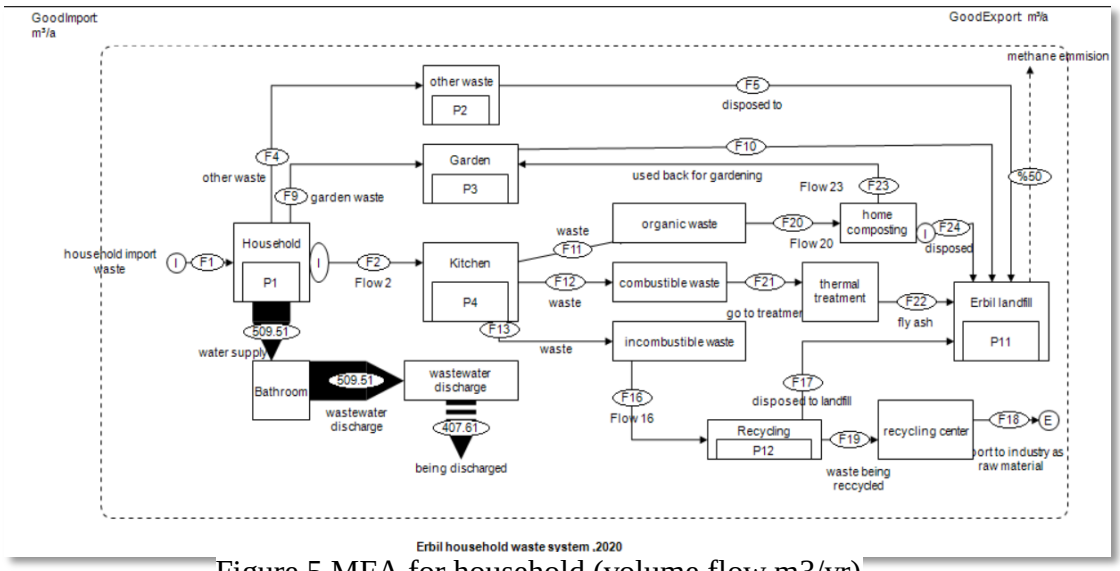

Figure 5 MFA for household (volume flow m3/yr)

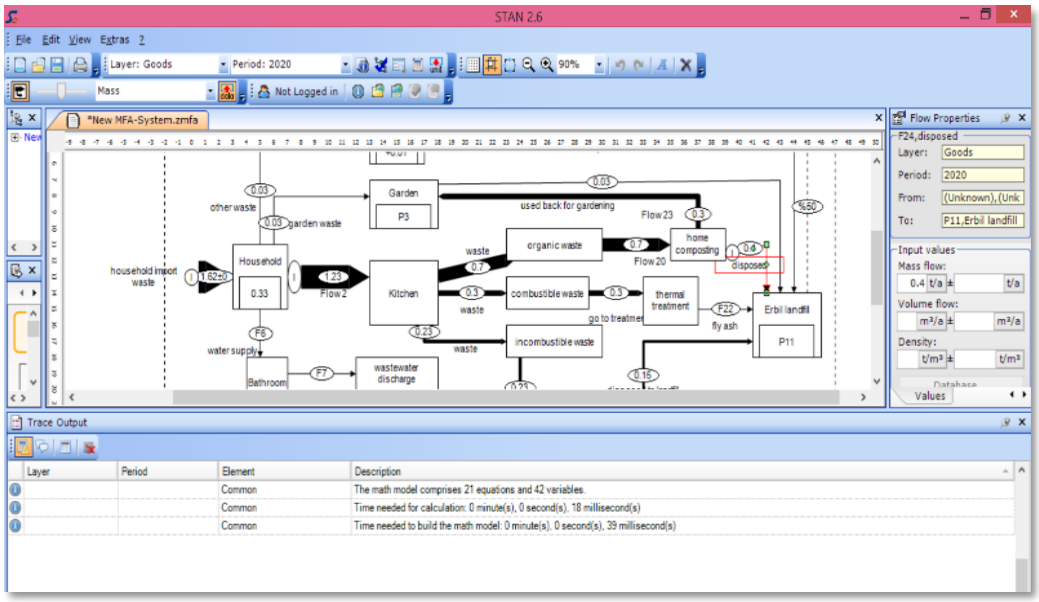

Figure 6 MFA calculations with no error in the system

3. CONCLUSION

In this study the following concludes have been determined. MFA applied for the assessment of waste management in Erbil city. Basic principles of mass balance conservation are used to define the processes of the system.

1. It is concluded that majority of household waste generation comes from combustible and non - combustible.
2. The organic waste (food waste) is covers about 75%, combustible is about 17% and incombustible is 7%.
3. The total import of the household waste is 1.62 ton/year that is divided into four parts which are 1.23 tons/year is for kitchen waste (organic, combustible and incombustible), 0.03 tons/year for garden waste, and 0.03 tons/year for other waste and 0.33 for stocks material.
4. The household requires to be minimized from the quantity of organic wastes.
5. Some of the materials can be separated from incombustible waste which can be used for as a raw material in the industrial.
6. Moreover, some parts of organic waste can be used in the home composting that is used for gardens and other large part is going to the landfill sites.
7. The MFA system has able to obtain the management of the household waste in cities in a more sustainable way.

REFERENCES

ABDII A. & SCHLOSSER S. 2019. Determining Of Heavy Metals Content In Three Leafy Vegetables Treated With Compost Produced By Quashie Municipal Solid Waste Plant. *Journal of University of Duhok., Vol. 22, No.1 (Agri. and Vet. Sciences), Pp 122-131.*

ABDULLAH, R. A., ALI, H., & MOHAMMED, M., 2020. Characteristics of Erbil wastewater. Online at *https://www.researchgate.net/publication/342004577_CHARACTERISTICS_OF_ERBIL_WASTEWATER*

AZIZ, S. Q., AZIZ, H. A., BASHIR, JK. M., & YUSOFF, M. S., 2011. Appraisal of domestic solid waste generation, components, and the feasibility of recycling in Erbil, Iraq. *Journal of Waste Management & Research, 29(8), pp.880-887.*

BRUNNER, P. & RECHENBERG, H., 2004. Practical Handbook of Material Flow Analysis. Boca Raton, *FL: Lewis Publ.*

BUREECAM, C., CHAISOMPHOB, T. & SUNGSOMBOON, P., 2018. Material flows analysis of plastic in Thailand. *journal of Thermal Science , 22(6 Part A), pp.2379-2388.*

CENCIC, O. & H. RECHBERGER. 2008. Material flow analysis with software STAN. *Journal of Environmental Engineering and Management 18(1): 3–7.*

CONDEIXA, K., HADDAD, A. & BOER, D., 2017. Material flow analysis of the residential building stock at the city of Rio de Janeiro. *Journal of Cleaner Production, 149, pp.1249-1267.*

General Director of water and sewage in Kurdistan region.

GHANI, L.A., MAHMOOD, N.Z., MUHAMMAD, Z., BAHRI, S. & SAPUTRA, J., 2019. The energy flow for maize production: An application of material flow analysis (MFA) and giddens

structural theory. *Journal of Southwest Jiaotong University, 54(4).*

LANER, D., RECHBERGER, H., & ASTRUP, TH., 2014. Systematic Evaluation of Uncertainty in Material Flow *Analysis, research and analysis journal, Volume 18, Number 6.*

MADRON, F., VEVERKA, V. & VANĚČEK, V., 1977. Statistical analysis of material balance of a chemical reactor. AIChE *Journal, 23(4), pp.482-486.*

NURUL Q., FARAHIN S., & NORASHIKIN AHMAD KAMAL, 2017. Evaluation of Solid Waste Management Using Material Flow Analysis (MFA) for a Waste Utilization System in Shah Alam. *Journal of Engineering and Applied Sciences, 12: 6450-6455.*

TANG, J. & BRUNNER, P.H., 2013. Globalising MFA–decision support for waste management in cities based on the software STAN. *ISWA Guidelines & Reports.*

TRAN, H., SCHAUBROECK, T., NGUYEN, D., HA, V., HUYNH, T. & DEWULF, J., 2018. Material flow analysis for management of waste TVs from households in urban areas of Vietnam. *Resources, Conservation and Recycling, 139, pp.78-89.*

VIDAL, B. 1985. Histoire de la Chemie. Paris: P*resses Universitaire de France.*

YOSHIDA, A., TASAKI, T., TERAZONO, A., 2009. Material flow analysis of used personal computers in Japan, *journal of Waste Management 29, 1602–1614.*

ZANCO Journal of Pure and Applied Sciences
The official scientific journal of Salahaddin University-Erbil
https://zancojournals.su.edu.krd/index.php/JPAS

ISSN (print):2218-0230**, ISSN (online):** 2412-3986**, DOI: http://dx.doi.org/10.21271/zjpas**

RESEARCH PAPER

Coordination of Traffic Signals on Arterial Streets in Duhok City

Dilshad Ali Mohammed 1, Aso Faiz Saeed Talabany*,2
[1] Department of Civil Engineering, College of Engineering, Duhok University, Kurdistan Region, Iraq
[2] Department of Civil Engineering, College of Engineering, Salahaddin University-Erbil, Kurdistan Region, Iraq

A B S T R A C T:

Duhok City lies in the north of Iraq and it has mountainous terrain. The poor road infrastructure of the city and also the daily increasing number of vehicles had left no choice other than applying traffic control systems to solve congestion problems in the city streets. Traffic control signal coordination which is one of efficient method of traffic control system that can improve the traffic operation and safety for series of signalized intersections along the arterials in the city. In this study the benefit of actuating traffic signal coordination was evaluated, and comparison in control delay against the same signalized intersection in case of being isolated was made. To achieve this four successive signalized intersections on Barzani street and three successive signalized intersections on Zakho street which are two major arterials in Duhok City were chosen. Traffic data (traffic volumes, vehicle link and approach speeds, and passenger car equivalent) during peak hours were collected. Also, geometric data and signalization data were collected using different methods, such as video recording technique, moving vehicle method and manual methods. To check the coordination attainability, the coupling index and key intersection was determined, then time-space diagrams were constructed representing one-way coordination for the intersections on Barzani and Zakho Streets, and others represented two-way coordination for the intersections on Zakho Street with acceptable progression bandwidth efficiency. The results of this study showed that a progression bandwidth of 54 seconds for east direction coordination and 17 seconds for west direction coordination on Barzani Street under suggested controlled speed of 60 kph pleasant with the present data. For Zakho Street, the progression bandwidth is 19 seconds for east direction coordination and 18 seconds for west direction coordination under suggested controlled speed of 40 kph. The results show that traffic signal coordination had led to high reduction in intersection control delays. On Barzani arterial street the reduction was between 16.2% and 51.8%, while for Zakho arterial street the reduction ranges between 16.93% and 26.11%.

KEY WORDS: Traffic Signal; Signal Coordination; Arterial Coordination
DOI: http://dx.doi.org/10.21271/ZJPAS.33.5.2
ZJPAS (2021) , 33(5);8-23 .

1.INTRODUCTION :

The increased usage of vehicles has led to congestion, not only in urban metropolitan areas, but also in rural small and mid-size cities. In most areas, the networks operate at capacity or near capacity, during the morning and evening peak hours (Zaher Khatib, et al, 2001).

When traffic signals are located in close proximity, the presence of the upstream traffic signals alters the arrival pattern of traffic at the downstream traffic signals from random arrivals to arrivals in platoons.

This means that improved traffic flow can be achieved if the green signal at the downstream traffic signal is arranged to coincide with the arrival of the platoon. To achieve this, traffic signals are coordinated, sometimes called "linked". This improves the level of service on a road network where the spacing of traffic signals is such that isolated operation causes excessive delays (Luk, J.Y.K. and Sims, A.G., 1982).

Traffic signal coordination can be applied when two or more traffic signals are working together so that cars moving through a group of traffic signals will make the least number of stops possible. In order to perform such process, each traffic signal in the group of signals must allow

*** Corresponding Author:**
Aso Faiz Saeed Talabany
e-mail: aso.talabany@su.edu.krd
Article History:
Received: 29/03/2021
Accepted: 06/06/2021
Published: 20/10/2021

for a green light for desired directions of travel during the correct fixed time period. However, traffic signal coordination does not mean that drivers will never have to stop for red light because of some reasons which affect the amount of time available for green light in that direction. Those reasons are pedestrian crossings, cross traffic, left turn signals, two-way traffic flow and off-peak traffic periods (City of Kent Development assistance brochure, 2001).

Advantages of signal coordination include the following (Martin Rogers, 2003):

1- Reduced energy and fuel consumption
2- Reduced vehicle emissions
3- Bolstered local economies
4- Eliminated or delayed street widening needs
5- Improved emergency response
6- Reduced motorist frustration and road rage
7- Increased control of travel speeds
8- Reduced diversionary flows in neighbourhoods
9- Real-time traffic monitoring
10 Advanced equipment monitoring

The main disadvantage of signal coordination is that side street traffic typically experiences a longer wait time.

The objective of this research is to apply coordination of traffic signals for sets of successive isolated intersections on two arterial streets in Duhok City in order to get best progress and greatest number of vehicles through a corridor with the fewest stops in the safest and most efficient manner; hence, reducing delay and optimizing the capacity of these intersections in the direction of progression.

William A. Stimpson and Gerald M. Takasaki (1982) developed a study (Coordinating vehicle-actuated traffic signals to reduce vehicular fuel consumption) in Britain. They stated that: Test car fuel consumption was reduced through signal retiming and co-ordination by greater percentage than was travel time; indeed, over the full 29-link route, reductions in morning fuel use were accompanied by increases in travel time. This phenomenon resulted from reductions in stop frequency coupled with increases in stopping time. It appears that changes in signal timing are not related simply to corresponding changes in travel time.

Masaki Koshi (1989) showed fundamental relationships between the cycle time and delay as well as number of stops of a signalized corridor based on some assumptions with the field experiment results. The study showed that cycle time can be optimized through on-line feedback techniques and demonstration of results of experiments made by the author.

Chang, E C and Koothrappally, J (1994) studied the effect of actuated traffic signals used on isolated intersections in Kingsville, Texas. The purpose of the study was to develop an analytical methodology for improving the overall design and operation of actuated controllers, determining the best way to use the added flexibility of actuated control in a coordinated system, and generate feasible coordination parameters for arterial progression. The field examination of the coordinated, actuated operations of a real arterial traffic signal system in Kingsville, Texas, is described. The validity of the simulation study was proven. Signal system improvements of semi-actuated coordinated timing was compared with that of either fully actuated or pretimed coordinated timing plan was used.

Wei Li and Andrew P. Tarko (2007) used Synchro and SimTraffic software package to optimize signal coordination. The research outcome is expected to help traffic systems engineers reach reasonable signal settings in a shorter time. The final part of the research was the investigation of the robustness of the arterial signal coordination procedure. In current practice, signals are optimized to traffic volumes that represent a single time interval. In spite of the randomness of traffic, these plans are executed for a long period of time until obvious insufficiencies of the signal timings are noticed and re-timing is necessary.

Hirsh Muhammad Majid and Aso Faiz Talabany (2007) studied number of adjacent intersections in Sulaimani City-Kurdistan-Iraq. The attainability of coordinating these intersections by calculating the coupling index as a treatment of some traffic problems which exist in these intersections, like congestion, delay and traffic jam due to heavy traffic volume, and poor timing of traffic signals. The coordination between mamostayan and yakgirten intersections (Mamostayan2) and between palace, aqare and engineering intersections (Salm1 and Salm2 respectively) is studied. For each intersection in

this study data were collected by various methods such as video camera, manual method or by moving vehicle method for finding the elements which are necessary to obtain the coordination goal. The elements are peak hour volume, passenger car equivalent, saturation flow, link speed, spot speed approach and intersection stopped and approach delays and intersection control delay before coordination and after coordination. In addition, the authors checked the two-way coordination availability for application by calculating the attainability factor and finding its efficiency. It was found by the researchers that the coordination between these intersections give good results, moreover, the coordination between Palace and Aqare intersection (Salm1), in one-way or two-way progression, gives the best results.

2. METHODOLOGY

The methodology to achieve the of this research, includes the main methods and equations which was used to obtain the necessary elements for the data collection and data analysis.

2.1 Passenger Car Equivalent (PCE)

HCM 2000 tables were used to find Passenger Car Equivalent for trucks and buses as it reports PCEs according to percent and length of grade and proportion of heavy vehicles.

The terrain in the studied segments is a combination of horizontal and vertical alignment permits heavy vehicles to maintain approximately the same speed as passenger cars. Therefore, the terrain is assumed to be level terrain, and the value of PCE is equal to 1.5 for trucks and buses.

2.2 Link Speeds

Moving vehicle method was used to obtain average link travel speeds between intersections on the arterial streets. For reliable results a minimum of six test runs were performed in each direction under comparable conditions (Pignataro, L. J., 1973).

Also spot speed study at selected locations were used to determine the Mid-Link spot speed, a sample size of at least 50 and preferably 100 vehicles are usually obtained. The spot speed data are collected using the stopwatch.

2.3 Traffic Volume

Traffic volume studies are conducted to determine the number, type of movements, and classification of vehicles at study locations using Moving vehicle method to obtain link volume on arterial streets and video recording technique for the determination of intersection volumes at peak hours dividing the period of data collection into 5-minute intervals to obtain PHF

2.4 Saturation Flow Rate

HCM2000 method was used for the determination of saturation flow which is used for the computation of both cycle time and traffic control delay for the signalized intersections.

2.5 Coordination of Traffic Signals

The Intersection Control Strategy was determined for each intersection. The relationship between each signalized intersection's location and the adjacent signalized intersections was determined using the coupling index (Alexandar Skabardonis, 1998).

The Coupling Index is a simple methodology to determine the potential benefit of coordinating operation of two signalized intersections. The theory is based on Newton's law of gravitation, which states that the attraction between two bodies is proportional to the size of the two bodies (traffic volume) and inversely proportional to the distance squared. In equation form, the Coupling Index is:

$$Ic = V / d_L^2 \quad \ldots\ldots\ldots\ldots \quad \ldots\ldots\ldots \quad (1)$$

Where:

I_C = Coupling Index

V = Two-way total traffic volume peak hour (vph)

d_L = Distance between signals (meters)

When Ic is greater than 0.5, signal progression is recommended. As the link volume increases, so the need to provide signal progression is essential. Based on the coupling index, the signal is classified as an isolated, arterial, crossing arterial, or dense network intersection as follows:

Isolated	$Ic \leq 0.5$ for all directions
Arterial	$Ic > 0.5$ for major street only
Crossing arterial	$Ic > 0.5$ for major street, and at least one side street link
Dense network	$Ic > 0.5$ for both the major street and minor street links

The Measure of Effectiveness (MOEs) associated with the green bands in the Time-Space Diagram (TSD) are Bandwidth Efficiency and Bandwidth attainability (Minnesota Department of Transportation, 2005).

Bandwidth Efficiency which is simply the proportion of the cycle that is included in through green bands, extending the entire length of the system. A simple Time-Space Diagram showing perfect time-space progression illustrates the concept. Mathematically, efficiency is calculated as (Minnesota Department of Transportation):

$$E = \frac{B_f + B_r}{2C} \quad \ldots\ldots\ldots\ldots\ldots\ldots\ldots \quad (7)$$

Where:

B_f, B_r Bandwidths in the forward (f) and reverse (r) directions with respect to the arterial orientation (sec).

C Cycle time, sec.

E Bandwidth efficiency

Bandwidth attainability as a measure of how much of the maximum available green is used for through progression was calculated. The bandwidth attainability is the ratio of the total bandwidths to critical phase lengths for each of the directions on the arterial and is computed as (Minnesota Department of Transportation):

$$A = \frac{B_f + B_r}{G_f + G_r} \quad \ldots\ldots\ldots\ldots\ldots\ldots\ldots\ldots \quad (8)$$

Where:

A Bandwidth attainability

Gf, Gr The critical (or minimum) green periods (including change periods) in the two directions.

In this study the following types of coordination was applied:

1. One-way street: - The simplest form of coordinating signals is along a one-way street or to favor one direction of traffic on a two-way street that contains highly directional traffic flows. Essentially, the mathematical relationship between the progression speed S and the offset L can be described as (Minnesota Department of Transportation):

$$S(mph) = D(ft)/1.47L$$

$$or\ S(kph) = D(m)/0.278L \quad \ldots\ldots \quad (9)$$

Where: D Spacing of signals (m or ft)

2. Two-way street: For a two-way movement, many modes of operation are possible, the relative efficiency of any of these modes is dependent on the distances between signalized intersections, the speed of traffic, the cycle length, the roadway capacity, the amount of friction caused by turning vehicles, and parking and unparking maneuvers (Institute of Traffic Engineers, 1978).

2.6 Traffic Delay

Delay estimate measures reflect the driver discomfort, frustration, fuel consumption and lost travel time. The (HCM) approach control delay equation was used for the determination of control delay for each lane group, approach and the whole intersection. Then the Level of Service (LOS) was determined from a predefined range of average control delay values.

3. SELECTION OF STUDY AREA

Two arterial streets were selected for the purpose of this study, Barzani and Zakho Streets. While the studied links on Barzani Street are 6 - lane sub urban, arterial dual carriageway road, the studied links on Zakho Street are 4 - lane urban, arterial divided road. The lengths of the links on both arterial streets are measured using mechanical distance meter, as shown in Tables (1) and (2).

Table (1) Link Speed and Volume Data on Barzani Street

Link	Link length (m)	Travel speed (km/h)	Running speed (km/h)	Mid-Link Spot Speed			Volume (vph)	% of Directional Distribution
				Sample size (N)	Mean (km/h)	Standard Deviation		
SRS-SIL	1.05	35.46	44.80	116	71.7	10.65	3125	50.8
SIL-SRS	1.05	38.10	44.27	111	62.2	10.10	3019	49.2
SIL-R	0.305	13.76	28.75	105	48.4	9.33	2913	49.0
R-SIL	0.305	27.61	27.61	101	64.7	11.65	3024	51.0
R-SK	1.10	42.20	47.96	109	78.2	11.24	2747	49.6
SK-R	1.10	28.43	43.72	104	77.7	11.63	2782	50.4

Table (2) Zakho Street Links Speed and Volume Data

Link	len	speed	speed	Mid-Link Spot Speed	ume	ona l

				Sample size (N)	Mean (km/h)	S.D		
K-A	425	16.33	28.51	105	50.2	8.21	905	41.90
A-K	425	14.44	28.35	103	42.8	7.44	1254	58.10
A-D	416	19.12	30.65	106	63.3	7.56	1369	44.50
D-A	416	16.88	28.62	104	54.9	8.00	1710	55.50

Four successive intersections on Barzani street were studied: Sarsink (SRS), Silav (SIL), Raza (R) and Sarok (SK) Intersections. These intersections have approximately the same geometry they are three-leg three approach actuated signalized intersections. Also three successive signalized intersections on Zakho Street were studied they are: Kawa (K), Azadi (A) and Daristan (D) intersections. These intersections also have approximately the same geometry they are three-leg three approach actuated signalized intersections except Azadi intersection which is four leg actuated intersection. The arterials and intersections are shown in Figures (1) through (9).

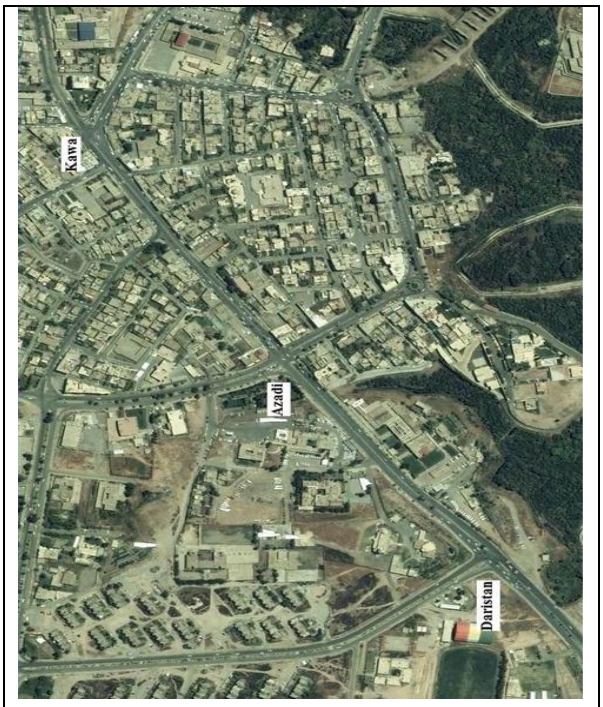

Figure (6) Google image of Zakho street showing the three studied intersecions (Directorate of Traffic, Traffic Engineering Department, Duhok City, 2009)

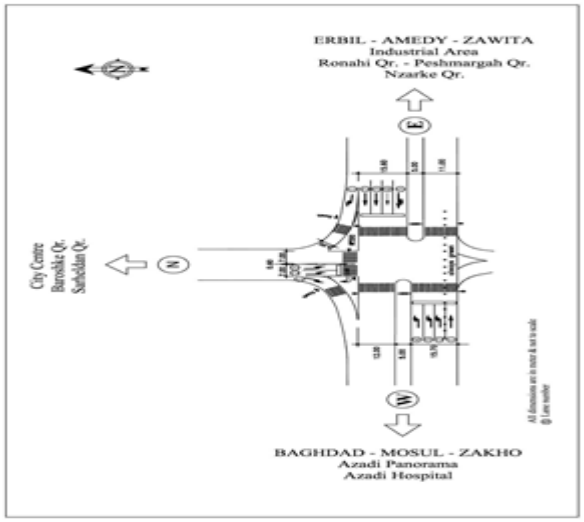

Figure (2): Sarsink Intersection (SRS) Plan (Directorate of Traffic, Duhok City, 2009)

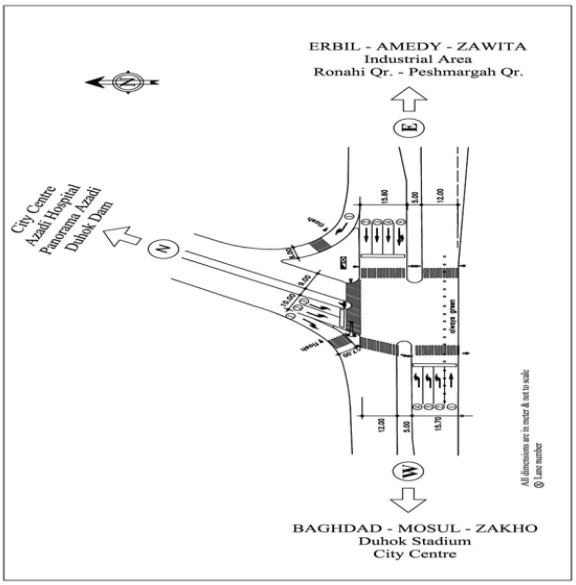

Figure (3): Silav Intersection (SIL) Plan (Directorate of Traffic, Duhok City, 2009)

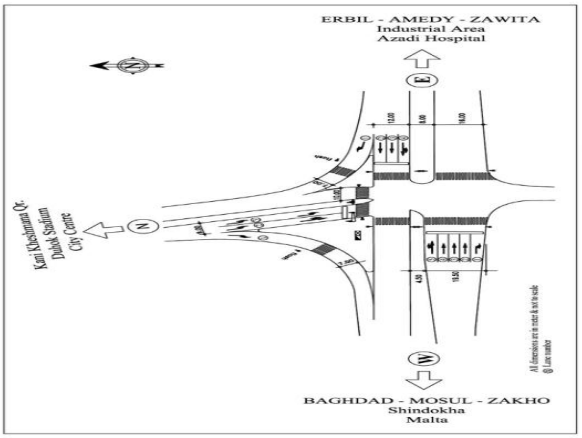

Figure (4): Raza Intersection (R) Plan (Directorate of Traffic, Traffic Engineering Department, Duhok City, 2009)

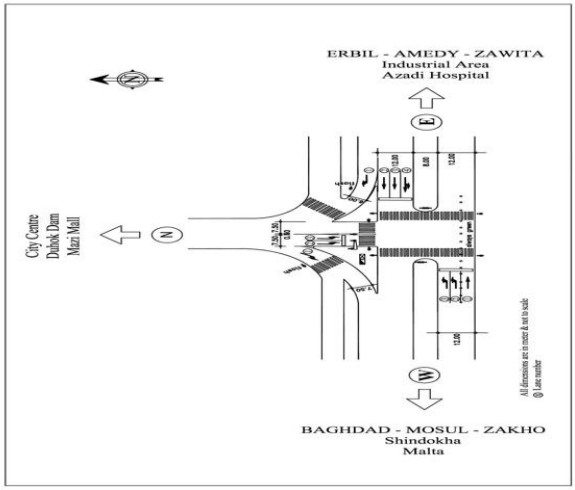

Figure (5): Sarok Intersection (SK) Plan (Directorate of Traffic, Traffic Engineering Department, Duhok City, 2009)

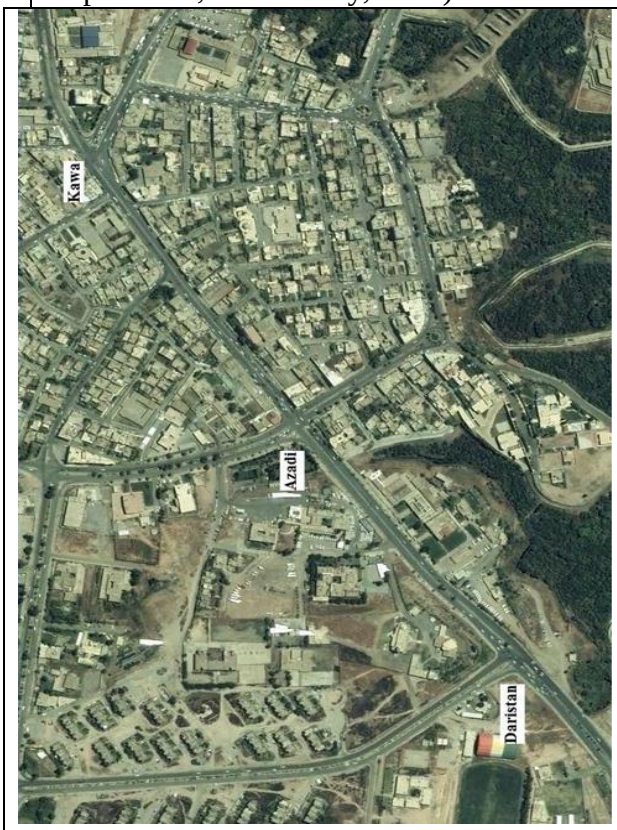

Figure (6) Google image of Zakho street showing the three studied intersecions (Directorate of Traffic, Traffic Engineering Department, Duhok City, 2009)

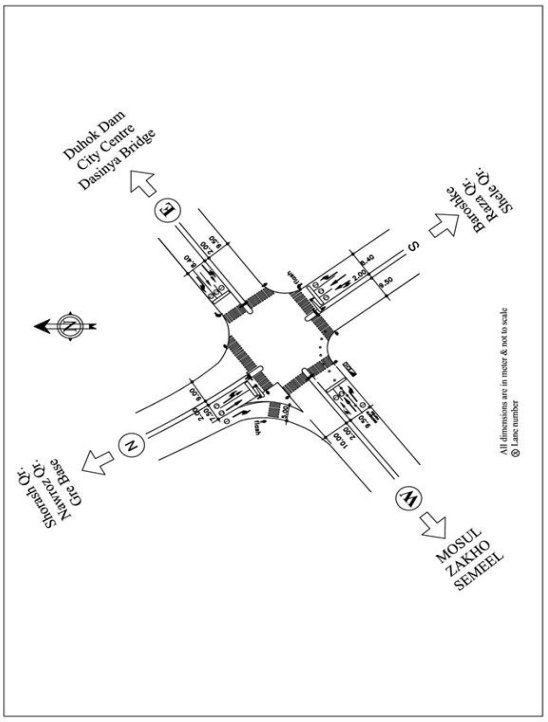

Figure (7): Azadi Intersection (A) Plan (Directorate of Traffic, Traffic Engineering Department, Duhok City, 2009)

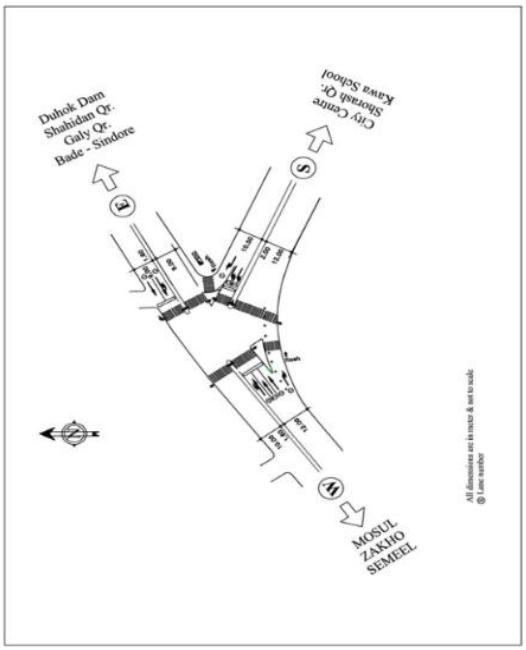

Figure (8): Kawa Intersection (K) Plan (Directorate of Traffic, Traffic Engineering Department, Duhok City, 2009)

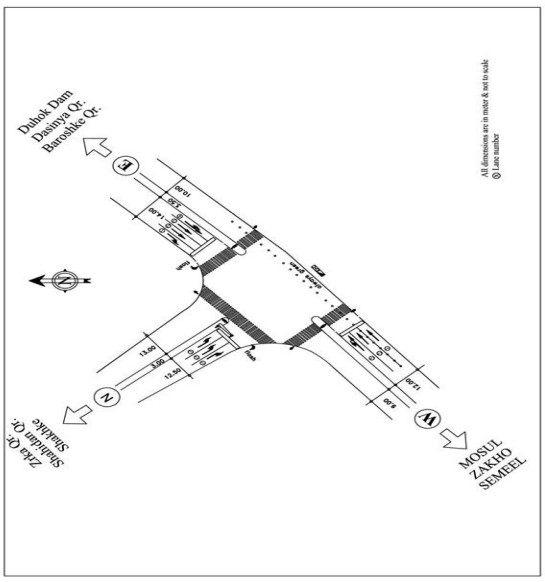

Figure (9): Daristan Intersection (D) Plan (Directorate of Traffic, Traffic Engineering Department, Duhok City, 2009)

4. DATA COLLECTION

To achieve the objective of this study, data was collected on intersections and links geometry, approach counts, AM and PM peak hour counts, posted speed on all links and approaches, percent of heavy vehicles. Morever, all the data required for field studies such as travel time and approach delay, signal timing and phasing data was collected

The determination of time period for data collection has its own importance in satisfying statistical evaluation for traffic activities. For this purpose, data collection was made by choosing different time periods from 7:30 AM to 7:30 PM according to the traffic activity. The study had avoided collecting data during weekends and other holidays as they don't represent the actual traffic activity and finding the peak periods.

Different methods of data collection were used in this study. The manual method was used to collect the intersection geometry, detectors measurements, approach speed and mid link spot speed. Moving vehicle method was used to collect the speed and volume data for the links between the studied intersections, while video camera technique was used to collect all other necessary data, which were not collected manually or by moving vehicle. The video camera data was abstracted using a computer program named EVENT (Al-Neami, A.H.K., 1995).

5. DATA ANALYSIS

5.1 Link Speeds and Volumes

It can be realized that there is a big difference between Mid-link average spot speed and link average running speed, (1.5-2) times the running speed. This may be due to the acceleration and deceleration near approaches to intersections and uncontrolled crossing walk for pedestrian in the link. Therefore, this was not used in the traffic signal coordination.

The spot speed data for mid-links on both streets were statistically analyzed using SPSS version (17) software. The chi-square test (Pignataro, L. J.,, 1973) showed that these speeds may be considered to be normally distributed at 95% confidence level.

The posted speed limit is 60 km/h for Barzani street. Mid-link spot speed and average travel and running speeds for all studied links on this street were obtained. The running speed values are approximately equal for studied links, because the link geometric conditions are not much different except (SIL-R or R-SIL) link which has a shorter length causing the vehicle to move at speed less than the speed of other links. These speed values can be combined to an average running speed (Barzani street running speed) to use it as progression speed in the coordinated system. Table (1) shows the results of spot speed and link running and travel speeds for the studied links on Barzani street.

On Zakho street, the speed limit is 40 km/h. Mid-link spot speed and average travel and running speeds for all studied links on this street were also obtained. For the links on Zakho Street, the running speed values are very close to each other as the geometric conditions of the links are similar. Therefore, these speeds also can be combined to an average running speed (Zakho street running speed) to use it as progression speed in the coordinated system. Table (2) shows the results of spot speed and link running and travel speeds for the studied links on Zakho street.

The links volumes and the directional distribution for studied links on both streets were observed. Tables (3) and (4) show results of peak hour volumes and saturation flow rate for the intersections.

5.2 Coordination of Traffic Signals on Barzani Street Intersections

Lane groups, design cycle time, green splits, yellow time, all-red time and red time for all the studied intersection on both Barzani and Zakho

Streets for isolated intersection plan strategy are shown in Tables (5) and (6) respectively.

It can be noticed that Raza Intersection has the maximum value of cycle time of 118 seconds among the other intersections on Barzani Street. While Azadi Intersection has a cycle time of 88 seconds which is the maximum cycle time value for the intersections on Zakho Street.

For coordinated plan, it should be noted that all signals within the same signal system must generally have the same cycle length, to make it possible for the pattern of timings to repeat every cycle.

Table (3) Design hourly volume and saturation flows for intersections on Barzani street (pcph)

Inter`.	Parameter		Approach								
			E			W			N		
			L	T	R	L	T	R	L	T	R
SRS	Volume (vph)	Total	0	2693	57	361	1888	0	26	0	85
		Bus%	0	4	0	0	1	0	0	0	0
		Truck%	0	3	0	0	2	0	0	0	0
	PHF			0	0.913	0.712	0.727	0.959	0	0.722	0
	Saturation Flow pcphgpl) *		1604			1721			1459		
SIL	Volume (vph)	Total	0	2085	1012	669	1417	0	763	0	408
		Bus%	0	4	2	0	5	0	1	0	1
		Truck%	0	3	1	0	4	0	2	0	1
	PHF			0	0.899	0.937	0.785	0.921	0	0.827	0
	Saturation Flow pcphgpl) *		1396			1465			1708		
R	Volume (vph)	Total	193	1644	620	334	1081	47	600	125	387
		Bus%	0	2	0	0	4	0	0	0	0
		Truck%	0	4	0	0	5	0	0	0	0
	PHF			0.782	0.851	0.771	0.705	0.932	0.734	0.787	0.744
	Saturation Flow pcphgpl) *		1568			1293			1734		
SK	Volume (vph)	Total	0	1790	372	361	1074	0	397	0	350
		Bus%	0	3	1	1	4	0	2	0	1
		Truck%	0	5	2	2	6	0	2	0	1
	PHF			0	0.883	0.721	0.737	0.962	0	0.735	0
	Saturation Flow pcphgpl) *		1595			1436			1470		

- Determined using HCM method

Table (4) Design hourly volume and saturation flows for intersections on Zakho Street

Inter.	Parameter		Approach											
			E			S			W			N		
			L	T	R	L	T	R	L	T	R	L	T	R
K	Volume (vph)	Total	406	481	0	983	0	305	0	540	706	0	0	0
		Bus%	0	0	0	0	0	0	0	0	0	0	0	0
		Truck%	0	0	0	0	0	0	0	0	0	0	0	0
	PHF		0.914	0.868	0	0.826	0	0.794	0	0.854	0.828	0	0	0
	Saturation Flow pcphgpl)		1864			1806			1627			-----		
A	Volume (vph)	Total	226	473	59	521	313	121	75	464	596	323	319	50
		Bus%	0	0	0	0	0	0	0	0	0	0	0	0
		Truck%	0	0	0	0	0	0	0	0	0	0	0	0
	PHF		0.871	0.949	0.912	0.956	0.932	0.843	0.821	0.945	0.932	0.873	0.891	0.912
	Saturation Flow pcphgpl)		1615			1590			1515			1728		
D	Volume (vph)	Total	0	887	243	0	0	0	330	763	0	461	0	199
		Bus%	0	0	0	0	0	0	0	0	0	0	0	0
		Truck%	0	0	0	0	0	0	0	0	0	0	0	0
	PHF		0	0.811	0.883	0	0	0	0.871	0.922	0	0.883	0	0.781
	Saturation Flow (pcphgpl)		1527			-----			1619			1853		

The suggested values of, green, yellow and all-red times as well as cycle time for all the studied intersections on both Barzani and Zakho Streets are shown in Tables (7) and (8) respectively. The maximum cycle time of Raza intersection (118 seconds) was used for the system. The green times for other intersections was extended proportionally so that the cycle time equals to 118 seconds.

Table (5) Signal Timing for Isolated Intersections on Barzani Street

Int.	Phase No.	Lane Group	Green (sec)	Yellow (sec)	All-Red (sec)	Cycle time (sec)
SRS	I	$T_E+T_E+T_E+(T_E+L_E)$	62	4	2	99
	II	$L_W+L_W+L_W$	10	4	2	99
	III	LN+LN	9	4	2	99
SIL	I	$T_E+T_E+T_E+(T_E+L_E)$	48	4	2	97
	II	$L_W+L_W+L_W$	12	4	2	97
	III	L_N+L_N	19	4	2	97
R	I	$T_E+T_E+(T_E+L_E)$	54	4	2	118
	II	$T_W+T_W+T_W+(L_W+T_W)$	28	4	2	118
	III	$(T_N+L_N)+L_N$	18	4	2	118
SK	I	$T_E+T_E+(T_E+L_E)$	47	4	2	87
	II	L_W+L_W	9	4	2	87
	III	L_N+L_N	13	4	2	87

Table (6) Signal Timing for Intersections on Zakho Street (Isolated Plan)

Int.	Phase No.	Lane Group	Green (sec)	Yellow (sec)	All-Red (sec)	Cycle time (sec)
K	I	$T_E+(T_E+L_E)$	14	4	2	71
	II	$T_W+T_W+(T_W+L_W)$	24	4	2	71
	III	L_S+L_S	15	4	2	71
A	I	$R_E+T_E+(T_E+L_E)$	15	4	2	88
	II	$T_N+(T_N+L_N)$	21	4	2	88
	III	$T_W+(T_W+L_W)$	14	4	2	88
	IV	$R_S+T_S+(T_S+L_S)$	14	4	2	88
D	I	$T_E+(TE+LE)$	15	4	2	55
	II	$T_W+T_W+(T_W+L_W)$	10	4	2	55
	III	L_S+L_S	12	4	2	55

Table (7) Signal Timing for Coordinated Intersections on Barzani Street

Int.	Phase No.	Lane Group	Green (sec)	Yellow (sec)	All Red (sec)	Cycle time (sec)
SRS	I	E	75	4	2	118
	II	W	13	4	2	118
	III	N	12	4	2	118
SIL	I	E	60	4	2	118
	II	W	16	4	2	118
	III	N	24	4	2	118
R	I	E	54	4	2	118
	II	W	28	4	2	118
	III	N	18	4	2	118
SK	I	E	66	4	2	118
	II	W	14	4	2	118
	III	N	20	4	2	118

Table (8) Signal Timing for Intersections on Zakho Street (Coordinated Plan)

Int.	Phase No.	Lane Group	Green (sec)	Yellow (sec)	All-Red (sec)	Red (sec)	Cycle time (sec)
K	I	E	19	4	2	65	88
	II	S	31	4	2	53	88
	III	W	20	4	2	64	88
A	I	E	15	4	2	69	88
	II	S	21	4	2	63	88
	III	W	14	4	2	70	88
	IV	N	14	4	2	70	88
D	I	E	28	4	2	56	88
	II	W	20	4	2	64	88
	III	WN	23	4	2	61	88

The coordination application on the arterial streets should be checked in order to achieve excellent results before starting the work. Coupling index for each link on Barzani and Zakho streets are calculated from two-way peak hour volumes and link length to determine the need of providing signal progression. The coupling index is greater than 0.5 for all links as shown in Tables (9) and (10) therefore, signal progression is recommended for all intersections on both Arterials.

Table (9) Coupling Index for Links on Barzani Street

Link	Link Volume veh/h	Length (m)	Coupling Index $Ic=V/d_L$
SRS-SIL	3125	1050	5.85
SIL-SRS	3019		
SIL-R	2913	305	19.47
R-SIL	3024		
R-SK	2747	1100	5.03
SK-R	2782		

Table (10) Coupling Index for Links on Zakho Street

Link	Link Volume veh/h	Length (m)	Coupling Index $Ic=V/d_L$
K-A	905	425	5.08
A-K	1254		
A-D	1369	416	7.40
D-A	1710		

5.2.1 One Direction Coordination Under Prevailing Conditions

In this case, the prevailing traffic conditions was used in the analysis without improvements. The running speeds, calculated from the moving car method, were used in the analysis. One direction coordination of traffic signals has more flexibility in dealing with bandwidth values. By using this

way, a greater value of bandwidth could be achieved.

The time-space diagram for the one direction coordination of traffic signals for all the intersections located on Barzani Street under prevailing conditions are shown in Figure (10). This Figure shows the coordination of the east approach of an intersection with the east approach of the next intersection along the arterial which represents the east direction coordination. Table (11) shows offsets and bandwidths resulted from the coordination operation. The offsets are 84 – 4 - 87 seconds while the band width is 54 seconds.

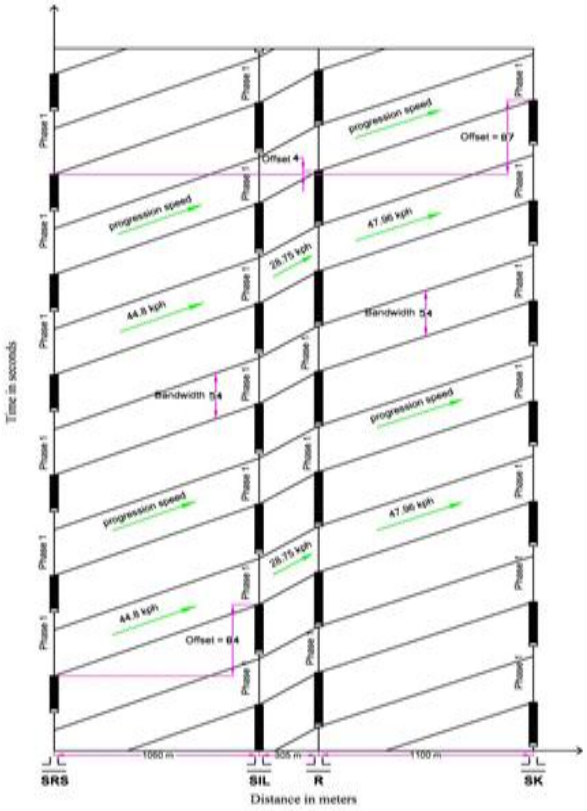

Figure (10) Time-Space Diagram for East Direction Coordination of Traffic Signals on Barzani Street under Prevailing Conditions

Table (11) Offsets & Bandwidths for One Direction Coordination of Traffic Signals on Barzani Street

Coordination Direction	Offsets (sec)	Bandwidth (sec)	Figure
East (prevailing)	84 - 4 – 87	54	(10)
East (constant speed)	84 - 4 – 87	50	(11)
East (controlled)	63 – 81 – 29.3	54	(12)

The coordination for other approaches on Barzani street are not significant, as there is already an always-green lane for the West Approach of all intersections except Raza Intersection, and also most of the vehicles during the green time move to the left direction except few vehicles that move straight and continue moving to the next intersection.

5.2.2 One Direction Coordination Using Street Average Speed (Constant Speed)

As mentioned, one running speed which was obtained by equalizing the speeds into Barzani street average speed (constant speed) was used in order to improve the coordination performance as shown in Figure (11). Table (11) shows offsets and bandwidths resulted from the coordination operation. Kell method resulted in a lower value of bandwidth therefore, it was not used in this study. The offsets are 84 – 4 - 87 seconds while the band width is 50 seconds. This means that the offsets remain the same while the band width decreased. Again, the coordination for other approaches are not significant for the same reason.

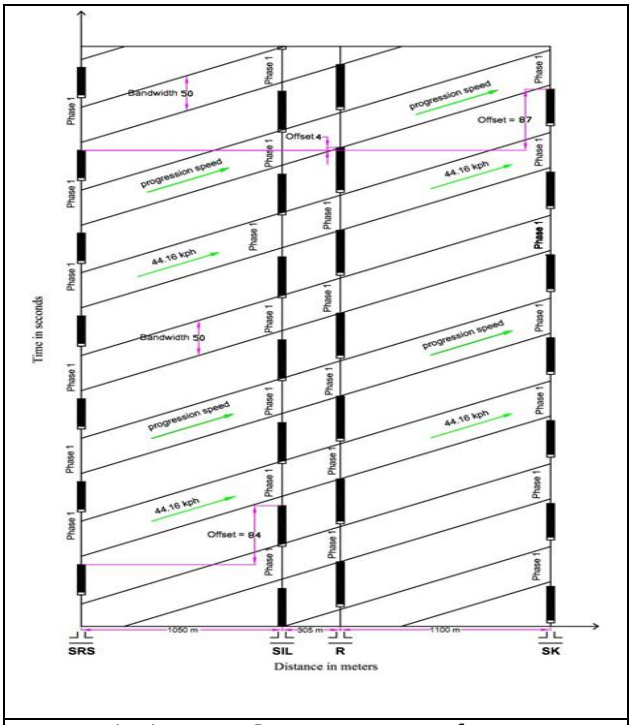

Figure (11) Time-Space Diagram for East Direction Coordination of Traffic Signals on Barzani Street under a Constant Speed

5.2.3 One Direction Coordination of Traffic Signals Under Controlled Conditions

To increase the efficiency and attainability of the traffic signals in the two studied Arterials, some improvements are recommended. One of these suggested improvements is increasing the running speed by preventing pedestrians from crossing the

roadway, except at crossing areas and using traffic signs and enforcement to assure the posted speed limit.

For the speeds on Barzani Street, the constant speed of the East Direction Coordination was changed from 44.16 km/h to the posted limit speed of this street which is 60 km/h. The controlled conditions give a greater bandwidth than the prevailing conditions as shown in Figure (12). Table (11) shows offsets and bandwidths resulted from the coordination operation.

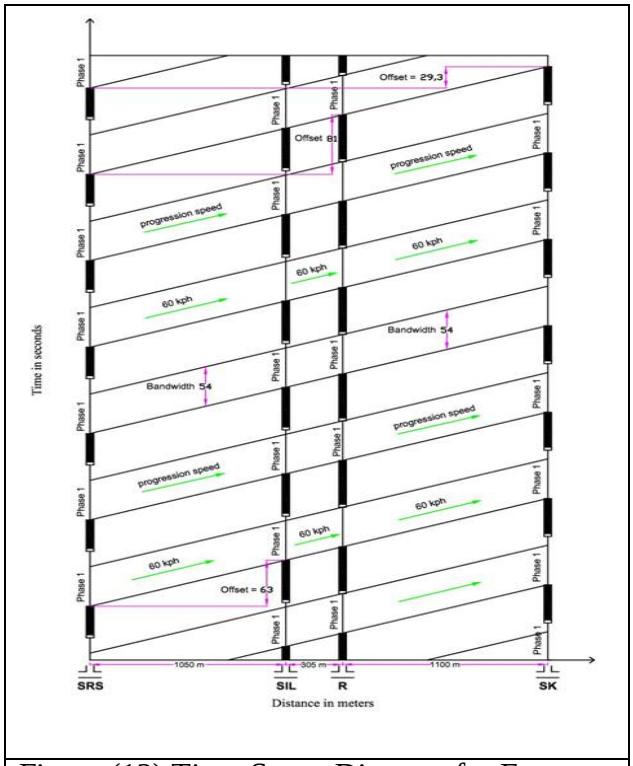

Figure (12) Time-Space Diagram for East Direction Coordination of Traffic Signals on Barzani Street under Controlled Conditions

It can be noticed that, the offsets changed to 63 – 81 – 29.7 seconds, while the bandwidth increased to a value of 54 seconds under a posted speed limit of 60 km/h. This value could also be increased to 58 seconds if the yellow time added to the green time to insure greater bandwidth (FHWA, 2008). Bandwidth of 54 seconds is adopted since the 54 seconds are sufficient for the platoon to move through all intersections.

5.2.4 Two Direction Coordination

The two-direction coordination for the traffic signals on Barzani street is not applicable and may be impossible to be executed. This is because of the left turn that is existing on the West Approach of each intersection that couldn't be ignored. Therefore, one direction coordination is more preferable for this arterial as there is always-green lane for all intersections except Raza Intersection, which helps the west direction to act as a coordinated direction all over the time.

5.3 Coordination of Traffic Signals on Zakho Street Intersections

5.3.1 One Direction Coordination Under Prevailing Conditions

The time-space diagram was drawn to show one direction coordination of traffic signals for the intersections located on Zakho Street under prevailing conditions or east and west directions respectively. The offsets are 54 – 15 seconds and 53 – 19 seonds for east and west approaches respectively, while the band widths 19 seconds and 18 seconds. The time space diagram, offsets and bandwidths from the coordination operation are shown in Figures (13) and (14) and Table (12).

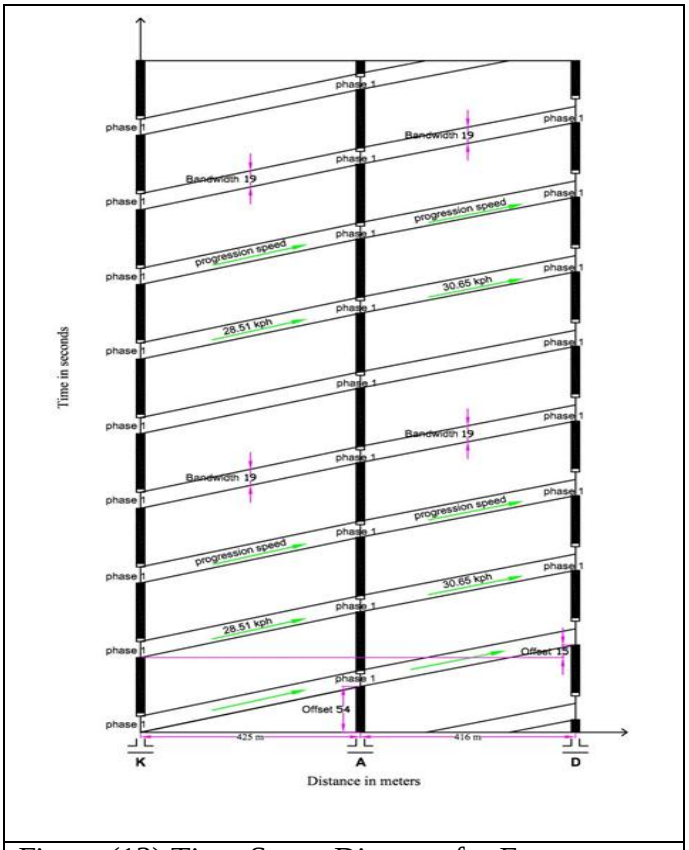

Figure (13) Time-Space Diagram for East Direction Coordination of Traffic Signals on Zakho Street under Prevailing Conditions

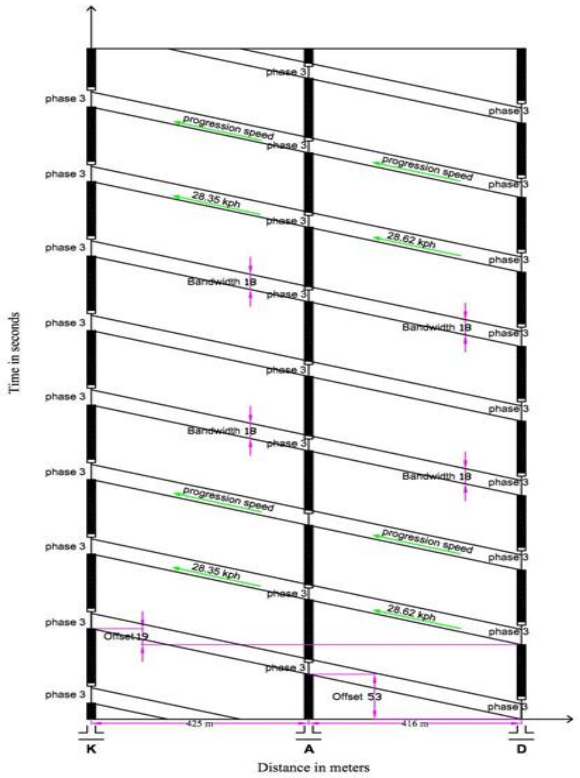

Figure (14) Time-Space Diagram for West Direction Coordination of Traffic Signals on Zakho Street under Prevailing Conditions

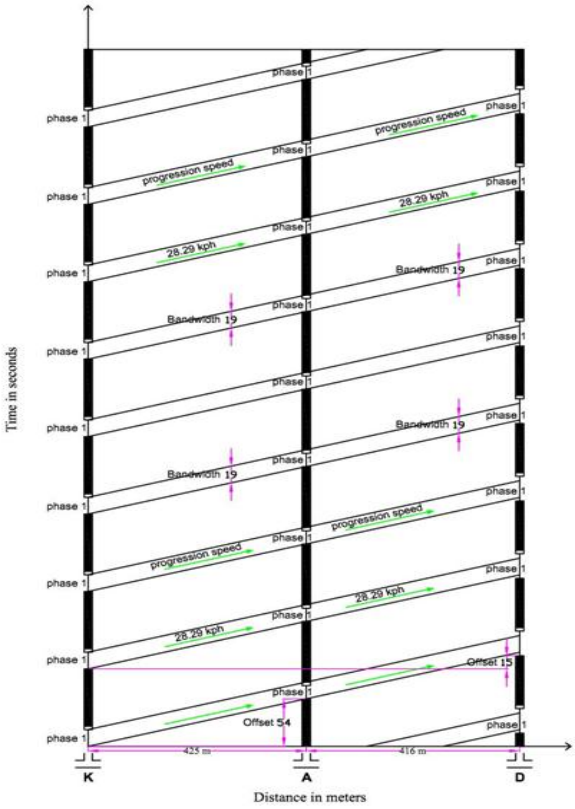

Figure (15) Time-Space Diagram for East Direction Coordination of Traffic Signals on Zakho Street under a Constant Speed

Table (12) Offsets & Bandwidths for One Direction Coordination of Traffic Signals on Zakho Street under Prevailing Conditions

Coordination Direction	Offsets (sec)	Bandwidth (sec)	Figure
East (prevailing)	54 – 15	19	(13)
West (prevailing)	53 – 19	18	(14)
East (constant speed)	54 – 15	19	(15)
West (constant speed)	53 – 19	18	(16)
East (controlled)	38.2 – 75.7	19	(17)
West (controlled)	37.5 – 75.7	18	(18)

5.3.2 One Direction Coordination Using Street Average Speed (Constant Speed)

It can be seen that there is no difference in bandwidths because coordination – through band – is restricted by the smaller (green plus yellow) time for both of east and west approaches of Azadi intersection. The offsets and band widths for east and west approaches are equal to that of prevailing speed and not changed. The time space diagram, offsets and bandwidths from the coordination operation are shown in Figures (15) and (16) and Table (12).

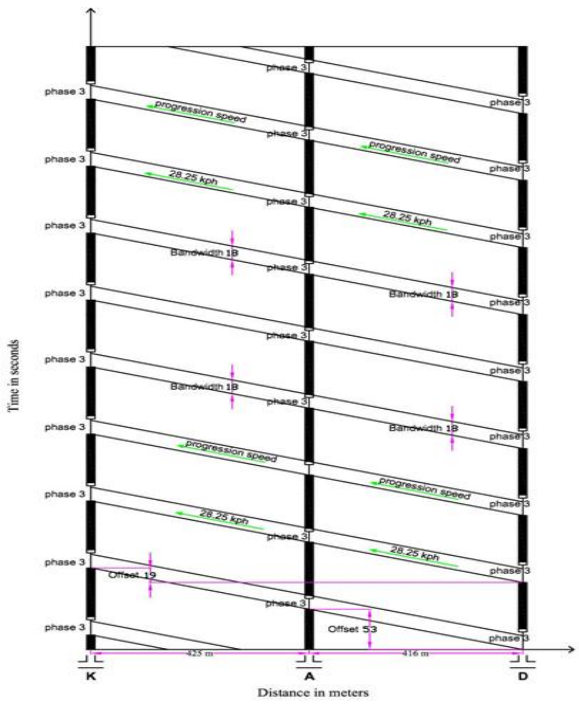

Figure (16) Time-Space Diagram for West Direction Coordination of Traffic Signals on Zakho Street under a Constant Speed

5.3.3 One Direction Coordination of Traffic Signals Under Controlled Conditions

For Zakho Street, the constant speeds of both east and west direction coordination was changed from 28.29 km/h and 28.25 km/h to the posted limit speed of this arterial which is 40 km/h the offsets and the bandwidths under controlled conditions.

The offsets are 38.2 – 75.7 seconds and 37.5 – 75.7 seconds for east and west approaches respectively, while no difference in bandwidths can be noticed after controlling the speed on Zakho Street, because coordination –through band– is again restricted by the smaller (green plus yellow) time for both of east and west approaches of Azadi Intersection, while the band widths remain as 19 seconds and 18 seconds for east and west approaches respectively. The time space diagram, offsets and bandwidths from the coordination operation are shown in Figure (17) and (18) and Table (12).

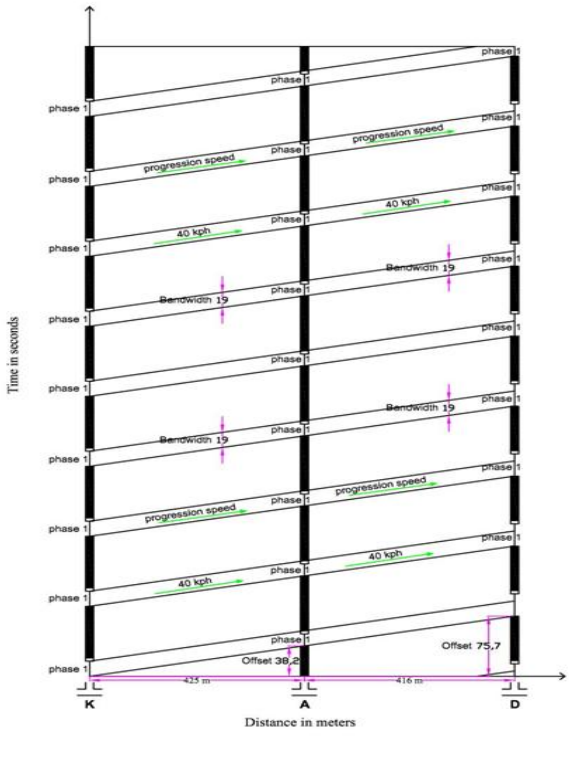

Figure (17) Time-Space Diagram for East Direction Coordination of Traffic Signals on Zakho Street under Controlled Conditions

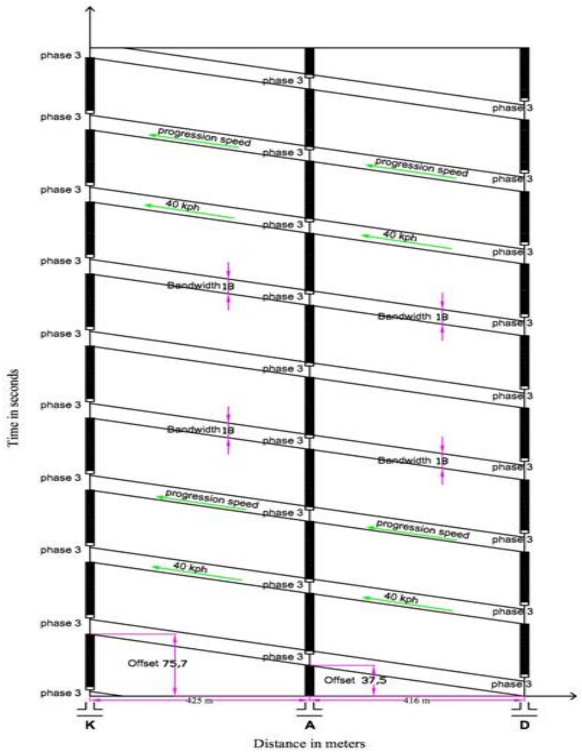

Figure (18) Time-Space Diagram for West Direction Coordination of Traffic Signals on Zakho Street under Controlled Conditions

5.3.4 Two Direction Coordination

The two-direction coordination can be designed for the traffic signals on Zakho Street, resulting in smaller value of bandwidth than one direction coordination. The design of the two-direction coordination was executed under controlled conditions as it's difficult to give good results under prevailing conditions. The offsets are 57 – 3.92 seconds and 42.08 – 87.08 seconds for east and west approaches respectively, while the band widths for both approaches are 16 seconds. The time space diagram, offsets and bandwidths from the coordination operation are shown in Figure (19) and Table (13).

The results show a higher value of bandwidth efficiency when applying coordination for two traffic signals, while coordination of three traffic signals gives less efficiency. Table (14) shows results of bandwidth efficiency which were obtained.

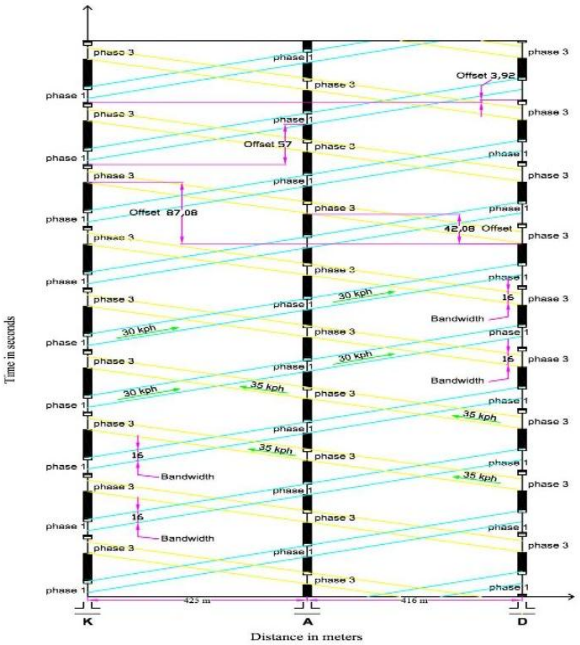

Figure (19) Time-Space Diagram for Two Direction Coordination (East-West) of Traffic Signals on Zakho Street under Controlled Conditions

Table (13) Offsets & Bandwidths for Two Direction Coordination of Traffic Signals on Zakho Street under Controlled Conditions

Coordination Direction	Offsets (sec)	Bandwidth (sec)
East (controlled)	57 – 3.92	16
West (controlled)	42.08 – 87.08	16

Table (14) Bandwidth Efficiencies for Two Direction Coordination on Zakho Street under Controlled Conditions

Link	Coordination type	B_f (sec)	B_r (sec)	Bandwidth Efficiency
K-A	Two-Way	18	18	20 %
A-D	Two-Way	18	18	20 %
K-A-D	Two-Way	16	16	18 %

It can be seen that the bandwidth attainability for coordination of two traffic signals is higher than the attainability for coordination of three traffic signals. Table (15) shows results of bandwidth attainability which was obtained.

Table (15) Bandwidth Attainability for Two Direction Coordination on Zakho Street

Link	Coordination type	B_f (sec)	B_r (sec)	G_f (sec)	G_r (sec)	Bandwidth Attainability
K-A	Two-Way	18	18	19	19	95 %
A-D	Two-Way	18	18	19	19	95 %
K-A-D	Two-Way	16	16	19	19	84 %

5.4 Control Delay

5.4.1 Approach Control Delay

Table (16) shows a comparison between approach control delays for the intersections on Barzani street before and after coordination. The Table also shows the percentage of improvement was obtained by decreasing delays for all the approaches.

Table (16) Approach Control Delays on Barzani Street before and after coordination

Int.	App.	Control Delay (sec/veh)		% Reduced Delay
		Before Coordination	After Coordination	
SRS	E	21.23	6.57	69.05
	W	54.81	51.95	5.21
	N	48.82	48.35	0.97
SIL	E	30.62	17.93	41.43
	W	99.14	71.16	28.23
	N	82.05	64.26	21.69
R	E	37.24	24.72	33.63
	W	77.50	68.79	11.25
	N	115.88	106.04	8.49
SK	E	26.75	12.51	53.23
	W	59.70	52.72	11.70
	N	63.43	51.40	18.97

It can be noticed that the best improvement was made in the east approach of Sarsink intersection with 69.05% reduction in delay. While the lowest improvement noticed on the north approach of the same intersection with 0.97% reduction in delay. Table (17) shows the comparison between approach control delays before and after coordination on Zakho Street. The best improvement was made in the east approach of Kawa intersection with 33.38% reduction in delay. While the lowest improvement was noticed on the west approach of the same intersection with 8.19% reduction in delay.

5.4.2 Intersection Control Delay

the comparison between intersection control delays before and after coordination on Barzani street was made to show the percent improvements. The highest improvement was made in Sarsink intersection with 51.79% reduction in delay. While the lowest improvement can be seen in Raza intersection with 16.21% reduction in delay. Table (18) shows the percentage of improvement obtained by

decreasing the intersection control delay for intersections on Barzani street.

Table (17) Approach Control Delays on Zakho Street before and after coordination

Int.	App.	Control Delay (sec/veh)		% Reduced Delay
		Before Coordination	After Coordination	
K	E	77.32	51.52	33.38
	S	32.40	25.41	21.57
	W	36.60	33.61	8.19
A	E	89.63	78.86	12.02
	S	62.76	49.94	20.44
	W	72.79	57.62	20.85
	N	76.97	64.15	16.65
D	E	31.59	25.18	20.29
	W	33.86	29.55	12.73
	N	31.90	27.52	13.72

Table (18) Intersection Control Delay Before and After Coordination on Barzani Street

Int.	Control Delay (sec/veh)		% Reduced Delay
	Before Coordination	After Coordination	
SRS	25.40	12.24	51.79
SIL	55.00	38.26	30.43
R	65.90	55.22	16.21
SK	37.13	24.26	34.65

For Zakho street, the highest improvement was made in Kawa Intersection with 26.11% reduction in delay. While the lowest improvement can be seen in Daristan intersection with 16.93% reduction in delay.

Table (19) shows the comparison between intersection control delays before and after coordination on Zakho Street.

As a result, the highest reduction in control delay value is for Sarsink intersection on Barzani Street, and for Kawa intersection on Zakho street.

Table (19) Intersection Control Delay Before and After Coordination on Zakho Street

Int.	Control Delay (sec/veh)		% Reduced Delay
	Before Coordination	After Coordination	
K	49.88	36.85	26.11
A	75.04	62.27	17.01
D	32.12	26.68	16.93

6. CONCLUSIONS & RECOMMENDATIONS

6.1 Conclusions

The following conclusions can be drawn based on the results of this study:

1. Intersections on Barzani Street have evening peak hour in the range between (5:30 to 6:30) PM in winter, while intersections on Zakho Street have evening peak hour in the range between (6:00-7:00) PM in spring.
2. The range of observed flow for intersections on Barzani Street was between 111 veh/h on North Approach of Sarsink Intersection, and 3070 veh/h on East Approach of Silav Intersection. While the range of observed flow for the intersections on Zakho Street was between 660 veh/h on North Approach of Daristan Intersection, and 1288 veh/h on South Approach of Kawa Intersection.
3. The range of saturation flow for intersections on Barzani Street was between 1293 pcphpl on West Approach of Raza Intersection, and 1734 pcphpl on North Approach of the same intersection. While for intersections on Zakho Street the range of saturation flow was between 1515 pcphpl on West Approach of Azadi Intersection, and 1864 pcphpl on East Approach of Kawa Intersection.
4. The coupling index values for the all links on Barzani and Zakho Arterial Streets were more than 0.5 which means that the coordination of traffic signal on both Arterials is applicable.
5. The average travel and running speeds are nearly equal for the links of both Barzani and Zakho Street as these links have approximately the same length and geometry on each street.
6. The coordination results under prevailing and controlled traffic conditions for both Barzani and Zakho Streets show an increase in bandwidths by controlling the progression speeds.
7. The intersection control delay and level of service values after coordination for the intersections on Barzani and Zakho Streets are improved.

6.2 Recommendations

1. Installing permanent video recording camera on streets and intersections for traffic volume counting and measuring speed of vehicles, this will simplify the process of data collection and data analysis for future studies.

2. Continuous maintenance for all the streets and intersections is needed including new marking lines and lightings.
3. Providing speed humps at the middle of the links that have long distances in order to avoid the probability of platoon dispersion. This mechanism is used to force the drivers to reduce their speeds at the point where the speed hump was installed, and then recollecting the platoon again so as to arrive together to the next intersection.
4. Offering a proposal for executing the east direction coordination on Barzani Street and the two-way coordination on Zakho Street as it gives the best results in this study.
5. As the coordination under controlled speed gives best results therefore, it is necessary to provide speed limit dynamic signs to show the speed required to reach the next intersection without interruption.

6.3 Further Research

Future research in this area will be aimed at:

1. Studies required to be made on networks in Duhok city and for Kurdistan Region wide.
2. Fuel consumption and Carbon Monoxide Emission studies for the coordinated traffic signals.

Acknowledgements

This paper is part of the MSc thesis at Salahaddin University-Erbil. The authors would like to acknowledge Civil department of College of Engineering in Salahaddin University - Erbil for helping to complete the study.

References

Alexander Skabardonis, Robert L. Bertini and Brian R. Gallagher "Development and Application of Control Strategies for Signalized Intersections in Coordinated Systems", paper No.: 981271, Publication: Transportation Research Record, March 1998.

Al-Neami, A.H.K.," Event, A Computer Program for Traffic Abstraction and Analysis" 1995.

Chang, E C and Koothrappally, J, "Field Verification of Coordinated Actuated Control", Transportation Research Record, No. 1456, Traffic Signing, Signals, and Visibility, pp. 83-90, (1994).

City of Kent Development assistance brochure "Frequently Asked Transportation Questions". Last revised February 21, 2001.

Directorate of Traffic, Traffic Engineering Department, Duhok City, 2009.

Hirsh Muhammad Majid, and Aso Faiz Talabany, "Fixed – Time Signal Coordination on Arterial Streets in Sulaimani City", Zanko Journal of Pure and Applied Sciences, Vol. 20, No. 4, 2008.

Institute of Traffic Engineers (ITE) "Transportation and Traffic Engineering Handbook", Prentice-Hall, INC., Englewood Cliffs. New Jersey, 1976.

Luk, J.Y.K. and Sims, A.G., "Selection of Offsets for Sub-Area Linkage in SCATS," Australian Road Research, Vol. 12, No. 2, June 1982.

Martin Rogers, "Highway Engineering", Department of Civil and Structural Engineering, Dublin Institute of Technology, Ireland. First published 2003

Masaki Koshi "Cycle Time Optimization in Traffic Signal Coordination", Institute of Industrial Science, university of Tokyo, Bunkyoku, Tokyo 113, Japan, Transp. Res.-A, Vol. 23A, No. 1, pp. 29-34, 1989.

Minnesota Department of Transportation "MnDOT Traffic Signal Timing and Coordination Manual", March 2005.

Pignataro, L. J., "Traffic Engineering – Theory and Practice", Prentice Hall, Inc, Englewood Cliffs, New Jersey, 1973.

Federal Highway Administration (FHWA) "Traffic Signal Timing Manual", publication number FHWA-HOP-08-024, 2008.

Wei Li and Andrew P. Tarko, "Effective and Robust Coordination of Traffic Signals on Arterial Streets", Joint Transportation Research Program, Vol. 1, Research Report, No. 8-4-75, January 2007.

William A. Stimpson and Gerald M. Takasaki "Co-ordinating Vehicle-Actuated Traffic Signals to Reduce Vehicular Fuel Consumption", (paper), Transportation Research Department, General Motors Research Laboratories, Traffic Engineering + Control, 1982.

Zaher Khatib, Ahmed Abdel-Rahim, Geoffrey Judd, and Krishnakanth Jagarapu, "Actuated Coordinated Signalized System", National Institute for Advanced Transportation Technology, University of Idaho, Research Report, November 2001.

ZANCO Journal of Pure and Applied Sciences
The official scientific journal of Salahaddin University-Erbil
https://zancojournals.su.edu.krd/index.php/JPAS

ISSN (print):2218-0230**, ISSN (online):** 2412-3986**, DOI: http://dx.doi.org/10.21271/zjpas**

RESEARCH PAPER

Out-put Characteristics of Low Power He-Ne Laser Efficiency Determination

Gullala. Y. Baker
Department of Physics, College of Education, Salahaddin University- Erbil, Kurdistan Region, Iraq

A B S T R A C T:

It is known that any laser has a pumping source, an amplifying medium and a resonator that oscillates the active mode representing the out-put wavelength of the laser. The suitable value for this ratio is 7:1 He/Ne in volume. These were to prepare under an ideal mixture of these gases as treated before by many experiment lists. The aim of this study to specify is to the basic portions of low power He-Ne gas lasers available in laboratories, and to test them in order to look for a probable factor of the efficiency as the whole. All calculations were performed, using calculators. The results were unique for all of them that the laser aperture also plays an important role in this criteria. The best fitting ratio between the radius of laser aperture and that of laser beam was determined and connected to the other parts of the efficiency, also the ratio of(ρ/ω) was fixed at 1.55.

KEY WORDS: Laser Efficiency; Out-put power; Laser aperture, Minimum pumping power, Laser Amplification.
DOI: http://dx.doi.org/10.21271/ZJPAS.33.5.3
ZJPAS (2021) , 33(5);24-30 .

1.INTRODUCTION :

When a gas is discharged in a low temperature plasma range, ionization is followed by a few consequent processes such as scattering, excitation, pair production and radiation(Hasted, 1976). Gas discharge in laser resonator has different functions since, the discharge followed by beam formation in Gaussian shape then amplification and saturation occurs in the medium(Yariv and Gordon, 1963). When a beam oscillates inside a laser resonator, the amplification quality depends in many factors including; end-mirror sizes, the plasma density and input electrical power (Born and Wolf, 1964). The overall process determines the laser efficiency which is different from other efficiencies in electrical and mechanical system.

* **Corresponding Author:**
Gullala. Y. Baker
E-mail: glalabakr@gmail.com
Article History:
Received: 17/03/2021
Accepted: 25/07/2021
Published: 20/10 /2021

This difference arises from that the laser resonator is an amplifying design, which concentrates the beam towards a tiny aperture of less than a millimeter in diameter(Hecht, 2018). In this study, few laser tubes were tested having out-put powers{1,2,3,5,10,15,20,30and35}m watts respectively. In all of these the basic parameters to be known are (Yariv, 1967)[5].

1-The electrical in put power [$P_{in}=V_{in}I_{in}$] which is the characteristic of the gases{He and Ne}with in the plasma tube V_{in} is entering Voltage and I_{in} is the input dc current.

2-The resonator geometry {length, mirror sizes and reflectivity's…. etc.

3-the plasma tube specifications including [cathode and anode} distance, the gas ratio He/Ne, the total pressure and discharge saturation times.

4- Physical and chemical properties of the laser coatings and their structure.

5-Finally, the power types are to be identified in order to specify and enhance their characteristics.

2.Theory:

From the parameters mentioned in the introduction one can get the formulas for basic parts of the power which ends of the outside plane of the output mirror, mentioned as the transmitted or useful out-put power(Abdul-Rahim and Mawlud, 2013).

In this case and according to their order of performance, these were the following:

1- The input electrical power coming from the step-up transformer as V_{in} and I_{in} respectively. So:

$P_{in} = V_{in} I_{in}$ in watts … (1)

2-Minimum pumping power (MPP) which is the necessary power needed to assure the desired process of population inversion, it is the function of the oscillating photon energy, the volume of the capillary tube and the lifetime of the upper level T_u in seconds(K. Evans and Sommerfield, 2015). This is

$MPP = h\nu \Delta N V/\tau_u$ …(2)

Here ΔN is the optimum population inversion density in m^{-3}, v is the volume of capillary tube in m^3 and τ_u is the mean life time of upper laser state.

The maximum output power stored in the resonator known as P_{sat}, which is:

$P_{sat.} = I_{sat.} A$ …(3)

Here A is the the cross-sectional area of the laser beam, $I_{sat.}$ is the saturated intensity of the laser beam and it is the characteristic of photon energy($h\nu$), the σ_{st} is the stimulated emission cross section, and the saturated life time of the process.τ_{sat} :

$\therefore I_{sat} = h\nu / \sigma_{st}. \tau_{sat}$ …(4)

In unit of watt/m^2 .

σ_{st}. is also the function of active medium characteristics.

4- the central power at the center of the resonator P_0, which is the (Urquhart, 2020).

$P_0 = Lg_0/2[1-(a_0/Lg_0)^{1/2}]^2 I_{sat} A$ … (5)

Where Lis the resonator length, g_0 is the gain coefficient, a_0 is the loss factor is equal to 0.005, and in equ.5 the whole bracket $[1-(a_0/Lg_0)^{1/2}]$ represents the aperture efficiency.

Now, on the behalf of these information's, the individual parts of the laser efficiency could be defined as(Morace et al., 2019):

a- $\eta_{pump} = \frac{MPP}{Pin}$ …(6)

b- $\eta_{res} = \frac{P0}{Psat}$ …(7)

c- $\eta_{ap} = 1-e^{-2\rho 2/\omega 2}$ … (8)

Where η_{pump} is the pumping efficiency, η_{res} is the resonator efficiency η_{ap} is the aperture efficiency. In equ.8, ρ is the radius of laser aperture and ω is the radius of the beam.

2.Results and discussion:

Throughout the whole work, parameters are the Own of the laser tubes such as their out-put their length, density and geometric parameters, and the He:Ne ratio was fixed as7:1 involves. From these the calculated portions of the efficiency were drown individually as in Figures1, and2, respectively, the results show that their values are different, according to different input parameters, the common values of these were (Bartal et al., 2012).

1-The small signal gain coefficient, $g_o = 0.1 m^{-1}$

2-The scattering and absorption coefficient, $a_0 = 0.005$

3-Stimulated emission cross-section,$\sigma_{st} = 3*10^{-17} m^2$

4-life time of upper laser level,$\tau_u = 3*10^{-8}$ sec.

5-Population inversion density ,$\Delta N = 5*10^{15} m^{-3}$.

From these, one can determine the fixed ratio ρ/ω, which was optimum for all laser tubes as (1.5). Also, the idea of the laser aperture to be part of the process was clear in calculating the total power efficiencies as (Cockbill, 2017):

$M_{ap} = P_{out}/P_o$, here P_{out} and P_o are the out put power and the central power stored in the resonator. Where P_{out} ,

$P_{out} = P_{in}[1-e^{-2\rho 2/\omega 2}]$ ……(9)

The results revealed that the effective part of these was the resonator efficiency.

The results were very close to standard evaluation of total laser efficiency, since the optimum value of common produced He-Ne laser exceeds (10^{-4}) slightly.

Figure١ represents the graph of the resonator efficiency as the function of Pout for the laser. Figure2 is the plot of (ρ/ω) as the function Transitions of out put mirror $[1-e^{-2r2/\omega 2}]$ r is the variable value of ρ. Finally, Figure٣ is the variation of Resonator Efficiency as the

function of total power stored in the resonator .

Figure ٤ is the variation of power output against the power stored of the laser.

Table 1: Variation of the efficiency resonator as a function of output power.

P_{out}	$\eta_{res.}$	P_{out}	$\eta_{res.}$
1	4094116.6330839800	16	8140995.4877139800
2	4363160.8667709000	17	8411403.5125626300
3	4632349.7439486100	18	8681866.3268220600
4	4901671.0285245500	19	8952381.4203046600
5	5171114.1180711600	20	9222946.4688368900
6	5440669.7538544300	21	9493559.3155148900
7	5710329.7938613800	22	9764217.9543208100
8	5980087.0328641500	23	10034920.5157464000
9	6249935.0581287300	24	10305665.2541313000
10	6519868.1325000000	25	10576450.5364722000
11	6789881.0987705900	26	10847274.8325000000
12	7059969.3007809600	27	11118136.7058526000
13	7330128.5178064100	28	11389034.8061998000
14	7600354.9095944200	29	11659967.8621976000
15	7870644.9700126400	30	11930934.6751675000

Table 2: Variation of aperture to beam radius ratio against the transitions of output mirror.

$1-e^{-2(r/w)2}$	0.95606	0.96414	0.97092	0.97902	0.98508	0.99074	0.9927	0.9950	0.9956
ρ/ω	1.25	1.29	1.33	1.39	1.45	1.53	1.57	1.63	1.65

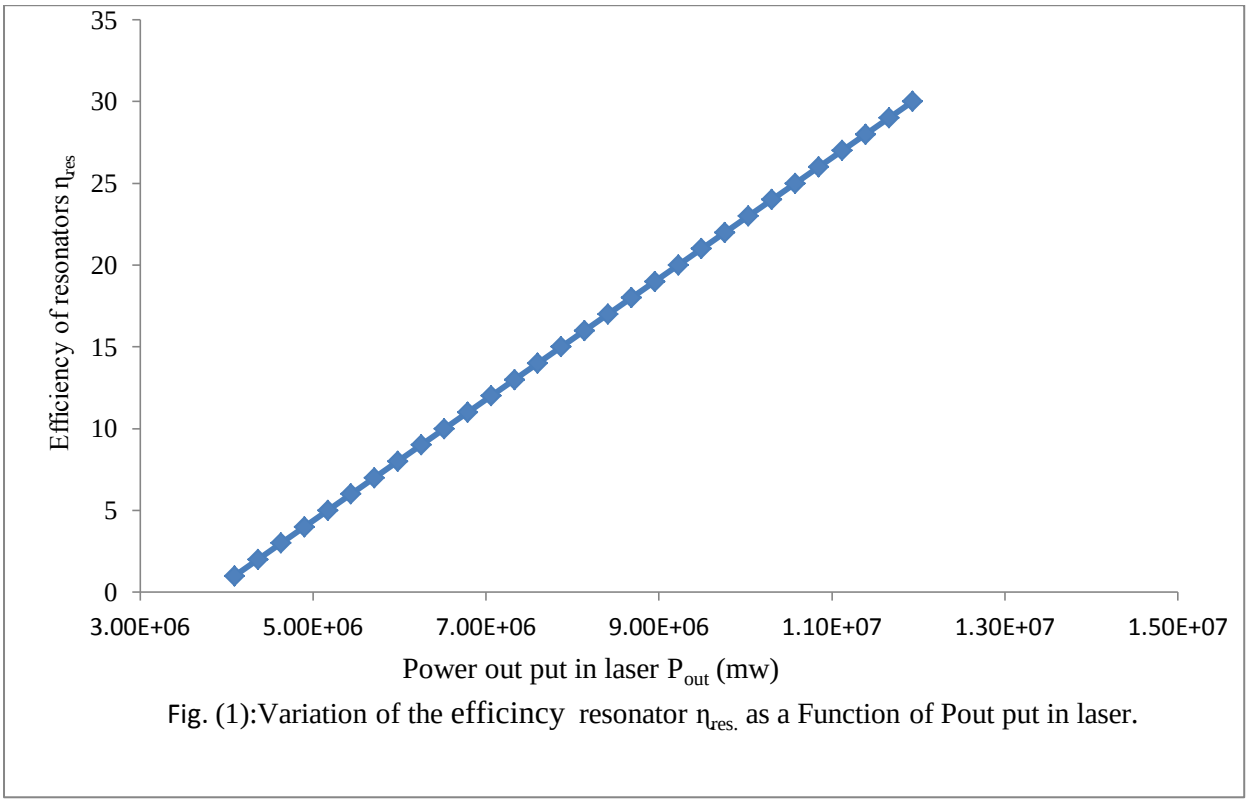

Fig. (1):Variation of the efficincy resonator $\eta_{res.}$ as a Function of Pout put in laser.

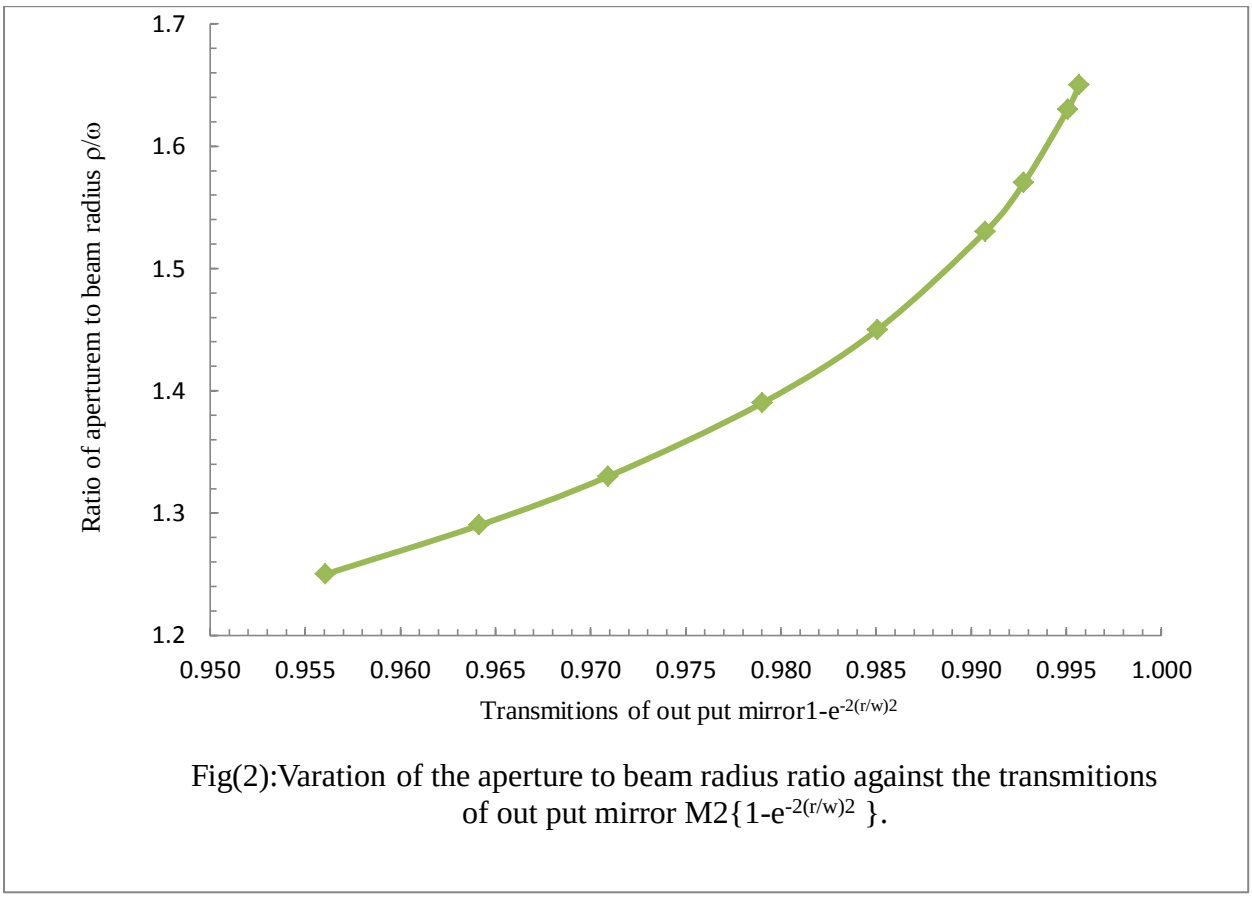

Fig(2):Varation of the aperture to beam radius ratio against the transmitions of out put mirror M2{1-$e^{-2(r/w)2}$ }.

Table 3: Variation of resonator efficiency as a function of total power stored in resonator.

P_{stored}	4.415	6.413	6.791	15.698	20.113	54.328
$\eta*10^{-2}$	0.167	0.195	0.225	0.426	0.715	1.3883

Table 4: Variation of power output against the power stored of the laser.

P_{stored}	P_{out}	P_{stored}	P_{out}
4.0941166331	1	8.1409954877	16
4.3631608668	2	8.4114035126	17
4.6323497439	3	8.6818663268	18
4.9016710285	4	8.9523814203	19
5.1711141181	5	9.2229464688	20
5.4406697539	6	9.4935593155	21
5.7103297939	7	9.7642179543	22
5.9800870329	8	10.0349205157	23
6.2499350581	9	10.3056652541	24
6.5198681325	10	10.5764505365	25
6.7898810988	11	10.8472748325	26
7.0599693008	12	11.1181367059	27
7.3301285178	13	11.3890348062	28
7.6003549096	14	11.6599678622	29
7.8706449700	15	11.9309346752	30

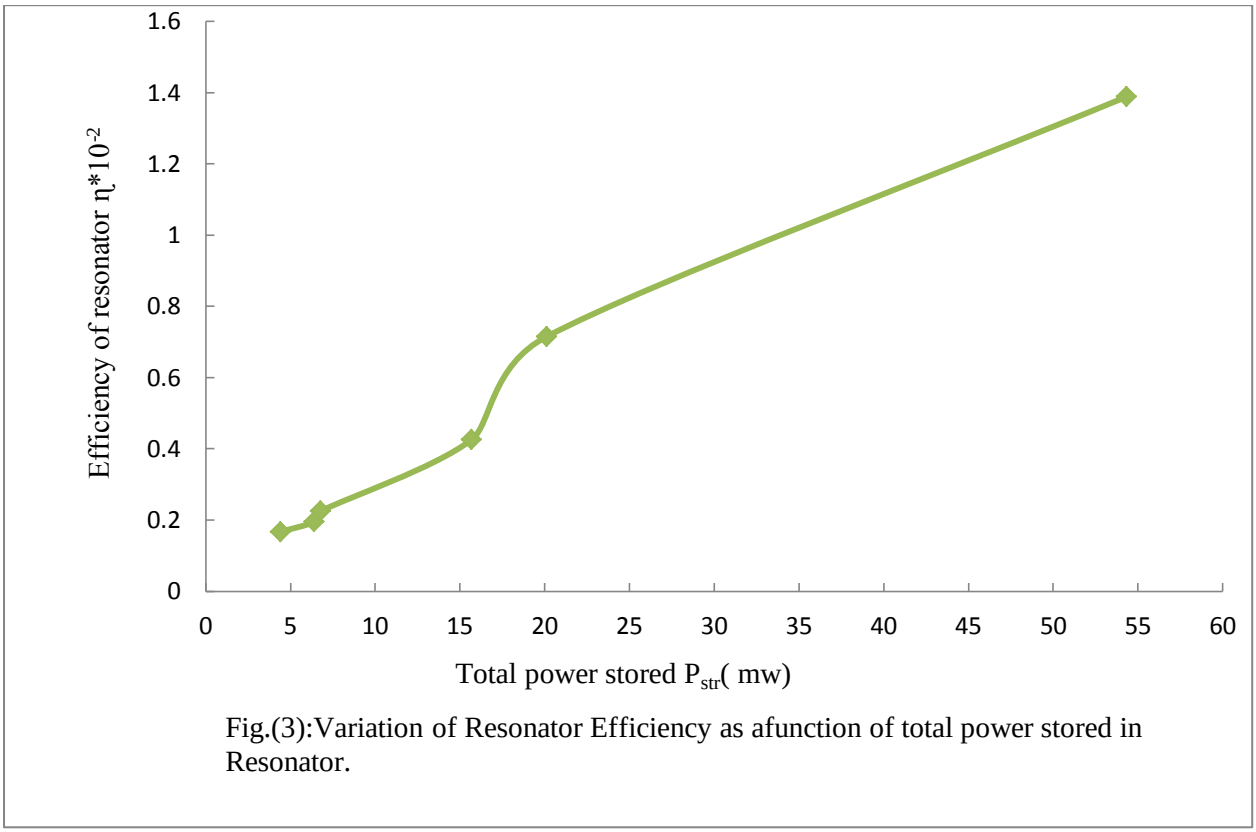

Fig.(3):Variation of Resonator Efficiency as afunction of total power stored in Resonator.

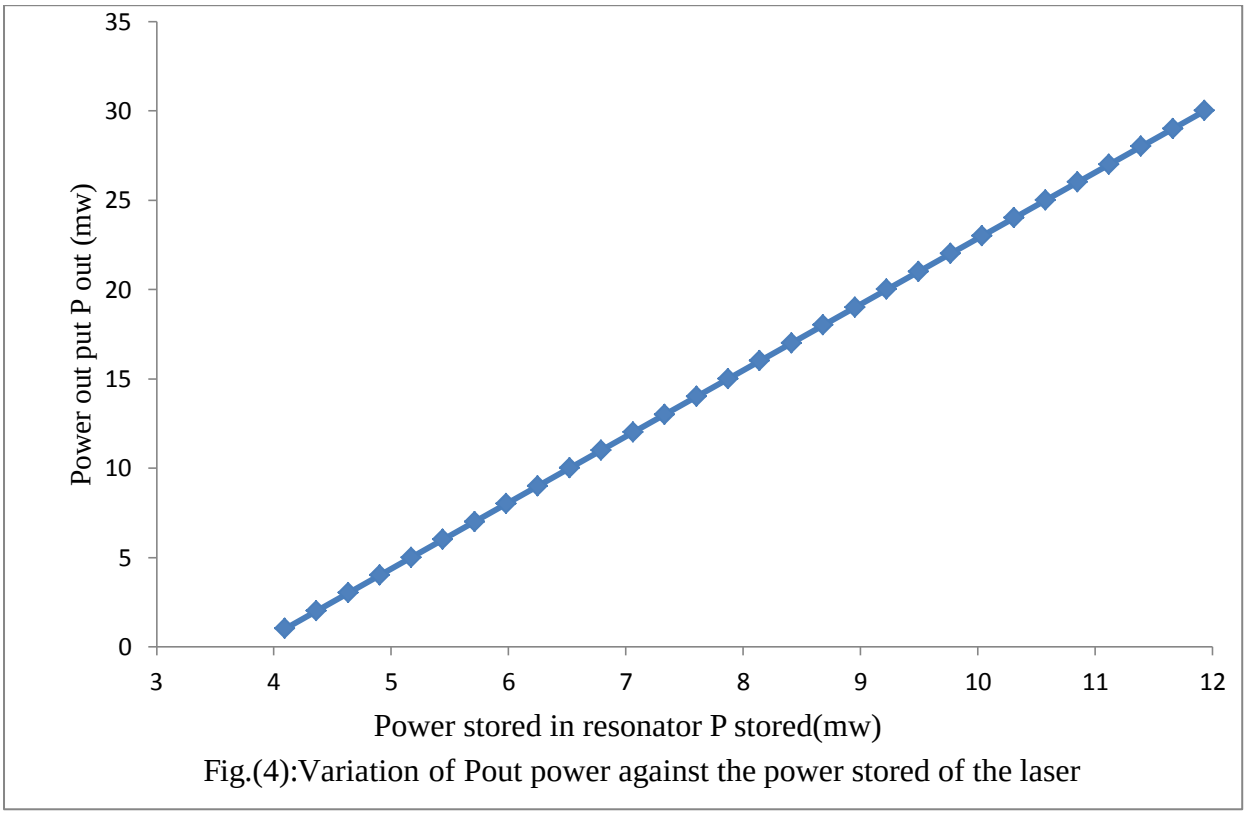

Fig.(4):Variation of Pout power against the power stored of the laser

4. Conclusion

Throughout the whole work, it was clear that estimation of the overall efficiency of any laser tube is a very complicated process, since it is a non- liner combinations of many parts. The essential parts are the laser aperture, the input power and the resonator efficiencies. From

efficiencies of these one can conclude the following:

1-Both the aperture radius and the input power changes linearly with the output power. This Means they have no saturation limit for gas lasers.

2-The only part effective on the total efficiency of the gas laser is the power stored in the resonator ,since this part depends on the geometry of the resonator and the other two parts mentioned above.

3-For low-power He-Ne gas lasers, the jump in resonator efficiency between [1-10] mw, due to the very low efficiency of the input power and aperture efficiency ,almost between [10^{-5}-10^{-4}].

4-Finally, the efficiency of high power gas lasers, such as,Co_2 lasers are much higher than low power He-Ne lasers, since He-Ne lasers have very low efficiencies, unfortunately there were no any relevant references for this.

Reffrenses

ABDUL-RAHIM, D. O. & MAWLUD, S. Q. 2013. Optimization of the Geometrical Parameters for the Output Mirror in a He-Ne Laser. *Science Journal of University of Zakho,* 1**,** 383-387.

BARTAL, T., FOORD, M. E., BELLEI, C., KEY, M. H., FLIPPO, K. A., GAILLARD, S. A., OFFERMANN, D. T., PATEL, P. K., JARROTT, L. C. & HIGGINSON, D. P. 2012. Focusing of short-pulse high-intensity laser-accelerated proton beams. *Nature Physics,* 8**,** 139-142.

BORN, M. & WOLF, E. J. N. Y. 1964. Principles of Optics MacMillan. 19592**,** 671-691.

COCKBILL, L. 2017. Operating silicon-based lasers with high quantum efficiency above room temperature. AIP Publishing LLC.

HASTED, J. 1976. Physics of Ionized Gases. *Europhysics News,* 7**,** 10-10.

HECHT, J. 2018. Low- Power Laser Applications. 425-473.

K.EVANS & SOMMERFIELD, N. 2015. Laser Quantity and efficiency in Han cement. *Journal of applied Optics,* 116.

MORACE, A., IWATA, N., SENTOKU, Y., MIMA, K., ARIKAWA, Y., YOGO, A., ANDREEV, A., TOSAKI, S., VAISSEAU, X. & ABE, Y. 2019. Enhancing laser beam performance by interfering intense laser beamlets. *Nature communications,* 10**,** 1-9.

URQUHART, P. 2020. Fibre laser resonators. *The Physics and technology of laser resonators.* CRC Press.

YARIV, A. 1967. Quantum electronics.

YARIV, A. & GORDON, J. 1963. The laser. *Proceedings of the IEEE,* 51**,** 4-29.

ZANCO Journal of Pure and Applied Sciences
The official scientific journal of Salahaddin University-Erbil
https://zancojournals.su.edu.krd/index.php/JPAS

ISSN (print):2218-0230**, ISSN (online):** 2412-3986**, DOI: http://dx.doi.org/10.21271/zjpas**

RESEARCH PAPER

Real Time Pain Detection Using Facial Action Units in Telehealth System

Dalya Abdullah Anwar
Department of Computer Science and information technology, College of Science, Salahaddin University-Erbil, KRG-Iraq.

A B S T R A C T:

During the Covid-19 pandemic, to reduce staff exposure to ill people, minimize the impact of patient surges on facilities, and preserve personal protective equipment, the recommendations are made by the World Health Organization to change the way that health care is delivered. Several telehealth systems are utilized including live audio-video interaction or real-time telephone typically with a patient using a computer, smartphone, or tablet. During these appointments, the doctors need to know the pain levels of the patient to be able to prescribe the correct medicine and diagnose the disease proficiently. In this paper, a real-time 4-pain levels recognition based on facial expression during telehealth is proposed. Generally, the pain is measured via verbal communication, normally the patient's self-report. However, if the patient has a disability and unable to communicate with others due to being impaired mentally or having breathing problems or the child self-reporting may not be a perfect way to measure the pain. The proposed system consists of two methods to detect pain from a patient's facial expressions. The AAM_Based method detects the face and facial landmarks from each video frame using Active Appearance Model AAM, these landmarks are used to compute the facial features. The AU_Based method uses Facial Action Units AU which objectively describes facial muscle activations that are considered as Region of Interest. Support Vector Machine classifier is utilized to detect the levels of pain. A labeled dataset such as Biovid is used to train test, and the AAM_based method, while and UNBC is used for the second method. The findings show that it is possible to depend on facial expression to detect pain level 1 and level 4 very accurately, while it is very tricky to detect pain level 2, and 3 because the AUs for them are similar for most of the patients.

KEY WORDS: Pain assessment, Face expression, AAM, SVM, COVID-19, Telehealth.
DOI: http://dx.doi.org/10.21271/ZJPAS.33.5.4
ZJPAS (2021) , 33(5);31-42 .

1.INTRODUCTION :

Globally, the pandemic virus called COVID-19 has infected about 1.6 million patients and killed around 100,000 patients all around the world since April 10, 2020 (Mervosh et al, 2020). The daily lives of everyone have been affected by this virus (Isaac et al, 2020). People have been to stay at home. Several businesses had to transition into telehealth or virtual by using online video conference software such as Zoom, Google meet, and WebEx (Hardy, 2020). Recently, many pain assessment applications have been developed, however, most of them are dependent on subjective self-reported pain levels and suffering low accuracy rate (Rosser and Eccleston, 2012).

Pain assessment using facial expression is an important subject and attracts the researcher's attention in the field of computer vision (Craig, 1992, Craig et al, 2011) and deep learning approaches (Werner et al, 2012, Kächele et al, 2015). The social context and personal factors are influence pain expression directly (Prkachin and Craig, 1995). The main advantage of using facial expression to detect the pain levels is to reduce the distress caused by recording the brain activities or other physiological signals such as electrocardiogram ECG and electromyogram EMG that required sensors to be contacted directly to patient's body/skin (Kunz and Lautenbacher, 2019). An international competition aimed to create a platform for the comparison of multimedia processing methods of chronic pain

* **Corresponding Author:**
Dalya Abdullah Anwar
E-mail: dalya.anwar@su.edu.krd
Article History:
Received: 18/05/2021
Accepted: 07/09/2021
Published: 20/10 /2021

assessment form human behavior and multi-model machine learning is conducted by the EmoPain 2020 challenge team (Egede et al., 2020).

Many researchers avoid the expressiveness problem while investigating an automatic pain recognition system and prefer visible pain reaction to label the video frames or images (Lucey et al, 2012, Kaltwang et al, 2012, Sikka et al, 2014, Rudovic et al, 2015). The main problem while evaluating several proposed methods is that the subjects show no facial reaction to pain (Kunz and Lautenbacher, 2014). A wrist-worm EDA device that transmits pain information and displays it into the user's smartphone via Bluetooth is proposed (Kong et al, 2020). Detecting pain levels for cancer patients via smartphone is proposed using their facial expression, the proposed method applied angular distance and SVM for the classification of the system (Hasan et al, 2016). Extensive research is detecting pain levels deploying the Facial Action Coding System (FACS) especially from human facial emotion (Ekman and Friesen, 1978). A facial emotions detection system using the Active Shape Model and SVM is utilized to identify the patient's psychological state in real-time (Anwar et al, 2016).

A stress detection of a smartphone user using an electrical dermal activity is proposed (Ayzenberg et al, 2012). A proposed method consists of three stages is proposed, the first stage is called the pre-processing stage, where the face is detected from each video frame, cropped, resized, and normalized using image processing methods. The next stage is called the feature extracting stage, in this stage, the facial features are extracted using the fine-tuned pre-trained CNN framework, then PCA is applied to reduce the extracted features dimensions. The third stage is called, the classification stage, in this stage an Enhanced Joint Hybrid classifier approach such as BilSTM is proposed to obtain the pain severity level (Ghazal Bargshady et al, 2020).

A study aims to provide a systematic review of deep learning applications only for pain detection is presented. The study aims to help the researchers in AI to know the deep ANN methods, used datasets, and tools needed to build a smart automatic pain detection system (Al-Eidan et al, 2020). Another study that focuses on analyzing the communication between measurements of pain and their prediction from a deep learning method is proposed. The authors explore several ways of using FACS Action Units AUs to combine them with their proposed extended multitask learning model (Xu & de Sa, 2020). Deep learning is utilized to train dataset and activity method to guide patient orientation, the method separated pain thresholds into 3 stages: no pain, start having pain, having pain (Pikulkaew, 2021). Deep convolution neural network DCNN is employed to detect pain, the proposed method is evaluated and tested using UNBC-McMaster shoulder pain dataset (Semwal et al, 2021).

In this paper, the contribution can be summarized in the following:

1. Building an automatic real-time pain detection system during a telehealth system.
2. Delivering the detected pain levels in a CSV format to the physicians to help them diagnose and treat the patients accordingly.
3. Utilizing two labeled datasets that content a to enhance pain detection reliability.
4. Calculating and adding three pain levels equations to the UNBC dataset, those pain levels are PA1, PA2, and PA3. Adding the three computed pain levels equations helped during the training process and improved the detection accuracy of the proposed method.
5. Comparing two methods for pain detection based on the patient's facial expression.

The work in this paper is arranged as follows: In section 2, the datasets are described. Section 3 includes the components of the developed method. Section 4 shows our findings. Section 5 includes the conclusion and future research.

2.DATASETS

A. Bovid Heat Pain Dataset

Heat with 4 intensities is used in the Biovid dataset to induce pain. Each subject in the dataset has a pain tolerance pain threshold used to adjust the temperature of the heat. In the Biovid database, there are 87 subjects and 5 pain levels, those levels are pain-baseline, L1, L2, L3, and L4. There are 20 samples for each class, each sample is 5 seconds in length, and the stimuli of the heat last for about 4s and have around 12s pause (The biovid heat pain database, 2021). In this paper, the Biovid dataset is used with AAM_based method.

B. UNBC Shoulder Pain Database

The facial expression of 25 subjects suffering from the pain of their shoulder is utilized to record 200 video series in UNBC Shoulder (upper back) Pain dataset (Prkachin et al, 2011). In total there are 48,398 frames coded using FACS (facial action coding system) (Friesen et al, 2002). For each frame in the UNBC dataset, there are pain scores depend on Prkachin and Solomon Pain Intensity (PSPI) scale. PSPI scale computed based on Facial Action Coding System FACS code that used tool for describing facial movements. The FACS code includes 9 different Action Units AUs in upper part of the face, 18 AUs in lower part of the face, and 5 AUs in neither lower nor upper part of face. Moreover, the FACS defines 11 AUs for head position, 9 for describing states of eyes, and 14 for other actions. Prkachin and Solomon are calculated pain level 4 using the FACS code. Below is the equation to calculate PSPI with the help of FACS for pain level 4. Other pain levels are calculated using PSPI with/out AU43, AU9, or AU6 (Prkachin and Solomon, 2008).

$$PSPI = AU34+(AU7 \text{ or } AU6) + (AU10 \text{ or } AU9) +AU4 \quad (1)$$

As shown in the above equation, the PSPI final score is the result of adding Action Unit AU7, AU6, or Au4 (the higher intensity AU will be added), Au9, or Au10 (the higher intensity AU will be added), and AU43. Figure 1 shows the AUs used in equation 1. Each AU is coded in six intensity levels, those levels are in the range 0 = absent, 5 = maximum. The AU43 is coded as 0 for close eyes and 1 for open eyes. The dataset provides 66 landmarks, they are used to compute the similarity normalized shape features (SPTS), and to reduce the landmarks' dimensionality, Principal Component Analysis is applied. 99% of the variance is kept this reduced the frame-level features from 132 to 29 dimensions. An example of different PSPI scores for the same subject is shown in figure 2 (Saha et al, 2016). In this paper, the UNBC dataset is used with AU_based method.

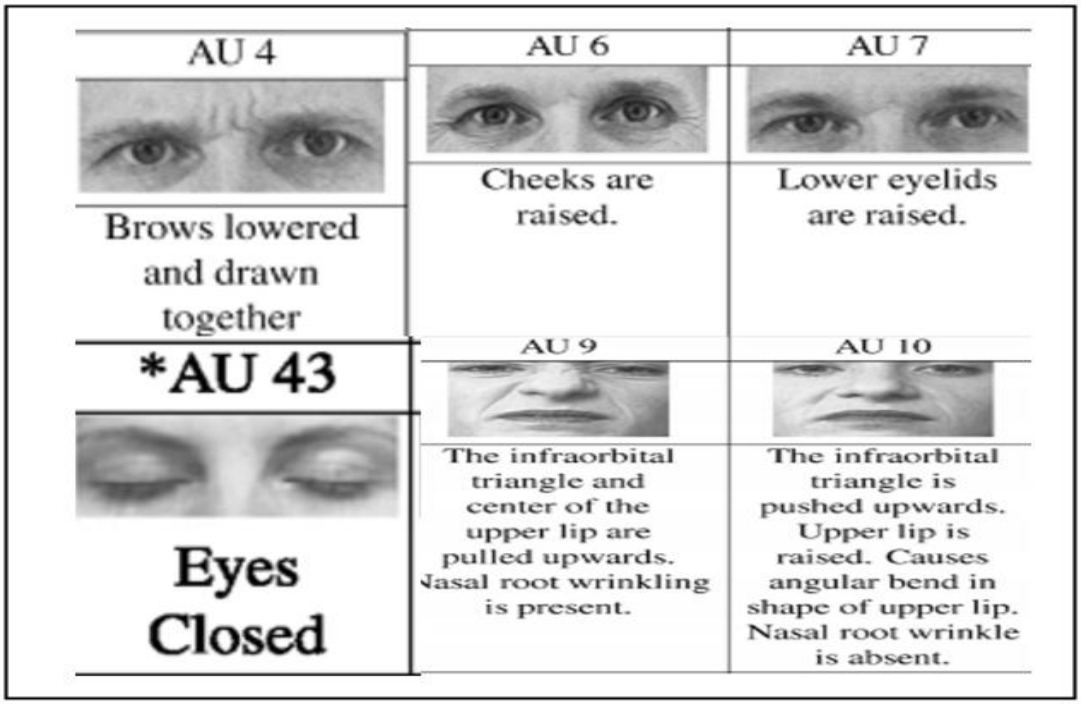

Figure 1: Action Units AUs that are used in PSPI scores appeared in equation 1

Figure 2: Sample of the same participant with different PSPI scores from UNBC_Mc Master dataset (Friesen et al, 2002)

3.PAIN DETECTION PIPELINE

In this section, the core technology utilized by the proposed system pipeline to detect pain is represented. First, an explanation of how the facial landmarks (features) are detected and tracked is provided. Second, a description of how these features is utilized to compute the Action Units AUs intensity. Finally, the Support Vector Machine classifier role is explained to classify the pain level of the patient in real-time.

In this paper, two methods are proposed to patient's detect pain level during the telehealth appointment. The first method named Active Appearance based methods AAM_based method, in this method, the facial features are extracted for modeling purpose for pain detection. The second method named AU_based method, in this method, the facial expression coding FACS is generally utilized for pain assessment.

The pain detection process starts by detecting the patient's face, crop it, and extracting the landmarks. The extracted features are used to find the region of interest ROI using the two proposed methods separately. For classification the Support Vector Machine classifier is used to detect the pain level for each method, and the results for each frame will be saved in a CSV file to and deliver to the physician for better treatment. Figure 3 shows the pipeline of the work proposed in this paper. Following is the mathematical model for the proposed method:

S= {∑, F, □, C}

S = Pain Detection

∑ = Set of input symbols = {datasets video, images, pain classes}

□ = 1 Start

2. Read dataset N*N

3. Resize image dimension N^2 *1

4. Select training set N^2 * M, M: Number of samples in the dataset

5. Extract 166 landmark using Active Appearance Model AAM
6. Apply Principal Component Analysis PCA
7. Apply Support Vector Machine SVM for classification
8. End

F = Set of output symbols = {pain levels PA0 (no pain), PA1, PA2, PA3, PA4 (highest pain), csv file}

A. Face Detection

In this stage, the person's face in each video frame is searched, cropped, and detected. By using Intel open-source framework known as OpenCV (Shervin Emami, 2010)), face detection is performed easily and reliably. The advantage of OpenCV is being a multi-platform framework; it is compatible with Linux, Windows, and Mac OS X. OpenCV provides many basic computer vision algorithms to use as a key for achieving a good facial detecting and tracking result. In this paper, several OpenCV modules are used such as CXCORE, CV, CVAUX, and CVCAM key namespaces.

$$S = S_0 + \sum_{i=0}^{n} P_i S_i$$

In this section, the generation of the appearance model for the faces is explained. In each video frame, both models of the shape and appearance variation are combined in a normalized shape frame. To indicate the essential features, a training set of facial images with landmark points at interesting positions is required to create a statistical pattern of shape variation.

$$x = \underline{x} + P_g b_g$$

Where $\underline{x}$ the computed mean of shape model, P_g is the orthogonal variation modes, and b_g is a list of shape variables. The triangulation algorithm is used to generate the statistical model for appearance's grey level for

$$g = \underline{g} + P_g b_g$$

Where $\underline{g}$ is the ger-level normalized mean vector, P_g is a list of grey-level variation's orthogonal modes and b_g is a set of parameters for the grey-level model. P_g and b_g vectors are

$$b = Qc$$

Where c is a set of parameters for the appearance model that control the shaper and the model's grey level and Q are b's eigenvectors.

B. AAM_Based Method

Upon detecting faces using an OpenCV algorithm such as Haar cascade, AAM_based method an Active Appearance Model (Cootes and Taylor, 1994) was used as a statistical technique to match image templates. For the aim of finding parameters that reduce the discrepancy between the synthesized image and observed image, the AAM is used in this paper. AAM is a parametric model of both texture and shape, considered as the basis of efficient method to align an image's predefined template with the features of the face. The shape model is extended by n eigen shapes S_i added to the average shape S_0.

(2)

The facial landmarks 2D-points represent the shape of the face, these set of 2D-points is aligned into a spread co-coordinate frame and introduces as a vector, v by employing Procrustes alignment. After generating the features vector, a Principal Component Analysis PCA is utilized it using the following equation:

(3)

every video frame by matching the mean shape with landmark points. After normalizing the vector g to reduce the effect of maximum lighting variation. Then PCA is applied to obtain the linear equation:

(4)

symbolizing the appearance and any video frame generated using AAM. A further PCA is applied to the data to generate the concatenated vector and give a further model.

(5)

The selected list of eigenvectors Q are multiplied by the matrix c to create a reduced eigenface.

In this paper, a training sets Biovid and UNBC are utilized to build the facial appearance

model. Each frame had 122 landmark points surrounding the main features. The shape model includes 23 parameters is generated. The shape model required 10,000-pixel points to create the facial patch.

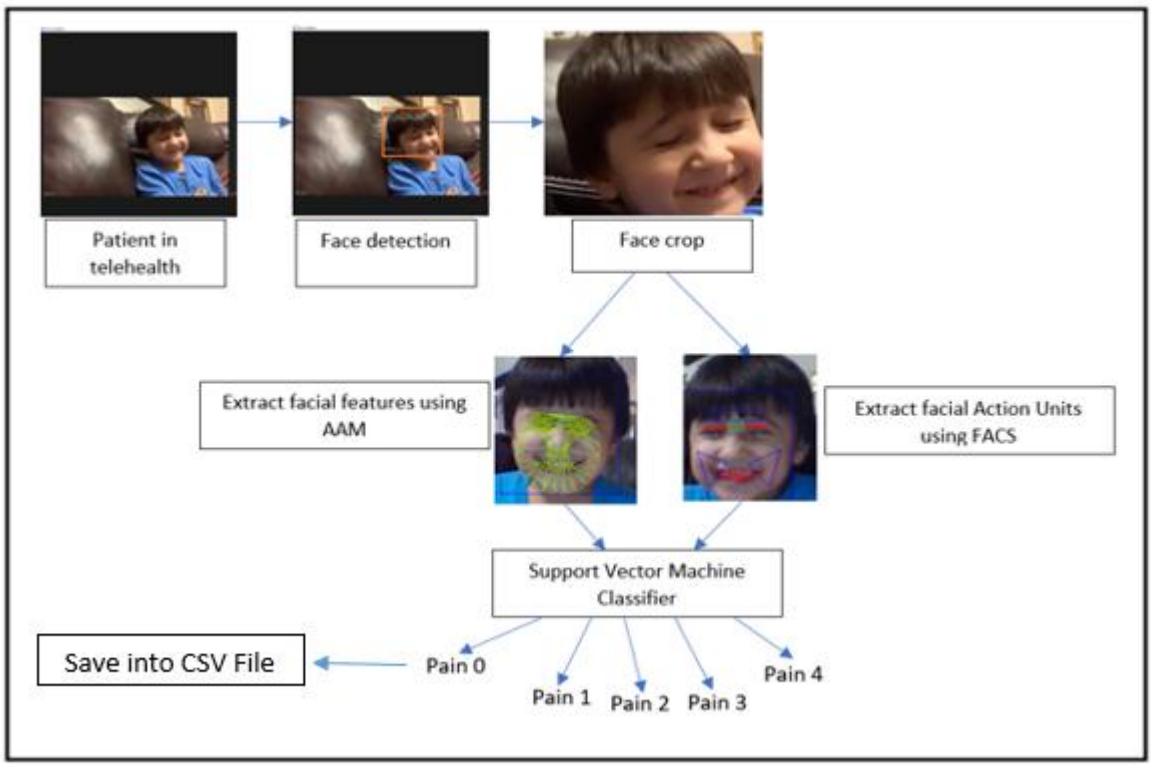

Figure 3: Pain detection system pipeline

C. AU_Based method

Many behavioral science studies show that human facial expression has a strong relationship with pain detection. The pain is encoded from the facial muscles' movement into a set of Action Units, depend on the coding system called FACS. Figure 4 shows a sample of some facial action units AUs 4, 6, 7, 9, 10, and 43 associated when the patient is in pain.

The four AUs in figure 4 were founded by Prkachain (Prkachin and Craig, 1995) considered as the four core actions linked to pain and they contained most of the pain input data. These actions defined the patient's pain by adding the intensities of lowering the eyebrow (AU4), tightening the orbital (AU7 and AU6), elevator contraction (AU10, AU9), and closing the eyes (AU43) as shown in equation 1 that calculates PSPI.

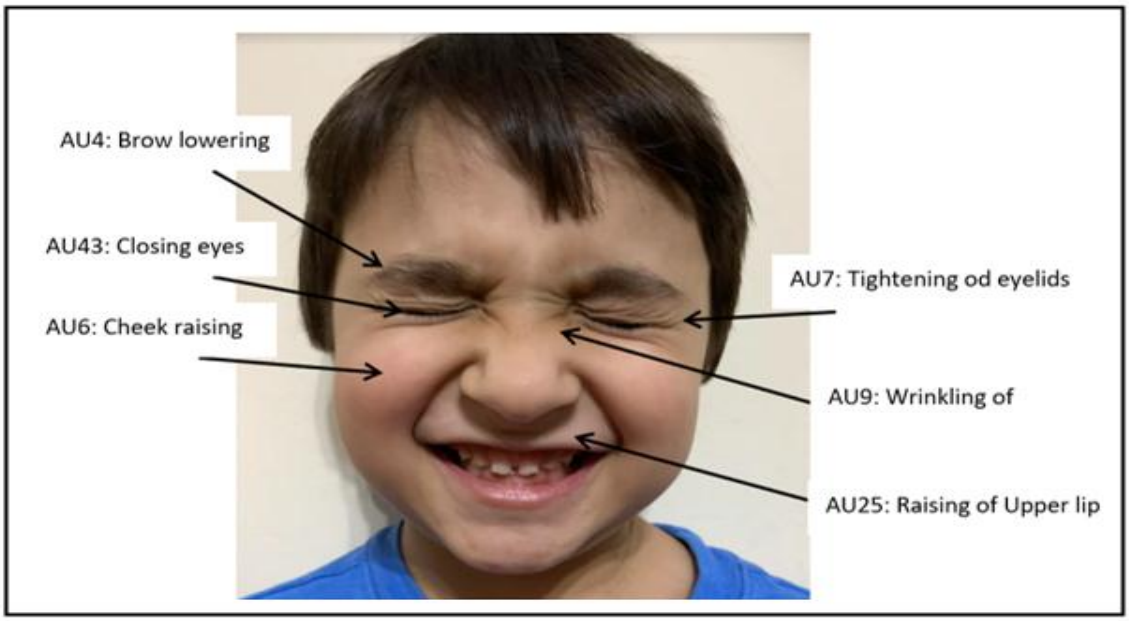

Figure 4: An example of facial action units AUs for a patient in pain level 4

Equation 1 uses to detect PA4, in this paper combination of action units AUs are used to compute the other pain levels (PA1, PA2, and PA3) as shown in table 1. AU1 represents a contribution to emotions such as surprise, sadness, and fear with a frontalis muscular basis. AU15 represents a contribution to sadness and disgust emotions with underlying facial muscle. AU23 represents a contribution to anger with an orbicular orris muscular basis. AU24 represents a contribution to affective anger emotion with an underlying facial muscle. The three computed pain levels are added to the dataset and a classifier are trained and tested to predict the patient's pain level during the telehealth appointment.

Table 1: The pain equations for each level

PA	AUs	Emotions
PA1	AU1+AU15	Surprise + Sadness + Fear + Disgust
PA2	AU1+AU6+AU23	Surprise + Sadness + Fear + Anger + Happiness
PA3	AU4+AU6+AU24	Anger + Happiness

D. Support Vector Machine

SVMs have been used as a classifier for many patterns recognition tasks such as facial action recognition. In this paper, the SVM classifier is used for detecting pain from a patient's facial actions because it is the best suited binary classifier for this task. The main season to select SVM as a classifier in this paper is to generate a sizeable volume of training samples and construct the compact discriminative model automatically. For a specific class, SVM found the hyperplane that increases the negative and positive observations margin. The decision of the linear SVM classifier is obtained for an observation X^* by the following equation:

$$W^T X^* > \text{b } True \quad (6)$$
$$< \text{b } False$$

Where w is the vector that separates the basis b and the hyperplane.

4.FINDINGS

To evaluate the proposed system two sets of experiments are devised. The first experiment was conducted on method 1 that detects the patient's pain in each video frame using pain intensity. The second experiment was conducted on AU_based method that detects pain using a patient's facial actions.

A. Environment

A laptop with the following configuration is used to conduct all experiments in this paper: 2.3 GHz Intel Core i7, 0.92 megapixels for still image, and 1280x720 (HD) for video at 30 fps and 16 GB RAM.

B. AAM_Based Method Results

The Biovid database is used to test the performance of AAM_based method. The facial features from each frame utilized as inputs to the SVM classifier. The output scores produced by SVM determine the pain level in each video frame. The results of applying AAM_based method on ten samples of the Biovid dataset are shown in figure 5. The data results contain a pain level from each frame is saved in a csv file for further research usage. As shown in figure 5, pain L0 and pain L4 have the highest accuracy rate. The precision for pain is 78% for AAM_based method.

C. AU_Based Method Results

To test the performance of AU_based method, the UNBC dataset is used. The AUs are utilized as baseline input features to the SVM classifier, The SVM used a grid search to find the best parameters for pain detection. The results show that the precision for pain is 89.3%. In figure 6, the results of detecting pain for ten UNBC video samples show that pain level-0 and level-4 have the highest accuracy rate. Figure 7 shows the result of implementing the proposed system on sample 1 of the Biovid dataset. In the figure the pain levels are represented in the source code as PainLV0, PainLV1, PainLV2, PainLV3, and PainLV4 and they are equivalent to PA1, PA2, PA3, and PA4 in this paper respectively. Where PainLV0 is the baseline level indicates no pain and PainLV4 indicates highest pain level. As mentioned before in section 3, the UNBC dataset includes only two pain levels; PA0 (no pain) and PA4 (pain as bad as could be) and in this paper the other three pain levels PA1, PA2, and PA3 are computed, added to the dataset to help in training procedure and improve the outcome during the testing stage.

D. Results Comparison

In table 2, these results of AU_based method are compared with Lucey et al, and Sikka et al, both methods used UNBC pain dataset to evaluate their proposed methods. Lucy et al. used three pain classes (PA1-0, PA2-3, PA4-5) to group all samples in the UNBC dataset and extracted the canonical normalized appearance features (CAPP), while Sikka et al. used two classes (PA 0 and PA 3-5). The experiment was conducted with both variants and different frame-level features. The accuracy which indicates the number of samples that correctly classified divided by the total number of samples. The AU_based method outperformed the other methods by using simple linear SVM, which proved the superiority of the AU_based method's temporal integration. Comparing the three methods regarding the different frame - level features observed that the AUs-based method's shape performed better with the appearance features than the Lucey et al. and Sikka et al.

Table 2: Comparing AUs_based method with other similar methods

Method	Frame-level features	Classifier	Accuracy
Lucey et al.	SPTS + CAPP	SVM	0.610
Sikka et al.	Dense Sift BoW	MS-MIL	0.837
AU_based proposed method	SPTS (PCA + 29 dim)	SVM	0.893

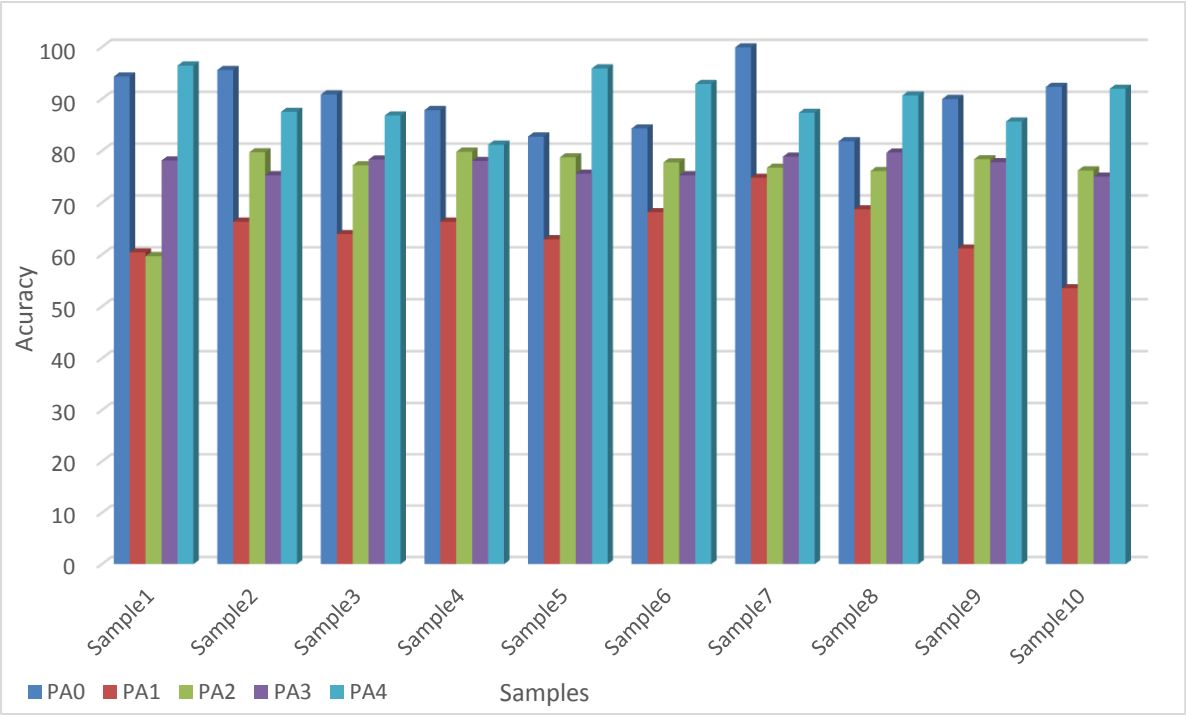

Figure 5: The result of performing the AAM_based method on 10 Biovid dataset video samples

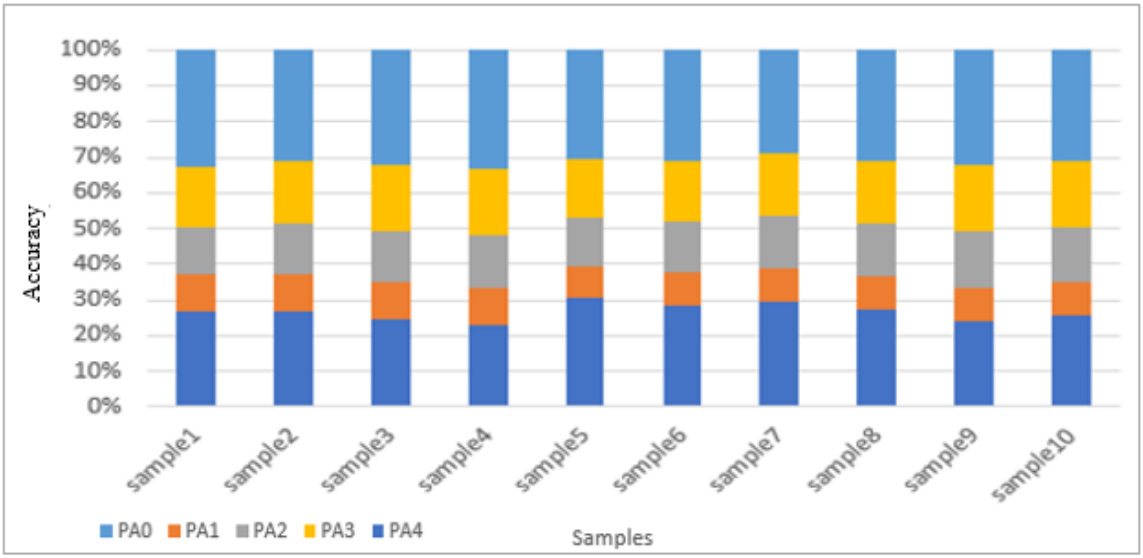

Figure 6: The result of performing AU_based method on 10 UNBC dataset video samples

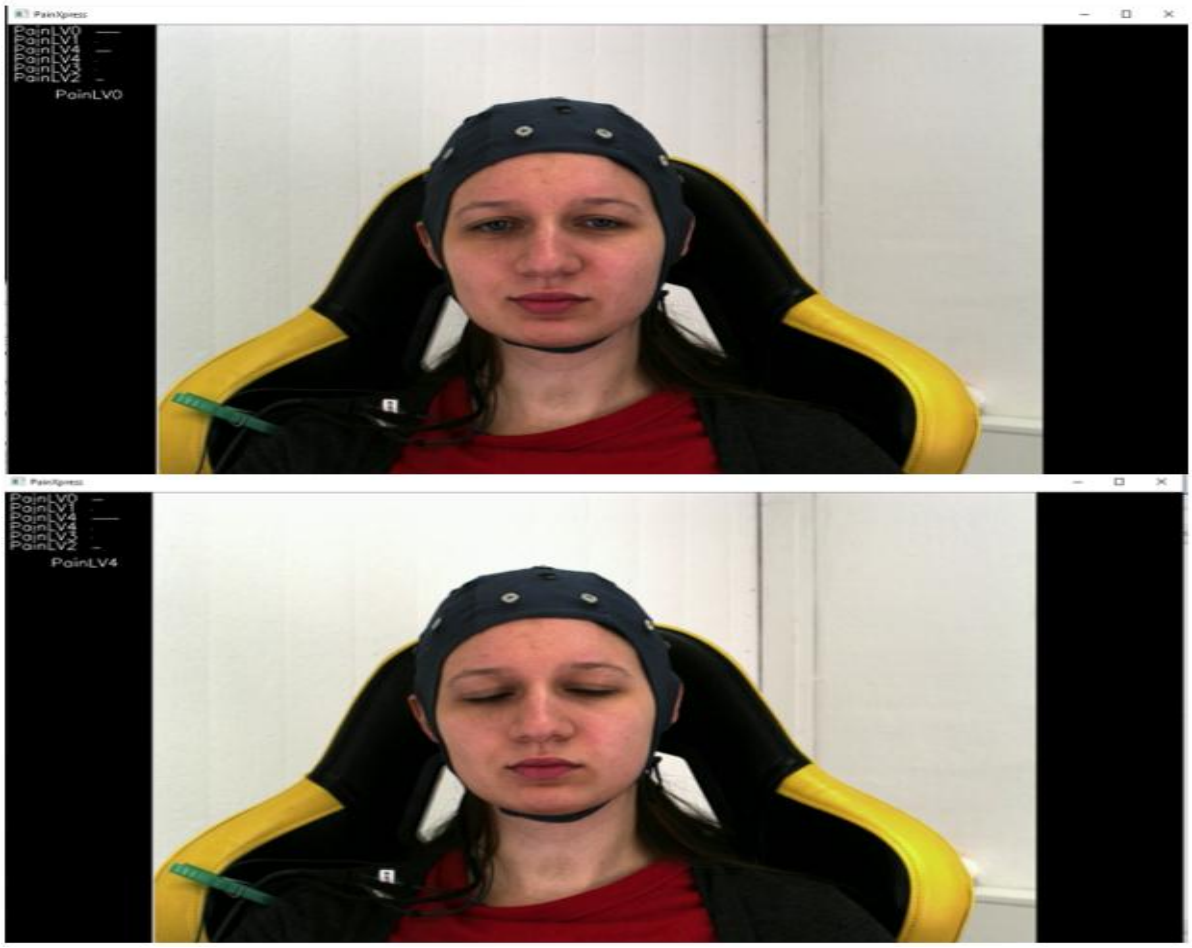

Figure 7: The result of implementing the proposed system on the Biovid video dataset

5.CONCLUSION

In this paper, a real-time pain recognition system based on the patient's facial expression during telehealth is proposed. The proposed automated system detects the patient's pain during telehealth using two approaches based on the patient's facial expressions. AAM_based method uses the extracted facial features directly to detect the level of the pain, while AU_based method uses a set of AUs to detect the pain levels. Two databases are used to test the performance of the developed system. These two datasets are UNBC which includes patients with shoulder pain and Biovid which uses heat to induce subjects with four pain intensities. These datasets missing several facial expressions that lead to minimizing the accuracy of the proposed method. Extract facial expressions from the video sequences such as anger, surprise, and sadness are added to the training datasets. The added emotions lead to add more AUs to AU_based method such as AU12, AU25, and AU20 to compute the different pain equations. Adding extra facial emotion increased the accuracy for the proposed system from 66% to 78% in AAM_based method and from 70% to 89.7% in AU_based method. The results of evaluating the system's performance indicated that in both methods the proposed system able to detect PA0 (no pain) and PA4 (high pain) more accurately compared with other pain levels.

In future research, a plan to include head movement, eye gaze, body movement, and audio will be examined to improve the performance of the proposed automated pain detection system which will be also a useful framework to detect depression emotions.

6.REFERENCES

Face Detection and Recognition using OpenCV, (2010) Article, http://shervinemami.info/faceRecognition.html, Published by Shervin Emami.

Al-Eidan, M. R.; Al-Khalifa, H.; Al-Salman, (2020) A. Deep-Learning-Based Models for Pain Recognition: A Systematic Review. Appl. Sci., 10, 5984.

Anwar, S., Milanova, M., Bigazzi, A., Bocchi, L. and Guazzini, A. (2016) Real time intention recognition," IECON 2016 - 42nd Annual Conference of the IEEE Industrial Electronics Society, Florence, pp. 1021-1024, DOI: 10.1109/IECON.2016.7794016.

Ayzenberg, Y., Hemandez J. and, Picard R., (2012) FEEL:Frequent EDA and Event Logging- A Mobile Social Interaction Stress Mointoring System, CHI.

Cootes, T. and Taylor, C. (1994) Modeling object appearance using the grey-level surface. In E. Hancock, editor, 5th British Machine Vision Conference, pages 479–488, York, England. BMVA Press.

Craig, K. D. (1992) "The facial expression of pain Better than a thousand words?" APS Journal, vol. 1, no. 3, pp. 153–162. 1, 4.

Craig, K. D., Prkachin, K. M. and Grunau, R. E. (2011) The facial expression of pain, in Handbook of Pain Assessment, D. C. Turk and R. Melzack, Eds. Guilford Press, 2011. 1, 4.

Egede J. O. et al., "EMOPAIN Challenge 2020: Multimodal Pain Evaluation from Facial and Bodily Expressions," 2020 15th IEEE International Conference on Automatic Face and Gesture Recognition (FG 2020), 2020, pp. 849-856, doi: 10.1109/FG47880.2020.00078.

Ekman, P. and Friesen, W. (1978) Manual for Facial Action Coding System, Palo Alto: Consulting Psychologists Press.

Friesen, W., Ekman, P., and, Hager, J. (2002) Facial action coding system: Research nexus in Salt Lake City UT USA: Network Research Information.

Ghazal Bargshady, Xujuan Zhou, Ravinesh C. Deo, Jeffrey Soar, Frank Whittaker, Hua Wang, (2020) Enhanced deep learning algorithm development to detect pain intensity from facial expression images", Expert Systems with Applications, Volume 149, 2020, 113305, ISSN 0957-4174, https://doi.org/10.1016/j.eswa.2020.113305. (http://www.sciencedirect.com/science/article/pii/S0957417420301305)

Hardy, Q. (2020) COVID-19 And Our Surprising Digital Transformation.

Hasan, M. K. G. M. T. Ahsan, Ahamed, S. I., Love, R. and Salim, R. (2016) Pain Level Detection from Facial Image Captured by Smartphone, J. Inf. Process, vol. 24, no. 4, pp. 598-608.

Isaac, M., Yaffe-Bellany, D. and Weise, K. (2020) Workplace vs. Coronavirus: 'No One Has a Playbook for This.

Kächele, M., Thiam, P., Amirian, M. Werner, P. Walter, S., Schwenker, F. and Palm, G. (2015) Multimodal Data Fusion for Person-Independent, Continuous Estimation of Pain Intensity, in Engineering Applications of Neural Networks, Springer, pp. 275–285, DOI: 10.1007/978-3-319-23983-5_26. 1.

Kaltwang, S., Rudovic, O. and Pantic, M. (2012) Continuous Pain Intensity Estimation from Facial Expressions, in Advances in Visual Computing, Springer, pp. 368–377.

Kong, Y., Posada-Quintero, H. F. and Chon, K. H. (2020) Pain Detection using a Smartphone in Real Time*, 2020 42nd Annual International Conference of the IEEE Engineering in Medicine & Biology Society (EMBC), Montreal, QC, Canada, pp. 4526-4529, DOI: 10.1109/EMBC44109.2020.9176077.

Kunz, M. and Lautenbacher, S. (2014) The faces of pain: a cluster analysis of individual differences in facial activity patterns of pain, European Journal of Pain, vol. 18, no. 6, pp. 813–823.

Kunz, M., D. Meixner, and Lautenbacher, S. (2019) "Facial muscle movements encoding pain–A systematic review," Pain, vol. 160, no. 3, pp. 535–549, Mar. 2019.

Lucey, P., Cohn, J. F., Prkachin, K. M., Solomon, P. E., Chew, S. and Matthews, I. (2012) Painful monitoring: Automatic pain monitoring using the UNBC-McMaster shoulder pain expression archive database, Image and Vision Computing, vol. 30, no. 3, pp. 197–205.

Mervosh, S. Lu, D. and Swales, V. (2020) See Which States and Cities Have Told Residents to Stay at Home.

Pikulkaew K. and V. Chouvatut, "Enhanced Pain Detection and Movement of Motion with Data Augmentation based on Deep Learning," 2021 13th International Conference on Knowledge and Smart Technology (KST), 2021, pp. 197-201, doi: 10.1109/KST51265.2021.9415827.

Prkachin, K. and Solomon, P. (2008) The structure reliability and validity of pain expression: Evidence from patients with shoulder pain, Pain, vol. 139, pp. 267-274.

Prkachin, K. M. and Craig, K. D. (1995) Expressing pain: The communication and interpretation of facial pain signals, Journal of Nonverbal Behavior, vol. 19, no. 4, pp. 191–205, Dec. 1995. 1, 4.

Prkachin, K.M., Solomon, P., Lucy, P., Cohn, J. F. and Matthrews, I. (2011) Painful data: The UNBC-McMaster shoulder pain expression archive database, Proc. IEEE Int'l Conf. Automatic Face and Gesture Recognition.

Rosser, B. A. and Eccleston, C. (2012) Smartphone applications for pain management, J. Telemed. Telecare, vol. 17, no. 6, pp. 308-312.

Rudovic, O., Pavlovic, V. and Pantic, M. (2015) Context-Sensitive Dynamic Ordinal Regression for Intensity Estimation of Facial Action Units, IEEE Transactions on Pattern Analysis and Machine Intelligence, vol. 37, no. 5, pp. 944–958.

Saha, P., Roy, S. D., Bhowmik, M. K. and Ghosh, A. K. (2016) An approach for automatic pain detection through facial expression", Procedia Comput. Sci., vol. 84, pp. 99-106.

Semwal A. and N. D. Londhe, "Automated Facial Expression based Pain Assessment Using Deep Convolutional Neural Network," 2020 3rd International Conference on Intelligent Sustainable

Systems (ICISS), 2020, pp. 366-370, doi: 10.1109/ICISS49785.2020.9316099.

Sikka, K., Dhall, A. and Bartlett, M. S. (2014) Classification and weakly supervised pain localization using multiple segment representation, Image and Vision Computing, vol. 32, no. 10, pp. 659–670.

The biovid heat pain database, [online] Available: http://www.iikt.ovgu.de/BioVid.html [Accessed 8 Feb. 2021].

Werner, P. Al-Hamadi, A. and Niese, R. (2012) Pain Recognition and Intensity Rating based on Comparative Learning," in IEEE International Conference on Image Processing (ICIP), pp. 2313–2316. 1.

Xu, X., & de Sa, V. R. (2020). Exploring Multidimensional Measurements for Pain Evaluation using Facial Action Units.

ZANCO Journal of Pure and Applied Sciences
The official scientific journal of Salahaddin University-Erbil
https://zancojournals.su.edu.krd/index.php/JPAS

ISSN (print):2218-0230**, ISSN (online):** 2412-3986**, DOI: http://dx.doi.org/10.21271/zjpas**

RESEARCH PAPER

Prediction of solar direct irradiance in Iraq by using artificial neural network

Zana Saleem Mohammed[1], Gzing Adil Mohammed[2].

[1] Lafargeholcim, Kurdistan region of Iraq, Sulaymaniyah.

[2] Department of Oil, Gas and Energy administration, Public Administration and Natural Resources, Charmo University.

A B S T R A C T:

Global solar irradiance is one of the main significant factors for designing and considering the volume of any solar station beside of it is usage in agricultural and building issue. Due of lack a precise information about the irradiance in Iraq metrological organization and seismology, this study is aimed to adopt the historical global data, build numerical analysis via using artificial neural network and predicting hourly irradiance. The test is applied over three locations Erbil, Bagdad, and Basra for being references to their closest locations. A foreword neural network (FNN) is the learning algorithm that is used in this study with relying on seven input variables consisting of Temperature, Precipitation, Humidity, Wind speed, Wind direction Sunshine duration and Date. After normalizing and standardizing data, an iteration method is used for determining the optimum number of neuron(s) in a hidden layer. It yields a least Root Mean square error (RMSE) between 2.5 to 3. The computed correlation coefficients are between 0.94 -0.96 for the mentioned locations.

KEY WORDS: Renewable energy, Solar system, Artificial neural network, Prediction.
DOI: http://dx.doi.org/10.21271/ZJPAS.33.5.5
ZJPAS (2021) , 33(5);43-50 .

1.INTRODUCTION :

Sun light is one of the most evolution resource among the renewable energy projects over the recent period. Irradiance measurements get a wide focus of data collection due of having an own merit in many fields such as crop growing, electricity resource, structure and building design (David, Gerrit, & R.W., 1994). Demanding of electricity is raised up in Iraq and it is depending dominantly on Fossil fuel for generating electricity (S. & M., 2009). Solar photovoltaic investment starts to be convinced after the reflection of shortage of generating national electricity source beside of increasing service cost for the commercial power that produce by local generators.

Variant geographical aspects need to be considered to design the solar system applications. Distribution of solar irradiance is the one of the significant factors that need to be paid attention through being involved in variety projects, thus resulting least project cost impact.

Investing solar energy in Iraq need to be focused which will boost the national electricity production. In high electric demand season, supplying electrical power to many industries are limited due to shortage of electrical production. Accordingly these businesses are continuously looking for alternative resources to cover the gap.

Many climate variables have influential factor of photovoltaic (PV) module and their performance. Generally, the average daily sunshine in Iraq is around 7-8 hours in winter, while it is around 10-11 hours in summer. Getting an accurate predicted data for weather, irradiance

* **Corresponding Author:**
Zana Saleem Mohammed
E-mail: zana.saleem82@gmail.com
Article History:
Received: 10/04/2020
Accepted: 07/08/2020
Published: 20/10 /2021

and solar power are continuously demanded in many cities in Iraq. Build a prediction model is helping in designing the relevant application such as solar power generation system. Other factors have impact on the PV system such as temperature, precipitation, and wind.

A common algorithm used for modeling irradiance prediction is Artificial neural network (Adel & Soteris, Artificial intelligence techniques for photovoltaic applications: A review, 2008), this tool is learned from experience and historical data. The model will be precise as much as the data is available (Negnevitsky, 2002).

2.Review of literature

Many aspects in solar irradiance prediction have been developed over the last ten years, **(Alzahrani, Kimball, & Dagli, 2014)**. The model was formulated by considering the inputs as time, day of the year, sky cover, pressure and wind speed and used by many researchers. Increase the accuracy of irradiance prediction by using nonlinear autoregressive neural network resulting a better performance than liner regression method. In Zimbabwe **(Chiteka & Enweremadu, 2016)** try to predict the irradiance with rely on neural network by selecting altitude, latitude, longitude, humidity, pressure, clearness index and average temperature as input. The absolute percentage error was 2.56%.

Monthly average solar radiation has been predicted in four locations in Uganda by (Mubiru & Banda, 2007). The used method was depending on artificial neural network with 8 neurons and one layer. Sunshine duration, temperature, cloud cover and location have been used as an input. The mean square error was 0.38 $MJ.m^2$. Multi-layer neural network was used by (Adel & Alessandro, A 24-h forecast of solar irradiance using artificial neural network: Application for performance prediction of a grid-connected PV plant at Trieste, 2010) to develop correlation coefficient for sunny and cloudy day. Try and error was used for finding the best activation function.

Solar irradiance corelates with various weather and geographical data, which considered as non-linear relation, artificial neural network is common method which used for such application (Adel M. , 2008).

In this article, the focus is on selecting a sufficient transfer function, getting the best number of neurons and improving the status of training ratio versus validation ratio via using forward neural network (FNN). This tool producing a high effective result to deploy prediction module.

3.Material and methods

3.1 Locations and data preparation

Three main locations are selected at Erbil, Baghdad, and Basra. The aim study is to test prediction algorithm and to get a reliable mathematical model and programming statements to build a rapid and accurate prediction architecture. Lacks of solar database in Iraq metrological organization and seismology in targeted sites in Iraq were the main struggle in this study. In addition, requiring a specific tool for measuring irradiance in different part of Iraq are costly and hard to be applied. The data are collected from MeteoBlue website as global weather database for one month period Feb, 2021, (meteoblue, 2006).

The collected wide range of dataset is on hourly bases. Each sites latitude and longitude are addressed in Table 1. The results can be reflecting into surrounded and closed area (Kais, Munya, & Zahraa, 2012).

Set of historical weather variables have been assigned as inputs. The model is mainly based on geographic, temperature, wind, and precipitation parameters. Table 2, represents the details of each input factor with hourly based data during one complete month.

Table 1 Geographic coordinate system for three cities.

Location	Latitude	Longitude
Erbil	36.199	44.0737
Baghdad	33.3793	44.4501
Basra	30.494	47.8398

Table 2 Corresponding input climate data.

Variable	Unit
Temperature	°C
Precipitation Total	Mm
Relative Humidity	%
Wind Speed	km/h
Wind Direction	°
Sunshine Duration	Min
Direct Shortwave Radiation	W/m²

3.2Standardizing and Normalizing data

This study is based on automated recognition method with combining and correlating wide range input values. This variety of input ranges will suppress the acceleration of such automated tools such as machine learning, this impact on the performance of the formulating model (Adel & Alessandro, A 24-h forecast of solar irradiance using artificial neural network: Application for performance prediction of a grid-connected PV plant at Trieste, 2010). Initially, pre-processing data for such a huge range of inputs is the crucial step, accordingly Min -Max normalization tool are the most efficient way to improve input status, this will be speeding up the machine learning performance and time for having a positive influence in this study (Kevin & Paul, 2005). Min -Max normalization representing in Eq.1.

$$x = Target_{min} + (Target_{max} - Target_{min}) * \frac{x - x_{min}}{x_{max} - x_{min}}$$

$Target_{max}$, $Target_{min}$ is corresponding normalized value (which considered to be $Target_{max}$=1&$Target_{min}$ =0). While x v [x_{max}, x_{min}]. After completing the process of correlation, the de-normalizing should be applied for getting the real value.

3.3Forward neural network methodology

Artificial neural network (ANN) is the most popular branch of machine learning, it forms a mathematical model depending on historical data, this can be interpreted as a process that is taught from experience. ANN can represent the brain mechanism for analyzing data, improving the act of sophisticated model and take a precise approach. The relation between brain biological structure and the mathematical statement is developed tightly. Neurons (As data input) address within initial layer that interconnected to subsequent nerves (intermediate layer or Hidden layer) by a specific strengthen link. The rate of strength (weight) will be changed upon learning epoch. The relative nerves are triggering neighborhood nerves until they combined to their eventual destination (output) to perform action (Michael, 2011). Figure 1 show the platform of Simulink equivalent model and each of initial weight, bias, activation function can be corresponding as a block in MATLAB. Eq 2, explains a simple mathematical expression for ANN excluding posting hidden layer. Activation functions transform the input data to more reasonable range.

$$Y = Sigmoid\left(\sum_{n=1}^{m} Input_n * Weight_n - Bias_n\right)$$

$$Simoid(A) = \frac{1}{1 + e^{-A}}$$

3.4Optimizing model through iteration and prediction performance evaluation

Posting hidden layer between input and output layer is to characterized input, increase a chance of manipulating the weights and corelated with the actual behavior (Michael, 2011). Serval statistical tools are commonly used for evaluating prediction deployment, Eq 3 and Eq 4 are Root mean square error (RMSE) and correlation coefficient (R) consequently are the most popular indicators.

$$RMSE = \sqrt{\frac{\sum_{n=1}^{m}(Y_{predicted} - Y_{Desired})^2}{m}}$$

$$R = \frac{\sum_{n=1}^{m}(Y_{Desired(n)} - \bar{Y}_{Desired})(Y_{predicted(n)} - \bar{Y}_{predicted})}{\sqrt{\sum_{n=1}^{m}(Y_{Desired(n)} - \bar{Y}_{Desired})^2 . \sum_{n=1}^{m}(Y_{predicted(n)} - \bar{Y}_{predicted})^2}}$$

Within FNN algorithm, data can be grouped into three sets randomly: trained (70% of data), validation (15% of data) and test (15% of data). Selecting optimum number of neurons in hidden layer has a direct influence of FNN. In this study, sets of neurons in hidden layer sequentially iterated and used for indicating the minimum RMSE between trained and validated sets (Jinchuan & Xinzhe, 2008).

4.Result and discussion

This study is performed by applying Matlab (Toolbox, 2019) and used neural network pattern. The input datasets, that including seven inputs, are recorded for one months over three location Erbil, Baghdad, and Basra. It is lunched with normalizing input through substitute it within Eq 1 and logarithmic the output to ensure that they have same weight and to accelerate the training process. The inputs transformation goes between zero and one. High commonly algorithm is Levenberg-Marquardt backpropagation that considered as recommended option to model prediction problem and used it in this study. 762 inputs dataset are gotten for each input, they are randomly set and partition into a specific group such as: choosing 70% as training set and 30% as validation set. The aim is to make the model in better condition. We have chosen the right number of hidden layers by training the model with different number of neurons (1 to 60 neurons). The optimum number of neurons were selected regarding to their matching of the least RMSE record between training and validation test. A very reasonable RMSE had gotten (between 2.5 – 3) and obtained among the three sites. As they are illustrated in Figure 2. After calculating the training coefficient regarding to each location, this model can be used easily for tracking the irradiation for each separated zone. It is notice that the greater number of neuron usage can't guarantee obtaining the minimum number of RMSE for training and validation set, thus it can't generalize well.

Figure 3 is plotting 70% of the predicted and desired output. A satisfied result with little of variance occurred between them and it is never far away from ideal case that represent as actual output value.

As shown in Figure 4, the statistical performance between estimated and desired value is presented. Since the output was normalized by logarithm their value, the range is transformed between 0 to 6.4. this transformation doesn't not change the property of data. The plotted regression (R) was greater than 0.94 for the three sits, that give the fit reasonably accurate model between actual and the desired value. The training and validation set both are well fitted.

For evaluating neural network design and analyzing the model performance, as the dataset are randomly split into validation and trained groups, selecting optimum iteration point that can be appeared between underfitting and overfitting is need. Figure 5 shows the best validation performance which considered as a least Mean Square error over the three modeled cities that resulted between 0.8-1.4.

1 Conclusion

As a conclusion, hourly climate data are deployed to predict hourly irradiance in high accuracy range. The better performance for the model coming out, in a descending sort, Erbil and Basra then followed by Baghdad. Substituting the neuron in a sequential iteration in the hidden layer is an effective tool for generalizing the model between training and validation set. Increasing number of neurons is add a complicity of data and can't improve the fitness between training and validation set. It is realized that the neuron increment has a slight impact on making the model overfitted. The agreement between training and validation set in a minimum RMSE resulted for almost all the data indexes.

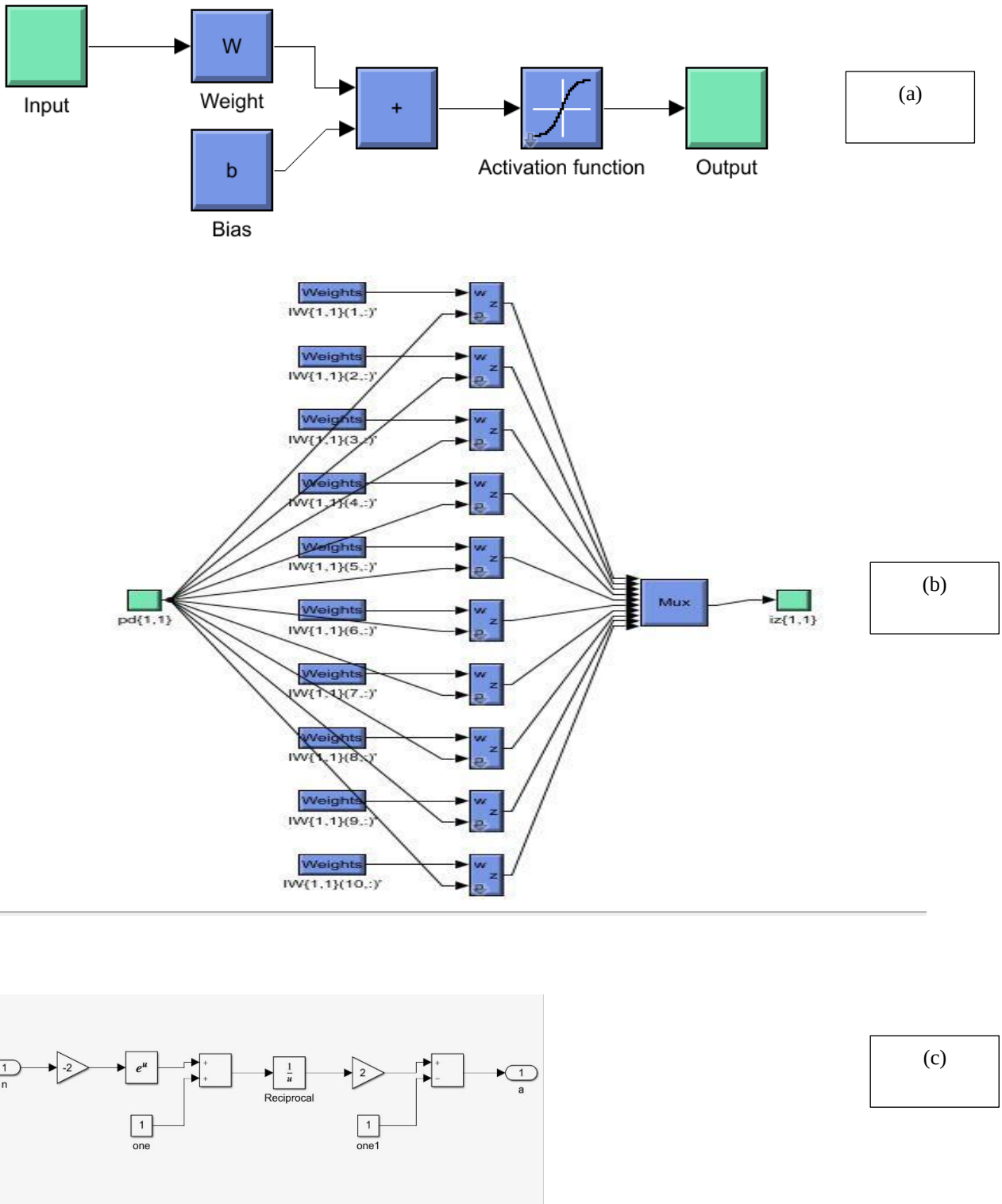

Figure 1 (a) Simple artificial neural network structure, (b) Generated simulink for one of the layer, (c) block for activation function.

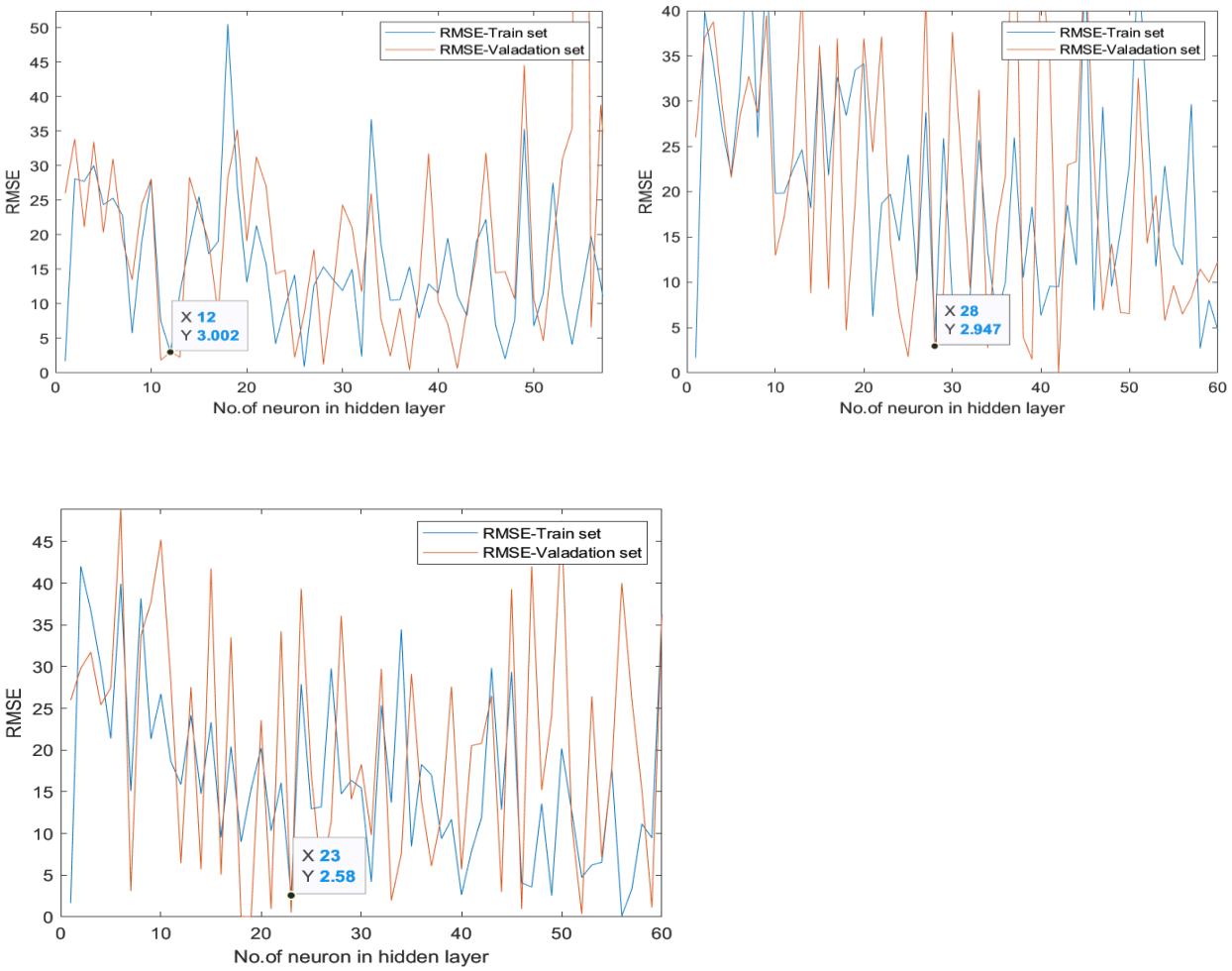

Figure 2 Different neurons in hidden layers Vs RMSE (For Erbil, Baghdad, and Basra)

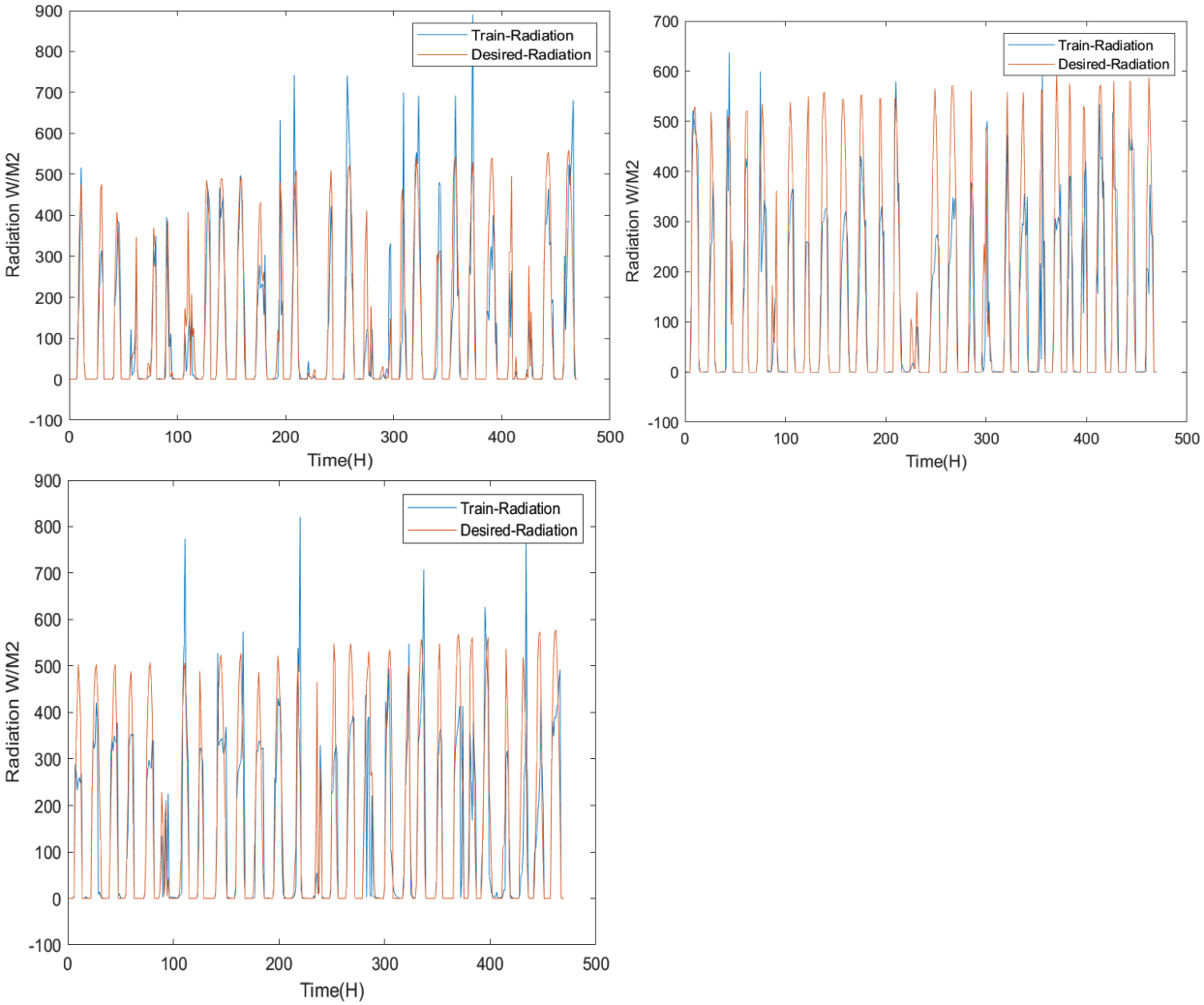

Figure 3 Actual Vs Predicted Irraidaince (For Erbil, Baghdad, and Basra)

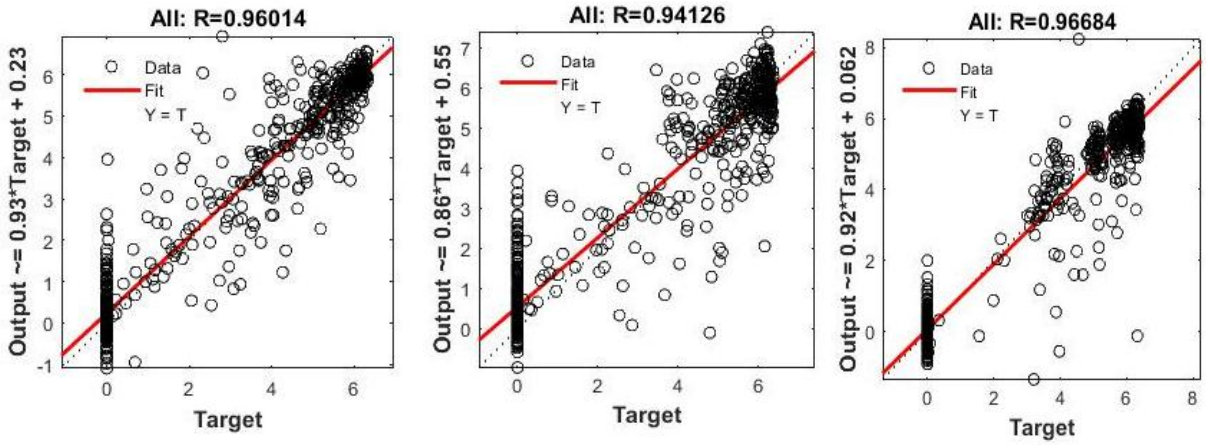

Figure 4 correlation coefficient for normalized actual Vs predicted output (Erbil, Baghdad, and Basra).

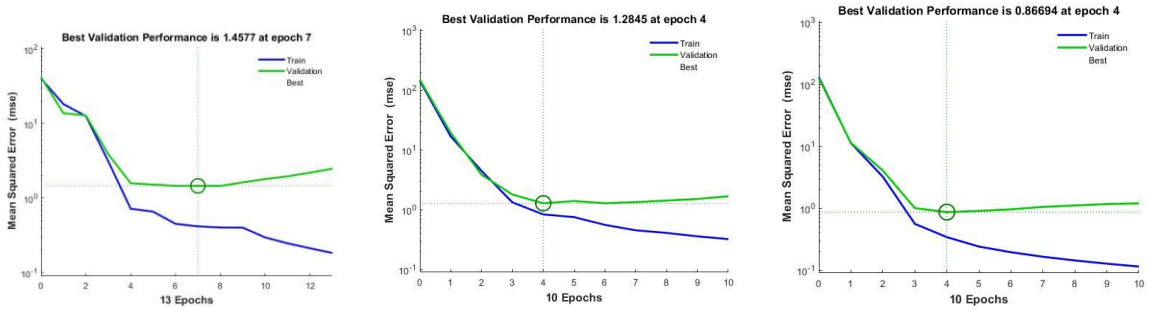

Figure 5 Mean square error Vs iteration with best validation performance (Erbil, Baghdad, and Basra).

Bibliography

Adel, M. (2008). Artificial Intelligence technique for modelling and forecasting of solar radiation data: a review. *Int. J. Artificial Intelligence and Soft Computing*.

Adel, M., & Alessandro, M. P. (2010). A 24-h forecast of solar irradiance using artificial neural network: Application for performance prediction of a grid-connected PV plant at Trieste. *ELSEVIER*.

Adel, M., & Soteris, A. K. (2008). Artificial intelligence techniques for photovoltaic applications: A review. *ELSEVIER*.

Alzahrani, A., Kimball, J., & Dagli, C. (2014). Predicting Solar Irradiance Using Time Series Neural Networks. *ELSEVIER*.

Chiteka, K., & Enweremadu, C. (2016). Prediction of global horizontal solar irradiance in Zimbabwe using artificial neural networks. *ELSEVIER*.

David, E., Gerrit, H., & R.W., M. (1994). Development of a neural network model to predict daily solar radiation. *ELSEVIER*.

Jinchuan, K., & Xinzhe, L. (2008). Empirical Analysis of Optimal Hidden Neurons in Neural Network Modeling for Stock Prediction. *IEEE Pacific-Asia Workshop on Computational Intelligence and Industrial Application*.

Kais, J. A.-J., Munya, F. A.-Z., & Zahraa, S. M. (2012). Estimation of clear sky hourly global solar radiation in Iraq. *INTERNATIONAL JOURNAL OF ENERGY AND ENVIRONMENT*.

Kevin, L. P., & Paul, E. K. (2005). *Artificial neural networks : an introduction.* The Society of Photo-Optical Instrumentation Engineers.

meteoblue. (2006). Retrieved from https://www.meteoblue.com/en/weather/week/basra_iraq_99532

Michael, N. (2011). *Artificial Intelligence: A Guide to Intelligent Systems.* Pearson Education Canada.

Mubiru, J., & Banda, E. (2007). Estimation of monthly average daily global solar irradiation. *elsevier*.

Negnevitsky, M. (2002). *Artificail intelligence a guide of intelligent system.* Pearson.

S., R., & M., M. (2009). Estimation of Diffuse Fraction of Global Solar Radiation Using Artificial Neural Networks. *Taylor & Francis Group, LLC*.

Toolbox, S. M. (2019). *MATLAB*. Retrieved from Mathworks Inc.

ZANCO Journal of Pure and Applied Sciences
The official scientific journal of Salahaddin University-Erbil
https://zancojournals.su.edu.krd/index.php/JPAS

ISSN (print): 2218-0230**, ISSN (online):** 2412-3986**, DOI: http://dx.doi.org/10.21271/zjpas**

RESEARCH PAPER

Gyrodactylus angorae (Monogenea: Gyrodactylidae): First Occurrence on the Body of Two Nemachilid Fishes from Iraq

Younis S. Abdullah[1]

[1]Department of Medical Laboratory, Technical College of Health, Sulaimani Polytechnic University, Kurdistan Region, Iraq

A B S T R A C T:
The monogenean *Gyrodactylus angorae* Ergens & Ibragimov, 1979 was identified on the skin, fin and gills of two nemacheilid loaches *Oxynoemacheilus zarzianus* Freyhof & Geiger, 2017 and *Eidinemacheilus proudlovei* Freyhof, Abdullah, Ararat, Hamad & Geiger, 2016 from Tabin Stream, Sulaimani Prvovince, Kurdistan Region, Iraq for the first time. The description and measurements of this parasite are given in the present study. The prevalence and mean of intensity were also shown.

KEY WORDS: *Gyrodactylus angorae*, Monogenea, Nemacheilidae, Tabin Stream.
http://dx.doi.org/10.21271/ZJPAS.33.5.6
ZJPAS (2021) , 33(5);51-56 .

1.INTRODUCTION :

Stone loaches or Nemacheilidae are small fishes found in freshwaters of Asia, Europe, and northeast Africa (Coad 2017). Due to their small size and low economic value, nemachilid fishes are poorly known group of freshwater fishes (Kottelat 2012; Mafakheri *et al*. 2015). The Euphrates and Tigris river drainages are the major hotspot of nemachilid loach species (Freyhof *et al*. 2019). In Iraq Nemacheilidae is the second largest freshwater fish family after Cyprinidae. There are 13 known nemachilid fish species were reported (Code 2010; Freyhof & Abdullah 2017; Abdullah *et al*., 2020).

* **Corresponding Author:**
Younis Sabir Abdullah
E-mail: younis.abdullah@spu.edu.iq
Article History:
Received: 24/02/2021
Accepted: 01/07/2021
Published: 20/10 /2021

Gyrodactylus Nordmann, 1832 is a genus of the Mono-pithocotylean monogenean trematode, belonging to the family Gyrodactylidae which is worldwide distribution, they are hermaphroditic, viviparous, one-host direct life cycle. Generally permanent ectoparasites on the body surface, fins and gills of fresh, brackish and marine water fishes attached by posterior adhesive organ, they possess a high degree of host-specificity (Margolis & Kabata 1984; Bakke *et al*. 2004; Woo 2006; Buchmann 2012). According to Bakke *et al.* (2002), *Gyrodactylus* have high species richness but low morphological and biological diversity. Many different species of *Gyrodactylus* were found on a single fish host species. While, some other gyrodactylid species was host specific.

The major identification characters of *Gyrodactylus* are presence of opisthaptor which equipped with one pair of large median hooks and 16 marginal hooks. The most prominent feature of this genus is presence of developed embryo in the uterus. Sometime, the embryo may have own

embryo (Buchmann 2012). The identification of *Gyrodactylus* at the species level depends on the morphology and measurements of the attachment organs (Mo & Appleby 1990).

This worm (*Gyrodactylus*) may harm its host by injuries the epithelial cells during attachment process as a result of inserting their marginal hooks and the median hooks into the epidermis in addition to its feeding activities and the consequence of secondary bacterial infections. *Gyrodactylus* is the causative agent of gyrodactylosis in fishes, this disease has been reported worldwide. It is characterized by epithelial damage, excessive mucous secretion, and producing potential hemorrhagic lesions (Johnsen & Jensen 1991; Buchmann, 2012). In addition, *Gyrodactylus* can directly transfer between hosts as adults, and leading to records of accidental transfers. Within the last this is creating confusion in the literature of fish parasite (Harries *et al.* 2004).

In Iraq, the first gyrodactylid species was known principally from early work by Ali & Shaaban (1984), in which they reported *Gyrodactylus elegans* on the gills of *Cyprinus carbio* and *Planiliza abu* (reported as *Liza abu*). After that, many *Gyrodactylus* species have been recorded from freshwater fishes in different Iraqi water bodies (Ali *et al.* 1988; Mhaisen *et al.* 1990; Al-Zubaidy 1998; Abdullah & Mhaisen 2004; Abdullah & Abdullah 2013; Kritsky *et al.* 2013a; Abdul-Ameer & Atwan 2017; Sheyaa & Abdul-Ameer 2019; Abdul-Ameer & Sheyaa 2020). According to Mhaisen (2021) there are 55 different *Gayrodactylus* species are known in Iraq. However, there is no any report regarding the parasitic fauna of nemachilid fish in Iraq.

In the present study, the occurrence of *Gyrodactylus angorae* from skin, fins and gills of two nimachilid fish collected from Tabin Stream in Sulaimani Province, Kurdistan Region-Iraq was reported for the first time in Iraq. Furthermore, the parasite description and measurements have been also depicted.

2. MATERIALS AND METHODS

2.1. Study area

Tabin Stream is located in Surdash Region in Sulaimani Province, Kurdistan Region-Iraq. It is located between Sulaimani City and Dukan District. It is bounded by Daban-Halaj Mountains from the north, Yakhian Mountains from the east, Bardazaro Mountain from the south and by Qashan Mountain from the west (Fig. 1).

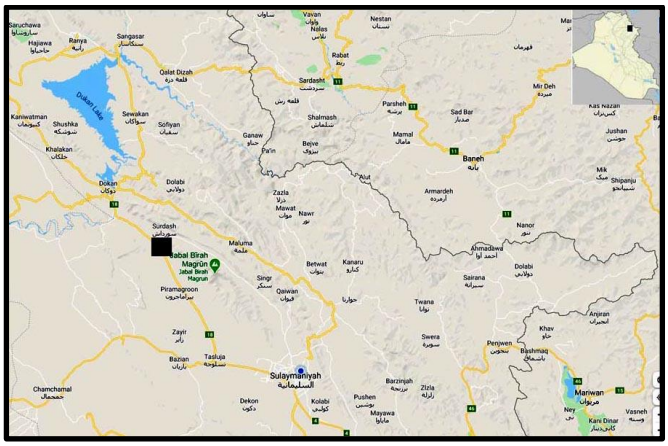

Figure 1: Location of the study area (marked with black square) in Sulaimani Province, Kurdistan Region-Iraq.

2.2 Sampling

A total of 45 stone loaches belonging to family Nemacheilidae (*Eidinemacheilus proudlovei* (n=38) and *Oxynoemacheilus zarzianus* (n=7)) were collected from Tabin Stream near Kanishok Village (N 35.83360 E 45.1045440) in Sulaimani Province, Kurdistan Region-Iraq by using electro-shock device (SAMUS 1000, Made in Poland). The fish were placed in a container with local stream water and transported to the parasitological laboratory as soon as possible and examined to detect the parasites. The fishes were identified according to Freyhof *et al.* (2016), and Freyhof & Geiger (2017).

2.3 Specimen preparation

In the laboratory, fish fins, body and gills were inspected under a dissection microscope. The gills of the fishes were removed and placed in a separate petridishes with only small amount of normal saline solution (0.9%). Pieces of the gill filaments were tiered with a fine needle. After leaving the gills, the worms were removed from the petridishes by a plastic dropper and placed on a clean slide with a few drop of tap water. Then, the specimen covered with a cover slip with glycerin-gelatin. A piece of melted glycerin-gelatin (40°C) was dropped with cover slip on to

the worm. The cover slip was dried carefully with a blotting paper (Kritsky *et al.* 2004). The skin and fins scrape was smeared onto a clean microscope slide and examined directly under optical microscope. The measurements of the worms were done with the aid of ocular micrometer. The parasite identification was recommended by Bykhovskaya-Pavlovskaya *et al.* (1962); Gussev *et al.* (1993); Pugachev *et al.* (2010). Photos were taken with Sony camera, 16.1

3. RESULTS AND DISCUSSION

In the current study, only monogenean parasites were recovered from two species of freshwater nemachilid fishes *Eidinemacheilus proudlovei* and *Oxynoemacheilus zarzianus* from Tabin Stream in Sulaimani Province in Kurdistan Region-Iraq. The study revealed that both fishes were infected with *Gyroductylus angorae* (Table 1). The following is a brief account of this parasite:

Class: Monogenea Carus, 1863
Order: Gyrodactylidea Bychowsky, 1937
Family: Gyrodactylidae Cobbold, 1864
Gyrodactylus angorae Ergens & Ibragimov, 1979
Host: *Eidinemacheilus proudlovei* and *Oxynoemacheilus zarzianus*
Site of infection: Skin, fins and gills
Locality: Tabin Stream, Sulaimani Province, Kurdistan Region-Iraq.

Table (1) Prevalence of *Gyrodactylus angorae* and mean of intensity in nemachilid fish in the present study.

Host	Fish		Prevalence %	Mean intensity	Site of infection
	Examined	Infected			
E. proudlovei	38	2	5.2	7.5	Gill, skin, caudal fin
O. zarzianus	7	2	28.5	6.5	Gill, caudal fin

Description:

The worm is fusiform and the greatest width occurs at the uterus level when it contains an embryo, peduncle is short and tapering toward haptor. Cephalic lobes are well developed, cephalic glands composed of bilateral groups of unicellular glands which are located anterolateral to the pharynx. Haptor is subcircular in shape.

Body length is about 0.34-0.38 mm, total length of the marginal hooks is 0.017-0.019 mm, total length of anchors is 0.036-0.038 mm, main parts 0.020-0.023mm, point 0.022-0.024 mm and inner root 0.014-0.016 mm. Size of ventral bar is 0.003-0.004 x 0.013-0.016 mm, membrane 0.005-0.008 mm. Size of dorsal bar is 0.001-0.004 x 0.010-0.013 mm (Fig. 2).

The description and measurements of the present specimens are closely similar to those reported by Pugachev *et al.* (2010) for *Gyrodactylus angorae* found on fins and skin of *Oxynoemacheilus bergiana* (reported as *Barbatula bergiana*) from Lenkoranka River from Azerbaijan. This monogenean parasite was never been reported from any fish species in Iraq before. Therefore, the present parasite is considered as the first record in Iraq.

Among the viviparous gyrodactylids, *Gyrodactylus* von Nordmann, 1832 is the most diverse genus in the world, with in excess of 500 nominal species (Harris *et al.* 1983; Kritsky *et al.* 2013b). According to Mhaisen (2021), the monogenean *G. angorae* Ergens & Ibragimov, 1979 is not previously recorded from any fish species in Iraq before. Hence, this is the first record in Iraq. Both *Eidinemacheilus proudlovei* and *Oxynoemacheilus zarzianus* are considered here as the first two fish hosts for this monogenean in Iraq.

So far, 56 *Gyrodactylus* species are known from fishes of Iraq in addition to some unidentified *Gyrodactylus* species from 18 different fish host species in Iraq (Mhaisen, 2021). In addition, no any *Gyrodactylus* species was reported earlier from *Eidinemacheilus proudlovei* and *Oxynoemacheilus zarzianus* in Iraq.

Also, in Kurdistan Region-Iraq 15 species of *Gyrodactylus* (*G. baicalensis*, *G. barbi*, *G. cyprinid*, *G. elegans*, *G. gobioninum*, *G. gussevi*, *G. katharineri*, *G. kherulensis*, *G. longoacuminatus*, *G. macracanthus*, *G. medius*, *G. molnari*, *G. shulmani*, *G. sprostonae* and *G. vicinus*) were reported from different fish species (Abdullah & Mhaisem, 2017). In addition, more surveys on nemachilid fish parasites are necessary in order to identify more species and to match the growing information on the parasitic fauna of

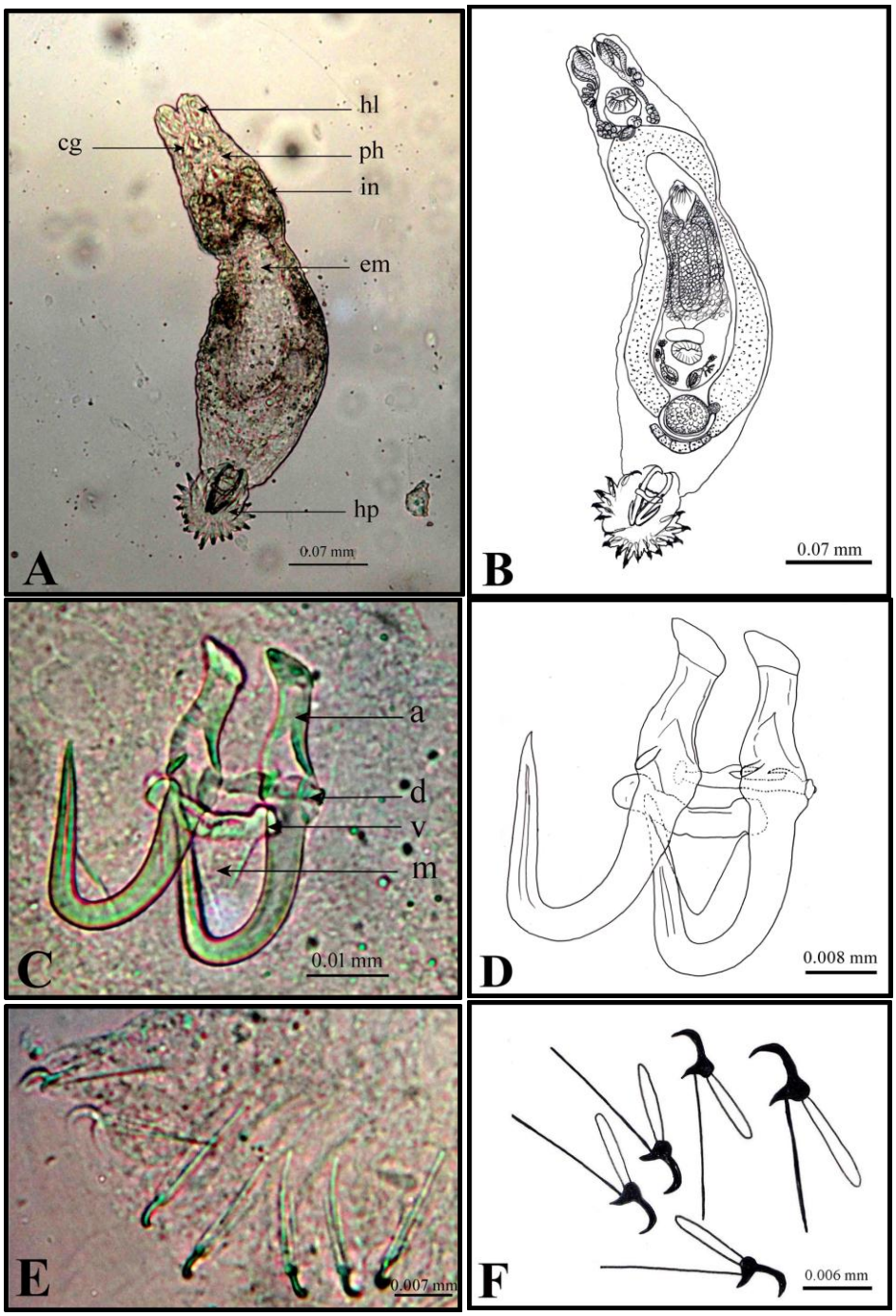

Fig. (2): A: Photomicrograph of *Gyrodactylus angorae* ventral view
B: Camera lucida of drawing of *Gyrodactylus angorae* ventral view
C: Photomicrograph of attachment apparatus
D: Camera lucida of drawing of attachment apparatus
E: Photomicrograph of marginal hooks (hooklets)
F: Camera lucida of drawing of marginal hooks (hooklets)
hl= head lob; **ph=** pharynx; **in=** intestine; **em=** embryo; **hp=** haptor; **cg=** cephalic glands; **a**= anchor; **d**= dorsal bar; **m**= membrane; **v**= ventral bar

these types of fishes in Iraq. This is because Nemacheilidae regarded as the largest freshwater fish family after Cyprinidae in Iraq. Furthermore, the nimachilid fishes have a great biodiversity in Kurdistan Region of Iraq.

Acknowledgements

The author would to appreciate and thank, Prof. Dr. Furhan T. Mhaisen for providing necessary information from his index-catalogue of parasites and disease agents of fishes of Iraq.

References

ABDUL-AMEER, K. N. and ATWAN, F. K. 2017. First record of four species of the genus *Gyrodactylus* Nordmann 1832 (Monogenea: Gyrodactylidae) from some Iraqi freshwater fishes. J. Kerbala Agric. Sci. (Proc. 3rd Sci. Conf., Fac. Vet. Med.), Univ. Kerbala, 10 April 2017. p. 289-297.

ABDUL-AMEER, K. N., and SHEYAA, F. A.-R. 2020. First record of *Gyrodactylus longiradix* Malmberg, 1957 (Monogenea: Gyrodactylidae) from three Iraqi freshwater fish species. Biol. Appl. Environ. Res., 4(1). p. 48-52.

ABDULLAH, S. M. A. and MHAISEN, F. T. 2004. Parasitic infections with monogenetic trematodes on fishes of Lesser Zab and Greater Zab rivers in northern Iraq. Zanco J. Pur. And Appl. Sci., 16(4). p. 43-52.

ABDULLAH, S. M. A. and MHAISEN, F. T. 2017. Parasites of fishes of Kurdistan Region, Iraq: checklists. Biol. Appl. Environ. Res., 1(2). p. 131-218.

ABDULLAH, Y. S. & ABDULLAH, S. M. A. 2013. Monogenean infections on fishes from Darbandikhan Lake in Kurdistan Region, Iraq. Basrah J. Agric. Sci., 26 (Spec. Issue 1). p. 117-131.

ABDULLAH, Y. S.; ABDULLAH, S. M. A. and HUSEEIN, R. H. 2020. Biodiversity of fishes in Sulaimani Province in Kurdistan Region, Iraq. Zanko J. Pur. And Appl. Sci., 32(1). P. 39-44.

ALI, N. M.; MHAISEN, F. T.; ABUL-EIS, E. S. and Kadim, L.S. 1988. First occurrence of the monogenetic trematode *Gyrodactylus kherulensis* Ergens, 1974 in Iraq on the gills of the common carp *Cyprinus carpio*. J. Biol. Sci. Res., 19(3). p. 659-664.

ALI, M. D. and SHAABAN, F. 1984. Some species of parasites of freshwater fish raised in ponds and in Tigris- Al-Tharthar canal region. Seventh Sci. Conf. Iraqi Vet. Med. Assoc., Mosul: 23-25 Oct. 1984: p. 44-46. (Abstract).

AL-ZUBAIDY, A. B. 1998. Studies on the parasitic fauna of carps in Al-Furat fish farm, Babylon province, Iraq. Ph. D. Thesis, Coll. Sci., Univ. Babylon: 141 pp. (In Arabic).

BAKKE, T. A.; HARRIS, P. D. and CABLE, J. 2002. Host specificity dynamics: Observations on gyrodactylid monogeneans. Int. J. Parasitol., 32(3). p. 281-308.

BAKKE, T. A.; NILSEN, K. B. and SHINN, A. P. 2004. Chaetotaxy applied to Norwegian *Gyrodactylus salaris* Malmberg, 1957 (Monogenea) clades and related species from salmonids. Folia Parasitol., 51(2/3). p. 253-261.

BUCHMANN, K. 2012. *Gyrodactylus salaris* and *Gyrodactylus derjavinoides*. In: Woo, P.T.K. and Buchmann, K. (Eds.). Fish parasites: Pathology and protection. CAB Int., Wallingford, p. 193-208.

BYKHOVSKAYA-PAVLOVSKAYA, I. E.; GUSEV, A. V.; DUBINIA, M. N.; IZYUMOVA, N. A.; SMIRNOVA, T. S.; SOKOLOVSKAYA, I. L.; SHTEIN, G. A.; SHUL'MAN, S. S. and EPSHTEIN, V. M. 1962. Key to parasites of freshwater fish of the U. S. S. R, Akad. Nauk, S. S. S. R., Moscow, 727 pp. (In Russian).

COAD, B. W. 2010. Freshwater fishes of Iraq. Pensoft Publishers, Sofia, 275 pp.

COAD, B. W. 2017. Freshwater Fishes of Iran. http://www.briancoad.com. Retrieved 23/2/2021.

FREYHOF, J.; ABDULLAH, Y. S.; ARARAT, K.; HAMAD, I. and GEIGER, M. F. 2016. *Eidinemacheilus proudlovei*, a new subterranean loach from Iraqi Kurdistan (Teleostei; Nemacheilidae. Zootaxa, 4173(3). p. 225-236.

FREYHOF, J. and GEIGER, M. 2017. *Oxynoemacheilus zarzianus*, a new loach from the Lesser Zab River drainage in Iraqi Kurdistan (Teleostei: Nemacheilidae). Zootaxa, 4273(2). p. 258-270.

FREYHOF, J.; KAYA, C.; TURAN, D. and GEIGER, M. F. 2019. Review of the *Oxynoemacheilus tigris* group with the description of two new species from the Euphrates drainage (Teleostei: Nemacheilidae). Zootaxa, 4612(1). p. 29-57.

GUSSEV, A. V.; ALI, N. M.; ABDUL-AMEER, K. N.; AMIN, S. M. and MOLNÁR, K. 1993. New and known species of *Dactylogyrus* Diesing, 1850 (Monogenea, Dactylogyridae) from cyprinid fishes of the river Tigris, Iraq. Syst. Parasitol., 25(3). p. 229-237.

HARRIS, P. D. 1983. The morphology and life–cycle of the oviparous Oögyrodactylus farlowellae gen. et sp. nov. (Monogenea, Gyrodactylidea). Parasitology, 87(3). p. 405-420.

HARRIS, P. D.; SHINN, A. P.; CABLE, J. and BAKKE, T. A. 2004. Nominal species of the genus *Gyrodactylus* von Nordmann 1832 (Monogenea: Gyrodactylidae), with a list of principal host species. Syst. Parasitol., 59(1). p. 1-27.

JOHNSEN, B. O. and JENSEN, A. J. 1991. The *Gyrodactylus* story in Norway. Aquaculture, 98(1-3). p. 289-302.

KOTTELAT, M. 2012. Conspectus Cobitidum: An inventory of the loaches of the world (Teleostei: Cypriniformes: Cobitoidei). The Raffles Bulletin of Zoology 26(Suppl. 26). p. 1-199.

KRITSKY, D. C.; ALI, A. H. and KHAMEES, N. R. 2013a. *Gyrodactylus* aff. *mugili* Zhukov, 1970 (Monogenoidea: Gyrodactylidae) from the gills of mullets (Mugiliformes: Mugilidae) collected from the inland waters of southern Iraq, with an evaluation of previous records of *Gyrodactylus* spp. on mullets in Iraq. Folia Parasitol., 60(5). p. 441-447.

KRITSKY, D. C.; BOEGER, W. A.; MENDONZA-FRANCO, E. F. and VIANNA, R. T. 2013b. Neotropical Monogenoidea. 57. Revision and phylogenetic position of Scleroductus Jara & Cone, 1989 (Gyrodactylidae), with descriptions of new species from the Guatemalan chulin Rhamdia guatemalensis (Günther) (Siluriformes: Heptapteridae) in Mexico and the barred sorubim Pseudoplatystoma fasciatum (Linnaeus) (Siluriformes: Pimelodidae) in Brazil. Syst. Parasitol., 84(1). p. 1-15.

KRITSKY, D. C.; PANNDEY, K. C.; AGRAWAL, N. and ABDULLAH, S. M. A. 2004. Monogenoids from the gills of spiny eels (Teleostei: Mastacembelidae) in India and Iraq, proposal of *Mastacembelocleidus* gen. n., and status of the Indian species of *Actinocleidus*, *Urocleidus* and *Haplocleidus* (Monogenoidea: Dactylogyridae). Folia Parasitol., 51(4). p. 291-298.

MAFAKHERI, P.; EAGDERI, S.; FARAHMAND, H.; MOSAVII-SABET, H. 2015. Descriptive Osteology of Oxynoemacheilus kermanshahensis (Bănărescu And Nalbant, 1966) (Cypriniformes, Nemacheilidae). Croat. J. Fish., 73(3). p. 115-123.

MARGOLIS, L. and KABATA Z. 1984. Guide to the parasites of fishes of Canada Part I. National Printers Press, Canada (Ottawa) Inc., 209 pp.

MHAISEN, F. T. (2021). Index-catalogue of parasites and disease agents of fishes of Iraq. (Unpublished: mhaisenft@yahoo.co.uk).

MHAISEN, F. T.; ALI, N. M.; ABUL-EIS, E. S. and KADIM, L. S. 1990. Parasitological investigation on the grass carp (*Ctenopharyngodon idella*) of Babylon fish farm, Hilla, Iraq. Iraqi J. Biol. Scs., 10(1). p. 89-96.

MO, T. A. and APPLEBY, C. 1990. A special technique for studying haptoral sclerites of monogeneans. Syst. Parasitol., 17. p. 103-108.

PUGACHEV, O. N.; GERASEV, P. I.; GUSSEV, A. V.; ERGENS, R. and KHOTENOWSKY, I. 2010. Guide to monogenoidea of freshwater fish of Palaeartic and Amur regions, Ledizioni Ledipublishing, Milano. 567 pp.

SHEYAA, F. A.-R. and ABDUL-AMEER, K. N. 2019. Record of *Gyrodactylus bychowskianus* Bogolepova, 1950 (Monogenea, Gyrodactylidae) for the first time in Iraq from gills of the cyprinid fish *Arabibarbus grybus*. Bull. Iraq Nat. Hist. Mus. 15(3). p. 287-291.

WOO, P. T. K. (2006). Fish diseases and disorders, volume 1: Protozoan and metazoan infections. Second Ed. CAB Int., Wallingford: 791 pp.

ZANCO Journal of Pure and Applied Sciences
The official scientific journal of Salahaddin University-Erbil
https://zancojournals.su.edu.krd/index.php/JPAS

ISSN (print):2218-0230**, ISSN (online):** 2412-3986**, DOI: http://dx.doi.org/10.21271/zjpas**

RESEARCH PAPER

Vascular Plants of Bani Harir Mountain (Harir intramural bound)

Shahban K. Abbas[1] and Jawhar F. Saeed[2]

[1]Department of Biology, College of Education-Shaqlawa, Salahaddin University- Erbil, Kurdistan Region, Iraq
[2]Department of Biology, College of Education, Salahaddin University- Erbil, Kurdistan Region, Iraq

A B S T R A C T:

Field work survey conducted in this investigation area Bani Harir Mountain (MRO, Kurdistan-Iraq) and their adjacent places. The important goals of this study are to determine vascular plant species of this mountain and their adjacent because of have rich plant diversity which has not been surveyed in detailed by previous botanists up to now and it's not signified in Flora of Iraq. For this purpose, new localities for plant species should be reorganized in flora of Iraq. This survey includes all species of natural local flora of vascular plants which are distributed at the mountains and their adjacent. All the plants those are were determined, only they are new record according to the surveyed area. To constitute the floristic composition, field survey duration was from beginning of spring season 2020 and continued to spring season of 2021. For this purpose; field works were divided to 7 sections and more than 950 plant samples were collected. At the result 247 plant species from 67 families and 183 genera were determined and identified. The 3 largest families in the area of this study is fabaceae family (33 species; 13.36%), the second largest is Asteraceae family (30 species; 12.14%), and the third largest family is Poaceae (22 species; 8.9%). These 3 families followed by Brassicaceae family with (13 species), and Rosaceae family with (12 species).

KEY WORDS: Vascular plants, Plant surveying, Plant collection. Bani Harir mountain Kurdistan-Iraq.
DOI: http://dx.doi.org/10.21271/ZJPAS.33.5.7
ZJPAS (2021) , 33(5);57-68 .

1.INTRODUCTION :

Plant Surveying should be systematic and comparable; data collection, storage and plant identification standards should be observed (Heard and Channon, 1997). Objectives for surveys may be to detect new invaders early, to locate the maximum number of species, to locate the most populations of a single (known) species, or to gather landscape-level data (Allard and Moore, 2011). The field works related with Flora of Iraq started in 1960 as a project of the National Herbarium, Ministry of Agriculture-Baghdad in collaboration with Royal Botanic Gardens, Kew, UK. The Flora of Iraq, with its wealth of over ±3300 species, was planned to be published in 9 volumes (Ghazanfar and Edmondson, 2013).

* **Corresponding Author:**
Shahban Karasul Abbas
E-mail: Shahban.karasul88@gmail.com
Article History:
Received: 06/04/2021
Accepted: 05/07/2021
Published: 20/10/2021

An analysis of the distribution of the flora in the different physiographic regions and districts of Iraq shows the Mountain Region (northern mountains of Iraq) and the Central Alluvial Plains District in the Lower Mesopotamian Region to be the most species rich (Ghazanfar and McDaniel, 2016). An analysis of the distribution of species by physiographic regions and districts shows that the northern regions are the most species rich, with the mountain region containing 40% of the total flora (Zohary, 1973). Many taxonomists have worked in the region, they've always tried to complete the Iraqi flora despite scientific source of very limited, there studies similar to this study conducted previously in different districts and different regions such as; Survey of vascular plants of Sinjar Mountain (Khalaf, 1980). Survey of vascular plants of Piramagrun Mountain (Fars, 1984). Saeed, Surveyed of the Flowering plants of Gali Ali Beg region in Erbil-Iraq (Saeed,

2002). Survey to the vascular plants of Gomaspan strait and around region (Ahmed, 2010). Survey to the vascular plants of Hawraman region (Ahmed, 2013). Survey vascular plant taxa of Hujran Basin (Hameed, 2016). Plant Biodiversity and Ethnobotanical Properties of Various Plants in Choman (Darwesh, 2017).

- Goal of this work:

1- To survey the Bani Harir mountain.
2- To determination families, genera and species of this mountain.
3- To determination of new species or new record.
4- Mention some of the ecological or beneficial uses of included plants.

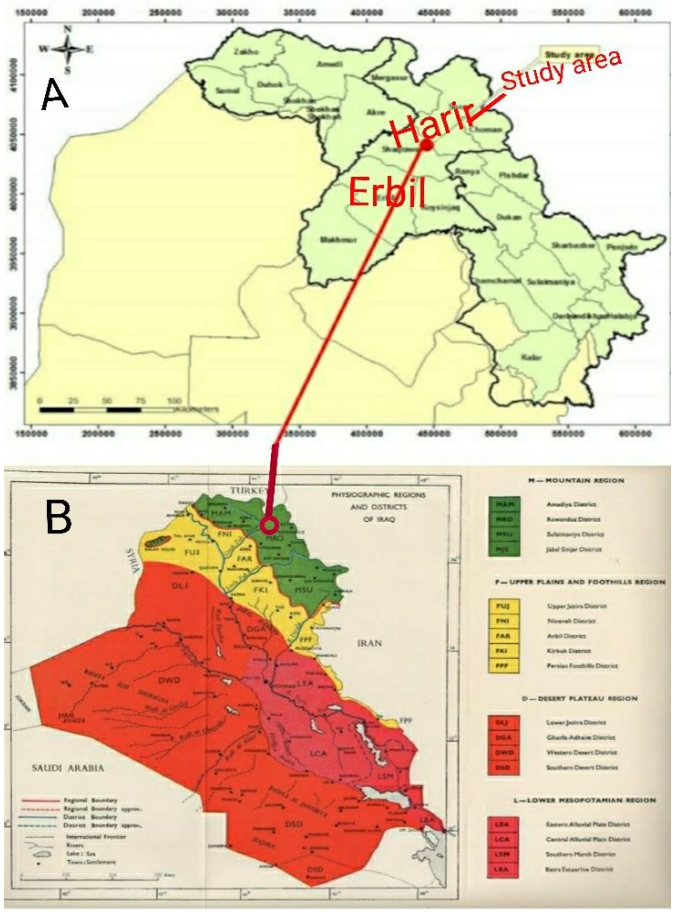

Plate 1 A- Location map of surveyed Area (Ghaib, 2016), (B)Physiographic regions map of Iraq (Guest, 1966).

LOCATION AND GEOLOGY

The republic of Iraq is in southwest Asia between latitudes 29° 5' and 37° 22' N and longitudes 38° 45' and 48° 45' E; it forms the eastern border of the Arab countries. (Omer, 2011). Kurdistan region northern of Iraq mostly mountain area, varying from some (500-800m) in altitude in the lowest valleys to (2000-3600m) at the top of the highest area, Study area is part of the mountain region Rowanduz district (abbreviated by MRO) according to Guest (1966) division (Guest, 1966). The Studied area is located within the Folded Zone of Iraq according to the well-known (Dunnington, 1958) tectonic subdivision of the Iraqi territories, The geological reasons are that the limestone of the Bekhme Formation (The main aquifer in northern Iraq) has a very steep dip on the southwestern limb of the Harir Anticline, Harir area is located within the Zagros high folded zone, which is characterized by relatively long and high-amplitude anticlines (Ghaib, et al, 2009). Harir sub district is about 60 km northeast of Erbil city which situated in north east of Iraq (Iraqi Kurdistan region).

Harir Mountain is located north and north eastern of Harir city, it's divided to both Harir and Khalifan City boundaries. The most extended stretch in the study area also it length is about 29 km', it is high from the highest point about 1550 m according to sea level and its area about 250 km. The study area lies between longitudes 44°16′ and 44°30′ East and latitudes 36°22′ and 36° 38′ North, within the Iraqi Kurdistan Region. The Anticline has two or double draft, asymmetrical and cylindrical shape (Al-Nabawi, 2002). The Longitude and Latitude of studied area are received from lower most places to highest of it.

MATERIALS AND METHODS

Plant samples are the materials of this study which collected and dried according to standard herbarium technique (Bridson and Forman, 1998). The plant samples are collected in primitive spring season 2020 and continued to spring season of 2021. For the perfect and accurate identification process, complete characters both vegetative and reproductive must be present predominately. The specimens morphologically analysis with dependent (stem, flower, fruit and leaves) has been cross-sectioned by hand and most of the taken species were photographed in their habitat. Two main techniques for plant surveys are generally used: random wander and systematic splits, the random wander are useful in difficult terrain or irregularly-shaped localities. The identification process dependent on the available floras, journals, scientific papers, plant field guides and dissertation pertinent to the flora of Iraq and neighboring countries. During this study about 950 specimens were collected at 7 sections

on 46 trips. The identification process was followed on the present floras; Flora of Iraq, (Khalaf, 1980), (Fars, 1983). (Saeed, 2002), (Fatah, 2003), (Ahmed, 2010), (Ahmad, 2013), (Hameed, 2016), and (Darwesh, 2017). Surveyed area divided to 7 sections, usually for division dependent for the area each of the village region ownership for the mountain. Gulak village was represented section 1, it ownership the area of Mountain from the Hamlton road side to highlands of it, parallel to the Darbandok Village boundary. Each of Gulak, Darbandok, Harir, Khrwatan, Bawyan, Sisawa, and Shexmamudian are the villages represented Sections 1, 2, 3, 4, 5, 6, 7, respectively. As showed from (Plate 2). As well as Longitude and Latitude of sections (Table 1).

Table 1. Geographical locations of the surveyed area

Section 1	Gulak Village, Longitude: 700-1300 m, 36° 36'24.6" N, Latitude 44°19'37.4" E. to Longitude: 36° 30'37.3" N, Latitude 44°24'41.3" E.
Section 2	Darbandok Village, 730-1400 Longitude: 36° 34'32.7" N, Latitude 44°20'16.1" E. to Longitude: 36° 30'37.3" N, Latitude 44°24'41.3" E.
Section 3	Harir Town, 730-1500 Longitude: 36° 33'59.7" N, Latitude 44°21'26.1" E. to Longitude: 36° 30'37.3" N, Latitude 44°24'41.3" E.
Section 4	Khrwatan Village, 750-1500 Longitude: 36° 32'09.3" N, Latitude 44°23'08.3" E. to Longitude: 36° 30'37.3" N, Latitude 44°24'41.3" E.
Section 5	Bawian Village, 750-1510 Longitude: 36° 30'57.4" N, Latitude 44°23'43.1" E. to Longitude: 36° 30'37.3" N, Latitude 44°24'41.3" E.
Section 6	Sisawa Village, Longitude, 740-1500 36° 29'47.5" N, Latitude 44°24'35.8" E. to Longitude: 36° 30'37.3" N, Latitude 44°24'41.3" E.
Section 7	Shexmamudian Village, 750-1520 Longitude: 36° 28'05.8" N, Latitude 44°26'17.2" E. to Longitude: 36° 30'37.3" N, Latitude 44°24'41.3" E.

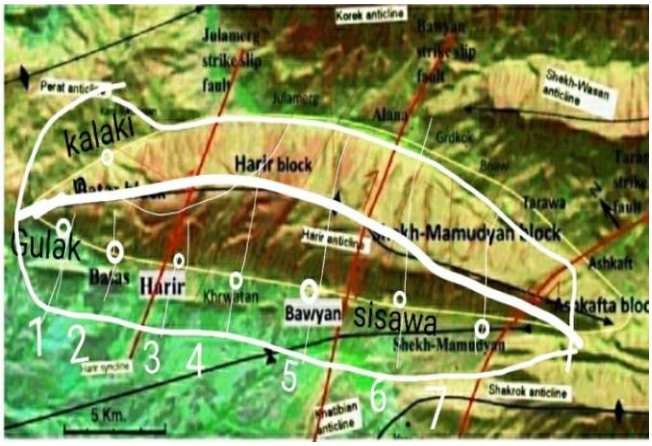

Plate 2. Physiography of the surveyed area
After founding of plants at the field usually some of them capable to interlace but others need to spade to dig out and collection of them, then usually they dried in a shadow place under simple pressure in a newspaper for two or three days with a suitable shape for the purpose revelation all parts of the plant. Some of plants are identified from the field but some of other need to superfine identification with dependent different source, then put them to special labeled. For easy referencing, an alphabetic arrangement of all plant species was used from family to the variety ranks. Family limits and generic placements follow (Mabberly, 2008). The Longitude and Latitude of studied area are received from lowermost place to highest of it. Beside of natural plants some of artificial vegetation (Tree) that suitable for the characteristic species of the habitat are surveyed mostly includes Suburban, Waterside, Garden and wayside vegetation.

ABBREVIATIONS

The abbreviations used in the text and in the floristic list of Bani Harir mountain are as follows: **an:** annual plants**, bi:** biennial plants, **pe:** perennial plants, **Tr**: Tree, **Sh**: Sh, **Fe**: Fern according to plant distribution, **(M)** for other mountain districts in Kurdistan-Iraq, **I:** for Iran, **S:** for Syria, **T:** for turkey, **Vo**: Voucher number for plant specimens.

RESULTS and DISCUSSIONS

A total of 247 plant species from 67 families and 183 genera were identified. Of these, ١٨٠ species belonged to Spermatophyta, which included 3 taxa from Gymnospermae and 241 plant species from Angiospermae. Also the remaining 3 taxa belonged to Pteridophyta as there showed from See (Table 2) and (Table 3). About 950 plant samples were collected from studied area. Generally, division of all plants to their families, genera and taxa according to the large taxonomical groups illustrated from these two. The five largest families given as follow; Fabaceae with 33 plant species, Asteraceae with 30 plant species, Poaceae with 22 plant species, Brassicaceae with 13 plant species, and Rosaceae 12 plant species, as from Table4.

The plants were collected from the process of plant surveying, usually they are different in Results according to family numbering, genus and species numbering from a section to another section of study area, which it's dependent of some factors such as, attempt of researcher, capability of researcher, biological factor and environmental factors of the study area. Most of the plant cover of Bani Harir Mountain and the areas around it is of thick or lush herbs (Herbaceous plants), that covering the slopes, valleys and the top of the studied area, along with the Hills and plains on both sides. Most of the forests were descried from the eastern and northern of the Mountain and rich in plant community if compared with other sides because western and southern of the Mountain is mostly rocky soil, slope surface, also it's nearness from inhabited and shady place which helps to deliverance of trees to drought through reduction of rain fall. All the plants that are recorded and determined, they were new record according to the surveyed area, The largest life cycle of identified 247 vascular plant species are herbs with 208(%84.21) plant species, of these 121 (%58.17) of which are `annual; 4 (%1.92) of which are `biennial; 83 (%39.9) of which are `perennial`, (Table 5). The others; 15 shrubs (%6.07), 21 trees (%8.5) and 3 ferns (%1.21), (Table ٥) and (Table 6). See list of the flora in the supplement.

Table 2. Plant groups according to their taxa

	Number of Families	Number of Genera	Number of species
Pteridophyta	٢	٣	٣
Spermatophyta	65	١٨٠	٢٤٤
Total	67	١٨٣	٢٤٧

Table 3. Groups of Spermatophyta

	Number of Families	Number of Genera	Number of species
Gymnosperme	٢	3	3
Angiospermae	٦٣	١٨٠	241
Total	٦٥	١٨٣	٢٤٤

Table 4. Ratio of ٥largest families with their species number:

Family	**Taxa number**	**Ratio(Total flora)**	**Ratio (five largest family)**
Fabaceae	33	13.36	30
Asteraceae	30	12.14	27.27
Poaceae	22	8.9	20
Brassicaceae	13	5.26	11.8
Rosaceae	12	4.85	10.9
Total	**110**	**%44.51**	**%100**

Table 5. Plant duration:

Life cycle	**Species number**	**Ratio**
Annual herbs	121	58.17
Biennial herbs	4	1.92
Perennial herbs	83	39.9
Total	٢٠٨	١٠٠.٠٠

Table 6. Plant habit:

Life spans	**Taxa number**	**Ratio**
Herb	٢٠٨	٨٤.٢١
Shrub	١٥	٦.٠٧
Tree	٢١	٨.٥
Fern	٣	١.٢١
Total	٢٤٧	١٠٠.٠٠

Supplement: Flora list of the study area

The systematic list is given as follow;

1. ACERACEAE
1. ***Acer monspessulanum*** L.
(Tr, M, I, T, S), Section, 4, (Vo-160).
2. ADIANTACEAE
2. ***Adiantum capillus-veneris*** L**.**
(Fe, M, I, S, T), Section, 1, 2, 3, 4, 5, (Vo-185).
3. ***Chelianthes persica*** (Bory) Mett. ex Kuhn.
(Fe, M, T, I), Section, 1, 3, 4, 5, (Vo-220).
3. ALLIACEAE
4. ***Allium ampeloprosum*** L.
(Pe, M, S, T, I), Section, 2, 3, 4, 5, (Vo-100, 301).
5. ***Allium rotundom*** L.
(pe, M, S, T, I), Section, 3, (Vo- 125).
4. AMARANTHACEAE
6. ***Amaranth albus*** L.
(an, M, S, T, I), Section, 4, 5, (Vo-186).
7. ***Amaranth retroflexus*** L**.**
(an, M, S, T, I), Section, 4, 7, (Vo- 14).
5. ANACARDIACEAE
8. ***Pistacia eurycarpa*** Yalt.
(Tr, M, I, S, T), Section, 1, 2, 3, 4, 5, 6, 7, (Vo- 3, 437).
9. ***Pistacia khinjuk*** Stocks.
(Sh, M, I, S, T), Section, 1, 2, 3, 4, 5, 6, 7, (Vo-221, 504).
10. ***Pistacia vera*** L.
(Tr, M, S, T, I), Section, 3, (Vo-126).
11. ***Rhus coriaria*** L.
(Sh, M, S, T, I), Section, 3, 6, (Vo-25).
6. APIACEAE *(*UMBELLIFERAE*)*
12. ***Ainsworthia trachycarpa*** Boiss.
(an, M), Section, 2, 4, (Vo-52).
13. ***Apium nodiflorum*** (L.) Lag.
(pe, M), Section, 3**,** 4, 6 (Vo-37, 508)
14. ***Eryngium campestre*** L**.**
(Pe, P, M, I, T), Section, 2, 3, 7, (Vo-151).
15. ***Lagoecia cuminoides*** L.
(an, M S, T, I), Section, 2, 7, (Vo-187).
16. ***Smyrnium cordifolium*** Boiss.
(bi, M, I, T, S), Section, 3, 4, (Vo-65).
17. ***Scandix stellata*** L.
(an, M, T, I, S), Section, 3, 4, 6, (Vo-227).
18. ***Turgenia latifolia*** (L.) Hoffm.
(an, M, S), Section, 1, (Vo-76).
19. ***Torilis leptophylla*** (L.) Rchb.f.
(an, Th, M, I, T, S), Section, 4, (Vo- 189).
7. APOCYNACEAE
20. ***Nerium oleander*** L.
(Sh, M, I, S, T), Section, 1, 4, 7, (Vo-101, 305).
8. ARACEAE
21. ***Eminium spiculatum*** (Blume) Schott
(pe, M, I, T), 3, 4, (Vo-53)
9. ARISTOLOCHIACEAE
22. ***Aristolochia bottae*** Jaub. & Spach.
(pe, M, S, T, I), Section, 3, 4, 5, 6, (Vo-152).
10. ASPARAGACEAE
23. ***Bellevalia kurdistanica*** Feinbrun.
(pe, M, I, T), Section, 3, 4, (Vo-188).
24. ***Ornithogalum krdicum*** Bornm.
(pe,), Section, 3, 4, (Vo- 77)
11. **ASPLENIACEAE**
25. ***Cetarach officinarum*** Willd.
(Fe, M, S, T, I), Section 1, 3, 4, 5, 6, 7, (Vo-223, 405).
12. ASTERACEAE (COMPOSITAE)
26. ***Anthemis pseudocotula*** Boiss.
(an, M, S, I) Section, 1, 2, 3, 4, 5, 6, 7, (Vo-306)
27. ***Callendula arvensis***.
(an, M, S, T), Section, 2, 3, 4, 5, 6, , (Vo-38, 412).
28. ***Carthamus oxyacantha*** M. Bieb.
(an, M, I, T), Section, 1, 2, 3, 4, 5, 6, 7, (Vo-102, 440).
29. ***Carlina corymbosa*** L.
(pe, M), Section, 2, (Vo-190).
30. ***Centaurea behen*** L.
(pe, M, I), Section, 8, (Vo-310)
31. ***Centaurea iberica*** Trev. ex Spreng.
(pe, M, I, T, S), Section, 2, 3, 4, (Co-128, 402).
32. ***Centaurea solstitialis*** L.
(pe, M, I, T), Section, 1, 3, 4, 7, (Vo-154, 410).
33. ***Cichorium intybus***.
(an, M, I, T, S) Section, 2, 3, 4, 5, 6, 7, (Co-224,442).
34. ***Conyza bonariensis*** (L.) Cronquist.
(an, M, T), Section, 2, 3, 4, (Vo-54).
35. ***Crepis sancta*** (L.) Babcoc.
(an, M, T, I), Section, 3, 4, 5, (Vo-193).
36. ***Crupina crupinastrum*** (Moris) Vis.
(an, M, I, T, S), Section, 3, 4, 6, 7, (Vo-129).
37. ***Echinops*** sp.
(Pe, M, I), Section, 1, 2, 3, 4, 5, 6, 7, (Vo-26, 221).
38. ***echinops spinosissimus*** L**.**
(Pe, M, I), Section, 1, 3, (Vo-15)
39. ***Filago pyramidata*** L.
(an, M, S, T) Section, 2, 6, (Vo-103)
40. ***Gundelia tournefortii*** L.

(pe, M, I, T, S), Section, 1, 2, 3, 4, 5, 6, 7, (Vo-225, 413).
41. ***Hedypnois rhagadioloides*** (L.) F.W.Schmidt.
(an, M, I, T), Section, 4, 6, (Vo-194).
42. ***Helichrysum arenarium*** (L.) Moench
(pe, M, T, I), Section, 3, 4, 5, (Vo- 613)
43. ***Lactuca serriola*** L.
(bi, M, S, T, I), Section, 1, 2, 3, 4, 5, 6, 7, (Vo-155, 414).
44. ***Lactuca saligna*** L.
(an, M), Section, 4, (Vo-130).
45. ***Matricaria aurea*** (Loefl.) Sch.Bip.
(an, M, S, T), Section, 3, (Vo-226).
46. ***Notobasis syriaca*** (L.).
(an, M, I, T, S), Section, 1, 2, 3, 4, 5, 6, 7, (Vo-156, 311).
47. ***Onopordum carduchorum*** Bornm. Beauverd.
(bi, M, I, T, S), Section, 1, 3, 4, 6, (o- 78).
48. ***Picnomon acarna*** (L.) Cass.
(an, M, I, T, S), Section, 2, 4, 5, 7 , (Vo-192).
49. ***Scorzonera pseudolanata*** Grossh.
(pe, M, I, T), Section, 4, (Vo-66).
50. ***Rhagadiolus stellatus*** (L.) Gaertn.
(an, M, I, T), Section, 3, (Vo-55).
51. ***Senecio vernalis*** Waldst. & Kit.
(an, M, S, T), Section, 3, 4, 5, 6, (Vo-131)
52. ***Silybum marianum*** (L.) Gaertn.
(an, M, I, T, S), Section, 1, 2, 3, 4, 5, 6, 7, (Vo-227, 442).
53. ***Sonchus oleraceus*** (L.) L.
(an, M, S, T, I), Section, 3, 4, (Vo- 4)
54. ***Steptorhamphus tuberosus*** (Jacq.) Grossh.
(pe, M), Section, 1, (Vo- 621)
55. ***Urospermum picroides*** (L.) Scop. Ex F.W.Schmidt.
(an, M, S, T), Section, 5, (Vo- 79)
56. ***Xanthium strumarium*** L.
(pe, M, I, T, S), Section, 1, 3, 4, 6, 7, (Vo- 195)
13. BERBERIDACEAE
57. ***Bongardia chrysogonum*** (L.) Spach.
(pe, M, I, T), Section, 4, (Co- 104)
14. BORAGINACEAE
58. ***Anchus azurea*** Mill.
(pe, M, S, T), Section, 2, 3, 5, 6, 7, (Vo- 518)
59. ***Echium italicum*** L.
(pe, M, I, T), Section, 2, 3, 5, 6, 7, (Vo-228).
60. ***Onosma alborosea*** Fisch. & C. A. Mey.
(pe, M, T), Section, 1, 2, 3, 4, (Vo- 39).
15. BRASSICACEAE *(*CRUCIFERAE*)*
61. ***Alyssum strigosum*** Banks & Sol.
(an, M, T, I, S), Section, 3, 4, (Vo-16).
62. ***Biscutella didyma*** L.
(an, M, T, I, S), Section, 3, 6, (Vo-158).
63. ***Brassica nigra*** L.
(an, M, T, I, S), Section, 2, 3, 4, 5, 6, (Vo-132).
64. ***Capsella bursa-pastoris*** (L.) Medik.
(an, M, I, T, S), Section, 2, 3, 4, 7, (Vo- 196).
65. ***Clypeola jonthlaspi*** L.
(an, M, S, T), Section, 2, (Vo-56).
66. ***Conringia perfoliata*** (Crantz) Link.
(an, M, S, T), Section, 3, (Vo-197).
67. ***Erysimum repandum*** L.
(an, M, S, T), Section, 3, (Vo-127).
68. ***Isatis Lusitanica*** L.
(an, M, S, T), Section, 3, 4, (Vo-133).
69. ***Lepidium draba*** L.
(an, M, I, T, S), Section, 3, (Vo-198).
70. ***Lepidium sativum*** L.
(an, M, I, S, T), Section, 4, (Vo-5).
71. ***Nasturtium officinale*** R.Br.
(pe, M, I, S, T), Section, 1, 3, 4, 7(Vo-159, 447)
72. ***Sisybrium irio*** L.
(an, M, S, T), Section, 3, 4, 6, (Vo-229).
73. ***Sisymbrium officinale*** (L.) Scop.
(an, M, S, T), Section, 1, 3, 7, (Vo-54)
74. ***Sinaps arvensis*** L.
(an, M, I, S, T) Section, 4, 5, 6, (Vo-105).
16. CAMPANULACEAE
75. ***Mechauxia nuda*** A.DC.
(bi, M, S), Section, 1, 4, (Vo-199).
17. CAPPARIDACEAE
76. ***Capparis spinosa*** **L.**
(Sh pe, M, I, S, T), Section, 2, 3, 4, 7(Vo-134)
18. CAPRIFOLIACEAE
77. ***Cephalaria syriaca*** (L.) Schrad.
(an, M, I, S, T), Section, 1, 2, 3, 4, 5, 8, (Vo- 232)
78. ***Pterocephalus kurdicus*** Vaill. ex Adans.
(Pe, M, I, T), Section, 1, 2, 4, 5, 6, 7, (Vo-6)
79. ***Valerianella vesicaria*** **(**L.) Moench.
(an, M, I, T), Section, 3, 4, 5, (Vo-17).
19. CARYOPHYLLACEAE
80. ***Dianthus strictus*** Banks et Sol.
(pe, M, T, I), Section, 3, 6, (Vo-28).
81. ***Minuartia hamata*** (Hausskn.) Mattf.
(an, M, T), Section, 2, 3, 4, (Vo-230).
82. ***Silene aegyptiaca*** (L.) L.f.
(an, M, T), Section, (Vo- 41).
83. ***Vaccaria hispanica*** Mill.
(an, M, S, T, I), Section, 3, 4, 5, (Vo- 160)
20. CISTACEAE
84. ***Helianthemum ledifolium*** (L.) Mill.
(an, M, I, S, T), Section, 2, 3, (Vo- 67).

21. CONVOLVULACEAE
85. *Convolvulus arvensis* L.
(pe, M, I, S, T), Section, 2, 3, 4, (Vo-200, 440).
86. *Convolvulus stachydifolius*L.
(pe, M, I, S, T), Section, 3, 5, (Vo- 106).
87. *Cuscuta* sp.
(an, M, S, T, I), Section, 3, (Vo- 135).
22. CRASSULACEAE
88. *Rosularia radiciflora* Boriss.
(pe, M, T), Section, 2, 3, (Vo- 136).
89. *Umbilicus horizontalis* (Guss.) DC.
(pe, M, S, T), Section, 1, 2, 3, 4, 5, 6, 7, 8, (Vo-201, 266)
23. CUCURBITACEAE
90. *Bryonia multiflora* L.
(pe, M, I, S, T), Section, 3, (Vo-231).
91. *Citrullus colocynthis* (L.) Schrad.
(pe, M), Section, 3, 5, (Vo- 161, 340).
24. CUPRESSACEAE
92. *Cupressus sempervirens* L. **var. Pyramidata** (Mill.) Loudon
(Tr, M, I, S, T), Section, 1, 3, 5, (Vo-107).
93. *Thuja orientalis* (L.) franco.
(Tr, M), Section, 1, 2, 3, 6, (Vo-539)
25. CYPERACEAE
94. *Carex diluta* M.Bieb.
(pe, M, I, S, T), Section, 2, 3, 8, (Vo-738)
95. *Carex pachystylis* J.Gay.
(pe, M, I, T), Section, 2, 3, 6, (Vo-198)
96. *Cyperus longus* L.
(pe, M, I, S, T), Section, 5, 7, (Vo- 138).
97. *Cyperus rotundus* L.
(pe, M, S, T, I), Section, 3, 7, (Vo- 202).
26. EUPHORBIACEAE
98. *Andrachne telephoides* L.
(pe, M, I, S, T), Section, 1, 3, 5, 6, (Vo- 139).
99. *Andrachne aspera* Spreng.
(pe, M, I, S, T), Section, 1, 3, 6, (Vo- 18, 272).
100. *Chrozophora tinctoria* (L.).
(an, M, I, S, T), Section, 2, 3, 4, 5, 6, 7(Vo-18).
101. *Euphorbia aleppica* L.
(an, M, S, I, T), Section, 1, 3, 6, (Vo- 163).
102. *Euphorbia helioscopia* L.
(an, M, I, S, T), Section, 2, (Vo- 233).
103. *Euphorbia macroclada* Boiss.
(pe, M, S, I, T), Section, 2, 6, (Vo- 233).
104. *Euphorbia falacta* L.
(an, M, I, S, T), Section, 4, 6, (Vo- 30).
105. *Euphorbia petiolata* Banks & Sol.
(an, M, S, T) , Section, 3, 4, (Vo- 108).
27. FABACEAE (LEGUMINOSAE)
106. *Alhagi graecorum* Boiss.
(Pe, M, I, T, S), Section, 2, 3, 4, (Vo- 203).
107. *Astragalus gossypinus* L.
(pe, M, T, I, S), Section, 1, 6, (Vo- 164, 278).
108. *Astragalus spinosus* (Forssk.) Muschl.
(pe, M), Section, 1, 2, 6, (Vo- 82, 449).
109. *Astragalus hamosus* L.
(an, M, I, T, S), Section, 3, (Vo- 234).
110. *Cicer arietinum* L**.**
(an, M, I, T, S) , Section, 2, 4, 5, 6, 7, (Vo- 83).
111. *Glycyrrhiza glabra* L.
(pe, I, T, S), Section, 1, 6, 7, (Vo- 68).
112. *Hippocrepis unisiliqusa* L
(an, M, I, T, S), Section, 3, (Vo- 165).
113. *Hymenocarpus circinnatus* (L.) Savi
(an, M, I, T, S), Section, 3, (Vo- 43).
114. *Lathyrus aphaca* L.
(an, M, I, T), Section, 3, 4, (Vo- 140, 270).
115. *Lathyrus inconspicuus* L.
(an, M, S, T), Section, 5, (Vo- 204).
116. *Lathyrus annus* L.
(an, I, T), Section, 3, 4, (Vo- 31).
117. *Medicago minima* (L.) L.
(an, M, S, T), Section, 2, 3, 4, (Vo- 166, 450).
118. *Medicago orbicularis* (L.) Bartal.
(an, M, I, T, S), Section, 2, 3, 4, (Vo- 109, 430).
119. *Medicago polymorpha* L.
(an, M, I, T, S), Section, 3, (Vo- 56).
120. *Medicago radiate* L.
(an, M, I, T), Section, 3, 4, (Vo- 235).
121. *Medicago lupulina* L.
(an, M, S, T, I), Section, (Vo- 69).
122. *Medicago sativa* L.
(an, M, I, S, T), Section, 6, (Vo- 19).
123. *Medicago rigidula* (L) all.
(an, M, T, I, S), Section, 1, (Vo- 7).
124. *Melilotus indica* (L.) All. , Fl. Pedem.
(an, M, S, T, I), Section, 4, (Vo- 205).
125. *Onobrychiscaput-galli* (L.) Lam.
(an, M, I, T, S), Section, 3, 4, (Vo- 141).
126. *Pisum sativum* L.
(an, M, I, T, S), Section, 3, 4, 5, (Vo- 167).
127. *Prosopis farcta* (Banks & Sol.) J.F.Macbr.
(pe, M, I, T, S), Section, 1, 2, 3, 4, 6, 7, (Vo- 32, 431).
128. *Scorpiurus muricatus* L.
(an, M, I, T, S), Section, 1, 2, 3, 4, 5, 6, 7(Vo- 92)
129. *Trifolium campestre* Schreb.
(an, M, I, S, T), Section, 2, 6, (Vo- 44).
130. *Trifolium resupinatum* L.
(an, M, S, T), Section, 3, 4, 6, (Vo- 110, 455).
131. *Trifolium grandiflorum* Schreb.
(an, M, I, S, T), Section, 6, (Vo- 45).

132. *Trifolium purpureum* Loisel.
(an, M, I, S, T), Section, 1, 2, 3, 4, 5, (Vo- 142).
133. *Trifolium repens* L.
(an, M, I, T, S), Section, 6, (Vo- 206).
134. *Trifolium stellatum* L.
(an, M, I, T, S), Section, 1, 2, 3, 4, 5, 6, (Vo- 168, 432).
135. *Trifolium hirtum* L.
(an, M, S, T), Section, 2, 3, 4, 5, 7, (Vo- 56).
136. *Trifolium tomentosum* L.
(an, M, I, T), Section, 3, 4, 5, (Vo- 237).
137. *Vicia narbonensis* L.
(an, M, I, S, T), Section, 3, (Vo- 69).
138. *Vicia sativa* L.
(an, M, I, S, T), Section, 4, 5, 6, (Vo- 143, 371).
139. *Vicia faba* L.
(an, M, I, S, T), Section, 4, 5, 6, (Vo- 221).
28. FAGACEAE
140. *Quercus aegilops* L.
(Tr, M, I, S, T), Section, 1, 2, 3, 4, 5, 6, 6, 7, (Vo- 20, 462).
141. *Quercus infectoria* Oliv.
(Tr, M, I, S, T), Section, 1, 2, 3, 4, 5, 6, 7, (Vo- 207, 279).
29. GENTIANACEAE
142. *Gentiana olivieri* Griset.
(pe, M, I, T), Section, 3, 4, (Vo- 111).
30. GERANIACEAE
143. *Erodium cicutarium* (L.) L'Hér.
(an, M, S, T), Section, 3, (Vo- 33).
144. *Gernium molle* L.
(pe, M, S, T), Section, , (Vo- 543)
145. *Gernium rotundifolium* L.
(an, M, I, S, T,), Section, 3, 6, (Vo- 238).
31. HYPERICACEAE (GUTTIFERAE)
146. *Hypericum triquetrifolium* Turra., Farsetia nov Pl.
(pe, M, I, S, T), Section, 1, 2, 3, 4, 5, 6, (Vo-8).
32. IRIDACEAE
147. *Gladiolus atroviolaceus* Boiss.
(pe, M, I, S, T), Section, 2, 3, (Vo- 46).
148. *Gladiolus italicus* Mill.
(pe, M, I, S, T), Section, 2, 3, 6, (Vo- 149).
33. IXIOLIRIONACEAE
149. *Ixiolirion tataricum* (Pall.) Schult & Schult.f.
(pe, M, I, S, T), Section, 1, (Vo- 482)
34. JUGLANDACEAE
150. *Juglans regia* L
(Tr, M, I, S, T), Section, 3, 6, (Vo- 208).
35. JUNCACEAE
151. *Juncus bufonius* L.
(an, M, I, T), Section, 3, (Vo- 58).
152. *Juncus rigidus* Desf.
(pe, M, I, T, S), Section, 1, 7, 8, (Vo- 170)
36. LAMIACEAE (LABIATAE)
153. *Ajuga chamaepitys* (L.) Schreb.
(Pe, M, I), Section, 1, 3, 6, (Vo- 47).
154. *Eremostachys laciniata* (L.) Bunge
(pe, M, I), Section, 3, 4, 5, (Vo- 112).
155. *Lamium amplexicaule* L.
(an, M, I, S, T), Section, 2, 3, 4, 6, (Vo- 39).
156. *Marrubium cuneatum* Banks & Sol.
(pe, M, I, T), Section, 2, 4, 6, (Vo- 86).
157. *Mentha longifolia* (L.) L.
(pe, M, I, T), Section, 1, 2, 4, 5, 6, 7, (Vo- 171).
158. *Molucella laevis* L.
(Pe, M, I, T), Section, 2, 5, (Vo-209).
159. *Phlomis kurdica* Rech.f.
(pe, M, I, S, T), Section, 4, (Vo-470).
160. *Salvia indica* L.
(pe, M, I, T), Section, 1, 2, 3, (Vo- 69).
161. *Teucrium polium* L.
(an, M, S, T, I), Section, 1, 2, 3, 4, 5, (Vo- 85).
162. *Vitex agnus-castus* L.
(Sh, M, S, T, I) ,Section, 1, 4 , (Vo- 172).
163. *Ziziphora capitata* L.
(an, M, I, S, T), Section, 3, 4, (Vo- 113).
37. LILIACEAE
164. *Gagea* sp.
(pe, M), Section**,** 3, (Vo- 682)
165. *Scilla autumnalis* L.
(pe, M), Section, 1, 2, 3, 4, (Vo-127, 564)
38. LINACEAE
166. *Linum corymbosum* Reichb.
(an, M, I, S, T), Section, 2, 3, (Vo- 565)
167. *Linum mucronatum* Bertol**.**
(pe, M, I, S, T), Section, 1, 2, (Vo-392)
39. MALVACEAE
168. ***Alcea kurdica*** Alef.
(pe, M, I, S, T), Section, 1, 2, 3, 4, 5, 6, 7, (Vo- 210, 436).
169. *Malva neglecta* Wallr.
(pe, M, I, S, T), Section, 1, 2, 3, 4, 5, 6, 7, (Vo- 240. 472).
40. MELIACEAE
170. *Melia azedarach* L.
(Tr, M), Section, 3, (Vo- 145).
41. MORACEAE
171. *Ficus carica* L.
(Sh, M, I, S, T), Section, 1, 3, 4, (Vo-9, 376).
172. *Morus alba* L**.**

(Tr, M, I, S, T), Section, 1, 3, 4, 6, (Vo- 21).
42. MYRTACEAE
173. *Eucalyptus* sp L'Hér**.**
(Tr, M, S, T, I), Section, 1, 2, 3, 6, (Vo- 211).
43. OLEACEAE
174. *Olea europaea* L**.**
(Sh, M, S, T, I), Section, 2, 3, (Vo- 114).
44. ORCHIDACEAE
175. *Orchis collina* Banks & Sol. ex Russell.
(pe, M, I, S, T), Section, 4, (Vo- 241).
45. OROBANCHACEAE
176. *Orobanche aegyptiaca* Pers.
(an, M, I, S, T), Section, 2, 4, (Vo- 146).
46. PAPAVERACEAE
177. *Papaver decaisnei* Hochst. & Steud. ex Elkan.
(an, M, I, S, T), Section, 1, 3, 4, 6, (Vo- 22, 476).
178. *Papaver fugax* Poir.
(an, M, I, T), Section, 1, 2, 3, 4, 6, 7, (Vo- 212).
47. PINACEAE
179. *Pinus halepensis* Mill.
(Tr, M), Section, 1, 2, 3, 4, (Vo- 215, 480).
48. PLATANACEAE
180. *Platanus Orientalis* L.
(Tr, M, I, S, T), Section, 3, 5, (Vo- 149).
49. PLANTAGINACEAE
181. *Plantago major* L.
(Pe, M, I, S, T), Section, 6, (Vo- 175).
182. *Plantago cretica* L.
(an, M), Section, 3, (Vo-118).
183. *Plantago lanceolata* L.
(an, M, I, S, T), Section, 2, 4, 5, 7, (Vo- 243).
184. *Veronica anagallis* aquatic L.
(an, M, I, T), Section, 3, 4, (Vo- 1).
50. PLUMBAGINACEAE
185. *Plumbago europae* L.
(pe, M, I, S, T), Section, 2, 4, 6, (Vo- 12, 486).
51. POACEAE (GRAMIEAE)
186. *Aegilops columnaris* Zhuk.
(an, M, S, T, I), Section, 2, (Vo- 34).
187. *Avena fatua* L.
(an, M, I, S, T), Section, 2, 3, 4, 5, 7, (Vo- 216).
188. *Bromus tomentellus* Boiss.
(pe, M, I, S, T), Section, 3, 4, 7, (Vo- 60).
189. *Bromus tectorum* L.
(an, m, I, S, T), Section, 2, 3, 5, (Vo-176, 281).
190. *Bromus danthoniae* L.
(pe, M, S, T), Section, 2, 3, 5, (Vo- 72).
191. *Catabrosa aquatic* (L.) P. Beauv.
(pe, M, S, T), Section, 4, (Vo- 48).
192. *Cynodon dactylon* **(** L.) Pers
(pe, M, I, S, T) , Section, 1, 2, 3, 4, 5, 6, 7, (Vo- 119, 391).
193. *Echinaria capitata* (L.) Desf.
(an, M, I, S, T), Section, 3, 7, (Vo- 23).
194. *Echinochloa colonum* L.
(an, M, S, T, I), Section, 6, (Vo- 61).
195. *Hordeum glaucum* Steud.
(an, M, I, T, S), Section, 1, 2, 3, 5, (Vo- 150).
196. *Hordeum spontaneum* K.Koch.
(an, M, I, S, T), Section, 1, 2, 3, 4, 5, (Vo- 217).
197. *Hordeum vulgare* L.
(an, I, S, T), Section, 3, 4, 5, (Vo- 49).
198. *Hordeum bulbosum* L.
(Pe, m, I, S, T), Section, 3, 4, (Vo-244).
199. *Imperata cylindrica* (L.) P.Beauv.
(Pe, M, I, S, T), Section, 3, 4, (Vo-699)
200. *Lolium persicum* Boiss. & Hohen.
(an, M,T), Section, 7, (Vo-62).
201. *Lolium rigidum* Gaud.
(an, M, I, S, T), Section, 4, (Vo-13).
202. *Phalaris minor* Retz.
(an, M, S, T, I), Section, 4, 5, 6, (Vo- 177, 485).
203. *Phragmites australis* (Cav.) Trin. ex Steud.
(pe, M, I, S, T), Section, 2, 3, 7, (Vo- 120, 398).
204. *Poa bulbosa* L.
(pe, M, I, S, T), Section, 2, 3, 5, (Vo- 73).
205. *Poa annua* L**.**
(pe, M, I, S, T), Section, 3, 6, (Vo-84).
206. *Sorghum halepensis* (L.) Pers
(pe, M, I, S, T), Section, 3, 4, 6, (Vo-121).
207. *Polypogon monspeliensis* (L.) Desf.
(an, M, M, I)**,** Section, 6, (Vo-63).
208. *Triticum durum* Desf.
(an, M, I, T, S), 3, 4, 5, 6, 7, (Vo-218, 282).
52. POLYGONACEAE
209. *Polygonum aviculare* L.
(an, M, I, T**)**, Section, 3, (Vo-178).
210. *Rumex crispus* L.
(pe, M, I, T), Section, 1, 2, 3, 4, 5, (Vo-245).
211. *Rhuem ribes* L.
(Pe, M, I, T), Section, 6, (Vo-24).
53. PORTULACEAE
212. *Portulace oleraceae* L.
(an, M, I, S, T), Section, 4, 6, (Vo-122).
54. PRIMULACEAE
213. *Anagallis arvensis* L.
(an, M, I, S, T), Section, 1, 2, 4, 5, 6, (Vo-246).
55. PUNICACEA
214. *Punica granatum* L**.**
(Sh, M, I, T), Section, 1, 2, 3, 4, 5, 7, (Vo-179).
56. RANUNCULACEA
215. *Adonis aestivalis* L.

(an, M, S, T), Section, 2, 3, 4, 5, (Vo-35).
216. ***Adonis microcarpa*** DC.
(an, M, I, S, T), Section, 1, 2, 3, 4, 5, 6, 7, (Vo-123, 400).
217. ***Anemone coronaria*** L.
(pe, I, S, T), Section, 1, 2, 3, 4, 5, 6, 7, (Vo- 64).
218. ***Ranunculus arvensis L***.
(an, M, I, S, T), Section, 1, 2, 3, 6, (Vo- 14).
219. ***Ranunculus macrorhynchus*** Boiss.
(an, M, S, T), Section, 1, 2, 5, 6, (Vo-36, 490).
57.RHAMNACEAE
220. ***Paliurus spina-christi*** Mill.
(Sh, M, S, T, I), Section, 2, (Vo-219).
58. ROSACEAE
221. ***Crataegus azarolus*** L.
(Tr, M, I, S, T), 1, 2, 3, 4, 5, 6, 7 (Vo-180).
222. ***Crataegus monogyna*** L
(Tr, M, I, S, T) Section, 6, (Vo- 124).
223. ***Potentilla reptans*** L.
(pe, M, I, S, T), Section, 6, (Vo-51).
224. ***Poterium sanguisorba*** L.
(pe, M), Section, 2, 3, 6, (Vo-247, 500).
225. ***Prunus amygdalus*** Batsch.
(Tr, M, I, S, T), Section, 3, (Vo-212).
226. ***Prunus arabica*** (Oliv.) Meikle.
(Sh, M, I, S, T), Section, 1, 2, 3, 4, 5, (Vo-213).
227. ***Prunus argentea*** (Lam.) Rehd.
(Sh, M, I, S, T), Section, 2, 3, 4, (Vo- 115).
228. ***Prunus microcarpa*** C.A.Mey.var. ***pubescens*** (Bornm.') Meikle.
(Sh, M, I, S, T), Section, 1, 2, 3, 4, 5, (Vo-10).
229. ***Pyrus syriaca*** Boiss.
(Tr, M, I, S, T), Section, 4, (Vo-181,477).
230. ***Pyrus communis*** Boiss.
(Tr, M, I, T, S), Section, 3, 6, (Vo- 58).
231. ***Rosa canina*** L.
(Sh, M, I, S, T), Section, 6, (Vo- 70).
232. ***Rubus sanctus*** Schreb.
(Sh, M, S, I), Section, 1, (Vo- 242).
59. RUBIACEAE
233. ***Callipeltis cucullaris*** (L.) DC.
(an, M, I, T, S), Section, 3, 4, (Vo- 147).
234. ***Galium aparine*** L.
(an, M, I, T, S), Section, 3, 4, 5, 6, 7, (Vo-59).
235. ***Galium setaceum*** Lam. subsp.
(an, M, I, T, S), Section, 3, 4, (Vo-182).
236. ***Galium tricornutum*** Dandy.
(an, M, I, T, S), Section, 4, (Vo-25).
237. ***Sherardia arvensis*** L.
(an, M, I, S, T), Section, 5, 6, (Vo-87).
238.***Theligoniumcynocrambe***L.
(an, M, S, T, I), Section, 1, 3, 4, (Vo- 162).
60. SALICACEAE
239. ***PopuLus alba*** L.
(Tr, M, I, S, T), Section, 3, 6, (Vo-379).
240. ***Salix acmophylla*** Boiss.
(Tr, M, I, S, T), Section, 1, 3, 6, (Vo-116).
61. SOLANACEAE
241. ***Solanum S. nigrum*** L.
(an, M, I, T)Section, 4, 5, (Vo- 71).
62. TAMARICACEAE
242. ***Tamarix ramosissima*** Ledeb.
(Sh, M, I), Section, 7, (Vo-183).
63. TYPHACEAE
243. ***Typha lugdunensis*** P. Chab.
(pe, M, I, T), Section, 3, 7, (Vo-148).
64. ULMACEAE
244. ***Celtis tournifourtii*** Lam.
(Tr, M, I, S, T), Section, 1, 2, 3, 4, 5, 6, 7, (Vo-243, 479).
65. URTICACEAE
245. ***Urtica pilulifera*** fera.
(an, M, S, T, I), Section, 3, (Vo- 11)
66. VITACEAE
246. ***Vitis vinifera*** L.
(pe, M, I, T), Section, 1, 3, 4, 5, 6, (Vo- 117)
67.ZYGOPHYLACEAE
247. ***Tribulus terrestris*** **L.**
(an, M), Section, 3, 6, (Vo- 184, 293).

REFERENCES

Ahmad, S. A. (2013). Vascular plants of Hawraman Region in Kurdistan Iraq, Doctoral dissertation, Ph. D., Faculty of Agriculture Science, Sulaimani University, Iraq.

Ahmed, K. H. (2010). Vascular plants of Gomaspan Strait and their around-Erbil/Iraq.

Allard, G., & Moore, B. (2011). Invasive Species Survey Techniques: Plant Survey. *Protection and Health. Beijing*.

Al-Nabawi, A. K. (2002). *Hydrogeology and Hydrochemistry* of Harir basin-Iraqi Kurdistan, (Doctoral dissertation, M. Sc. Thesis, Salahaddin Univ., Erbil, 154p).

Authority, E. P. (2016). Technical Guidance-Flora and

Vegetation Surveys for Environmental Impact Assessment. *Perth: EPA*.

Beghin, T., Cope, J. S., Remagnino, P., & Barman, S.

Bor, N.L., Guest, E.1968. Flora of Iraq, Vol. 9. Ministry of Agriculture, Baghdad. Bridson, D., Forman, L. 1998. The Herbarium. Handbook. Royal Botanical Gardens, Kew, p.334.

Brummitt, R.K. and Powell, C.E. 1992. Authors of plant Names. Kew: Royal Botanic Gardens.

Darwesh, T. D. (2017). Plant biodiversity and Ethnobotanical properties of various Plants in Choman (Erbil-Iraq). Master Thesis, Department of Bioengineerring and Science. Kahraman Marash-Turkey.

Davis, P.H., 1965-1985. Flora of Turkey and the East Aegean Islands, Vol I-IX., Edinburgh University Press, Edinburgh.

Faris, Y. S. 1983. The Vascular Plant of Pira Magrun Mountain. Msc. Thesis, University of Salahaddin (In Arabic).

Ghaib, F. A., Al-Dawoody, A. M., & Koyi, H. A. (2009). Geological significance of Bouguer anomalies in Harir plain, northwest Zagros folds-thrust belt (Iraqi Kurdistan Region). *Nat Sci*, *7*, 43-51.

Ghazanfar, S. A., & McDaniel, T. (2016). Floras of the Middle East: a quantitative analysis and biogeography of the flora of Iraq. Edinburgh Journal of Botany, 73(1), 1-24.

Ghazanfar, A.A., Edmondson, J.R., 2013. Flora of Iraq vol. 5 part 2. Lythraceae to Campanulaceae. Ministry of Agriculture Republic of Iraq by Royal Botanic Gardens, KEW.

Guest, E. (1966), Flora of Iraq. Pub. By Ministry of Agriculture of Republic of Iraq. Bagdad.Vol. 1.

Hameed, M., A. (2016). Vascular Plant Taxa of Hujran Basin-Erbil/Iraq. KSU Journal of Natural Sciences, 19(3): 279-295.

Heard, L., & Channon, B. (1997). Guide to a native vegetation survey (Agricultural Region) using the Biological Survey of South Australia methodology. *Department for Environment and Heritage, South Australia*, 49.

Khalaf, M. K. 1980. The Vascular Plants of Sinjar Mountain. M.Sc. Thesis, Baghdad University. (In Arabic).

MabberLY, D, J. (2008). Moberly's Plant-Book. Cambridge University press.https://www.cambridg org/core/s/mabberleys-plantbook.

Saeed, J, F. (2002). Flowering plants of Gali Alibag (George). Zanco, Journal of pure Applied Science. Salahaddin University Vol.1. 2002.

Towsend, C. C., Guest, E., 1966-1985. Flora of Iraq Vol. 1-8."Baghdad: Ministry of Agriculture, Iraq

Whiting, D., A. O'Connor, J. Jones, L. Potts. (2014). State Taxonomic Classification. Color University. Extension. CMG Garden Notes. Research Report. 122(1-8) *P*

Zohary, M. (1973). Geobotanyical Foundation of the Middle East, Vol I-II, Guestav Fischer Verlag, Stutgart.

ZANCO Journal of Pure and Applied Sciences
The official scientific journal of Salahaddin University-Erbil
https://zancojournals.su.edu.krd/index.php/JPAS

ISSN (print):2218-0230**, ISSN (online):** 2412-3986**, DOI: http://dx.doi.org/10.21271/zjpas**

RESEARCH PAPER

Association of Afamin Concentration with Type 1 and Type 2 Diabetes Mellitus

Rebwar Jalal Ali , Sardar Nouri Ahmed

Department of Basic Science-Biochemistry Unit, College of Medicine, Hawler Medical University-Erbil, Erbil City, Kurdistan Region, Iraq

A B S T R A C T:

Afamin is a protein in humans that plays a major role in the regulation of glucose metabolism, insulin sensitivity, so it may be related to diabetes mellitus. The aim of this study to evaluate the afamin concentration level in diabetic patients. This study was a case-control study blood samples were collected from 130 patients of Diabetes mellitus (DM) which divided into two groups (65 types1 DM and 65 type 2 DM) from Laila Qasim center for diabetes in Erbil City. In addition90 healthy volunteers used as a control. Serum was separated to determine afamin concentration. The results showed that the level of afamin in type 2 diabetic patients were significantly higher than those of healthy adults (75.09 $\pm$ 10.09 mg/L), and (65.62 $\pm$ 7.18 mg/L) respectively, No significant differences in the concentration of afamin were observed between control and type 1 DM were (58.47 ± 8.13), and (63.07 ± 5.53) respectively. Our finding showed that increase serum afamin concentration in type 2 diabetes patients can be used as a biomarker for predicting diabetes mellitus.

KEY WORDS: Serum afamin, type 1 DM, type 2 DM
DOI: http://dx.doi.org/10.21271/ZJPAS.33.5.8
ZJPAS (2021) , 33(5);69-75 .

1.INTRODUCTION :

Afamin also named vitamin E binding protein is a protein in humans encoded by the *AFM* gene, which was founded in 1994 as the fourth constituent of the human albumin gene family which is comprised of four genes, and these four genes encode structurally-related serum transport proteins or binding protein. Afamin is an 87 kDa glycoprotein with five predicted N-glycosylation sites with 15% carbohydrate content and 55% amino acid sequence similarity to albumin. Human afamin gene (AFM) sequence size 1981 bp. AFM gene in humans has 15 exons and composed of 599 amino acids. Genomic location on chromosome 4q13-3 in humans is mainly expressed in the liver and secreted into the bloodstream (Lichenstein et al., 1994).

Afamin protein acts similarly to albumin as a transport protein for small hydrophobic molecules. A high-level amount of this protein found in plasma but circulating plasma afamin is primarily of hepatic origin; the brain, kidney, testes, and ovaries have been found as additional afamin-expressing tissues, body fluids, like follicular, cerebrospinal, and seminal fluid. A strong association between afamin protein levels in these fluids (Jerkovic et al., 2005).

Prevalence of diabetes have been steadily increasing worldwide according to this data in the years 2017, 463 million people had diabetes worldwide, , approximately 90% of diabetes were type 2 DM (Vos et al., 2012). Another study shows that the number of patients with diabetes mellitus globally has four times more than in the past three decades (Zheng et al., 2018)

Diabetes mellitus divided into two main types which are type1 diabetes (T1DM) and type2

* **Corresponding Author:**
Rebwar Jalal Ali
E-mail: rebwara11@yahoo.com
Article History:
Received: 26/02/2021
Accepted: 03/07/2021
Published: 20/10 /2021

diabetes (T2DM) the major difference between these two types are relate following criteria first of all age, amount of loss of Beta Cell function, and insulin resistance or associated autoantibodies. Also, there are several causes for diabetes classification which are obesity at a young age and genetic factors for T1DM and T2DM(Leslie et al., 2016)

T1 DM named insulin-dependent diabetes mellitus (IDDM), this name come from that the pancreas cannot produce enough insulin as a result of a loss of B cell, T1DM commonly known in children and early age population.

T2DM named non-insulin-dependent diabetes mellitus (NIDDM) because cells fail to respond to the insulin produced by B cell properly means cells of the body resist to insulin, therefore, named insulin resistance, T2DM more common in adult and old age persons but causes due to excessive body weight, lifestyle, healthy diet and insufficient exercise (Delhi, 2012).

The study results show that the strong relationship between afamin plasma levels and all the components of metabolic syndrome were shown to occur not only at baseline, but also at follow-up, these findings of hyperlipidemia, hyperglycemia, and obese phenotype suggest a possible role of afamin protein infrequently observed metabolic disturbances, such as metabolic syndrome (Kronenberg et al., 2014).

Another study concluded that the value of afamin plasma levels in the female with polycystic ovary disorder (PCOS), a disease directly associated with the related signs of metabolic syndrome and type 2 diabetes mellitus, regarding the presence of insulin resistance. Furthermore, women with insulin resistance exhibited higher levels of afamin, regardless of the presence of PCOS. The researchers concluded that afamin serves as a prognostic marker of insulin resistance in young women with PCOS (Seeber et al., 2014).

The data of a pooled study showed that more than 20,000 participants, according to this study afamin protein level can be used or having benefits in clinical diagnostic. Each elevated afamin concentration level by 10 mg/l was related to an increase in the prevalence of type 2 diabetes mellitus, while afamin protein was also determined to be positively associated with insulin resistance. The data of this study concluded that the afamin levels are positively and significantly related to insulin resistance and type 2 diabetes mellitus therefore afamin can be used as a novel marker for the detection of type 2 diabetes (Kollerits et al., 2017).

According to the last new study that the afamin protein level in T1DM lower than the healthy children when compared it, according to this study Adropin, afamin, and neudesin are regulatory peptides may play a large role in the regulation of glucose metabolism especially carbohydrate metabolism, There are a few article papers about afamin in type 1 diabetes mellitus in children (Polkowska et al., 2019)

The aim of the study was to found concentration of afamin protein level and demonstrate it to investigate the suitability of using afamin as an early marker for the detection of T2 DM and T1 DM, Also Compare the results of the afamin protein concentration between type1 and type2 diabetes patients.

2.Materials and methods

The study was a case-control study consisted of 220 blood samples aged from (2 – 81) years (Male 115 female 105). During the period from January 2020 to September 2020. Collected samples include 130 patients with diabetes mellitus having the clinical symptoms were diagnosed by laboratory tests such as blood glucose and HbA1c, who were treated at Laila Qasim center for diabetic patients in Erbil City from Kurdistan region, which divided into two equal groups (65) of type 1 DM and (65) of type 2 DM , in addition to intact 90 volunteers without clinical signs of any diseases used as a control, after taking informed consent a standard questionnaire was filled out for the patients and controls, Statistical analysis was based on anthropometric parameters such as age, height, and weight and laboratory tests (HbA1c) using standard methods we included children and adults for both group case and control

Serum was separated to perform by Enzyme-linked immunosorbent assay (ELISA) (ELx800-BioTeK80, U.S.A) in Medical Research Center we used human afamin (AFM) kit produced by fine test Biotech Company to examine the association of afamin protein with diabetes mellitus (company, 2020).

Statistical Analysis

Statistical Package for Social Science (SPSS) software version 26 was used for data analysis. , while quantitative variables were stated as the

mean standard deviation (SD) . A P value at p ≤0.05 was measured statistically significant (Di Leo and Sardanelli, 2020).

3.Results:

The healthy group was (n=90) and the diabetic group also categorized into two types of patients type2 (n=65) and type1 (n=65) diabetes, which control was two groups, therefore the study populations group divided into four groups which were separated to type 1 diabetes with control of type 1 and type 2 diabetes with control of type 2.

Table 1 shows that the mean age of type 1 participants (13.88 ± 4.34) years and controls of type 1 were (14.95 ± 9.9) years, about mean age T2DM were (52.82 ± 11.92) years and controls of type 2 were (43.44 ± 15.71) years.

The study results showed the different afamin concentration level ranges when compare type 1 and type 2 diabetes with the control group, Table 2. Shows that the significant results of elevated afamin concentration in type 2 diabetes by (9.5 mg/L) compared control group the mean serum afamin in T2DM were (75.09 ± 10.09 mg/L) and control group was (65.62 ± 7.18 mg/L). About type 1 diabetes the result showed a significant result that the mean afamin protein levels in type 1 diabetes participants were (58.47 ± 8.13) this value lower by (4.6 mg/L) than the mean of a control group for type 1 diabetes (63.07 ± 5.53).

According to table 3 the biochemical tests which were glucose, glycated hemoglobin (HbA1c), and albumin level in type 1, diabetes and control group of type 1 DM. The results demonstrate statically significant (p< 0.001) for both glucose and (HbA1C). The means glucose for patient and control were (232.77 ± 97.33), (91.85 ± 12.1) and the means for HbA1C for both groups were (9.18 ± 2.06), (4.93 ± 0.65) respectively but about albumin level statically was non-significant (p> 0.05), the means of albumin level for T1DM and control were (4.71 ± 0.59), (4.72 ± 0.466).

Table 4 showed glucose, glycated hemoglobin (HbA1c), and albumin level in type 2 diabetes with the control group of type 2 the results describe statically significant (p<0.001)for both glucose and (HbA1C). The means glucose for patient and control were (253.38 ± 128.78), (99.48 ± 11.35) with the means for HbA1C for both groups were (9.26 ± 2.12), (5.5 ± 0.39), but about albumin level statically was non-significant (p< 0.01), the means of albumin level for T2DM and control were (4.17 ± 0.455), (4.56 ± 0.65) respectively.

The data of body mass index (BMI) in table 5 for both types of diabetes and controls the results of mean BMI in type 1 diabetes group and control group were (19.12 ± 3.15), (18.85 ± 3.54) respectively. Results statically non-significant (p> 0.05), BMI measured significantly higher among T2DM patients than control group data shows statically significant (p< 0.001) the means were (28.54 ± 3.7), (24.36 ± 2.4) respectively.

4.Discussion

The present study demonstrated that serum afamin concentration has related to diabetes mellitus especially type 1 and type 2 diabetes. And this results is confirmed by many scientific papers.

Afamin concentrations have been founded in various other types of diabetes except type 1 and type 2 diabetes such as gestational diabetes mellitus (Koninger et al., 2018). Afamin protein expression was investigated in various disease studies such as carcinoma which were breast cancer and thyroid cancer (Wang et al., 2020). Relate to this protein more studied done about it which are metabolic syndrome patients and diabetes especially type 2 diabetes but about type 1 diabetes we evaluated afamin level in children, till now have little information about it, Further research is needed about afamin level in type 1 diabetes (Kronenberg et al., 2014).

Data showed that the afamin level was increased in type 2 diabetes patients mean overexpressing human afamin in type 2 diabetes, in the other side the results of our analysis show that the mean afamin concentration were statistically lower children with diabetes type 1 compared to the control group, the results in our study found that the afamin concentration was significantly associated with diabetes mellitus.

Our results were in agreeement with another studies results were done about type 2 diabetes before which confirmed that overexpression of serum afamin by (9.5 mg/l) in our results the mean afamin concentration was (75.09 ±10.09 mg/l) in type 2 diabetes while in the healthy individual was (65.62 ± 7.18) our data close to another papers data (Kollerits et al., 2017).

Metabolic syndrome another factor that correlated with type 2 diabetes, metabolic syndrome is a combination of type 2 diabetes and cardiovascular

disease (CVD) including dyslipidemia, hyperglycemia and insulin resistance, abdominal obesity, and hypertension these factors have a role in elevated afamin concentration according to this study that the afamin is a promising novel marker for metabolic syndrome and related diseases, therefore by increasing obesity or body mass index (BMI) with type 2 diabetes serum afamin concentration increase, table 5 show that the mean (BMI) in T2DM was (28.54 ± 3.7) which is confirm with Kronenberg F. study (Kronenberg and Dieplinger, 2015). About type 1 diabetes mellitus from table 2 data showed that the mean serum afamin was lower than the control group by (4.6 mg/l), the explanation for our results afamin protein act as regulators of glucose metabolism according to a study which supports our data of afamin in type 1 diabetes a drop-in, afamin, and neudesin may play a major role in the glucose metabolism regulation (Polkowska et al., 2019).

Another criteria we founded from the mean age of table 1 was the comparison between the ages of both types of diabetes, the study described that the type 1 diabetes mellitus age in the early stages of life occur in children while T2DM occurs in adult age after 45 years (Leslie et al., 2016). The means age of type 1 and type 2 diabetes were (13.88 ± 4.34) and (52.82 ± 11.924) respectively. Because the exact cause unknown there are several causes first of all genetic factor and body's immune system in early age for type 1 DM (Leslie et al., 2016).

Table 1. The mean age of control and diabetic patients

	Control and patient	N	Mean ± SD	Minimum	Maximum
Age (Years)	Type 1 diabetesx	65	13.88 ± 4.34	6	25
	Control type1	40	14.95 ± 9.905	2	41
	Type 2 diabetes	65	52.82 ± 11.924	20	80
	Control type2	50	43.44 + 15.71	19	81

Table 2. Serum afamin concentraion in diabetes patient and control participant

	Control and patient	N	Mean ± SD	P-value
Afamin level Mg/L	Type 1 diabetes	65	58.47 ± 8.13	< 0.01
	Control type1	40	63.07 ± 5.53	
	Type 2 diabetes	65	75.09 ±10.09	< 0.001
	Control type2	50	65.62 ± 7.18	

Table 3.The levels of serum glucose, albumin, and blood (HbA1C) in type 1 DM and control groups

	Type1 diabetes N=65 Mean ± SD	Control N=40 Mean ± SD	P-value
Glucose (mg/dl)	**232.77 ± 97.33**	**91.85 ± 12.1**	**< 0.001**
HbA1C (%)	**9.18 ± 2.06**	**4.93 ± 0.65**	**< 0.001**
Albumin (g/dl)	**4.71 ± 0.59**	**4.72 ± 0.466**	**> 0.05**

Table 4. Levels of serum glucose, albumin, and blood (HbA1C) in type 2 DM and control groups

	Type2 diabetes N=65 Mean ± SD	Control N=50 Mean ± SD	P-value
Glucose (mg/dl)	**253.38 ± 128.78**	**99.48 ± 11.35**	**< 0.001**
HbA1C (%)	**9.26 ± 2.12**	**5.5 ± 0.39**	**< 0.001**
Albumin (g/dl)	**4.17 ± 0.455**	**4.56 ± 0.65**	**< 0.01**

Table 5. Comparison of BMI in type 1 and type 2 DM with control groups

	Control and patient	N	Mean ± SD	P-value
Body Mass Index (BMI) kg/m^2	**type 1 diabetes**	**65**	**19.12 ± 3.15**	**> 0.05**
	control type1	**40**	**18.85 ± 3.54**	
	type 2 diabetes	**65**	**28.54 ± 3.7**	**< 0.001**
	control type2	**50**	**24.36 ± 2.4**	

5.Conclusion

This study concluded according to the results that the serum afamin concentration was found significantly higher in type 2 diabetes mellitus group patients than healthy individuals these results help us to use afamin as a biomarker with diabetes mellitus especially with type 2 diabetes as well as in type 1diabetes our study demonstrate that the afamin concentration decreased compare to healthy child's, also we need further research to determine afamin level in type 1 diabetes, in the other side, the result showed that the persons with high body mass index, especially in type 2 diabetes mellitus, has more afamin concentration than normal BMI persons.

6.Recommendation

We can use afamin as a biomarker with diabetes mellitus especially with type 2 diabetes.

About afamin level in type 1 diabetes has a few studies to confirm our result we need further research to obtain significant data or use as a biomarker for type 1 diabetes patients. The metabolic syndrome is defined as the coexistence of several risk factors for both type 2 diabetes mellitus and cardiovascular disease. Therefore preventative and recommendation need to avoid the causes of metabolic syndrome by aggressive lifestyle modification focusing on weight-loss and physical activity.

ACKNOWLEDGMENT

We will express our gratitude to those who helped us especially my supervisor (Dr. Sardar Nouri Ahmed), and special thanks to Hawler Medical University-Medical Research Center and College of medicine/ department of the basic science-biochemistry unit for their support during the period of achievement of this research.

Reference:

COMPANY, F. T. 2020. Human AFM(Afamin) ELISA Kit [Online]. Available: https://www.fn-test.com/product/eh2493/ [Accessed].

DELHI, N. J. R. T. O. D. M. N. E. N. D. N. D. J. B. M. P. 2012. textbook of diabetes mellitus. 2nd ed, Jaypee Brothers Medical Publishers

DI LEO, G. & SARDANELLI, F. J. E. R. E. 2020. Statistical significance: p value, 0.05 threshold, and applications to radiomics—reasons for a conservative approach. 4, 1-8.

JERKOVIC, L., VOEGELE, A. F., CHWATAL, S., KRONENBERG, F., RADCLIFFE, C. M., WORMALD, M. R., LOBENTANZ, E. M., EZEH, B., ELLER, P., DEJORI, N., DIEPLINGER, B., LOTTSPEICH, F., SATTLER, W., UHR, M., MECHTLER, K., DWEK, R. A., RUDD, P. M., BAIER, G. & DIEPLINGER, H. 2005. Afamin is a novel human vitamin E-binding glycoprotein characterization and in vitro expression. J Proteome Res, 4, 889-99.

KOLLERITS, B., LAMINA, C., HUTH, C., MARQUES-VIDAL, P., KIECHL, S., SEPPALA, I., COOPER, J., HUNT, S. C., MEISINGER, C., HERDER, C., KEDENKO, L., WILLEIT, J., THORAND, B., DAHNHARDT, D., STOCKL, D., WILLEIT, K., RODEN, M., RATHMANN, W., PAULWEBER, B., PETERS, A., KAHONEN, M., LEHTIMAKI, T., RAITAKARI, O. T., HUMPHRIES, S. E., VOLLENWEIDER, P., DIEPLINGER, H. & KRONENBERG, F. 2017. Plasma Concentrations of Afamin Are Associated With Prevalent and Incident Type 2 Diabetes: A Pooled Analysis in More Than 20,000 Individuals. Diabetes Care, 40, 1386-1393.

KONINGER, A., MATHAN, A., MACH, P., FRANK, M., SCHMIDT, B., SCHLEUSSNER, E., KIMMIG, R., GELLHAUS, A. & DIEPLINGER, H. 2018. Is Afamin a novel biomarker for gestational diabetes mellitus? A pilot study. Reprod Biol Endocrinol, 16, 30.

KRONENBERG, F. & DIEPLINGER, H. J. C. L. 2015. Afamin is a promising novel marker for metabolic syndrome and related diseases. Clinical Lipidology, 10, 207-3.

KRONENBERG, F., KOLLERITS, B., KIECHL, S., LAMINA, C., KEDENKO, L., MEISINGER, C., WILLEIT, J., HUTH, C., WIETZORREK, G., ALTMANN, M. E., THORAND, B., MELMER, A., DAHNHARDT, D., SANTER, P., RATHMANN, W., PAULWEBER, B., KOENIG, W., PETERS, A., ADHAM, I. M. & DIEPLINGER, H. 2014. Plasma concentrations of afamin are associated with the prevalence and development of metabolic syndrome. Circ Cardiovasc Genet, 7, 822-9.

LESLIE, R. D., PALMER, J., SCHLOOT, N. C. & LERNMARK, A. J. D. 2016. Diabetes at the crossroads: relevance of disease classification to pathophysiology and treatment. 59, 13-20.

LICHENSTEIN, H. S., LYONS, D. E., WURFEL, M. M., JOHNSON, D. A., MCGINLEY, M. D., LEIDLI, J. C., TROLLINGER, D. B., MAYER, J. P., WRIGHT, S. D. & ZUKOWSKI, M. M. 1994. Afamin is a new member of the albumin, alpha-fetoprotein, and vitamin D-binding protein gene family. J Biol Chem, 269, 18149-54.

POLKOWSKA, A., PASIEROWSKA, I. E., PASLAWSKA, M., PAWLUCZUK, E. & BOSSOWSKI, A. 2019. Assessment of Serum Concentrations of Adropin, Afamin, and Neudesin in Children with Type 1 Diabetes. Biomed Res Int, 2019, 6128410.

SEEBER, B., MORANDELL, E., LUNGER, F., WILDT, L. & DIEPLINGER, H. 2014. Afamin serum concentrations are associated with insulin resistance and metabolic syndrome in polycystic ovary syndrome. Reprod Biol Endocrinol, 12, 88.

VOS, T., FLAXMAN, A. D., NAGHAVI, M., LOZANO, R., MICHAUD, C., EZZATI, M., SHIBUYA, K., SALOMON, J. A., ABDALLA, S. & ABOYANS, V. J. T. L. 2012. Years lived with disability (YLDs) for 1160 sequelae of 289 diseases and injuries 1990–2010: a systematic analysis for the Global Burden of Disease Study 2010. 380, 2163-2196.

WANG, W. K., TSAI, C. H., LIU, Y. W., LAI, C. C., HUANG, C. C. & SHEEN-CHEN, S. M. 2020. Afamin expression in breast cancer. Asian J Surg, 43, 750-754.

ZHENG, Y., LEY, S. H. & HU, F. B. 2018. Global aetiology and epidemiology of type 2 diabetes

mellitus and its complications. Nat Rev Endocrinol, 14, 88-98.

COMPANY, F. T. 2020. Human AFM(Afamin) ELISA Kit [Online]. Available: https://www.fn-test.com/product/eh2493/ [Accessed].

DELHI, N. J. R. T. O. D. M. N. E. N. D. N. D. J. B. M. P. 2012. textbook of diabetes mellitus. 2nd ed, Jaypee Brothers Medical Publishers

DI LEO, G. & SARDANELLI, F. J. E. R. E. 2020. Statistical significance: p value, 0.05 threshold, and applications to radiomics—reasons for a conservative approach. 4, 1-8.

JERKOVIC, L., VOEGELE, A. F., CHWATAL, S., KRONENBERG, F., RADCLIFFE, C. M., WORMALD, M. R., LOBENTANZ, E. M., EZEH, B., ELLER, P., DEJORI, N., DIEPLINGER, B., LOTTSPEICH, F., SATTLER, W., UHR, M., MECHTLER, K., DWEK, R. A., RUDD, P. M., BAIER, G. & DIEPLINGER, H. 2005. Afamin is a novel human vitamin E-binding glycoprotein characterization and in vitro expression. J Proteome Res, 4, 889-99.

KOLLERITS, B., LAMINA, C., HUTH, C., MARQUES-VIDAL, P., KIECHL, S., SEPPALA, I., COOPER, J., HUNT, S. C., MEISINGER, C., HERDER, C., KEDENKO, L., WILLEIT, J., THORAND, B., DAHNHARDT, D., STOCKL, D., WILLEIT, K., RODEN, M., RATHMANN, W., PAULWEBER, B., PETERS, A., KAHONEN, M., LEHTIMAKI, T., RAITAKARI, O. T., HUMPHRIES, S. E., VOLLENWEIDER, P., DIEPLINGER, H. & KRONENBERG, F. 2017. Plasma Concentrations of Afamin Are Associated With Prevalent and Incident Type 2 Diabetes: A Pooled Analysis in More Than 20,000 Individuals. Diabetes Care, 40, 1386-1393.

KONINGER, A., MATHAN, A., MACH, P., FRANK, M., SCHMIDT, B., SCHLEUSSNER, E., KIMMIG, R., GELLHAUS, A. & DIEPLINGER, H. 2018. Is Afamin a novel biomarker for gestational diabetes mellitus? A pilot study. Reprod Biol Endocrinol, 16, 30.

KRONENBERG, F. & DIEPLINGER, H. J. C. L. 2015. Afamin is a promising novel marker for metabolic syndrome and related diseases. Clinical Lipidology, 10, 207-3.

KRONENBERG, F., KOLLERITS, B., KIECHL, S., LAMINA, C., KEDENKO, L., MEISINGER, C., WILLEIT, J., HUTH, C., WIETZORREK, G., ALTMANN, M. E., THORAND, B., MELMER, A., DAHNHARDT, D., SANTER, P., RATHMANN, W., PAULWEBER, B., KOENIG, W., PETERS, A., ADHAM, I. M. & DIEPLINGER, H. 2014. Plasma concentrations of afamin are associated with the prevalence and development of metabolic syndrome. Circ Cardiovasc Genet, 7, 822-9.

LESLIE, R. D., PALMER, J., SCHLOOT, N. C. & LERNMARK, A. J. D. 2016. Diabetes at the crossroads: relevance of disease classification to pathophysiology and treatment. 59, 13-20.

LICHENSTEIN, H. S., LYONS, D. E., WURFEL, M. M., JOHNSON, D. A., MCGINLEY, M. D., LEIDLI, J. C., TROLLINGER, D. B., MAYER, J. P., WRIGHT, S. D. & ZUKOWSKI, M. M. 1994. Afamin is a new member of the albumin, alpha-fetoprotein, and vitamin D-binding protein gene family. J Biol Chem, 269, 18149-54.

POLKOWSKA, A., PASIEROWSKA, I. E., PASLAWSKA, M., PAWLUCZUK, E. & BOSSOWSKI, A. 2019. Assessment of Serum Concentrations of Adropin, Afamin, and Neudesin in Children with Type 1 Diabetes. Biomed Res Int, 2019, 6128410.

SEEBER, B., MORANDELL, E., LUNGER, F., WILDT, L. & DIEPLINGER, H. 2014. Afamin serum concentrations are associated with insulin resistance and metabolic syndrome in polycystic ovary syndrome. Reprod Biol Endocrinol, 12, 88.

VOS, T., FLAXMAN, A. D., NAGHAVI, M., LOZANO, R., MICHAUD, C., EZZATI, M., SHIBUYA, K., SALOMON, J. A., ABDALLA, S. & ABOYANS, V. J. T. L. 2012. Years lived with disability (YLDs) for 1160 sequelae of 289 diseases and injuries 1990–2010: a systematic analysis for the Global Burden of Disease Study 2010. 380, 2163-2196.

WANG, W. K., TSAI, C. H., LIU, Y. W., LAI, C. C., HUANG, C. C. & SHEEN-CHEN, S. M. 2020. Afamin expression in breast cancer. Asian J Surg, 43, 750-754.

ZHENG, Y., LEY, S. H. & HU, F. B. 2018. Global aetiology and epidemiology of type 2 diabetes mellitus and its complications. Nat Rev Endocrinol, 14, 88-98.

ZANCO Journal of Pure and Applied Sciences
The official scientific journal of Salahaddin University-Erbil
https://zancojournals.su.edu.krd/index.php/JPAS

ISSN (print):2218-0230**, ISSN (online):** 2412-3986**, DOI: http://dx.doi.org/10.21271/zjpas**

RESEARCH PAPER

Hematological and biochemical status of βeta-thalassemia major patients in Koya city.

Kochar Kh. Saleh[1,2], Esmail S. Kakey[3]

[1]Department of Community Health, Koya Technical Institute, Erbil Polytechnic University, Erbil, Kurdistan Region-Iraq
[2]Department of Biology, College of Science, Firat University, Elazığ, 23000, Turkey
[3]Department of Biology, Faculty of Science and Health, Koya University, Koya KOY45, Kurdistan Region-Iraq.

A B S T R A C T:

Thalassemia major is a severe anemia that requires blood transfusions. In this study, we searched into the hematological and biochemical status of βeta-thalassemia major patients in Koya. Hematological analysis revealed severe anemia in βeta-thalassemia patients when compared to controls. The hemoglobin levels in patients were less than 30% of that of controls. Furthermore, patients had a significant leukocytosis compared to the controls. Red blood cell incidences are decreased except RDW, which were Hct includes (23.8±2.9 % vs. 34.6±2.3 %), MCV (71.8±7.1 fl vs. 77.5±4.1 fl), MCH (20.2±2.4 pg vs. 23.5 ± 2.2 pg) and MCHC (30.8±0.7 g/dl vs. 30.1±1.2 g/dl), while RDW % (20.5±9.7 % vs. 14.2±2.5 %). The linear regression analysis showed non-correlation between iron overload with RBC, WBC, and red blood cell incidences (hemoglobin (Hb), hematocrit (Hct), mean corpuscle hemoglobin (MCH), and mean corpuscle hemoglobin concentration (MCHC), while PLT count, mean corpuscular volume (MCV) and red cell distribution width (RDW) showed a significant positive correlation with iron overload. The biochemical characteristics of the patients showed a significant increase in the levels of liver enzymatic parameters, ALP, ALT, and AST as compared to controls.

KEY WORDS: Anemia, βeta-thalassemia major, Hematological change, Biochemical change.
DOI: http://dx.doi.org/10.21271/ZJPAS.33.5.9
ZJPAS (2021) , 33(5);76-84 .

1. INTRODUCTION:

Thalassemia is a term referring to a class of genetic disorders caused by inadequate hemoglobin development, with a deficiency in hemoglobin synthesis. It is sometimes referred to as Mediterranean anemia. Thalassemia impacts European, African, and Asian people [1, 2].

Thalassemia is one of the world's most severe genetic disorders. It is the most common cause middle east persistent hemolytic anemia [3, 4]. In some nations, the distribution of beta thalassemia major appears dependent on ethnics and community relationships [5]. In order to understand how thalassemia influences the human body, we first need to understand how blood lais created. If the body does not generate enough globin alpha and beta chains, the red blood cells will not shape correctly and will not be able to carry enough oxygen. The effect is anemia that begins in early childhood and persists for life. Genes involved are those regulating the development of hemoglobin-containing alpha and

* **Corresponding Author:**
Kochar Khasro Saleh
E-mail: kochar.khasro.saleh@gmail.com or kochar.saleh@epu.edu.iq
Article History:
Received: 30/07/2020
Accepted: 08/07/2021
Published: 20/10 /2021

beta-globin [6]. Thalassemia may be identified by signs or by the impaired genes. The two major forms of thalassemia, alpha, and beta, are named for the two normal adult hemoglobin protein chains [7]. Beta thalassemia major is an inherited defect hemolytic state in the synthesis of the beta-globin chain, individuals with beta-thalassemia major usually present with severe anemia in the first two years of life, requiring regular transfusions of red blood cells (RBCs) to survive in life [8]. Impaired beta-globin biosynthesis contributes to an aggregation of unpaired alpha-globin string, the shorter life span of red cells, and iron deficiency triggering functional and physiological defects in many organ systems such as the pancreas, which lead to diabetic in some of the patients [9, 10]. The purpose of this study was to compare the liver function parameters, kidney function parameters, and hematological features of beta-thalassemia patients to a control group of children from Koya City.

2. MATERIALS AND METHODS

2.1. Study design:

The present investigation consists of 86 subjects divided equally between two groups as shown in (Figure 1), the first group consists of 43 β-thalassemia major children currently being transfused and managed for the clinical symptoms and manifestations of the disease at the Shaheed Dr. Khalid Teaching Hospital, and the second group consists of healthy control study design. No significant differences appear in the ages between patients and control groups The controls were patient age and sex-matched, the mean patient age (9.1±2.2 years) and the controls (8.8±1.9 years) of this study. Six 6 Milliliters of venous blood samples were collected from each patient with a disposable syringe prior to the planned blood transfusion. This was then used to predict checks on hematological and biochemical parameters.

2.2. Collection of data:

The analysis included 43 transfusion-dependent β-thalassemia majors of different ages and communities from different regions and villages in Koya. Both patients receive a daily transfusion of blood. Several patients underwent splenectomy and had additional iron deficiency surgical problems.

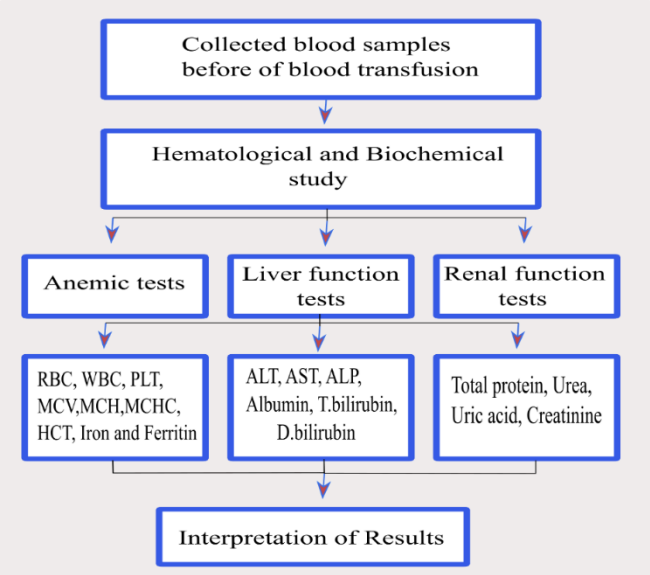

Figure 1. general design of the research.

In addition, the research data collected for the type of causative mutation, biochemical and hematological parameters of the β-thalassemic minor by questionnaire and blood test examination. Before blood transfusion, the consultation with the patients and their caregivers and relatives was held in Shaheed Dr. Khalid's general hospital. Specific information is taken from each person at the point of thalassemia diagnosis, including name, sex, race, residency, and education, in general, whether it was before or after one year of age. A detailed and thorough record of the disease provided then asked questions about the family history, which included consanguinity between parents (Figure 2), number of infected and unaffected children, number of dead siblings of any thalassemic kin.

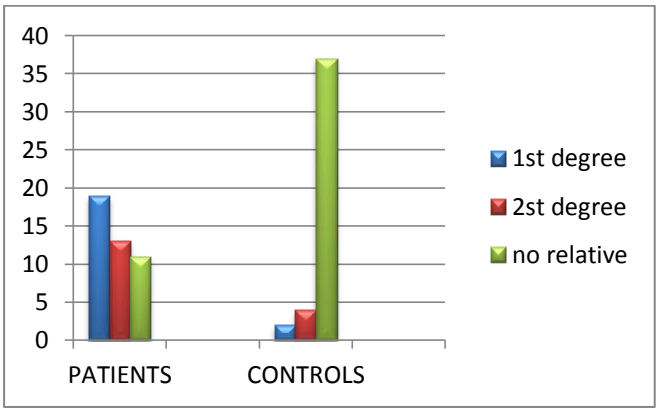

Figure 2. Degree of consanguinity among patients.

In general, data relating to blood transfusion (the total number and rate of blood transfusion and any transfusion-related complications) and chelation

therapy (chelation sort and regularity) were analyzed. Splenectomy was specifically asked about it and its pacing. Anemia, physical improvements, and skin pigmentation were then investigated by each person. In their visiting hours, they asked to fill out a survey application of medical review and before blood transfusion. Forty-three of the healthy people from various Koya groups (without Hemoglobin disorders) are spontaneously aged and paired with the patient populations used as a control group.

2.3. Biochemical analysis:

Fully automatic chemical analyzer used to evaluate biochemical parameters (Human Star-180), hematological parameters: blood samples are analyzed for blood parameters using a fully automated hematological analyzer in accordance with the protocol of the manufacturer. On the day the blood samples were taken, the hematological parameters (WBC, RBC, Hb, Plt, Hct, and MCV, MCH, and MCHC) are evaluated.

2.3. Statistical analysis:

The current study data were expressed as mean, a standard mean deviation (Mean ± S.D.M) and statistical software (SPSS) (Version 20) was used to analyze the data. Two T-test samples (independent student t-test between healthy and thalassemia patients and paired sample t-test between male thalassemia and female thalassemia) and correlation coefficient were used to analyze differences in mean values between 2 groups. The level of significance of P-value ($P<0.05$) was probably considered statistically significant.

3. RESULTS

Approximately 44% of the major children's parents with β-thalassemia are first-degree cousins compared to the control group with a percentage of less than 5%. In fact, the percentage of 2nd degree consanguineous marriages in the patient groups is significantly higher than that of the control group, 30.2 %, and 9.3 % respectively. The general characteristics of the study groups mentioned in (Table 1A).

3.1. Clinical characteristics of thalassemia

The general and clinical characteristics of the patients are summarized in (Table 1B) which revealed that the majority (67.4%) of the patients are receiving a blood transfusion every 2-3 weeks and 29.9 % every 4 -5 weeks. While only two patients (4.6%) require transfusion at longer intervals, more than 5 weeks.

Table 1A. General characteristics of the studied population.

Variables	Patients group (n=43)		
Age / year	Male	Female	Total
	8.9±2.3	8.8±1.4	9.1±2.2
Number	23	20	43
Percentage	53.48	46.51	100
Parents consanguinity	**Patients group (n=43)**		
Degree of consanguinity	1st degree	2nd degree	No relative
Number	19	13	11
Percentage	44.1	30.2	25.5
Results expressed as Mean ±SD			

Table 1B. General characteristics of the studied population.

Variables	**Controls group (n=43)**		
Age / year	Male	Female	Total
	9±2.3	8.7±3.1	8.8±1.9
Number	23	20	43
Percentage	53.48	46.51	100
Parents consanguinity	**Patients group (n=43)**		
Degree of consanguinity	1st degree	2nd degree	No relative
Number	2	4	37
Percentage	4.6	9.3	86.0
Results expressed as Mean ±SD			

Splenectomies thalassemic patients represented only 20.9% of the cases. Regarding iron chelation of the patients withdraw the overloaded iron through the subcutaneous pumps (deferral pumps) used by 46.5%, of the patients, through intramuscular infusion about 34.8%, while intravenous infusion about 11.6% and oral chelation (X-Jade) of iron is used by 6.9% of the patients. The presence of other thalassemic patients within the same family (brothers or sisters) is obvious and 67.3% of the current patients have other thalassemic brothers and /or sisters **(**Table 2).

Table 2. Clinical characteristics of thalassemia.

Period of transfusion	**Number**	**% Percentage**
2-3 weeks	29	67.4
4-5 weeks	12	27.9
More than 5 weeks	2	4.6
Iron chelation	**Number**	**% Percentage**
Desferal pump	20	46.5
Intramuscular infusion	15	34.8
Intravenous infusion	5	11.6
Oral (x-Jade)	3	6.9
Splenectomy	**Number**	**% Percentage**
Yes	9	20.9
No	34	79.0
Thalassemic brothers/sisters	Number	% Percentage
0	14	32.5
1	17	39.5
4	3	6.9
2	9	20.9

3.2. Incidence of the thalassemia

3.2.1. Distribution of age and sex:

Age ranged among the patient populations (1-19 years), 8 patients between the ages (1-4 years), 18 patients between the ages (5-9 years), 11 patients between the ages (10-14 years) and 6 patients between the ages (15-19 years), 53.4% male and 46.5% female.

3.2.2. Family history of thalassemia:

Twenty-one (48.8%) recruited patients had another sibling (either alive or deceased) or thalassemia relative and 22 (51.1%) patients had no sibling or thalassemia relative affected (either alive or deceased).

3.2.3. Age at first diagnosis:

Twenty-six (60.4 percent) of the recruited patients were diagnosed before two years of age, while the diagnosis was rendered after two years of age in the remaining patients.

3.2.4. Skeletal changes:

All patients assessed for skeletal changes and such changes were noted in 17 cases (39.53%) and included facial bone expansion characteristics, large skull, frontal bone bossing. Such bone modifications in the remaining 26 (60.46 percent) patients have been of varying degrees, ranging from mild to severe degrees, with no apparent or major structural shifts.

3.2.5. Skin pigmentation:

Skin pigmentation was observed in 19 patients (44.18%) which varied from a slight increase in skin pigmentation to very dark-colored skin, especially in the face and hands, and 23 remaining patients (53.48%) retained normal skin pigmentation.

3.2.6. Viral hepatitis assessment:

Most thalassemia patients checked for hepatitis B and C specifically for whole blood using a hepatitis B and C strip of the 43 patients surveyed, 27 patients tested positive for hepatitis C were nearly (62.7 percent), while none of our patients tested positive for hepatitis B.

3.3. Pre-transfusion levels of hemoglobin:

Pre-transfusion levels of hemoglobin were available in 36 (83.7%) of patients enrolled. The pre-transfusion distribution of hemoglobin levels in these patients and indicates that it was below 9 gm / L in 20 patients (66.6%) and below 16 gm / L in 12 patients (33.3%).

3.3.1. Hematological features of thalassemia:

Both complete blood counts parameters and red blood cell indexes in patients with beta-thalassemia assessed in this analysis have identified important issues. Compared to healthy controls, a severe anemic presentation was seen in patients. The rate of hemoglobin in patients decreased to about 30 percent of the amount reported in healthy controls,8.0±1.0 g / dL vs. 11.4±0.8 g / dL, while the incidence of red blood cells decreased with the exception of RDW, which included Hct (23.8±2.9 vs. 34.6±2.3), MCV (71.8±7.1fl vs. 77.5±4.1fl), MCH (20.2±2.4 vs. 23.5 ± 2.2), MCHC (30.8±0.7 vs. 30.1±1.2), and RDW percent (20.5±9.7 vs. 14.2±2. In contrast, severe leukocytosis was also found in patients relative to healthy controls 11.8 ± 4.6 vs.7.1±2.2 X 109/L, and linear regression testing was used in the current study to assess the association between blood cell rates (RBC, WBC, and PLT) and incidences of red blood cells (Hb, Hct, MCV, MCH, and MCHC) of iron excess concentrations

in thalassemia. no correlation was found between RBC and iron (r = - 0.036, P = 0.410), also for WBC no correlation was found with iron (r =0.069, P =0.030), while for PLT significant (r = 0.292, P = 0.029) positive correlation was found with iron, whereas for red blood cell incidences there is no correlation between blood cell incidences (Hb, Hct, MCH , MCHC and RDW) and iron, except MCV and RDW blood cell incidence, which have a significant positive correlation with iron overload (Table 3), (Table 4), and (Figure 3).

Table 3. Correlation between RBC incidences and iron overload.

	Iron overload	
parameters	Pearson correlation (r)	P-value (p)
Hb	r= - 0.036	P = 0.410
Hct	r= - 0.069	P =0.330
MCV	r= 0.232	P = 0.029
MCH	r= - 0.036	P = 0.410
MCHC	r= 0.069	P = 0.330
RDW	r= 0.292	P = 0.029

Table 4. Correlation between blood cell and iron overload.

	Iron overload	
parameters	Pearson correlation (r)	P-value (p)
RBC	r= - 0.036	P = 0.410
WBC	r= 0.069	P = 0.330
PLT	r= 0.292	P = 0.029

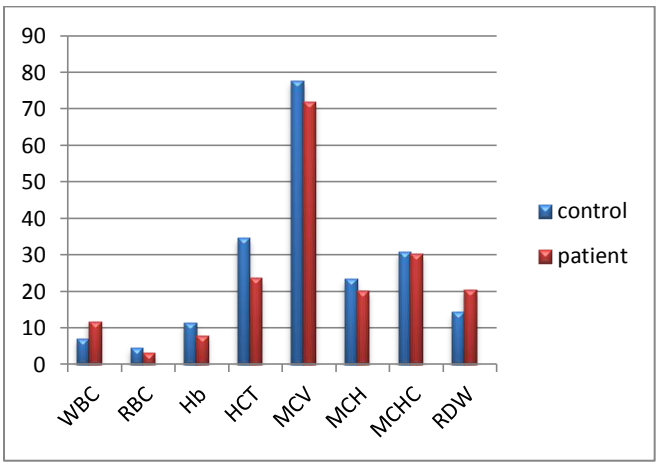

Figure 3. Hematological changes in thalassemia.

3.4. Biochemical characteristics of thalassemia

3.4.1. Renal function test parameters:

The results of the current study showed a significant decrease in serum total protein and serum creatinine levels in beta-thalassemia patients (6.1±0.6g / dl, 0.43±0.07mg / dl) compared to healthy controls of the same age and sex (6.9±0.4 g / dl, 0.51±0.9mg / dl), while thalassemia patients showed a significant increase in serum uric acid levels (4.4 ±0.4 g / dl, 0.51 ±0.9mg / dl), as it clear in the (Figure 4). In addition of it in the correlation relation between all renal parameters have no significant correlations as shown in the Table (5).

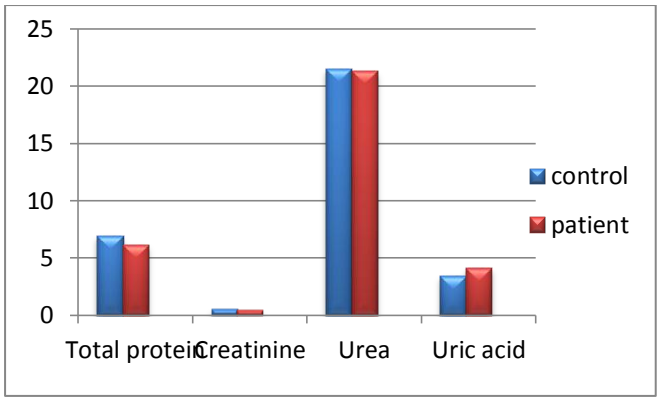

Figure 4. Changes in the renal function of thalassemia.

Table 5. Correlation between renal parameters and iron overload.

	Iron overload	
parameters	**Pearson correlation (r)**	**P-value (p)**
Creatinine	r= 0.097	P = 0.268
Uric acid	r= 0.190	P = 0.111
Urea	r= - 0.028	P = 0.430
Total protein	r= 0.096	P = 0.269

3.4.2. Liver function test parameters

3.4.2.1. Enzymatic liver parameters:

The findings of the current study show a significant increase in the level of liver enzymatic parameters ALP, ALT and AST (187.1 ± 51.3 UI / L, 47.5 ± 23.1UI / L and 56.3 ± 31.3UI / L) compared to healthy controls (83.2 ± 29.1UI / L, 16.3 ± 13.4UI / L and 25.9 ± 5.1UI / L) respectively (Figure 5) show a positive significant correlation between ALT and iron overload, while for ALP and AST shows no correlation with iron overload.

3.4.2.2. Non-enzymatic parameters of the liver:

The findings of the current study showed a significant improvement in the rate of non-enzymatic parameters of the liver, serum total bilirubin, serum direct bilirubin and serum indirect bilirubin (1.1±0.7mg / dl, 0.43 ± 0.39mg / dl and0.67±0.43mg / dl) compared to healthy controls of the same age and sex (0.6 ± 0.1mg / dl, 0.22 ± 0.08mg / dl and0.38±0.11mg / dl). Nonetheless, the findings of serum albumin rate liver-related non-enzymatic parameters showed a

significant decrease in stable regulation relative to its point (4.1 ±0.3 g / dl, 4.6 ±0.3g / dl). (Figure 6) comparisons of all non-enzymatic liver parameters with iron values in iron overload patients indicate poor non-significant correlations, full bilirubin, and indirect bilirubin parameters display low positive iron overload correlations, while specific bilirubin and albumin parameters show weak negative iron overload correlations.

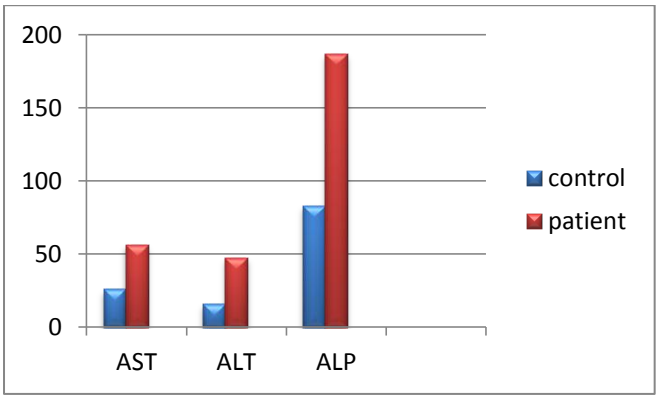

Figure 5. Changes in the enzymatic liver functions of thalassemia.

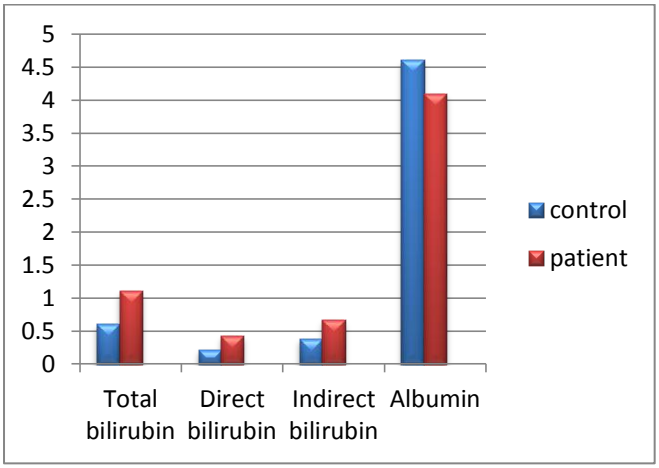

Figure 6. Changes in the non-enzymatic liver function parameters.

3.4.2.3. Iron profile:

The study findings showed significant changes in serum ferritin and iron (3132.0 ± 1012.1 ug / dl, 167.1 ±0.423 ng / ml) vs. (44.3 ± 22.3 ug / dl, 112.3 ± 0.68 ng / ml) relative to control point respectively. Furthermore, in the sample populations, association evaluation of iron profile (iron and ferritin) with iron overload in thalassemic patients shows high positive associations with iron values (r= 0.368, p=0.008).

4. DISCUSSION

4.1. Incidence of the thalassemia distribution

4.1.1. Beta-thalassemia major age distribution:

The information gathered in the context of a questionnaire. Patients involved in the actual research suggested the age and gender distribution of thalassemia patients. The age range was between (1-19 years) of the registered thalassemia patients. These include eight patients aged 1-4 years, 18 patients aged 5-9 years, 11 patients aged 10-14 years, and 6 patients aged 15-19 years. The patient's gender allocation proportions were male (53.4 percent) and woman (46.5 percent). Significant differences are observed in the consanguinity of parents of thalassemic patients and healthy controls, suggesting that consanguinity is correlated with the incidence of β-thalassemia in boys, this was clarified by the parents ' low health education and knowledge of the disorder, the findings of an earlier study designed to evaluate the consanguinity of parents with contrast, the proportions of 2nd degree consanguineous marriages in client populations are significantly higher than those of the control group, respectively 30%, and 9.3%. This result is consistent with the results published in preliminary studies [1, 11] in the current study, approximately twenty-one enrolled patients (48.8%) had another sibling either thalassemia relative (either alive or deceased) and (51.1%) had no sibling or thalassemia relative affected (either alive or deceased). Early reviews also found in another study showing that clinicians with thalassemia have another parent or family with thalassemia [2].

4.1.2. Viral hepatitis thalassemia:

Hepatitis is liver inflammation. For instance, medications, alcohol, chemicals, and autoimmune diseases may cause inflammation of the liver, but some viruses cause around half of all hepatitis in humans. Viruses that target liver specifically are referred to as hepatitis viruses. There are several varieties of hepatitis viruses; including types A, B, C, D, E. Varieties A, B, and C are the most prevalent and all hepatitis viruses that cause acute hepatitis, although persistent hepatitis may be triggered by viral types B and C. Thus, as a consequence of blood transfusion, most thalassemia patients had untreated hepatitis, of 43 patients surveyed around 27 patients (62.7%) tested positive for hepatitis C. None of our doctors, on the other side, tested positive for hepatitis B. It is also linked to the viral transmission pathway, the most common blood and needle transmission of HCV; hence it’s more

frequent in patients with thalassemia. Severe anemic occurs as a consequence of thalassemia and involves healthy red blood cells each month. Otherwise, HBV is the most common route of spread among thalassemia patients in the studied population [7].

4.1.3. Association of thalassemia with other diseases:

All patients evaluated for skeletal changes in this investigation, and such changes were noted in 39.53 percent of patients including characteristic facial bone expansion, large skull, and frontal bone bossing. Such shifts in the bone were of varying degrees, ranging from mild to severe degrees, the same skeletal feature as the previous study showed [12]. Bone defects present as rickets, scoliosis, extreme bone pain, spinal deformity, osteopenia, serious osteoporosis or multiple fractures, excess iron accumulation in the bones may affect the number and function of osteoblasts and interfere with mineralization, contributing to osteoporosis [13, 14]. No significant changes in the skeleton are found in the remaining 26 patients (60.46 percent). Skin pigmentation was observed in 19 patients (44.18%) which ranged from a slight increase in skin pigmentation to a very dark-colored skin, especially in the face and hands, while the other 23 patients (53.48%) retained normal skin color. Past [15] research affirms and aligns with these findings. Therefore, indicated that the majority of patients (67.4%) undergo blood transfusion every 2-3 weeks and 29.9% 4-5 weeks, whereas only two patients (4.6%) need a transfusion at longer intervals, more than 5 weeks, as stated by [16] agreement. Blood transfusions are the most common treatment for all major thalassemia types. Such transfusions are necessary in order to provide the person with hemoglobin capable of providing the oxygen needed by the body of the patient Splenectomy is clarified as it prevents the extra corpuscular process responsible for the increased degradation of healthy donor red cells in the bloodstream of the person. In respect to iron chelation, nearly half of clinicians extract the excessive iron through subcutaneous pumps (deferral pumps), 46.5% through intramuscular infusion, while 34.8% by intravenous infusion. 6.9% of clinicians used oral chelation (X-Jade) for titanium. Chelation therapy's key goal is to reduce tissue iron to a level where there is no iron-mediated toxicity. Therefore, chelate should have a high iron specificity [17].

4.2. Biochemical characteristics of thalassemia

4.2.1. Renal thalassemia parameters:

Results from this study showed that thalassemia patients renal function parameters changed significantly with the exception of serum urea. The findings showed a significant rise in the amount of serum uric acid relative to healthy volunteers, a significant reduction in the rate of serum creatinine according to its level of healthy controls. Such results confirm [18]. Total plasma protein concentrations were dramatically reduced in patients relative to healthy controls Similar results have been reported by [19] verifying our observations. Uric acid in red blood cells is considered to be the metabolically inactive end product of purine metabolism [20]. Rapid erythrocyte turnover in conjunction with reduced reabsorption of diluted uric acid from possible weakened renal tubules may explain the reported rise in serum uric acid concentrations in thalassemia patients [21]. Creatinine is a waste product usually processed out of the blood and excreted with the urine. High creatinine levels may be correlated with kidney function dysfunction or/and decreased muscle mass in thalassemic patients. The possible cause for reduced serum total protein, kidney disease, and liver disease [22], and there is no association of urea, creatinine, and albumin in the statistical analysis of the relationship between the renal parameters in thalassemic patients.

4.2.2. Liver parameters of thalassemia

4.2.2.1. Enzymatic liver parameters:

There was a substantial increase in thalassemic patients' liver enzymatic parameters compared to control samples in our studies. For adolescents with β-thalassemia, elevated liver enzymatic are suggestive of liver failure and liver enzyme leak into the plasma [1, 15]. Liver cell trauma allows the enzymes to escape into the bloodstream, in turn, enzyme parameter elevations are primarily used to assess whether the liver has been compromised and its activity is weakened liver disease, often correlated with frequent blood transfusions of thalassaemic patients and the effects of liver enzyme association testing. It is also correlated with the damage caused by iron overloading of liver cells during blood transfusion and contributes to leakage of enzymes into the blood circulation [23].

4.2.2.2. Non-enzymatic liver parameters:

Non-enzymatic liver variables such as overall bilirubin levels have increased dramatically in contrast to healthy control and specific bilirubin levels have significantly increased relative to healthy control. However, this observation is compatible with the findings of [24]. The increase and specific rates of bilirubin in thalassemic patients were consistent with the hemolytic cycle and reinforce the existing damage to the liver. The iron overload found in β-thalassemic patients could theoretically produce hepatic toxicity and, therefore, elevated overall and specific bilirubin levels, while the rate of albumin showed a significant decrease relative to normal regulation, the possible cause of decreased serum albumin is the secondary reduction of protein synthesis by the liver, its consent to findings were obtained [6, 10].

4.3. Iron profile:

The study findings showed a substantial increase in serum ferritin and iron compared to a healthy control group. This observation was compatible with the findings of [25]. This is a reasonable result where both transfusion iron deficiency and insufficient gastrointestinal absorption are observed in thalassemic patients. This observation was backed by several reports, such as [18] and [21]. From a biochemical point of view, it seems obvious that high iron concentrations have detrimental effects on the body organs and disrupt certain organs to conduct their own normal functions Lack of physiological process in beta-thalassemia major to remove excessive iron triggers their tissue deposition. Serum ferritin represents the state of the body's iron stores. Iron tissue overloaded is the most critical complication of β-thalassemia and is a major topic of management [26] and explanation of association study between iron overload and ferritin suggests a highly significant connection between iron overload and ferritin values in the body in positive states, indicating that as iron values rise in the body, ferritin values often increase in positive states.

4.4. Gender-related hematological and biochemical characteristics of patients:

The hematological and biochemical features of thalassemia males and females showed no significant gender differences. This demonstrated in population studies by the age of thalassemic patients as most of the thalassemic patients in population studies were under 16 years of age. This indicates that under the age of puberty, a thalassemic disorder often plays a major role in children's lag in puberty and development. Such results have been supported by previous [1, 26] studies.

CONCLUSIONS

In the present study, concluded that in patients with beta -thalassemia major, higher incidence of hematological and biochemical changes occurs in addition to iron overload in all patients. There is no any gender-related hematological and biochemical significantly changes.

Acknowledgments

We would like to express our deep appreciation to all patients suffering from Beta-thalassemia and their parents for allowing us to carry out this research and to their staff who have contributed to this study at the Shahid Dr. Khalid Hospital in Koya City.

Declaration of conflicting interests

Authors also confirmed that there are no potential conflicts of interest with regard to the study, authorship and/or publishing of this paper.

Funding

The author received no financial support for the research, authorship, and/or publication of this article.

References

[1] Saleh, K.K. and Kakey, E.S. (2018). Some Molecular Characterization of β-Thalassemia Major In Koya City, *International Conference on Pure and Applied Sciences*, C Vol. 4 (4), pp: 64-68.

[2] Ward, A., Caro, J.J., Green, T.C., Huybrechts, K., Arana, A., Wait, S., and Eleftheriou, A. (2002). An international survey of patients with thalassemia major and their views about sustaining life-long desferrioxamine use, *BMC clinical pharmacology*, C Vol. 2 (1), pp: 3.

[3] Galanello, R. and Origa, R. (2010). Beta-thalassemia, *Orphanet journal of rare diseases*, C Vol. 5 (1), pp: 11.

[4] Mehmetçik, G.J.Z.J.o.P. and Sciences, A. (2019). Estimation of MDA, CRP and Some hematological parameters in the mature Cypriot Thalassemia patients, *Zanco Journal of Pure and Applied Sciences*, C Vol. 31 (s4), pp: 143-149.

[5] Al-Awamy, B.H. (2000). Thalassemia syndromes in Saudi Arabia, *Saudi medical journal*, C Vol. 21 (1), pp: 8-17.

[6] Čokić, V.P., Smith, R.D., Biancotto, A., Noguchi, C.T., Puri, R.K., and Schechter, A.N. (2013). Globin gene expression in correlation with G protein-related genes during erythroid differentiation, *BMC genomics*, C Vol. 14 (1), pp: 116.

[7] Sabri, M.S. (2017). Biochemical Study on Splenectomy and Non Splenectomy Iraqi Major Thalassemic Patients, *Ibn AL-Haitham Journal For Pure and Applied Science*, C Vol. 23 (1), pp: 254-259.

[8] Jiffri, E.H., Bogari, N., Zidan, K.H., Teama, S., and Elhawary, N.A. (2010). Molecular updating of β-thalassemia mutations in the upper Egyptian population, *Hemoglobin*, C Vol. 34 (6), pp: 538-547.

[9] Khattak, S.T. and Khan, J. (2006). Heterozygous beta thalassemia in parents of children with beta thalassemia major, *Gomal Journal of Medical Sciences*, C Vol. 4 (2), pp.

[10] Saleh, K.K., Saman, R.A., and Rukhosh, E.M. (2019). Estimation of Serum Homeostasis Model Assessment-Insulin Resistance and Lipid Profile in Beta-thalassemia Major Patients and their Correlation with Iron Overload in Koya City, *Polytechnic Journal*, C Vol. 9 (2), pp. doi: 10.25156/ptj.v9n2y2019.pp125-132.

[11] Hamamy, H.A. and Al-Allawi, N.A.S. (2013). Epidemiological profile of common haemoglobinopathies in Arab countries, *Journal of community genetics*, C Vol. 4 (2), pp: 147-167.

[12] Napoli, N., Carmina, E., Bucchieri, S., Sferrazza, C., Rini, G.B., and Di Fede, G. (2006). Low serum levels of 25-hydroxy vitamin D in adults affected by thalassemia major or intermedia, *Bone*, C Vol. 38 (6), pp: 888-892.

[13] Attia, M.M.A., Sayed, A.M., Ibrahim, F.A., Mohammed, A.S., and El-Alfy, M.S. (2011). Effects of antioxidant vitamins on the oxidant/antioxidant status and liver function in homozygous beta-thalassemia, *Romanian J. Biophys*, C Vol. 21 93-106.

[14] Saleh, K.K., Dalkiliç, S., Dalkiliç, L.K., Hamarashid, B.R., and KIRBAĞ, S. (2020). Targeting cancer cells: from historic methods to modern chimeric antigen receptor (CAR) T-Cell strategies, *AIMS Allergy Immunol*, C Vol. 4 (2), pp: 32-49. doi: 10.3934/Allergy.2020004.

[15] Ghasemi, A., Keikhaei, B., and Ghodsi, R. (2014). Side effects of hydroxyurea in patients with Thalassemia major and thalassemia intermedia and sickle cell anemia, *Iran J Ped Hematol Oncol*, C Vol. 4 (3), pp: 114-7.

[16] Borgna- Pignatti, C., Cappellini, M.D., De Stefano, P., Del Vecchio, G.C., Forni, G.L., Gamberini, M.R., Ghilardi, R., Origa, R., Piga, A., and Romeo, M.A. (2005). Survival and complications in thalassemia, *Annals of the New York Academy of Sciences*, C Vol. 1054 (1), pp: 40-47.

[17] Waseem, F., Khemomal, K.A., and Sajid, R. (2011). Antioxidant status in beta thalassemia major: a single-center study, *Indian Journal of Pathology and Microbiology*, C Vol. 54 (4), pp: 761.

[18] Aldudak, B., Karabay Bayazit, A., Noyan, A., Ozel, A., Anarat, A., Sasmaz, I., Kilinc, Y., Gali, E., Anarat, R., and Dikmen, N. (2000). Renal function in pediatric patients with beta-thalassemia major, *Pediatr Nephrol*, C Vol. 15 (1-2), pp: 109-12. doi: 10.1007/s004670000434.

[19] Eldor, A. and Rachmilewitz, E.A. (2002). The hypercoagulable state in thalassemia, *Blood*, C Vol. 99 (1), pp: 36-43. doi: 10.1182/blood.v99.1.36.

[20] Salih, M.I., Abdoulrahman, K.K.J.Z.J.o.P., and Sciences, A. (2016). Estimation of Anemia parameters in chronic renal failure patients on hemodialysis in Erbil Governorate, *Zanco Journal of Pure and Applied Sciences*, C Vol. 28 (6), pp: 75-80.

[21] Ferru, E., Pantaleo, A., Carta, F., Mannu, F., Khadjavi, A., Gallo, V., Ronzoni, L., Graziadei, G., Cappellini, M.D., and Turrini, F. (2014). Thalassemic erythrocytes release microparticles loaded with hemichromes by redox activation of p72Syk kinase, *Haematologica*, C Vol. 99 (3), pp: 570-578.

[22] Elgammal, M., Mourad, Z., Sadek, N., Abassy, H., and Ibrahim, H. (2012). Plasma levels of soluble endothelial protein C-receptor in patients with β-thalassemia, *Alexandria Journal of Medicine*, C Vol. 48 (4), pp: 283-288.

[23] Meerang, M., Nair, J., Sirankapracha, P., Thephinlap, C., Srichairatanakool, S., Fucharoen, S., and Bartsch, H. (2008). Increased urinary 1, N6-ethenodeoxyadenosine and 3, N4-ethenodeoxycytidine excretion in thalassemia patients: markers for lipid peroxidation-induced DNA damage, *Free Radical Biology and Medicine*, C Vol. 44 (10), pp: 1863-1868.

[24] Shamshirsaz, A.A., Bekheirnia, M.R., Kamgar, M., Pourzahedgilani, N., Bouzari, N., Habibzadeh, M., Hashemi, R., Shamshirsaz, A.A., Aghakhani, S., and Homayoun, H. (2003). Metabolic and endocrinologic complications in beta-thalassemia major: a multicenter study in Tehran, *BMC endocrine disorders*, C Vol. 3 (1), pp: 4.

[25] Mishra, A.K. and Tiwari, A. (2013). Iron overload in Beta thalassaemia major and intermedia patients, *Maedica*, C Vol. 8 (4), pp: 328.

[26] Telfer, P., Prestcott, E., Holden, S., Walker, M., Hoffbrand, A., and Wonke, B. (2000). Hepatic iron concentration combined with long- term monitoring of serum ferritin to predict complications of iron overload in thalassaemia major, *British journal of haematology*, C Vol. 110 (4), pp: 971-977.

ZANCO Journal of Pure and Applied Sciences
The official scientific journal of Salahaddin University-Erbil
https://zancojournals.su.edu.krd/index.php/JPAS

ISSN (print):2218-0230**, ISSN (online):** 2412-3986**, DOI: http://dx.doi.org/10.21271/zjpas**

RESEARCH PAPER

Synthesis and Characterization of some divalent transition metal complexes with acid hydrazone ligand

Bayan A. Faiq,Bayan O. Ahmed
[1] Department of Chemistry, Collage of Science, Salahaddin University-Erbil, Kurdistan Region, Iraq.

A B S T R A C T:

Complexes with the general formula $[M(LH)_2]X_2$ where M=Mn(II),Co(II),Ni(II) and Cu(II) LH= 4-acetylpyridine benzoyl hydrazone and X=chloride ion were synthesized. The structures were confirmed by IR spectroscopy, and characterized by elemental analyses, UV-vis, ^{1}H.n.m.r ^{13}C-n.m.r, and conductivity measurements. Molar conductance values in DMSO indicate that all complexes are electrolytes with mole ratio (1:2) and chloride ions not participate in coordination to central metal ion except Mn complex. The ligand act as bidentate, they coordinates through azomethine nitrogen (>C=N-) and carbonyl oxygen′s.

KEY WORDS: Acid hydrazone; complexes; synthesis.
DOI: http://dx.doi.org/10.21271/ZJPAS.33.5.10
ZJPAS (2021) , 33(5);85-94 .

1.INTRODUCTION :

The condensation between substitution acid hydrazide with carbonyl compound (aldehydes, ketones) is the best method for hydrazone preparation or synthesis by the reaction of hydrazine with aldehydes, ketones in ethanol, methanol that have a general formula of $R_1R_2C = NNR_3R_4$ contains (N-N) linkage. The general formula for a substituted acylhydrazone is shown below: (Hamada et al., 2015)

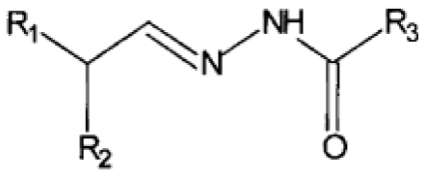

General formula of a substituted acylhydrazo

Hydrazone behave as bidentate ligands and owing of -NH-C=O group in acid hydrazone show keto-enol tautomerism, keto-form was absent in solid state while in solution enol- form is present and they exist as an equilibrium mixture keto and enol forms. (Bessy, 2009)

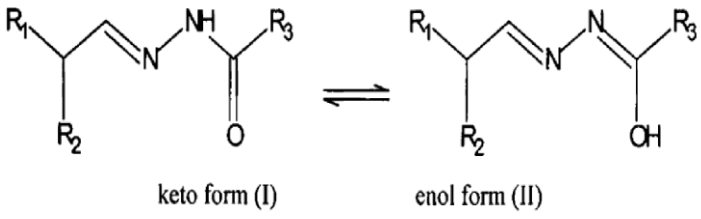

Tautomerism of acid hydrazone (keto-enol form)

Keto-enol Tautomerism makes it to form a stable complex with different transition metal ions make hydrazone ligand played a great role in inorganic chemistry. (Sreeja, 2004)

The arylhydrazones ligand R-CO-NH-N=CHR act as bidentate or chelating ligands and

* **Corresponding Author:**
Bayan A. Faiq
E-mail: bayan.ahmed@su.edu.krd
Article History:
Received: 03/04/2021
Accepted: 09/07/2021
Published: 20/10 /2021

coordinate with transition metal ions through the N atom of azomethine group and O atom of the carbonyl group, a five membered ring being produced. (Aurkie et al., 2008; Sajjad, et al., 2019; Adrian and Jack, 2009)

The most interest hydrazones and it′s complexes usage in clinical, analytical, biological fields like antibacterial (Ruth et al., 2006) antimicrobial, antifungal, anticonvulsant, (Marisa et al., 1999) anti-analgesic (Rafat et al., 2010), antimalarial, anti-inflammatory (Bhushankumar et al., 2011), anticancer (Basavaraj et al., 2011), antitumor (Wagnat, Naned, and Rafat, 2013), anti-tuberculosis, (Ahmet et al., 2010) antioxidant are some physiologically active of it (Bahaa et al., 2019; Deepa et al., 2015). They show activity against leukemia, sarcomas and other malignant neoplasms. industrially hydrazone used as plasticizers and as polymerization initiators antioxidants. Also play a great role in plant growth regulators, insecticides, rodenticides, herbicides, nematocides. (Livio et al., 2017)

The new complexes of Mn(II),Co(II),Ni(II) and Cu(II) with the ligand 4-acetylpyridine benzoyl hydrazone, having general the formula $[M((LH)_2]Cl_2$ where M = Mn(II), Co(II),Ni(II) while (H_2O) is participate as ligand in Cu complex. The result indicates that in all complexes, ligand was coordinated to metal via azomethine nitrogen (>C=N-) and carbonyl oxygen′s.

2.Materials and Methods

2.1 Experimental Notes:

All chemicals used were of reagent grade, supplied by either Merck, Fluka or (B.D.H). Melting Point of the complexes were measured using Electro thermal-IA 9000-England melting point apparatus. Thermo Mattson IR 300 spectrophotometer was used to recorded infrared spectra in the (400-4000) cm^{-1}range using KBr discs. The conductivity was measured for the (10^{-3} M) solution of the complexes in (DMSO), using WTW-conductometer inolab 749-Geermany. Electronic spectra were recorded on a UV-Vis. spectrometer, CE -3021- England. Elemental analysis was carried out on Elementary Analyses system GmbH in Kashan University (Iran). ^{1}H.n.m.r ^{13}C-n.m.r spectra of ligand and complexes were recorded by Bruker ultra-shield 300 MHz with TMS as internal reference, in Kashan University (Iran).

2.2 Preparation of Acid Hydrazone Ligand:

(4.11ml, 0.0375 mol) of 4-acetylpyridine was added to a solution of (5.1 gm, 0.0375 mol) benzoyl hydrazine which is dissolved in (50ml) absolute ethanol, heated to reflux for (1hr.). Filtered off and recrystallized in ethanol, washed with diethyl ether and dried under vacuum.

2.3 Preparation of metal complex:

Solid complexes were prepared by heating of ethanolic solution of metal chloride (0.000418 mol) was added to (0.000836 mol) of prepared ligand in (15 ml) absolute ethanol, heated to reflux for (1 hr.), a colored complex was formed. Filtered off and recrystallized in ethanol, washed with diethyl ether and dried under vacuum.

3.Result and Discussion:

Several methods, traditional and modern are available for elucidating the structure of ligand and their coordination complexes. The complexes are characterized by elemental analysis, Infrared Spectral, ^{1}HNMR, ^{13}C-NMR spectral, Molar conductivity measurement, Electronic Spectra and Magmatic susceptibility measurement.

3.1 Elemental analysis:

The complexes were analyzed for carbon, hydrogen and nitrogen. The results are given in the table (1). The stoichiometry of the complexes data was found to be (1:2) (M:L).

3.2 Infrared Spectral Studies:

The IR spectra of the complexes were analyzed and compared with free hydrazone ligand (LH) that show a strong absorption band at (1644 cm^{-1}) assigned to υ (C=O) and medium intensity band υ (C=N) at (1588 cm^{-1}). Both of these bands shift to lower wave number after complexation indicate that the ligand act as bidentate and coordination occur from oxygen′s carbonyl group and nitrogen′s azomethine to central metal (Morsy et al.,2011; Samar, 2017), other bands observed at (3200cm^{-1}) and (1448 cm^{-1}) assigned to the υ (N-H cm^{-1}) and υ $(C=N)_{py}$ respectively which is not affected on complexation. A new band appear in complex around (1065 cm^{-1}), (469-501 cm^{-1}), (422-424 cm^{-1}) which are attributed to υ (C–O), (M–O), (M–N) respectively. (Mariana et al., 2010; Ikechukwu and Peter, 2015; Ganesh, 2016; Abdul hakim and Salima, 2008)

Another broad band appear in Cu complex around (3432 cm^{-1}) due to υ (O-H) absorption band which is for participate H_2O in coordination. (Nakamoto, 1978)

3.3 Molar conductivity measurement:

Conductivity measurement of complexes carried out in 10^{-3} M (DMSO) solution. All molar conductance values are listed in table (2). These values showed that all complexes were electrolyte.

The value of the molar conductance ($cm2.ohm^{-1}. mol^{-1}$) are in the ranges (71.8-76.5) $cm^2.ohm^{-1}. mol^{-1}$) which correspond to (1:2) electrolytes, this is also confirmed with positive $AgNO_3$ test for chloride containing complexes except Mn complex which is not electrolyte.

3.4 Electronic Spectra:

Electronic spectra of octahedral manganese (II) complex exhibit six spin- forbidden transition in the visible region, three of the electronic transition bands around (15470) cm^{-1} which assigned to $^6A_1g \rightarrow {}^4T_1g$ (D), (23640) cm^{-1} transition s assigned to $^6A_1g \rightarrow {}^4T_2g$ (D) and (29455) cm^{-1} assignable to the charge transfer respectively for an octahedral geometry for Mn (II) complex. (Lever, 1984; Achut et al., 2010)

In the present work the electronic spectra of cobalt (II) complex was exhibit the electronic transition band at (17120) cm^{-1} which may be attributable to $^4A_2 \rightarrow {}^4T_1$ (P) in tetrahedral environment for cobalt complex, while the band at (23923) cm^{-1} is assigned to the (L→M) charge transfer (charge transfer). (Canpolat and Kaya, 2005; Sajid and Qin-han, 2008; Tejraj, 1984)

The electronic spectra of Ni(II) complex show one absorption band at (14710) cm^{-1} which may be assigned to $^3A_2 \rightarrow {}^3T_2$ (F) transition, suggestion the tetrahedral geometry around Ni (II). Both Co(II), Ni(II) complexes show an intense band at (23923- 24390) cm^{-1} which can be assigned to charge transfer transition of tetrahedral geometry.(Lever, 1984; Kasuga et al., 1984; George and Christos, 1985; Christian, 1962; Yamada and Takeuchi, 1982).

Finally square pyramidal geometry is proposed for Cu complex 4 based on the presence of two bands at (21978) cm^{-1} and (16393) cm^{-1}. These bands may be assigned to the $^2B_1 \rightarrow {}^2A_1$ and the $^2B_1 \rightarrow {}^2E$ transitions, respectively, based on assignments published before (James, 1978; Sudeep et al., 1996)

3.5 Magmatic susceptibility:

The effective magnetic moment values were calculated by using formula, μ eff =2.83 $(\chi M\ T)^{1/2}$ BM where, χM = molar susceptibility, T = absolute temperature.

The magnetic susceptibility for Mn (II) complex is that found is (1.92) B.M at 300 K compared with theoretical value (1.73B.M) expected for low spin d^5 Mn complex that evidence for octahedral geometry. (Achut et al., 2010)

The magnetic moment value for Co(II) complex was found (3.79) B.M that evidence for paramagnetic and tetrahedral geometry compared with theoretical value (3.84) B.M. (Sajid and .Qin-han, 2008)

Cu(II) complex had a magnetic moment of (1.89) B.M which is higher than the theoretical value of (1.73) B.M. due to John Teller distortion expected for a d^9 ion with one unpaired electron. (Temitope et al., 2019; F. Albert, 1999)

Ni(II) complex had magnetic moment of (2.71) B.M which is lower than theoretical value of (2.82) B.M. that indicate Ni complex is paramagnetic (Mohammed and Mostafa, 2001)

3.6. ^{1}H-NMR and ^{13}C-NMR Spectra:

The ^{1}H-NMR spectrums of synthesized ligand were recorded in DMSO-d 6 solution using TMS as internal standard show signals at 10.70 ppm (s, 1H) due to the -NH proton. The two doublet peaks with equal integration at 8.63 and 7.40 ppm belongs to the protons of the pyridine ring, were shown at significant different δ depending on their position to the electronegative nitrogen atom of the pyridine ring. The aromatic protons (Ar-H) show singlets at 7.50- 7.89 ppm. The singlet peak at 2.32 ppm with integration equal to 3 H's clearly belongs to the methyl group ($-N=CCH_3$))(Rosaleen et al., 2004). Moreover, the ^{13}C NMR spectrum of the ligand showed a signal at 163.58 ppm corresponding to the carbonyl group(C=O). The aromatic carbons of the phenyl ring are observed at 127.5, 128.8 ,132.2 and 138.4ppm (Bridson, 2003; El-Saied et al., 2017). The signal of the azomethine carbon(C=N) is observed at 149.14 ppm (Juvansinh et al., 2015). The chemical shift appeared at 14.24 ppm can be assigned to the methyl group (CH_3), and pyridine ring carbon show a signal at 124.1, 138.4and

147.7 ppm . The ^{1}H and ^{13}C - NMR spectra of ligands is full agreement with their proposed structure.

The essential features of the ^{1}H-NMR spectrum of the Co(II),Mn(II), Ni(II)and Cu(II) complexes as a representative case is similar to that of ligand. The ^{1}H- NMR spectrum of ligand shows a signal at (10.70 ppm) is assigned to amide proton (-CONH-) , which is downfield in the spectrum of the complex at (10.91)(10.97)(10.95)(11.2) respectively indicating coordination of oxygen of –CONH– with metal ion (Shivakumar et al., 2008), The presence of this signal in the free ligand and the complexes indicating that free ligand is mainly in keto form and coordinated to the metal ion in keto form also. The slight downfield shift of methyl group protons from (2.32 ppm) in the ligand to (2.45, 2.61, 2.55 and 2.67 ppm) respectively for the complexes may be considered as another evidence of coordination of the ligand through azomethine nitrogen. The signals of the atoms of carbon (C=O) and (C=N) in the ^{13}C- NMR spectrum present shifts of (2.76, 3.01, 2.88 and 2.95) ppm respectively (2.48, 2.55, 3.11 and 2.65) ppm in the complexes, and this downfield in the spectrum of the complex pointed clearly the involvement of the atoms of amide oxygen and azomethine nitrogen in coordination. The atoms of carbon in the pyridine ring have signals in the same region of the spectrum and the shift is very small and in this way is confirmed that the pyridinic nitrogen is not involved in the coordination.

Table 1. Analytical and physical data of the ligand and their complexes

Compd.	***Color***	***M.wt***	***(M.P)°C***	***$AgNO_3$ Test***	***Molar Conductivity***	***Analyses Found (Calc.%)***		
						C	***H***	***N***
$C_{14}N_3H_{13}O$ (LH)	Needly White	239.11	(172.5-172.8)	-------	-------	-------	-------	--------
$[Mn(LH)_2Cl_2]$	White	604.06	>225° decomp	- Ve	1.9	55.58 (55.66)	4.30 (4.33)	13.87 (13.91)
$[Co(LH)_2]Cl_2$	Turquoise-Blue	608.06	>165° decomp	+ Ve	74.2	55.24 (55.30)	4.28 (4.31)	13.79 (13.82)
$[Ni(LH)_2]Cl_2$	Green	607.82	>270° decomp	+Ve	71.8	55.26 (55.32)	4.25 (4.31)	13.73 (13.82)
$[Cu(LH)_2H_2O]Cl_2$	Pale- green	630.67	>145° decomp	+ Ve	76.5	53.28 (53.32)	4.39 (4.47)	13.26 (13.32)

Table 2. The IR spectra of the ligand and complexes and geometrical structure

Compd.	N-H	C-H	C=O	C=N	$(C=N)_{py}$	C-O	M-O	M-N	Geo. Str
$C_{14}N_3OH_{13}(LH)$	3200	3036	1644	1588	1448	-----	------	------	-----
$[Mn(LH)_2 Cl_2]$	3209	3023	1578	1532	1446	1075	477	422	O.h
$[Co(LH)_2]Cl_2$	3214	3056	1597	1524	1447	1068	501	418	T.h
$[Ni(LH)_2]Cl_2$	3189	3062	1600	1536	1447	1065	469	424	T.h
$[Cu(LH)_2H_2O]Cl_2$	3211	3058	1599	1506	1437	1068	477	423	Sq.py

Table 3. Magnetic moment and electronic spectral data of the complexes

No.	***Complex***	***Band absorption***		***Assignment***	***Magnetic moment B.M***
		Cm^{-1}	***Nm***		
1	***$[Mn(LH)_2Cl_2]$***	43859 39370 29455 23640 15470	228.0 254.0 339.5 423.0 646.4	$\pi \rightarrow \pi^*$ $n \rightarrow \pi^*$ C.T $^6A_1g \rightarrow {}^4T_2g$ $^6A_1g \rightarrow {}^4T_1g$	(1.92) O.h

2	***[Co(LH)$_2$]Cl$_2$***	40176 35273 23923 17120 14710	248.9 283.5 418.0 584.0 679.8	$\pi \rightarrow \pi^*$ $n \rightarrow \pi^*$ C.T $^4A_2 \rightarrow {}^4T_1$ (P) $^3A_2 \rightarrow {}^3T_2$ (F)	(3.79) T.h
3	***[Ni(LH)$_2$]Cl$_2$***	37835 29069 24390 14710	264.3 344.0 410.0 679.8	$\pi \rightarrow \pi^*$ $n \rightarrow \pi^*$ C.T $^3A_2 \rightarrow {}^3T_2$(F)	(2.71) T.h
4	***[Cu(LH)$_2$H$_2$O]Cl$_2$***	34305 26212 23724 21978 16393	291.5 381.5 421.5 455.0 610.0	$\pi \rightarrow \pi^*$ $n \rightarrow \pi^*$ C.T $^2B_1 \rightarrow {}^3A_1$ $^2B_1 \rightarrow {}^2E$	(1.89) Sq.py

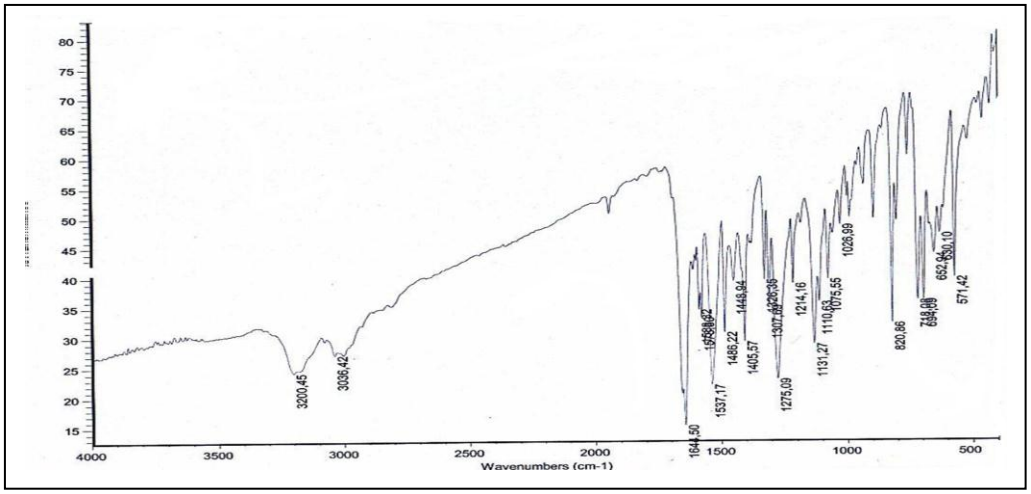

Fig (1) : Infra-red spectra of ligand

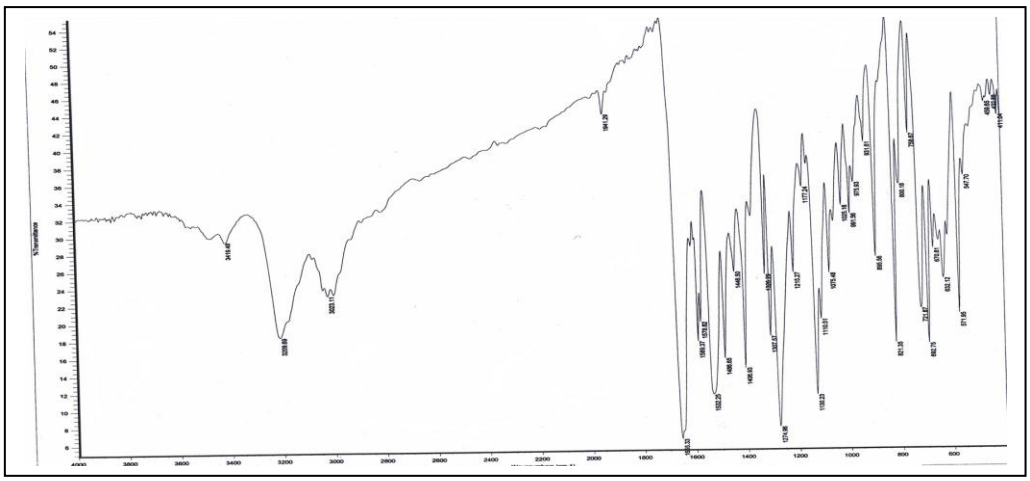

fig (2): Infra-red spectra of Mn complex

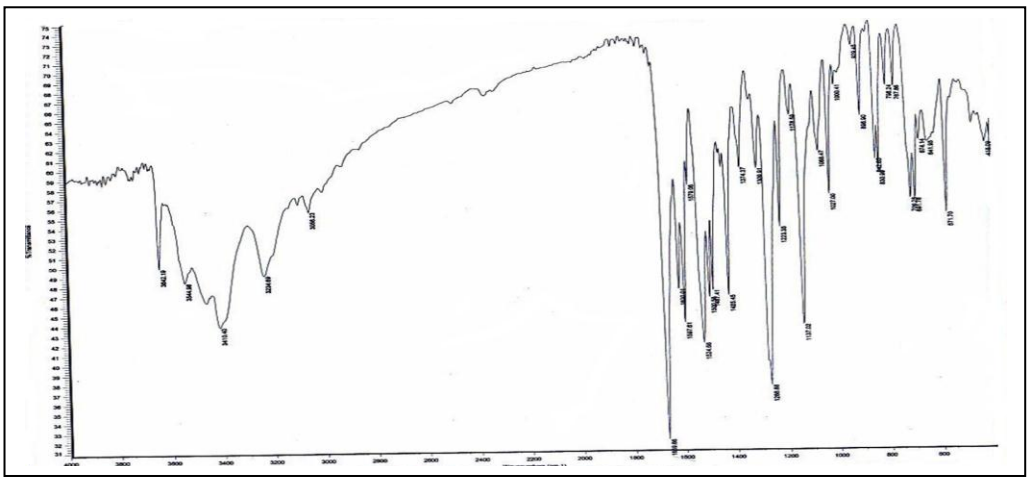

fig (3): Infra-red spectra of Co complex

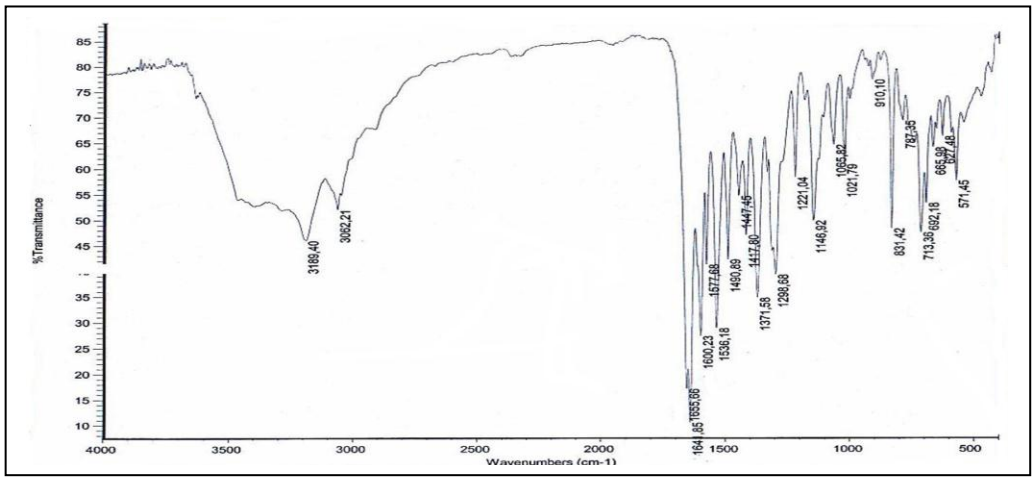

Fig (4): Infra-red spectra of Ni complex

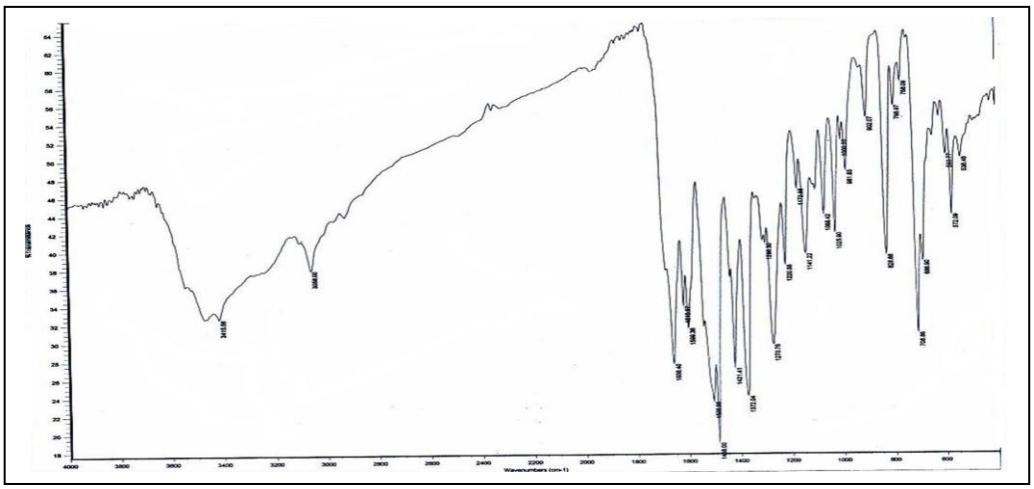

Fig (5): Infra-red spectra of Cu complex

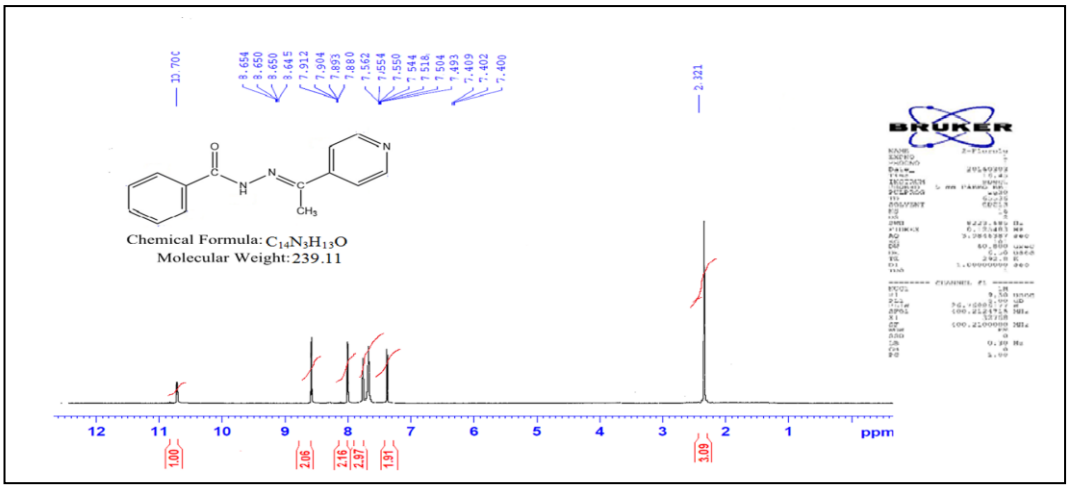

Fig (6) : ^{1}H NMR spectra of ligand

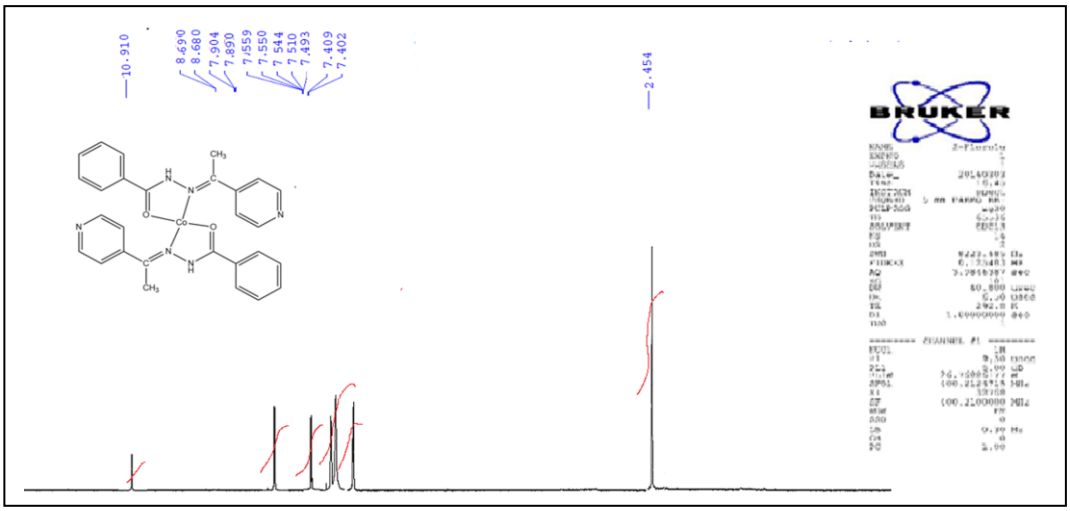

Fig (7) : ^{1}H NMR spectra of *$[Co(LH)_2]Cl_2$ complexes*

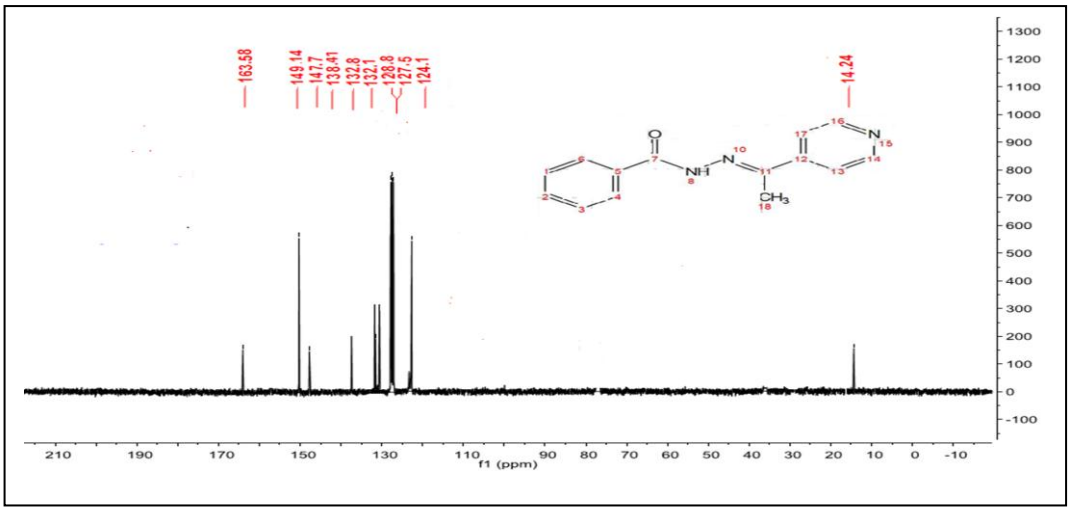

Fig (8) : ^{13}C NMR spectra of ligand

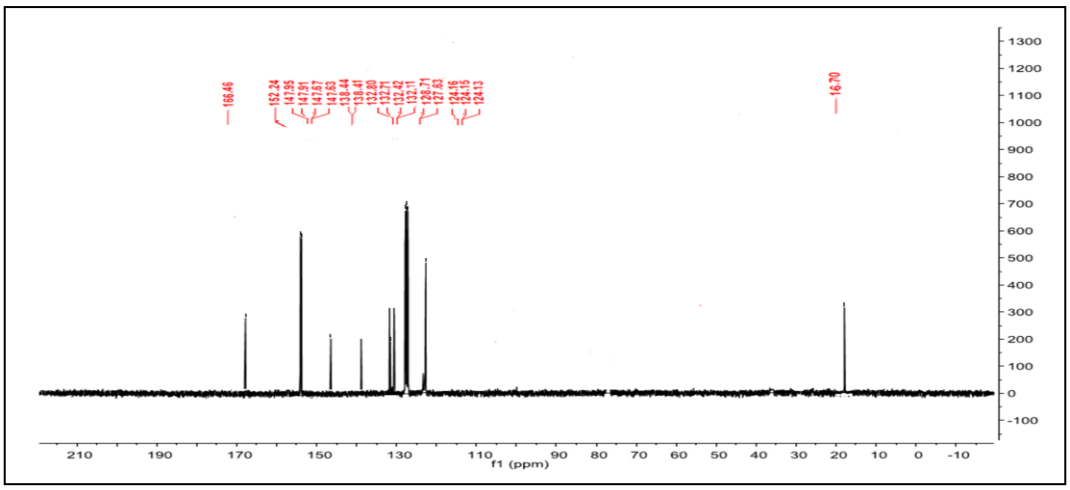

Fig (9) : ^{13} C NMR spectra of *$[Ni(LH)_2]Cl_2$ complex*

4.Conclusion:

In summary, the work reported involved synthesis and characterization of 4- acetyl pyridine benzoyl hydrazone and Mn(II), Co(II), Ni(II) and Cu(II) complexes have been investigated by spectroscopy and some other techniques (IR, UV-Vis spectroscopy, ^{1}HNMR, ^{13}C-NMR spectral molar conductivity and elemental analysis, magmatic susceptibility). In all the complexes, the hydrazone is associated with the metal through the carbonyl oxygen and the azomethine nitrogen to result in different geometrical structures.

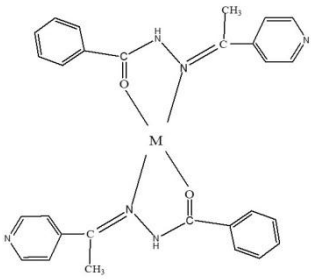

Structure of *$[M(LH)_2]Cl_2$, complexes where M=Co and Ni*

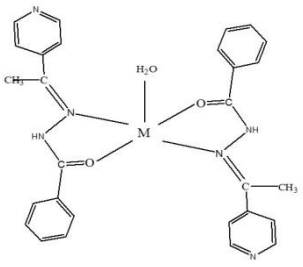

Structure of *$[Cu(LH)_2H_2O]Cl_2$ complex*

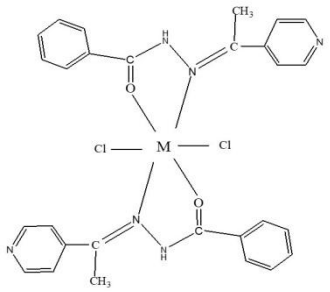

Structure of *$[Mn(LH)_2Cl_2]$ complex*

Acknowledgments:
We thank the College of Science Salahaddin University and Kashan University (Iran) for supporting this study. Magnetic susceptibility Balance Mode (MSB-MKI) Al-Nahrain University, College of Science.

Reference:

Abdul hakim A. Ahmed, Salima. A. BenGuzzi 2008. Synthesis and characterization of some transition metals complexes of Schif base derived from benzidine and acetylacetone. *J Science and Its Appl.*, 2(1):83.

Achut S. Munde, Amarnath N. Jagdale, Sarika M. Jadhav and Trimbak K. 2010. Complexes of an asymmetrical tetradentate Schiff base ligand, *J. Serb. Chem. Soc.*, 75(3), 349-359.

Adrian M. Stadler, Jack M. Harrowfield 2009. Bis-acyl-/aroyl-hydrazones as multidentate ligands Adrian, *Inorganica Chimica Acta*, 362, 4298–4314.

Ahmet Özdemir, Zafer A. Kaplancikli, Gülhan T. Zitouni, Gilbert Revial 2010. Synthesis of some novel hydrazone derivatives and evaluation of their anti

tuberculosis activity, *Marmara Pharmaceutical Journal*, 14, 79-83.

Aurkie Ray, Sambuddha Banerjee, Soma Sen, Ray J. Butcher, Georgina M. Rosair , Maria T. Garland and Samiran Mitra 2008. Two Zn(II) and one Mn(II) complexes using two different hydrazone ligands: spectroscopic studies and structural aspects, *Struct .Chem.*, 19(2):209–217.

Bahaa A. Salah, A. T. Kandil and M. G. Abd El-Nasser 2019. Synthesis, characterization, computational and biological activity of novel hydrazone complexes, *Journal of Radiation Research and Applied Sciences*, 12(1), 383–392.

Basavaraj R. Patil, Shrinath S. Machakanura, Rekha S. Hunoora, Dayananda S. Badigera, Kalagouda B. Gudasia, and S. W. Annie Bligh 2011. Synthesis and anti-cancer evaluation of cyclotriphosphazene hydrazone derivatives, *Der Pharma Chemica*, 3 (4):377-388.

Bessy Raj B. N. 2009. *Structural Characterization and Non-linear Optical Properties of Metal Complexes of Some Donor-Acceptor Substituted N-salicylideneN-aroylhydrazine Ligands***,** Ph.D Thesis, Cochin University of Science and Technology-India.

Bhushankumar S. Sathe, E. Jaychandran, Vijay. A. Jagtap and G. M. Sreenivasa 2011. Synthesis, characterization and vitro anti-flammatory evaluation of new Flurobenzothiazole Schiff's bases, *Int. J. Pharm.*,3,164.

A-K. Bridson, "Inorganic Spectroscopic Methods", Oxford University ,Press Inc, P; 42 (2003).

Canpolat E., Kaya M. 2005. Studies on Mononuclear Chelates Derived from Substituted Schiff Base Ligands (Part 4): Synthesis and Characterization of a New 5-Hydroxysalicyliden-P-Aminoacetophenoneoxime and Its Complexes with Co(II), Ni(II), Cu(II) and Zn(II), *Turk J Chem* ,29, 409-415.

Christian K. Jorgensen 1962. Absorption Spectra Of Transition Group Complexes Of Sulphur Containing Ligands, *J. Inorg. Nucl. Chem.*, 24, 1571-1585.

Deepa Chauhan, Ammar A. Siddiqui, Rajkumari Kataria 2015. Synthesis, characterization and antimicrobial evaluation of some new 1, 3-benzothiazole derivatives containing pyrazole moiety, *The Pharma Innov J*, 4(5): 90-93.

Dipesh P. Mahajan, Jitendra D. Bhosale and Ratnamala S.Bendre 2013, Synthesis, Characterization and Plant Growth Regulator Activity of Some Substituted 2-Amino Benzothiazole Derivatives, *Journal of Applicable Chemistry*, 2 (4):765-771.

El-Saied, F.A., Al-Hakimi, A.N., Wahba, M.A., Shakdofa, M.M.E., 2017. Preparation, characterization and antimicrobial activities of N'-((3-(hydroxyimino) butan-2-ylidene)-2 (phenylamino) acetohydrazide and its metal complexes. Egypt. J. Chem. 60 (1), 1–24.

F. Albert. Cottton, G. Wilkinson 1998. *Advanced Inorganic Chemistry*, Wiley-Interscience, New York.

Cotton F. A. 1999. *Advanced inorganic chemistry*. New York: Wiley.

Ganesh S. Kulkarni, Priyanka L. Anandgaonker, Digambar D. Gaikwad, Dnyandeo M. Janrao 2016. Efficient ultrasound synthesis and biology screening of metal complexes of N-(4methoxybenzylidene) Isonicitinohydrazone, *W J Pharma Research.*, 5(2),1153.

George E. Manoussakis and Christos A. Bolos 1985. Synthesis and Characterization of a Series of New Mixed Ligand Complexes of Manganese(III), Iron(III), Nickel(II), Copper(II) and Zinc (II) with Schiff Bases of N, Ndiethylamino-dithiocarbamate as Ligands, *Inorganica Chimica Acta*, 108, 215-220.

Hamada Abd El-Wahab, M. Abd El-Fattah, Ayman H. Ahmed, Ahmed A. Elhenawy and Alian, N. 2015. A. Synthesis and characterization of some arylhydrazone ligand and its metal complexes and their potential application as flame retardant and antimicrobial additives in polyurethane for surface coating**.** *Journal of Organometallic Chemistry*, 791,99-106,

Ikechukwu P. Ejidike , Peter A. Ajibade 2015. Synthesis, characterization and biological studies of metal(II) complexes of (3E)-3-[(2-{(E)-[1- (2,4-Dihydroxyphenyl) ethylidene]amino}ethyl)imino]-1-phenylbutan-1-one Schiff Base, *Molecules*, 20,9788.

James. E. Huheey 1978. *Inorganic Chemistry: principles of structure and reactivity*, 2nd ed., Harper &Row, New York.

Juvansinh, J., Mayank, M., Mitesh, G., Rohit, M., Manish, R., Shah, M.K., 2015. Synthesis, spectral analysis and evolution of antimicrobial activity of Schiff base of cyanoacetohydrazide. Int. Lett. Chem., Phys. Astron. 52, 100–110.

K. Kasuga, Y. Iida, Y. Yamamoto, M. Aihara and M. Kudo 1984. In-plane Ligand Effects on Oxygenation of Cobalt (I1) Schiff Base Complexes, *Inorganica Chimica Acta*, 84, 113-116.

Lever, A.B.P. 1984. *Inorganic electronic spectroscopy*, 2nd Edition, Elsevier, Amsterdam.

Livio R., Maja C., Nataša P., Petra R., Kristina S., Tomislav M., Maja M., Jasna D., Grace K. 2017. Synthesis and antioxidative potency of novel amidino substituted benzimidazole and benzothiazole derivatives, *Croat Chem Acta*, 90(2):187-195.

Mariana L. Oredana Dianu, Angela K., Nicholae S., Adina M.Musuc 2010. Transition metal M(II) complexes with isonicotinic acid 2-(9-anthrylmethylene)-hydrazide. *J Serb Chem Soc.* 75(11):1515.

Marisa B. Ferrari, S.Capacchi , G.Reffo, P.Tarasconi , P.Alberlini, S.Pinelli and P.Lunghi 1999. Synthesis, structural, characterization and biological activity of helicin thiosemicarbazone monohydrate and a copper(II) complex of salicylaldehyde thiosemicarbazone, *Inorganica Chimica Acta*, 286,134.

Md. Sajjad Hossain, Farzana K. Camellia, Nayon Uddin, Md. Kudrat-E- Zahan, Laila A. Banu and Md. Masuqu Haque 2019. Synthesis, Characterization

and Antimicrobial Activity of Metal Complexes of N-(4- methoxybenzylidene) Isonicotinohydrazone Schiff Base, *Asian Journal of Chemical Sciences*, 6(1): 1-8.

Mohammed M. Aboaly, Mostafa M.H. Khalil 2001. Synthesis And Spectroscopic Study Of Cu(II), Ni(II), and Co(II) Complexes Of The Ligand Salicylidene-2-Amino Thiophenol, *Spectroscopy Letters*, 34 (4), 495-504.

Morsy,M.A., Tahani, I.K., Samar A. A. 2011. Spectrochemical study and effect of high energetic gamma ray on copper(II) complexes. J. Solid State Sci. 13,2080-2085.

Nakamoto K. 1978. *Infrared and Raman Spectra of inorganic and coordination compounds*, 3rd ed, Wiley, New York.

Rafat M. Mohareb, Karam A. El-Sharkawy, Muhammad M. Hussein and Hend. M. El-Sehrawi2010. Synthesis of hydrazide-hydrazone derivatives and their evaluation of antidepressant, sedative and analgesic, *J. Pharm. Sci. & Res.*,2(4), 185-196.

Rosaleen J. Anderson, David J. Bendell and Paul W . Groundwater (Organic Spectroscopic Analysis) University of Sunderlan , Royal Society of Chemistry RS.C 2004.

Ruth C. Palenik, Khalil A. Abboud, Stephen P. Summers, Laurel L. Reitfort, Gus J. Palenik 2006. Synthesis, crystal structures, and bond valence sum analyses of lanthanide complexes with a planar pentadentate ligand. *Inorganica Chimica Acta*, 359, 4645-4650.

S. Yamada and A. Takeuchi 1982, The Conformation and Interconversion of Schiff Base Complexes of Nickel (II) and Copper (II), *Coordination Chemistry Reviews*, 43, 187-204.

Sajid H.Guzar and J.I.N.Qin-han 2008. Synthesis, Characterization and spectral studies of new Cobalt(II) and Copper(II) complexes of Pyrrol-2-Carboxaldehyde Isonicotinoyl hydrazone, *Journal of Applied Science*, 8(13), 2480-2485.

Samar A. A. 2017. Synthesis, characterization and antitumore activity of new copper(I) and mercury(II) complexes. Russ. J. General Chem. 87,1256-1263.

Shivakumar, K.; Sashidar, A.; Reddy, P.V.; Halli, M.B. (2008). Synthesis, spectral characterization and activity of benzofuran Schiff bases with Co(II),Ni(II),Cu(II),Zn(II),Cd(II) and Hg(II) omplexes. J. Coord.Chem.,61(14), 2274- 2287.

Sreeja P. B. 2004. *Synthesis, Spectral Characterization, Structural Studies And Biological Investigations Of Transitions Metal Complexes Of Some Acid Hydrazone*, Ph.D Thesis, Cochin University of Science and Technology, India.

Sudeep Bhattacharyya, Sujit Baran Kumar, Subodh Kanti Dutta, Edward R. T. Tiekink and Muktimoy Chaudhury 1996. Zinc(II) and Copper(II) Complexes of Pentacoordinating (N4S) Ligands with Flexible Pyrazolyl Arms: Syntheses, Structure, and Redox and Spectroscopic Properties, *Inorg. Chem.*, 35, 1967-1973.

Tejraj M. Aminabhavi, Ningond S. Biradar, G. V. Karajagi, Walter E. Rudzinski 1984. Spectral and Magnetic Studies of Amino-Acid Schiff Base Complexes of Nickel(II), *Inorganica Chimica Acta*, 91, 49-52.

Temitope A. Ajayeoba1, Olawale F. Akinyele, Ayowole O. Ayeni, Idowu J. Olawuni 2019., Synthesis, Characterisation and Acetylchol-inesterase Inhibition Activity of Nickel(II) and Copper(II) Complexes of 3-Hydroxybenzaldehyde-4-nitrobenzoic Acid Hydrazone, *American Journal of Applied Chemistry*, 7(2): 64-71.

Wagnat W. Wardakhani, Naned N. El-Sayed, Rafat M. Mohareb 2013. Synthesis and anti-tumor evaluation of novel hydrazide and hydrazide-hydrazone derivatives, *Acta Pharm.*, 63, 45-57.

ZANCO Journal of Pure and Applied Sciences
The official scientific journal of Salahaddin University-Erbil
https://zancojournals.su.edu.krd/index.php/JPAS

ISSN (print):2218-0230**, ISSN (online):** 2412-3986**, DOI: http://dx.doi.org/10.21271/zjpas**

RESEARCH PAPER

Hormonal aspects of skin hyperpigmentation in healthy Kurdish primigravida women in Erbil City

Renas Najat Saleem and Sarbaz Ibrahim Mohammed

Department of Biology, College of Science, Salahaddin University-Erbil, Kurdistan Region, Iraq

A B S T R A C T:

The present study aimed to determine some hormonal and biochemical aspects of skin pigmentation in pregnant women. The longitudinal study included forty-three healthy volunteers; ages ranged between 16-28 years, monitored from the beginning of gestation to delivery of birth. Then, women were divided into two groups (25 pigmented and 18 non-pigmented women) to evaluate hormonal and biochemical criteria. The result revealed a significant elevation in adrenocorticotropic hormones (ACTH), estrogen, progesterone hormone levels in pigmented women, and the progressing gestational period significantly changed the hormonal level, liver function parameters**.** At the same time**,** Alanine transaminase (ALT) reduced considerably in the first trimester. We concluded that skin pigmentation in primigravida women is associated with elevated ACTH, female sex hormones level, and liver enzymes. Hyperpigmentation was slightly evident in pregnant mothers with female fetuses than male fetuses.

KEY WORDS: ACTH; Primigravida; skin pigmentation; sex-hormones
DOI: http://dx.doi.org/10.21271/ZJPAS.33.5.11
ZJPAS (2021) , 33(5);95-104 .

1.INTRODUCTION :

The most generally recorded skin change during gravidity is hyperpigmentation (refers to dark spots or patches on the skin), which upgrade in around 90% of pregnant ladies, especially during the second trimester of pregnancy. Different types of pigmentation such as melasma, chloasma, stretch marks, linea nigra, acne, spider angiomas and varicose veins appear on the different part of the body. Hormonal changes may induce pigmentation during gestation, enhancing a temporary elevation in the quantity of melanin secretion by melanocytes (Ibrahim *et al.*, 2020; Motosko *et al.*, 2017; Bieber *et al.*, 2017; Fernandes and Amaral, 2015).

Gravidity is identifying by a change in endocrine hormones, metabolic, vascular, and immunity systems, led to deferent physiological and pathological changes in skin, including changes in coloration, alterations of the connective tissue, vascular system, and hormonal function. Pigmentation is highly related with female sex hormones and medications with estrogens and progesterone, such as the contraceptive tablet or hormone substitution therapy (Friedman *et al.*, 2019; Hurst and Jennifer 2016; Tyler 2015; Muller and Rees 2014).

The melanin synthesis and distribution process is called melanogenesis. It synthesised in melanocytes present among the epidermis' basal cells. Pigments formed in melanocyte melanosomes are then stored in the basal layer of epidermal cells and dermal macrophages, which

* **Corresponding Author:**
Sarbaz Ibrahim Mohammed
E-mail: Sarbaz.mohammed@su.edu.krd
Article History:
Received: 30/04/2021
Accepted: 13/09/2021
Published: 20/10 /2021

become melanophores (Ibrahim *et al.,* 2020; Maranduca *et al.,* 2019; Chaudhary *et al.,* 2015).

The melanin is a color which is delivered by melanocytes at the degree of melanosomes (the melanogenesis). Both melanocyte stimulating hormones (MSH) and ACTH are produced by the cleavage of proopiomelanocortin (POMC) after corticotropin-delivering factor (CRF) incitement and afterward MSH follows up on the skin causing hyperpigmentation. Expanded movement of the maternal adrenal and pituitary organs and a commitment from the creating fetal endocrine organs, expanded cortisone levels, sped up metabolism, and upgraded creation of progesterone and estrogenic chemicals are liable for most skin changes in gestation (Friedman *et al.,* 2019; Rofiq *et al.,* 2019).

Pregnancy-specific changes are the leading cause of abnormal liver function test during the pregnant state, particularly in the third trimester (Mutua *et al.,* 2019; Mishra *et al.,* 2016). Pregnant ladies are especially powerless against iron reduction because of significant increment of iron demands during pregnancy to help the development of erythrocyte mass and plasma volume, and fetal-placental development (Loy *et al.,* 2019; Fisher and Nemeth 2017; Breymann, 2015).

The present study aims to investigate hormonal and biochemical changes that may cause different type pigmented area during pregnancy.

2. MATERIALS AND METHODS

2.1. Subjects

The longitudinal study included forty-three healthy Kurdish primigravida volunteer women examined. They were admitted to a maternity teaching hospital in Erbil, who attended routine care, monitored from the beginning of gestation to delivery of birth. The pregnant women aged between (16-28) years. Other information was taken from the pregnant women by questioners before starting to evaluate hormonal and biochemical analysis. Women divided into two groups; group A included 25 women with gestational pigmentation, and group B had 18 women with no gestational pigmentation.

2.2. Collection of blood samples

The blood samples were collected three times through experiment from every 43 pregnant women during each trimester of pregnancy at 1-13, 14-26, and 27-40 weeks, respectively. After obtaining the information, about seven (7) ml of venous blood was obtained from each woman every three months by vein puncture, using a ten (10 ml) disposable syringe; the blood was added into sterile, plain tubes the serum by centrifugation at 3000 rpm for 15 min. (at $4c^{o}$, using cooling centrifuge) to separate serum and divide it into different parts and was stored frozen at -80c̊ (Sony, Ultra-low, Japan) to estimate later biochemical and hormonal tests.

2.3. Hormonal Analysis

2.3.1 Determination of adrenocorticotropic hormone (ACTH)

The ACTH Ref 7023 Biomerica ELISA kit provides materials for the quantitative measurement of ACTH in plasma.

2.3.2. Determination of estradiol (E2), progesterone hormone, and β-human chorionic gonadotropin

The Accubind ELISA Kit (code: 4925-300), (code: 4825-300), and (code: 825-300) were used for the quantitative Determination of estradiol E2, progesterone, and β-human chorionic gonadotropin levels respectively in human serum.

2.4 Biochemical analysis

Biochemical tests such as ALT, AST, triglyceride, alkaline phosphate (ALP), serum albumin, total protein, total bilirubin and direct bilirubin kit were measured by using Cobas c111 analyzer-Roche Diagnosis.

2.5. Statistical analysis

All data expressed as Means ± Standard Error. Statistical analysis of the obtained data has done according to independent samples t-test, complete randomized design, and qi-square to compare the means of pigmentation and non-pigmentation groups in the study. The statistical analysis carries out using statistically available software (SPSS version 17), using Matlab program for preparing standard hormonal curves and significant level at ($P \leq 0.05$).

3- RESULTS

This cross-sectional study had done on the healthy Kurdish primigravida volunteer women attending the maternity teaching hospital in Erbil. A total of 43 (25 pigmented and 18 no pigmented) pregnant women at different gestational periods had registered in the study after taking informed consent. The hormonal and biochemical result shown in table (1, 2, 3, 4, and 5).

3.1. Hormonal analysis

The ACTH, estrogen, progesterone and hCG values had measured in pigmented and non-pigmented mothers and in the first, second, and

third trimester of gestation, as shown in tables 1& 2.

The results displayed a significant increase of plasma ACTH in the first, second, and third trimesters, while estrogen and progesterone increased significantly in the second and third trimester with non-significant increase in first trimester for progesterone only in pigmented skin when compared with non-pigmented mothers.

In the present studies, there was a significant increase in ACTH, estrogen, progesterone and hCG level in the second and third trimester when contrasted with the first trimester.

Table 1. Some hormonal variations between pigmentation and non-pigmentation in all trimesters of healthy Kurdish primigravida women.

Parameters	First Trimester		P-Value	Second Trimester		P-Value	Third Trimester		P-Value
	No Pigmentation	Pigmentation		No Pigmentation	Pigmentation		No Pigmentation	Pigmentation	
ACTH (pg/ml)	9.685 ± 1.588	14.37 ± 1.054	0.01	13.42 ± 1.291	21.46 ± 3.254	0.05	14.71 ± 1.236	24.63 ± 4.283	0.05
Estradiol (pg/ml)	23.18 ± 4.470	22.42 ± 3.550	NS	25.17 ± 3.783	35.06 ± 3.008	0.05	32.67 ± 3.506	45.07 ± 3.964	0.05
Progesterone (ng/ml)	2957.0 ± 90.4	3408.0 ± 457.6	NS	6451.0 ± 606.1	7768.0 ± 303.8	0.05	7397.0 ± 643.3	8760 ± 266.6	0.05
hCG (mIU/ml)	678.0 ± 164.1	753.5 ±111.1	NS	821.6 ± 156.0	996.2 ± 121.2	NS	1153.0 ± 110.7	1226.0 ± 93.05	NS

NS: Non-Significant

Table 2. Some hormonal variations during the gestational period of healthy Kurdish primigravida women.

Parameters	First Trimester	Second Trimester	Third Trimester
ACTH (pg/ml)	12.43 ± 0.986^{a}	18.13 ± 2.092^{ab}	19.97 ± 2.712^{b}
Estradiol (pg/ml)	22.74 ± 2.734^{a}	31.42 ± 2.575^{b}	37.87 ± 3.589^{b}
Progesterone (ng/ml)	3222 ± 451.3^{a}	7257 ± 330.2^{b}	7886 ± 346.8^{b}
hCG (mIU/ml)	722.2 ± 92.58^{a}	924.0 ± 95.63^{a}	1196 ± 70.28^{b}

A similar line letters mean no significant differences; the various letters of a similar line mean significant differences.

3.2. Biochemical parameters

3.2.1. Liver function test

The results in table 3 show no significant differences in the mean values of total bilirubin, direct bilirubin, alkaline phosphatase, AST, albumins, and total protein values between pigmented and non-pigmented primigravida women in all trimesters. Except ALT level decreased significantly ($p<0.05$) in pigmented women compared with non-pigmented women in the first trimester.

The results of table (4) indicate that albumin and AST levels reduced in both the second and third trimester but**,** ALT and total protein was decreased only in the third trimester when compared with the first trimester. On the other hand, total bilirubin was increased significantly in both the second and third trimester. In contrast, direct bilirubin and alkaline phosphatase increased significantly only in the third trimester when compared with the first trimester.

Table 3. Liver functional test variations between non-pigmentation and pigmentation in all trimesters of healthy Kurdish primigravida women

Parameters	First Trimester		P-Value	Second Trimester		P-Value	Third Trimester		P-Value
	No Pigmentation	Pigmentation		No Pigmentation	Pigmentation		No Pigmentation	Pigmentation	
Total Bilirubin (mg/dl)	0.370 ± 0.028	0.374 ± 0.028	NS	0.588 ± 0.051	0.6148 ± 0.057	NS	0.465 ± 0.031	0.491 ± 0.018	NS
Direct Bilirubin (mg/dl)	0.127 ± 0.032	0.154 ± 0.021	NS	0.251 ± 0.009	0.291 ± 0.026	NS	0.455 ± 0.179	0.434 ± 0.141	NS
AST (U/L)	23.38 ± 1.888	22.62 ± 1.527	NS	17.66 ± 1.360	19.04 ± 1.066	NS	16.22 ± 1.345	18.12 ± 0.776	NS
ALT (U/L)	18.73 ± 1.660	14.74 ± 0.983	0.5	15.77 ± 2.109	15.40 ± 1.437	NS	11.62 ± 1.717	11.68 ± 0.782	NS
Alkaline phosphatase	81.69 ± 4.741	82.98 ± 3.962	NS	112.6 ± 10.38	95.48 ± 6.162	NS	201.6 ± 20.98	220.2 ± 11.84	NS

(Ul/L)									
Albumine (g/dl)	4.362 ± 0.149	4.268 ± 0.062	NS	3.871 ± 0.089	3.975 ± 0.064	NS	4.111 ± 0.134	3.879 ± 0.076	NS
Total Protein (g/dl)	6.587 ± 0.237	6.633 ± 0.124	NS	6.436 ± 0.152	6.421 ± 0.168	NS	6.191 ± 0.261	5.780 ± 0.181	NS

NS: Non-Significant

Table 4. Liver functional test variations during gestational period of healthy Kurdish primigravida women

Parameters	**First Trimester**	**Second Trimester**	**Third Trimester**
Total Bilirubin (mg/dl)	0.372 ± 0.020^{a}	0.603 ± 0.039^{c}	0.480 ± 0.016^{b}
Direct Bilirubin (mg/dl)	0.143 ± 0.018^{a}	0.274 ± 0.016^{ab}	0.443 ± 0.109^{b}
AST (U/L)	22.94 ± 1.176^{b}	18.46 ± 0.838^{a}	17.32 ± 0.726^{a}
ALT (U/L)	16.41 ± 0.938^{b}	15.55 ± 1.200^{b}	11.65 ± 0.838^{a}
Alkaline phosphatase (Ul/L)	82.44 ± 3.005^{a}	102.6 ± 5.708^{a}	212.4 ± 11.10^{b}
Albumin (g/dl)	4.307 ± 0.071^{b}	3.932 ± 0.052^{a}	3.976 ± 0.072^{a}
Total Protein (g/dl)	6.614 ± 0.121^{b}	6.427 ± 0.115^{b}	5.952 ± 0.153^{a}

A similar line letters mean no significant differences; the various letters of a similar line mean significant differences.

3.3 Baby gender and skin pigmentation

The present work Chi-square test revealed a non-significant relation between baby gender and skin pigmentation. The female gender percentage in non-pigmented women was (33.3 %) while in pigmented women was (58.3 %). On the other hand, the percentage of male gender in non-pigmented women was (66.7 %) and in pigmented women was (41.7%), i.e. male gender percentage is twice the female gender in non-pigmented women.

Table (5): Relation between baby gender and skin pigmentation during normal pregnancy.

Baby gender	Females	Males	P-Value
No Pigmentation	6 (33.3%)	12 (66.7%)	0.098
Pigmentation	14 (58.3)	10 (41.7)	

4.DISCUSSION

4.1Pigmentation during pregnancy

The commonly encountered physiological changes during pregnancy are pigmentary alterations, the most common colouration being melasma, linea nigra, palmar erythema (Ciechanowicz *et al.*, 2018; Urasaki, 2010).

Many factors have associated with the development of pigmentation, including hormonal influences of pregnancy, like elevated ACTH levels, estrogen and progesterone, ultraviolet radiation. Other possible factors are hepatic dysfunction, some haematological changes, nutritional deficiency, genetics, and racial (Cario 2018; Costin and Hearing, 2007; Damoa *et al*., 2006).

4.2Hormonal Analysis

4.2.1 ACTH

Results show a highly significant elevation in serum ACTH levels of first, second, and third trimesters in normal Kurdish primigravida pigmented ladies when compared with ACTH levels of non-pigmented healthy women, the present result in agreement with (Sandru *et al.*, 2019; Maranduca *et al.*, 2019; Sanson *et al*., 2003) they showed that ACTH levels increased throughout pregnancy reaching maximum levels during the third trimester. There is agreement that the proopiomelanocortin (POMC) peptides with huge melanogenic action are ACTH, α-MSH, and β-MSH. ACTH invigorates skin pigmentation, prevalently in sun-uncovered zones through a mechanism of binding ACTH to the epidermal melanocytic specific receptor (MC1-R), increased tyrosinase activity leads to melanin synthesis in which enhances skin pigmentation because of contribution large number and higher susceptibility of melanocytes receptors to hormonal stimulus in these areas and may be due to that the progressive well investigated stresses of primigravida to near the term and delivery, cause ACTH secretion from the anterior pituitary gland to suppress stresses pathway and lead to enhance pigmentation process (Maranduca *et al.*, 2019; Brenner and Hearing, 2008).

The observation of high ACTH concentration in pigmented pregnant women may be due to that CRH and vasopressin stimulate the POMC-derived peptide. The CRH is recognized as an inducible endocrine hormone from the placenta in the net-physiology of pregnancy, influencing ACTH release from the anterior pituitary lobe, raising the possible role in influencing skin pigmentation (Maranduca *et al.*, 2019; Petraglia *et al.*, 2010 and Brenner and Hearing, 2008).

On the other hand, a previous publication focused on a relationship between parity and increased stress. In normal pregnancies, there is evidence of oxidative stress related to the lipid changes observed in pregnancy (Brody *et al*., 2011).

The effects of the gestational period on the ACTH ratios indicate a significant increase of ACTH level in the third trimester compared with the first trimester. This result in agreement with previous studies (Sandru *et al.*, 2019; Karaca *et al*., 2010; Lindsay and Nieman, 2005), summarising that women of childbearing age tend to have larger glands, and upward convexity of the pituitary gland causes increased ACTH releasing, also include placental synthesis and release of biologically active CRH and ACTH. Furthermore, they found a positive correlation has observed between CRH and POMC; Proopiomelanocortin (POMC) is the polypeptide precursor of ACTH, which is physiologically present in blood originate from the anterior pituitary. Indeed, CRH levels increase exponentially during the late trimester,

lead to more releasing of POMC and subsequence production of ACTH (Maranduca *et al.,* 2019; Sandru *et al.,* 2019).

4.2.2 Sex hormones

Maternal estrogen results show a significant increase in the second and third trimester of gestation in pigmented mothers, this is in agreement with other findings (Friedman *et al*., 2019; Mahmood *et al*., 2011; Brenner and Hearing, 2008), and they provide the role of estrogen and progesterone in the causation of discolored patches and hyperpigmentation during pregnancy. It is due to the fact of the estrogens mechanism by which it progresses pigmentation. Probably, there are specific regional differences in the number of melanocytes in the skin (Cario, 2018).

Furthermore, the stimulating effects of estrogen on proliferation and tyrosinase role of epidermal melanocytes enhance melanin synthesis markedly. Where it accumulates within melanosomes, tend to develop chloasma observe in gravidity mother, often accompanied by elevated coloration in different areas of the body, including the linea alba, perineal skin and the areola, the majority of which generally blur following parturition (Rofiq *et al.,* 2019; Alves *et al*., 2005; Slominski *et al*., 2004).

Our data study for serum estrogen and progesterone demonstrate a significant increase in the second and third trimester when comparison with first trimester, agree with researches of (Cario 2018; Mahmood *et al*., 2011, Zen *et al*., 2010; Villaseca *et al*., 2005) indicating that in healthy pregnant women, serum estrogen level progressively increased throughout gestation, due to that additive production sites for estrogen rather than ovaries, include the corpus luteum, the placenta, and the fetal adrenal glands. Elliott *et al*., (2004) argue that estrogen may have evolved a pivotal role in establishing, maintaining, and culminating pregnancy. Also, estrogen influences muscle strength and increases uterine muscle contractility and during the gestational term progresses delivery (Cario 2018; Kristiansson and Wang, 2001)

The present study findings for progesterone are inconsistent with the results reported by (Rofiq *et al.,* 2019; Bolanca *et al.,* 2008), recording significant maternal serum elevations in the second and third trimester when compared with the first trimester. Progesterone's adaptive increases by placenta predominate later during pregnancy and the initial sources of corpus luteum, fetal and maternal adrenal glands. Propounding progesterone promotes uterine muscle relaxation for maintenance of pregnancy and fetal development, loosens up smooth muscle, which causes atony of the gastrointestinal and urinary system. Also, together with estrogens, stimulate the mammary glands' growth in the breasts in preparation for lactation. The estrogen stimulates the secretion of melanocyte-stimulating hormones higher than normal levels during gestation, in turn, leads to melanin pigment production, which is responsible for general gestation-induced pigmentary phenomena (Friedman *et al.*, 2019).

Physiologically increase in the level of hCG shown in pigmented mother compared with non-pigmented mothers' results supported by conclusions of (Petraglia, *et al.,* 2010 and Sanson *et al*., 2003) who showed that hCG, produced in the placenta implicated as important endocrine mediators in the physiology of pregnancy and parturition. Plasma hCG concentration correlated positively with gestational age and increased placental mass.

Moreover, a significant increase in hCG has shown in the third trimester when comparison with first trimester inconsistent by (Gallego *et al*., 2010; Tran, 2006), reporting that the gestational-related increase of maternal hCG serum levels reaches as the peak during the first and third trimester, during to the placental mass increasing in late pregnancy.

4.3 Biochemical parameters

4.3.1. Liver function test parameters

The results showed non-significant differences in the mean values of total bilirubin, direct bilirubin, ALP, AST, albumin and total protein value between the pigmented and non-pigmented primigravida women in all trimesters, whereas, ALT level was decreased significantly in pigmented women in the first trimester.

These results were dissimilar with findings documented (Mutua *et al.,* 2019; Mishra *et al.,* 2016; Jamjute *et al*., 2009), who showed that ALT and AST levels were slightly elevated, indicating liver diseases, spider naevi, pruritus and palmar erythema that may occur during normal pregnancy.

The current results indicate that albumin level decreased in the second and third trimesters and total proteins in last trimester compared with the first trimester. The present result agrees with studies of (Khatun *et al.,* 2020; Venugopal and Rajamma 2015; Gohel *et al.,* 2013; Suresh and Radfar, 2004), who showed a decline of serum albumin in the first ten weeks of pregnancy and slightly decreased toward term because there was a high plasma volume, the yields elevate in plasma volume proceeds from 50 cc at ten weeks pregnancy to 800 cc at 20 weeks. Also, excessive loss of urinary excretion may explain the fall in blood albumin level through late gestation (Khatun *et al*., 2020; Gohel, *et al.*, 2013; Jamjute *et al*., 2009).

On the other hand, the result of ALT, AST, total bilirubin, and direct bilirubin were dissimilar with findings documented (Khatun *et al.,* 2020; Venugopal and Rajamma 2015; Gohel, *et al.*, 2013) they showed serum ALT, AST concentration significantly high while serum total bilirubin, and direct bilirubin concentration as gestation advanced were due to a phenomenon called hemodilution could be responsible for the change in serum liver enzymes or liver damage.

Similar results found previously by (Mishra *et al.*, 2016; Venugopal and Rajamma 2015; Gohel, *et al.*, 2013; Tran 2006) reporting shifts in protein level and change gradually throughout gestation because the metabolic demands increased due to physiological and hormonal changes in the mother and growth of the fetus. Further explanation is that during gestation, micronutrients deficiencies may have severe consequences for pregnancy outcomes and, as a resulting decline, blood contents of proteins, vitamins and minerals (Khatun *et al.,* 2020; Venugopal and Rajamma 2015; Guerra *et al*., 2009).

The present study shows significantly higher alkaline phosphatase values in the third trimester and total bilirubin increased only in the second trimester compared with the first trimester. In agreement with (Mutua *et al.,* 2019; Mishra *et al.*, 2016; Suresh and Radfar, 2004), they summarised that alkaline phosphatase value ascendancy was at the binging of the last trimester. This increase is due to the leakage of placental alkaline phosphatase into the maternal blood (Mutua *et al.*, 2019; Mishra *et al.,* 2016; Suresh and Radfar, 2004)

Serum ALP concentration directly forwardly matches skeletal and fetus development and mineral storage in the maternal organs. Biological alterations in alkaline phosphatase value happen with regularity during the reproductive cycle. The greatness of alteration corresponds largely to anatomic growth and development (Khatun *et al*., 2020).

The result of total bilirubin and direct bilirubin in the current study agrees with previous investigations (Mishra *et al.,* 2016; Suresh and Radfar, 2004) show a significant elevation from the first to the third trimester. Hemodilution partially responsible for the diminishing of bilirubin levels because albumin is the protein carrier of bilirubin; decreased albumin concentrations during normal pregnancy interpret gestational bilirubin declines (Khatun *et al.,* 2020; Alonso, 2006)

4.4 Baby gender and skin pigmentation

The chi-square test has shown a non-significant correlation between baby gender and skin pigmentation in the present study. Ibrahim *et al.*, (2020) confirmed these results showed that chloasma is more likely to occur among female fetus than males, while Abdullah (2020) showed that hyperpigmentation was more evident in primigravida pregnant mothers with male fetuses than female fetuses. It may be related to hormonal, or any other haematological variation between these pregnancy cases and this must be confirmed and further studied.

CONCLUSIONS

The present research concluded the presence of ACTH and female sex hormones great effects in pregnancy women hyperpigmentation. Estimation in serum liver enzyme in all gestation trimesters is important for the diagnosis liver disease and anemia during gestation. Hyperpigmentation was more evident in pregnant mothers with female fetuses than male fetuses.

Acknowledgements

We wish to acknowledge all staff members of the haematology and the biochemistry labs in Erbil maternity teaching hospital for their assistance and co-operation during the research.

REFERENCES

Abdullah, G.A. 2020. Hyperpigmentation in primigravida pregnant ladies in relation to fetal gender. *Scholars literature.* 107 (3)

Alves, G. F., Nogueira, L. S. C. and Varella, T. C. N. 2005. Dermatology and pregnancy. *An Bras Dermatol.* 80 (2): 179-186.

Alonso A. G., (2006). Effect of pregnancy on pre-existing liver disease physiological changes during pregnancy. *Annals of hepatology*. 5 (3): 184- 186.

Bieber, A.K., Martires K.J., Stein J.A., Grant –Kels J. M., Driscoll M. S., and Pomeranz, M. K. 2017. Pigmentation and pregnancy: Knowing what is normal. *Obstet Gynecol*; 129:168–73.

Bolanca, I., Bolanca, Z., Kuna K., Vuković A., Tuckar N., Herman R. and Grubisić G., 2008. Chloasma- the mask of pregnancy. *Uni. Dep. of Obstetrics and Gynecology*. 32 (2): 139-141.

Brenner, M. and Hearing V. J. 2008. Modifying skin pigmentation – approaches through intrinsic biochemistry and exogenous agents. *Drug Discov Today Dis Mech.* 5 (2): 189–199.

Breymann, C. 2015. Iron deficiency Anemia in pregnancy. *Semin Hematol*; 52:339–47.

Brody, S. M., Stuebe, A., Dole, N., Savitz, D., Rubinow, D., and Thorp, J. 2011. Elevated corticotropin releasing hormone (CRH) during pregnancy and risk of postpartum depression (PPD). *J Clin Endocrinol Metab*. 96 (1): E40– E47.

Cario, M. 2018. How hormones may modulate human skin pigmentation in melasma: An in vitro perspective. *Experimental Dermatology WILEY*.

Chaudhary, R, Nirali, M., Ankur, C, and Khushbu, M. 2015. Dermatological Disorders in Pregnancy: A Cross-Sectional Study. *International Journal of Scientific Study*, 3(8).

Ciechanowicz, P., Mariusz, S., Karol, T., Agnieszka, R., Adriana, R., Bozena K., Miroslaw, W., Lidia, R. 2018. Skin changes during pregnancy. Is that an important issue for pregnant women? *Via Medica* 89 (8), 449–452

Costin, G. E. and Hearing, V. J. 2007. Human skin pigmentation: melanocytes modulate skin color in response to stress. *The Faseb Journal*. 21: 976 - 994.

Damoa, A. S., Lambert, W. C. and Schwartz, R. A., 2006. Melasma: Insight into a distressing Dyschromia. *Aesthetic Dermatology*. 8 (1): 1- 6.

Elliott K. J., Cable N. T., Reilly T., Sefton V., Kingsland C. and Diver M., (2004). Effect of supra-physiological changes in human ovarian levels on maximum force production of the first dorsal interosseus muscle. *Exp Physiol*. 90 (2). 215-223.

Fernandes L.B., and Amaral W.N. 2015. Clinical study of skin changes in low and high risk pregnant women. *An Bras Dermatol*; 90:822–6.

Fisher, A. L. and E. Nemeth 2017. Iron homeostasis during pregnancy. Am J Clin Nutr; 106 (Suppl):1567S–74S

Friedman, E. B. Richard, A S., and John, F. T. 2019. Management of pigmented skin lesions during pregnancy. *AJGP*. 48(9).

Gallego, M. J., Porayette, P., Kaltcheva, M. M., Bowen, R. L., Meethal, S. V. and Atwood. C. S., 2010. The pregnancy hormones human chorionic gonadotropin and progesterone induce human embryonic stem cell proliferation and differentiation into neuroectodermal rosettes. *Stem Cell Research & Therapy*. 1 (28): 1-13.

Gohel, M. G, Anant G. J., Jitendra S. A., Jemil S. M., and Chandrakant P.K. 2013.Evaluation of changes in liver function test in first, second and third trimester of normal pregnancy. *Int J Reprod Contracept Obstet Gynecol*; 2(4): 616-620.

Guerra, A. G., Neufeld, L. M., Cordero, S. H., Rivera, J., Martorell, R. and Ramakrishnan, U., 2009. Prenatal multiple micronutrient supplementation impact on biochemical indicators during pregnancy and postpartum. *Salud pública de méxico.* 51 (4): 327-335.

Hurst, H, and Jennifer, L. 2016. Diagnosing Dermatologic Conditions of Pregnancy. *The Journal for Nurse Practitioners – JNP*. 12(2).

Ibrahim, W. H., Heba, M. M. and Walaa, H. A. 2020. Relationship between Fetal Sex and pattern of Nausea, Vomiting and Cholasma among Pregnant women at Assuit city. *Assiut Scientific Nursing Journal.* 8 (20), pp (191-199)

Jamjute, P., Amer, A., Tarun, G., and Philip, B. (2009). Liver function test and pregnancy. *The Journal of Maternal-Fetal and Neonatal Medicine.* 22(3). 274-285.

Karaca, Z., Tanriverdi, F., Unluhizarci, K. and Kelestimur, F. 2010. Pregnancy and pituitary disorders. *European Journal of Endocrinology.* 162: 453–475.

Khatun, M. R., Amina Kh., Nowshad A. 2020. Comparison of Liver Function Tests in Normal Pregnancy with Non-pregnant Matched Controls. *TAJ;* 33(1)

Kristiansson, P. and Wang J. X. 2001. Reproductive hormones and blood pressure during pregnancy. *Human Reproduction*. 16 (1): 13-17.

Lindsay, J. R. and Nieman, L. K. 2005.The hypothalamic-pituitary-adrenal axis in pregnancy: challenges in disease detection and treatment. *The Endocrine Society.* 26 (6): 775–799.

Loy, S. L., Li, M. L., Shiao-Yng, C., Pei T. T., Yen, L. C., Phaik, L. Q., Jerry, K. Y. C., Kok H T, Fabian, Y., Keith, M. G., Lynette, P.C. S, Mary, F., Michael, S. K., Yap-Seng, C., and Claudia, C. 2019. Iron status and risk factors of iron deficiency among pregnant women in Singapore: a cross-sectional study. *BMC Public Health* 19:397

Mahmood, K., Nadeem, M., Aman, S., Abdul-Hameed and Kazmi, A. H. 2011. Role of estrogen, progesterone and prolactin in the etiopathogenesis of melasma in females. *Journal of Pakistan Association of Dermatologists.* 21(4): 241-247.

Maranduca, M. A., Daciana, B., Dragomir, N. S., Daniel, C. B., Gabriela, S., Nicuta, M. and Ionela, L. S. 2019. Synthesis and physiological implicationsof melanic pigments (Review). *ONCOLOGY LETTERS* 17: 4183-4187

Mishra, N. V. N. Mishra, Parineeta, T. 2016. Study of Abnormal Liver Function Test during Pregnancy in a Tertiary Care Hospital in Chhattisgarh. *The Journal of Obstetrics and Gynecology of India;* 66(S1): S129–S135

Motosko, C. C., Amy, K. B., , Miriam K. P., Jennifer, A. S., Kathryn, J. M. 2017. Physiologic changes of pregnancy: A review of the literature. *International Journal of Women's Dermatology* 3; 219–224.

Muller, I. and A. Rees. 2014. Melasma and Endocrine Disorders. *Journal of Pigmentary Disorders; S1*

Mutua, D. N, Eliud, N. M. N., and George, O. 2019. Liver Function Tests in Normal Pregnant Women. *J Liver*. 7 (2)

Petraglia, F., Imperatore, A., and Challis, J. R. G. 2010. Neuroendocrine mechanisms in pregnancy and parturition. *Endocrine Reviews.* 31 (6): 783– 816.

Rofiq, A, Shw, T., Widiatmoko, A. and Dyah, A. S. 2019. Correlation of Estradiol and Estriol Serum Levels to Melasma Severity in Pregnant Women. *Skin Diseases & skin care*. 4(3).

Sandru, F., Mihai, C. D., Simona, E. A., Mara, C., and Ana, V. 2019. Hyperpigmentation and ACTH – an overview of literature. *Ref: Ro Med J.;*66(4)

Sanson, R. M. L., Keyzer, Y. D. and Bertagna, X. 2003. Proopiomelanocortin, a polypeptide precursor with multiple functions: from physiology to pathological conditions. *European Journal of Endocrinology*. 149: 79–90.

Slominski, A., Tobin, D. J., Shibahra, S., and Wortsman, J. 2004. Melanin pigmentation in mammalian skin and its hormonal regulation. *Physiol Rev*. 84: 1228-1155.

Suresh, L. and Radfar, L. 2004. Pregnancy and lactation. *Endod*. 97 (6): 672-682.

Tran, H. A. 2006. Biochemical tests for abnormalities in pregnancy. *Aust Prescr. 29: 48–51.*

Tyler, K. H. 2015. Physiological Skin Changes During Pregnancy. *Clinical obstetrics and gynecology*, 58 (1), 119–124

Urasaki, M. B. M., (2010). Skin physiological alterations perceived by pregnant women attended at public health services. *Acta Paul Enferm. 23 (4): 519-525.*

Venugopal, S., and Rajamma C K. 2015. Liver function tests in first and third trimesters of normal pregnancy in a population of North Kerala. *Journal of International Medicine and Dentistry*; 2(3): 215-221

Villaseca, P., Campino, C., Oestreicher, E., Mayerson, D., Ferre, M. S. and Arteaga, E. 2005. Bilateral oophorectomy in a pregnant woman: hormonal profile from late gestation to post-partum: Case report. *Human Reproduction.* 20 (2): 397–401.

Zen, M., Ghirardello, A., Iaccarino, L., Tonon, M., Campana, C., Arienti, S., Rampudda M., Canova M. and Doria, A. 2010. Hormones, immune response, and pregnancy in healthy women and SLE patient. *Swiss Med WKLY;*140(13–14):187–201

ZANCO Journal of Pure and Applied Sciences
The official scientific journal of Salahaddin University-Erbil
https://zancojournals.su.edu.krd/index.php/JPAS

ISSN (print):2218-0230**, ISSN (online):** 2412-3986**, DOI: http://dx.doi.org/10.21271/zjpas**

RESEARCH PAPER

The Correlation of initial hematological feature with advanced stage in Chronic Lymphocytic Leukemia in Kurdistan Region of Iraq

Tavan Ismael Mahmood 1, Basil K. Abdulla2, Dana A. Abdullah3, Ahmed K. Yassin4, Kawa M. Hasan5 Zeki A. Mohamed 6, Nawsherwan S. Mohammed7, Hisham A. Getta8, Sana D. Jalal9, Rawand P. Shamoon10, Ranan Kardagh Polus11,Ghanim Salim Numan12,Bryar S. Rashid13, Zhala O. Ahmad14,Shokhan Mmustafa15,Shlan Salahaden Mohammed16,Lara Lateef Abdulrahman17, Marwa Nadhim Karam18, Rozh-hat A. yousif19.

1MBChB, KBMS-candidate, Department of Hematology, Hiwa Cancer hospital, Sulaymaniyah, Kurdistan Region, Iraq, tavan_esmaeel012@yahoo.com
2MBChB, FIMS-hemato-oncology, Department of Hematology, Hiwa Cancer hospital, Sulaymaniyah, Kurdistan Region, Iraq, basilonc@yahoo.com
3MBChB, MSc, PhD hematopathology, Department of Pathology, College of Medicine, University of Sulaymaniyah, Sulaymaniyah, Kurdistan Region, Iraq, dr_dana73@hotmail.com
4MBChB, DM, CABM, FIBMS, FRCP, Department of Medicine, College of Medicine, Hawler Medical University, Erbil, Kurdistan Region, Iraq, dahmedk@yahoo.com
5MBChB, FRCP, PhD, Department of Medicine, College of Medicine, Hawler Medical University, Erbil, Kurdistan Region, Iraq, mah_kawa@yahoo.com
6MBChB, MRCP, FIBMS, Department of Medicine, College of Medicine, University of Duhok, Duhok, Kurdistan Region, Iraq, barwari65@yahoo.com
7MBChB, FIBMS-path, Department of Pathology, College of Medicine, Hawler Medical University, Erbil, Kurdistan Region, Iraq, nawsherwan.sadiq@med.hmu.edu.iq
8MBChB, FIBMS-path, Department of Pathology, College of Medicine, University of Sulaymaniyah, Sulaymaniyah, Kurdistan Region, Iraq, haalrawi@yahoo.com
9MBChB, FIBMS-path, FRCPath, Department of Pathology, College of Medicine, University of Sulaymaniyah, Sulaymaniyah, Kurdistan Region, Iraq, dr.sanajalal612@gmail.com
10MBChB, PhDhematopathology, Department of Pathology, College of Medicine, Hawler Medical University, Erbil, Kurdistan Region, Iraq, rawand.shamoon@med.hmu.edu.iq
11MBChB, FIBMS-path, FFCAP, Department of Pathology , College of Medicine, Hawler Medical University, Erbil, Kurdistan Region, Iraq, ranan.kardagh@hmu.edu.krd
12MBChB, FIBMS-path, Department of Hematology, Nanakali Hospital, Erbil, Kurdistan Region, Iraq, ghanem_59@yahoo.com
13MBChB, KBMS- Department of Hematology, Hiwa Cancer hospital, Sulaymaniyah, Kurdistan Region, Iraq1MBChB, bryarsabah@gmail.com
14MBChB, KBMS-candidate, Department of Hematology, Hiwa Cancer hospital, Sulaymaniyah, Kurdistan Region, Iraq, zhala.ahamd@gmail.com
15MBChB, KBMS-candidate, Department of Hematology, Nanakali Hospital, Erbil, Kurdistan Region, Iraq, Shokhan.Mohammad@yahoo.com.
16MBChB, KBMS-candidate, Department of Hematology, Nanakali Hospital, Erbil, Kurdistan Region, Iraq, shlan.mohammad@yahoo.com
17MBChB, KBMS-candidate, Department of Hematology, Nanakali Hospital, Erbil, Kurdistan Region, Iraq, lara2018lateef@gmail.com
18MBChB, KBMS-candidate, Department of Hematology, Nanakali Hospital, Erbil, Kurdistan Region, Iraq, marwanadhim@gmail.com
19MBChB, KBMS-candidate, Department of Hematology, Azadi Hospital, Duhok, Kurdistan Region, Iraq, rojhat.duhoki1986@yahoo.com

* **Corresponding Author:**
Tavan Ismael Mahmood
E-mail:
Article History:
Received: 30/05/2021
Accepted: 28/07/2021
Published: 20/10 /2021

Background and objective: Chronic lymphocytic leukemia (CLL) is considered by an accumulation of matured lymphocytes in the blood, bone marrow, spleen. And lymph .We aimed to find the correlation of initial hematological feature with advanced stage in CLL. **Methods:** A retrospective study was conducted on 138 patients with CLL, confirmed by flow cytometry of peripheral blood collected in Hiwa Hematological and Oncological Hospital in Sulaimani, Nanakaly Hospital in Hawler, and Azadi Hematology - Oncology Center in Duhok, Kurdistan Region of Iraq dated from January 1, 2010, to December 31, 2020. **Results:** The mean age of 63.07±11 years with male predominance. The majority of patients at presentation were Rai Stage II and Binet stage A. The frequency of DAT positivity was found in (6.5%), which also established appositive relationship with advanced stage, there were statistically significant relation of hemoglobin level, platelet counts, LDH level to Rai stage and Binet stage disease (P value <0.001), No association were noted between different age groups and initial laboratory finding, also no relation of gender to staging. **Conclusion:** In the present study there was a significant relation between laboratory findings (hemoglobin, platelet count, LDH levels) to with staging, in addition DAT positivity demonstrated a significant correlation with advanced stage, those with High LDH levels associated with more advanced Rai stage.

KEY WORDS: Chronic lymphocytic leukemia; Initial laboratory; advanced stage, KRI.
DOI: http://dx.doi.org/10.21271/ZJPAS.33.5.12
ZJPAS (2021) , 33(5);105-115 .

1.INTRODUCTION :

Chronic lymphocytic leukemia (CLL) is considered by the accretion of matured-lymphocytes in the peripheral blood, bone marrow, spleen, and lymph nodes(Yun, Zhang and Wang, 2020). The diagnosis of CLL needs the presence of ≥5 × 109/L B lymphocytes in the peripheral blood, continued for at least 3 months with clonality confirmed by flow cytometry according to International Workshop on Chronic Lymphocytic Leukemia (IWCLL) criteria(Hallek *et al.*, 2018)Also express CD19, CD5, and CD23 with weak or no expression of surface immunoglobulin (Ig), CD20, CD79b, and FMC7, CLL is the furthermost common leukemia of adults in the west nations, Most CLL patients in the over-all population are elderly (median age 71.5 years)(Yun, Zhang and Wang, 2020).

The clinical presentation at diagnosis is very variable. About 60% of patients are asymptomatic, and the disease may be doubted after a routine complete blood count. While symptomatic, patients present with unclear symptoms of fatigue or weakness(Mercer, 2002). Patients generally have a good performance status at diagnosis, Lymphadenopathy with cervical and axillary lymph nodes bilaterally and symmetrically being affected, Splenomegaly is generally mild to moderate and is observed in nearly 50% of cases; hepatomegaly is less common, and rare at diagnosis, when the disease progresses, patients can have B symptoms (Rodrigues *et al.*, 2016).

Some of the chronic lymphocytic leukemia patients can presented with cytopenia's. These contain autoimmune hemolytic anemia, immune thrombocytopenic purpura, pure red cell aplasia and autoimmune agranulocytosis. Between CLL associated cytopenia's, autoimmune hemolytic anemia(AIHA) is the greatest common and considered by a positive direct antiglobulin test(DAT), known as Direct Coombs test with elevated serum bilirubin, increased reticulocytes and presence of spherocytosis on peripheral blood film examination (Haider *et al.*, 2019). AIHA is generally detected in advanced stages of disease and associated with poor prognostic group, DAT status at the time of disease appearance shows new prognostic indicator for overall survival (Abbas *et al.*, 2015).

Assessment of such patients should include a complete blood count with differential; flow cytometry of the peripheral blood to define the immunophenotype of circulating lymphocytes; and check of the peripheral smear, however Assessment of the bone marrow is not usually required, but should be examined in those patients with unexplained cytopenia's (Kanti RR, Stilgenbauer S and Aster JC, 2019).

The serological test in CLL, is standard and consist of Lymphocyte doubling time (LDT), serum beta2-microglobulin (s-β2M), serum thymidine kinase (s-TK) and lactic dehydrogenase (LDH) are the greatest common straight serum markers in CLL and expect poor results. LDT ≤ 12 months expects poor prognosis while LDT > 12 months associates with an extended treatment-free period and survive. LDH is an pointer of time to first treatment (TTFT) and related with shorter PFS, overall survival (OS) and Richter's transformation It is still of prognostic value in patients with trisomy 12 (Rosenquist *et al.*,

2013).it is commonly understood as reflecting high tumor burden or tumor aggressiveness and conveys a poor prognosis in CLL(Sagatys and Zhang, 2012).

The Rai and Binet clinical staging systems are useful to stratify patients, describing their risk and prognosis. (Hallek *et al.*, 2018).

Administration protocol for treatment of CLL consist of combination of immunotherapy and standard chemotherapy for patients with symptomatic, advanced or progressive disease. While for patients with stable disease the "watch and wait" algorithm is usually deployed (Hallek *et al.*, 2018),(Madu *et al.*, 2019) .

2. Materials and Methods:

2.1. Study design and patients

The present study was a retrospective observational study that involved 138 patients who had CLL were enrolled. The patients were admitted to Hiwa Hematological and Oncological Hospital in Sulaimani, Nanakaly Hospital in Hawler, and Azadi Hematology Oncology Center in Duhok, Kurdistan Region Iraq, from January 1, 2010, to December 31, 2020.

Patients involved in this study were established according to the International workshop on chronic lymphocytic leukemia (IWCLL)(Hallek *et al.*, 2018).

The inclusion criteria included all patients who had been diagnosed with CLL, (both gender male and female, age more than 35 years, newly diagnosis, and all races.)

Exclusion criteria all patients with

1-Incomplete data

2-Age younger than 35 years

3-Transforamtion of cases during data collection,

4-Small Lymphocytic Lymphoma

5- Hairy Cells Leukemia and others B-Cells Lymphoma.

The documented data about the patients was collected from the electronic databases of the mentioned hospitals, the demographic features containing (age, gender, race, residency, occupation, BMI.) , presenting features(anemia, fatigue, B-symptoms, lump), hematological panel (complete blood count, blood film, coombs test, retic count, blood group) , biochemical panel(lactate dehydrogenase), organomegaly ,peripheral lymphadenopathy confirmed with ultrasound and flow cytometry of peripheral blood was used to confirm the diagnosis but molecular and cytogenetic studies were not done as it was not available

Then we classified our patients according to Rai and Binet staging system (Hallek *et al.*, 2018). Also the patients were treated, followed up and assessed their response according to International Workshop on Chronic Lymphocytic Leukemia (IWCLL) criteria(Hallek *et al.*, 2018), some patients with a symptomatic early stage disease(Rai 0, Binet A) monitored without therapy, but patients with intermediate –risk and high-risk disease generally received treatment with chemo-immunotherapy and targeting therapy, and assessment of their response at least 2 months after completion of therapy.

2.2. Statistical analysis:

After data collection and prior to data entry and analysis, the questions of study were coded. Data entry performed via using an excel spreadsheet then the statistical analysis was performed by SPSS program, version 21 (IBM SPSS Statistical Package for the Social Sciences). The data presented in tabular forms showing the frequency and relative frequency distribution of different variables. Chi-square test used to compare different qualitative (categorical) variables of the study (to find their association) as comparing different laboratory finding with age groups, sex and the two types of staging (Benit and Modified Rai). Different types of Bar charts and Pie charts as well as arithmetic scale line graphs were used to describe some variables of the study diagrammatically.

2.3. Ethical consideration:

Research Ethical Committee of the Kurdistan Board of Medical Specialties (KBMS) and Cancer Center accepted the study proposal

3. Results

This study comprised 138 patients with CLL, the mean age of 63.07±11, 29 cases are female and 71 patients are male (ranged from 35 to ≥80 years). The major age group was in 50-64 years with 42.8 %. And male: female ratio is 2.45:1, as shown in (Table 1)

The majority of patients at presentation were Rai Stage II (44 cases, 31.9%), Binet stage A (58 cases, 42.0%) while minimum number of them had Rai Stage III (13 cases, 9.4%), Binet stage B (33 cases, 23.9%) as shown mentioned (Table 2).
The direct anti-globin test positivity was set up in (9 cases, 6.5%), negativity (129 cases 93%). LDH was measured in all patients, it was normal in 52.9 %(n=73) and in 47.1 %(n=65) was above the normal, the others hematological markers are shown in (Table 3).
The relation between different age groups and initial laboratory finding is statistically not significant (P >0.05) as shown in (Table 4).
Regarding the relation of the same age grouping to the staging systems of CLL, It was obvious that there was a highly significant correlation between age and Rai stage of presentation, with majority of patients of Stage II (P value 0.04), but correlation of age with Binet stage and modified Rai staging of presentation are also statistically not significant (P value> 0.05) as shown in table (Table 5)
Regarding the relationship of laboratory finding to the staging of presentation, there are statistically a significant relation of hemoglobin level, platelet counts ,LDH level to Rai stage and Binet stage disease (P value <0.001), but relation of lymphocyte groups, coombs test ,Blood groups of patients to Rai stage and Binet stage are statistically not significant(P value > 0.05) (Table 6).
We also want to discovery any relation between gender of patients and CLL staging systems in (Table 7), we found that more female patients have Rai Stage 0 and Binet stage A disease, while more male patients have Rai Stage II and Binet stage A disease, and both male and female have Modified intermediate risk, but again this relation is also statistically not significant (P value> 0.05).

Table (1): Age distribution of chronic lymphocytic leukemia in KRI

Age	**Frequency**	**Percent**
35 - 49 Years	22	15.9%
50 - 64 years	59	42.8%
65 - 79 years	47	34.1%
≥ 80 years	10	7.2%
Total	138	100.0%

Table (2): Staging systems of chronic lymphocytic leukemia patients:

Staging	category	Frequency	Percentage
Rai	0	30	21.7%
	I	15	10.9%
	II	44	31.9%
	III	13	9.4%
	IV	36	26.1%
Binet	A	58	42.0 %
	B	33	23.9 %
	C	47	34.1 %
Modified Rai	Low risk	30	21.7%
	Intermediate risk	59	42.8%
	High risk	49	35.5%

Table (3): Initial laboratory finding of CLL patients

Laboratory test	Frequency	Percentage
Hemoglobin		
≤ 10	31	22.5%
> 10	107	77.5%
Platelet level		
≥ 100	104	75.4%
< 100	34	24.6%
Lymphocyte groups		
5 – 10	81	58.7%
10.1 – 50	36	26.1%
> 50	21	15.2%
LDH		
Normal Normal (≤ 280 U/L)		52.9%
High (> 280 U/L)	65	47.1%
Coomb's test		
Positive	9	6.5%
Negative	129	93.5%
Blood group		
A + ve	28	29.8 %
B + ve	23	24.5 %
B - ve	1	1.1 %
AB + ve	5	5.3 %
AB - ve	1	1.1 %
O + ve	33	35.1 %
O – ve	3	3.2 %

Tabale (4): Relation between age distribution of CLL patients and initial laboratory finding

Laboratory test	35 - 49 Y	50 - 64 Y	65 – 79 Y	≥ 80 Y	Total	P value
Hemoglobin						
≤ 10	4	12	11	4	31	0.54
> 10	18	47	36	6	107	
Platelet level						
≥ 100	15	43	39	7	104	0.49
< 100	7	16	8	3	34	
Lymphocyte groups						
5 – 10	13	30	31	7	81	0.75
10.1 – 50	6	19	9	2	36	
> 50	3	10	7	1	21	
LDH						
Low (< 140 U / L)	7	22	16	5	50	0.93

Normal (140 - 280 U/L)	3	10	8	2	23	
High (> 280 U/L)	12	27	23	3	65	
Coomb's test						
Positive	1	4	2	2	9	0.32
Negative	21	55	45	8	129	
Blood group						
A+	3	13	9	3	28	0.78
B+	4	9	8	2	23	
B-	0	1	0	0	1	
AB+	1	1	3	0	5	
AB-	0	0	1	0	1	
O+	5	16	10	4	33	
O-	2	1	0	0	3	

Table (5): correlation between age distributions of CLL patients with staging systems

Staging	35 - 49 Y	50 - 64 Y	65 – 79 Y	≥ 80 Y	Total	P value
Rai staging						
0	1	11	15	3	30	0.04
I	6	8	1	0	15	
II	5	19	18	2	44	
III	2	4	5	2	13	
IV	8	17	8	3	36	
Binet staging						
A	9	24	21	4	58	0.52
B	3	15	14	1	33	
C	10	20	12	5	47	
Modified Rai staging						
Low risk	1	11	15	3	30	0.15
Intermediate risk	11	27	19	2	59	
High risk	10	21	13	5	49	

Table (6): correlation between laboratory findings of CLL patients with staging systems

Modified Rai staging

Lab. Finding / Rai Staging	Modified Rai staging			Total	P value
	Low risk	Intermediate risk	High risk		
Hemoglobin					
≤ 10	0 (0%)	0 (0%)	31 (100%)	31 (100%)	< 0.001
> 10	30 (28.0%)	59 (55.1%)	18 (16.8%)	107 (100%)	
Platelet level					
≥ 100	30 (28.8%)	59 (56.7%)	15 (14.5%)	104 (100%)	< 0.001
< 100	0 (0%)	0 (0%)	34 (100%)	34 (100%)	
Lymphocyte groups					
5 – 10	21 (26%)	30 (37%)	30 (37%)	81 (100%)	0.06
10.1 – 50	9 (25%)	18 (50%)	9 (25%)	36 (100%)	
> 50	0 (0%)	11 (52.4%)	10 (47.6%)	21 (100%)	
LDH					
Normal (≤ 280 U/L)	19 (26.0%)	25 (34.2%)	29 (39.7%)	73 (100%)	0.09
High (> 280 U/L)	11 (16.9%)	34 (52.3%)	20 (30.8%	65 (100%)	
Coomb's test					
Positive	2 (22.2%)	2 (22.2%)	5 (55.6%)	9 (100%)	0.36
Negative	28 (21.7%)	57 (44.2%)	44 (34.1%)	129 (100%)	
Blood group					
A+	7 (25%)	12 (42.9%)	9 (32.1%)	28 (100%)	0.70
B+	2 (8.7%)	9 (39.1%)	12 (52.2%)	23 (100%)	
B-	0 (0%)	1 (100%)	0 (0%)	1 (100%)	
AB+	1 (20%)	3 (60%)	1 (20%)	5 (100%)	
AB-	0 (0%)	1 (100%)	0 (0%)	1 (100%)	
O+	8 (24.2%)	15 (45.5%	10 (30.3%)	33 (100%)	
O-	0 (0%)	1 (33.3%)	2 (66.7%)	3 (100%)	

Lab. Finding / Benit Staging	Benit staging			Total	P value
	A	B	C		
Hemoglobin					
≤ 10	0 (0%)	0 (0%)	31 (100%)	31 (100%)	< 0.001
> 10	58 (54.2%)	33 (30.8%)	16 (15.0%)	107 (100%)	
Platelet level					
≥ 100	58 (55.8%)	33 (31.7%)	13 (12.5%)	104 (100%)	< 0.001
< 100	0 (0%)	0 (0%)	34 (100%)	34 (100%)	

Lymphocyte groups					
5 – 10	35 (43.2%)	18 (22.2%)	28 (34.6%)	81 (100%)	0.16
10.1 – 50	19 (52.8%)	8 (22.2%)	9 (25%)	36 (100%)	
> 50	4 (19%)	7 (33.3%)	10 (47.6%)	21 (100%)	
LDH					
Normal (≤ 280 U/L)	32 (43.8%)	14 (19.2%)	27 (37. 0%)	73 (100%)	< 0.001
High (> 280 U/L)	26 (40%)	19 (29.2%)	20 (30.8%)	65 (100%)	
Coomb's test					
Positive	3 (33.3%)	1 (11.1%)	5 (55.6%)	9 (100%)	0.34
Negative	55 (52.6%)	32 (24.8%)	42 (32.6%)	129 (100%)	
Blood group					
A+	10 (35.7%)	10 (35.7%)	8 (28.6%)	28 (100%)	0.47
B+	6 (26.1%)	6 (26.1%)	11 (47.8%)	23 (100%)	
B-	0 (0%)	1 (100%)	0 (0%)	1 (100%)	
AB+	3 (60%)	1 (20%)	1 (20%)	5 (100%)	
AB-	0 (0%)	1 (100%)	0 (0%)	1 (100%)	
O+	15 (45.5%)	8 (24.2%)	10 (30.3%)	33 (100%)	
O-	1 (33.3%)	0 (0%)	2 (66.7%)	3 (100%)	

Benit staging

Table (7): correlation between gender distributions of patients with staging

Gender/ Staging	**Gender**		**Total**	**P value**
	Male	**Female**		
Rai staging				
0	18	12	30	0.18
I	9	6	15	
II	33	11	44	
III	8	5	13	
IV	30	6	36	
Benit staging				
A	38	20	58	0.45
B	24	9	33	
C	36	11	47	
Modified RAI staging				
Low risk	18	12	30	0.25

Intermediate risk	42	17	59	
High risk	38	11	49	
Total	98	40	138	

4. Discussion

CLL is the greatest common form of adult leukemia in the Western countries, through maximum of cases in elders above 50(Basabaeen *et al.*, 2019) .

We retrospectively collected 138 patients, the mean age of presentation was 63.1 years old (ranged from 35 to ≥80 years) which are nearby to the results reported in other Iraq studies(Hasan, 2018), (Al-rubaie and Mohammed, 2018), also comparable to the result described in Iran(Payandeh, Sadeghi and Sadeghi, 2015). while the results show a decade younger than US (Brander *et al.*, 2017), (Pulte *et al.*, 2016). This difference can be qualified to the variance in population structure, residence, genetic tendency, environmental factor, disproportion in lifetime expectation and sample size among Iraq and western countries.

In our study the male to female ratio 2.45:1 which was comparable to that of western countries and other world studies (Brander *et al.*, 2017) (Pulte *et al.*, 2016),(Basabaeen *et al.*, 2019),(Abbas *et al.*, 2015). But it was higher than that described by other Iraqi studies (Al-rubaie and Mohammed, 2018),this may also due to variance in sample size. But in very studies clear finding of male predominance was stable. Which might be linked to genetic bases as revealed by results described by Cantu ES, McGill JR et al (Cantú *et al.*, 2013)

In the current study, most patient presented at Rai stage II (31.9%) or Binet stage A (42%) or modified Rai intermediate risk (42.8%), according to the data from other western world such as in brazil and USA are frequently primary seen in Rai stage II (35.6%), Modified Rai intermediate risk (43.2%) and Rai stage II (37.9%), Binet stage A (42.6%) respectively(Faria *et al.*, 2000) , (Pflug *et al.*, 2014). But according to the data from previous study of Iraq most of patients existing at an advance stage such as Rai stage III or IV (59.1%) Binet stage C (55.2%) (Hasan, 2018), (Naji, 2012). also in Iran greatest patient is realized in advanced stage (38.5%) which are various in present study.(Payandeh, Sadeghi and Sadeghi, 2015) may be due to regular review, services now available for initial recognition and diagnosis of the disease.

We tried to find any relation among staging and their gender but statistically it was not significant while both male and female mostly have modified Rai intermediate Risk and Binet stage A disease.

In current study in relation of age to staging our study showed that advance stage is more common in age 50-64years which was similar to the preceding study done in Iraq (Naji, 2012).also in USA (Parikh *et al.*, 2014).

Also, male was more frequently affected by the disease than female which is similar to a study done in Iran(Payandeh, Sadeghi and Sadeghi, 2015).

We found that in 138 pateints,44 patient blood group was not done(31.95%),majority of our patients have O-positive blood group(33 cases 35.1%) ; we didn't find any connection between blood group and staging in current study, and this may necessity further researches as we could not find any research about ABO blood grouping in CLL, except one paper speaking about the spreading of ABO blood type in patients with leukemia which displays that in CLL patients majority have blood Group O(Ochoa-garcía *et al.*, 2019).

The occurrence positive DAT in current study was (6.5%), Inadequate studies are available from Asian countries, Before only study showed in Erbil city of Iraq has reported 11% of CLL patients showing DAT positivity and its associated with significant anemia, this outcome was higher to that of our study(Hasan, 2018).Various studies conducted in United State, Spain, England and have re-counted a frequency of positive DAT in 4.5%,4.3% and 7.7% of CLL patients respectively However, the prevalence of DAT positivity in our patients appears to be more than in US, Spain, and less than in England these studies conducted in western world (Kyasa *et al.*, 2003)'(Moreno *et al.*, 2010)'(Ward, 2001) .

In this study on 138 CLL patients at diagnosis, DAT positive result was associated with more advanced stage, less predominant in stage A disease, as it was testified to another study in Iraq,

Asian and America(Hasan, 2018)'(Abbas *et al.*, 2015)'(Dearden *et al.*, 2008).

In current study we found that LDH has statistically significant relation with staging (p-value<0.001) which was comparable to that reported by Asian, Germany and Italy studies(Li *et al.*, 2017)'(Pflug *et al.*, 2014)'(Autore *et al.*, 2019).

Since LDH is an low-priced and usually performed laboratory parameter, also reflect tumor burden and such disease activity, we found that 73(52.9%) patients displayed levels within normal range, and 65(47.1%) patients exhibited elevated LDH levels, in compare elevated LDH levels to previous study in Iraq and Asian was lower (82.9%, 70%) respectively,(Hasan, 2018)'(Al-rubaie and Mohammed, 2018)'(Mozaheb, NazarAbadi and Aghaee, 2012) but in compare to Germany study in current study the elevated LDH level was more than in Germany study (47.1 %versus 34.8%) (Pflug *et al.*, 2014).

In current study Those with high LDH level showed (52.3%, 30.8%) associated with intermediate and high risk of modified Rai staging respectively and 40% with Binet Stage A, this was an arrangement to conducted study in Italy (Autore *et al.*, 2019).

5. Conclusion:

The median age was similar to that observed in Iraq and Iran. . Male –to-female ratio which was comparable to that of western countries and other world studied with male predominance which was obvious in all studies; however, patients more frequently presented at early stage comparable to the western population. And DAT positivity in our setting appears relatively similar to international studies, also an association of positive DAT was found with advanced stage like regional and western studies. Also there was statistically significant relation between laboratory finding to the staging (including hemoglobin, platelet count and LDH levels) similar to the regional and international studies, those with High LDH levels associated with advanced Rai stage.

Acknowledgment

We wish to extend our special thanks to the Smart Health Tower Research Center for their assistance.

Reference:

Abbas, S. A. *et al.* (2015) 'Direct coombs test positivity in B-chronic lymphoid leukemia: A marker of advanced clinical disease', *Asian Pacific Journal of Cancer Prevention*, 16(14), pp. 6007–6010. doi: 10.7314/APJCP.2015.16.14.6007.

Al-rubaie, H. A. and Mohammed, S. J. (2018) 'Assessment of Interleukin-8 in Patients with Chronic Lymphocytic Leukemia in Correlation with the Prognostic Factors : β2 -microglobulin , LDH and Binet Stage', 17(2).

Autore, F. *et al.* (2019) 'Elevated lactate dehydrogenase has prognostic relevance in treatment-naïve patients affected by chronic lymphocytic leukemia with trisomy 12', *Cancers*, 11(7), pp. 1–12. doi: 10.3390/cancers11070896.

Basabaeen, A. A. *et al.* (2019) 'Clinical presentation and hematological profile among young and old chronic lymphocytic leukemia patients in Sudan', *BMC Research Notes*, 12(1), pp. 12–17. doi: 10.1186/s13104-019-4239-7.

Brander, D. M. *et al.* (2017) 'Welcome & Introductions Living with Chronic Lymphocytic Leukemia (CLL)', (Cll), pp. 1–43.

Cantú, E. S. *et al.* (2013) 'Male-to-female sex ratios of abnormalities detected by fluorescence in situ hybridization in a population of chronic lymphocytic leukemia patients', *Hematology Reports*, 5(1), pp. 13–17. doi: 10.4081/hr.2013.e4.

Dearden, C. *et al.* (2008) 'The prognostic significance of a positive direct antiglobulin test in chronic lymphocytic leukemia: A beneficial effect of the combination of fludarabine and cyclophosphamide on the incidence of hemolytic anemia', *Blood*, 111(4), pp. 1820–1826. doi: 10.1182/blood-2007-07-101303.

Faria, J. R. de *et al.* (2000) 'Prognosis related to staging systems for chronic lymphocytic leukemia', *Sao Paulo Medical Journal*, 118(4), pp. 83–88. doi: 10.1590/S1516-31802000000400002.

Haider, M. S. *et al.* (2019) 'Autoimmune cytopenias in chronic lymphocytic leukemia', *Pakistan Journal of Medical Sciences*, 35(5), pp. 1334–1338. doi: 10.12669/pjms.35.5.369.

Hallek, M. *et al.* (2018) 'iwCLL guidelines for diagnosis, indications for treatment, response assessment, and supportive management of CLL', *Blood*, 131(25), pp. 2745–2760. doi: 10.1182/blood-2017-09-806398.

Hasan, K. M. (2018) 'Clinical aspects, immunophenotypic analysis and survival rate of chronic lymphocytic leukaemia patients in Erbil city, Iraq', *Sultan Qaboos University Medical Journal*, 18(4), pp. e461–e467. doi: 10.18295/squmj.2018.18.04.006.

Kanti RR, Stilgenbauer S and Aster JC (2019) 'Clinical features and diagnosis of chronic lymphocytic leukemia/small lymphocytic lymphoma - UpToDate [Internet] Updated May 2019', pp. 1–36. Available at: https://www.uptodate.com/contents/clinical-features-and-diagnosis-of-chronic-lymphocytic-

leukemia-small-lymphocytic-lymphoma.

Kyasa, M. J. *et al.* (2003) 'Autoimmune cytopenia does not predict poor prognosis in chronic lymphocytic leukemia/small lymphocytic lymphoma', *American Journal of Hematology*, 74(1), pp. 1–8. doi: 10.1002/ajh.10369.

Li, H. *et al.* (2017) 'Serum LDH level may predict outcome of chronic lymphocytic leukemia patients with a 17p deletion: A retrospective analysis of prognostic factors in China', *Chinese Journal of Cancer Research*, 29(2), pp. 156–165. doi: 10.21147/j.issn.1000-9604.2017.02.09.

Madu, A. J. *et al.* (2019) 'Presenting features and treatment outcomes of chronic lymphocytic leukaemia in a resource poor Southern Nigeria', *Malawi Medical Journal*, 31(2), pp. 144–149. doi: 10.4314/mmj.v31i2.7.

Mercer, R. (2002) 'Review articles', *The Antiquaries Journal*, 82, pp. 358–365. doi: 10.1017/S000358150007390X.

Moreno, C. *et al.* (2010) 'Autoimmune cytopenia in chronic lymphocytic leukemia: Prevalence, clinical associations, and prognostic significance', *Blood*, 116(23), pp. 4771–4776. doi: 10.1182/blood-2010-05-286500.

Mozaheb, Z., NazarAbadi, M. H. H. and Aghaee, M. A. (2012) 'Chronic lymphocytic leukemia and prognostic factors', *Asian Pacific Journal of Cancer Prevention*, 13(7), pp. 3009–3013. doi: 10.7314/APJCP.2012.13.7.3009.

Naji, A. S. (2012) 'Outcome of 49 Iraqi adult patients with Chronic Lymphocytic Leukemia treated with oral alkylating agent':, ٥٤ ,*مجلة كلية الطب*(2), pp. 126–130. doi: 10.32007/jfacmedbagdad.v2126-130.

Ochoa-garcía, P. P. *et al.* (2019) 'Association between the phenotype of the blood group system AB0 and', 30(4), pp. 639–644.

Parikh, S. A. *et al.* (2014) 'Chronic lymphocytic leukemia in young (≤ 55 years) patients: A comprehensive analysis of prognostic factors and outcomes', *Haematologica*, 99(1), pp. 140–147. doi: 10.3324/haematol.2013.086066.

Payandeh, M., Sadeghi, E. and Sadeghi, M. (2015) 'Survival and clinical aspects for patients with chronic lymphocytic leukemia in Kermanshah, Iran', *Asian Pacific Journal of Cancer Prevention*, 16(17), pp. 7987–7990. doi: 10.7314/APJCP.2015.16.17.7987.

Pflug, N. *et al.* (2014) 'Development of a comprehensive prognostic index for patients with chronic lymphocytic leukemia', *Blood*, 124(1), pp. 49–62. doi: 10.1182/blood-2014-02-556399.

Pulte, D. *et al.* (2016) 'Trends in survival of chronic lymphocytic leukemia patients in Germany and the USA in the first decade of the twenty-first century', *Journal of Hematology and Oncology*, 9(1), pp. 1–8. doi: 10.1186/s13045-016-0257-2.

Rodrigues, C. A. *et al.* (2016) 'Diagnosis and treatment of chronic lymphocytic leukemia: recommendations from the Brazilian Group of Chronic Lymphocytic Leukemia', *Revista Brasileira de Hematologia e Hemoterapia*, 38(4), pp. 346–357. doi: 10.1016/j.bjhh.2016.07.004.

Rosenquist, R. *et al.* (2013) 'Prognostic markers and their clinical applicability in chronic lymphocytic leukemia: Where do we stand?', *Leukemia and Lymphoma*, 54(11), pp. 2351–2364. doi: 10.3109/10428194.2013.783913.

Sagatys, E. M. and Zhang, L. (2012) 'Clinical and laboratory prognostic indicators in chronic lymphocytic leukemia', *Cancer Control*, 19(1), pp. 18–25. doi: 10.1177/107327481201900103.

Ward, J. H. (2001) 'Autoimmunity in chronic lymphocytic leukemia.', *Current treatment options in oncology*, 2(3), pp. 253–257. doi: 10.1007/s11864-001-0039-z.

Yun, X., Zhang, Y. and Wang, X. (2020) 'Recent progress of prognostic biomarkers and risk scoring systems in chronic lymphocytic leukemia', *Biomarker Research*, 8(1), pp. 1–11. doi: 10.1186/s40364-020-00222-3.

ZANCO Journal of Pure and Applied Sciences
The official scientific journal of Salahaddin University-Erbil
https://zancojournals.su.edu.krd/index.php/JPAS

ISSN (print):2218-0230**, ISSN (online):** 2412-3986**, DOI:**

RESEARCH PAPER

Removal of Bentazone Pesticide from Aqueous Solutions by Electro-oxidation Method

Mohammed Azeez Othman[1] ,Yusuf Yavuz [2]

1Department of Health and Environmental science , College of Science, Salahaddin University- Erbil, Kurdistan Region, Iraq
2Anadolu University, Dept. of Environmental Engineering, Turkey

A B S T R A C T:

The kinetics of the electro-oxidation degradation of prepared aqueous solutions containing bentazone as a model compound of the thiadiazine group of pesticides was studied in the lab. The oxidation process was conducted under galvanostatic polarization in natural model media using boron-doped diamond (BDD) cathode and anode. Chemical oxygen demand (COD) estimation along the electro-oxidation treatment processing allowed the assessment of kinetic of organic compounds decay as well as the instantaneous current efficiency. The obtained data reflected that the degradation of bentazone pesticide is significantly dependent on initial amount of bentazone pesticide, current density and electrolytes concentration. COD removal follows a pseudo first-order kinetic and the electro-oxidation process was under the control of mass transport within the range studied, regardless the conditions of experimental. The COD removal rate increases with applied current density until 20 mA/cm^2 and decreases for higher values. Two different concentrations supporting electrolyte (5mM, 10mM) were used. The rate of degradation increased significantly with increasing electrolyte concentration. The best obtained conditions for COD removal efficiency on the BDD electrode to degrade bentazone solutions (COD= 91.18 %) include operating at 20 mA/cm^2 and 10 mM Na^2SO^4 as supporting electrolyte. This arrangement and condition allow to approximately complete degradation of bentazone in just 80 min. A decrease in the relative toxicity index value along the electro-oxidation indicate toxic compounds disappearance. The initial toxicity EC50 (5 min) and (15min) were decrease by 81% and 94%

KEY WORDS: COD, Pesticides model wastewater, Electro-oxidation methods, COD removal, Removal efficiency.
DOI: http://dx.doi.org/10.21271/ZJPAS.33.5.13
ZJPAS (2021) , 33(5);116-121.

1.INTRODUCTION:

The conservation of freshwater resources has become a major concern for many countries around the world, and environment protection is an economic and political issue. Among the major sources of water pollution are organic pollutants, particularly pesticides and plant protection products used by farmers to increase crop yields. The widespread use of pesticides in agriculture, as well as excessive pesticide storage and disposal, a re major sources of pollution in rivers, ground wat er, reservoirs, rainwater, soil, and air.

Pesticides can be removed from water using a variety of advanced technologies. Among these technologies, electrochemical processes are the most recent methods for pesticide degradation. These approaches are safe for the environment and do not generate new radioactive waste. (Kapałka, et al., 2010 and Andrade et al., 2007).

In electro-oxidation process, the refractory compounds oxidation occurs at very high overpotential, choice of anode material is the most important factor. Electrochemical oxidation with a Boron-Doped Diamond (BDD) anode is well known as a promising treatment technique for the removal of available organic compounds. (Othman, M.A. 2018). Indeed, the high oxidation performance of the BDD by electro generation of

* **Corresponding Author:**
Mukhlis Hamad Aali
E-mail: mukhlis.aali@su.edu.krd or hamukhlis2@live.utm.my
Article History:
Received: 01/05/2021
Accepted:30/07/2021
Published: 20/10 /2021

hydroxyl radical (• OH) from water discharge (Eq. 1).

M+H2O-----M(OH.)+H+e (1)

The hydroxyl radicals on the BDD anode are quasi-free on the surface and can react massively with organics close to the anode (Mcbeath et al., 2000). The aim of the current work is to investigate the effect of electrochemical oxidation on bentazone removal in model solutions. Measurements of global parameters such as total organic carbon and chemical oxygen demand have been used to estimate the rate of mineralization. The effect of operating variables such as current density, type of electrolytes on the efficiency of COD and bentazone removal was investigated.

2. EXPERIMENTAL

2.1 Chemicals

All of the solutions in this study were made in the lab as a model solution. Where a concentration of 480g/L of a commercially available bentazone pesticide was chosen for the subsequent works, and deionized water is utilized to prepare the model solution. Bearing in mind that this concentration is identical to what farmers use in agricultural fields. The properties and structural of bentazone is given in table 1. To measure the chemical oxygen demand, sulfuric acid (H_2SO_4) reagent, standard solutions of potassium dichromate ($K_2Cr_2O_7$), and silver sulphate (Ag_2SO_4) were prepared. The value of COD reduction was evaluated using a closed reflux colorimetric method [16]. All chemicals used were reagent grade.

Table 1. Chemical structure of bentazone

Name	Structure
Bentazone Molecular Formula: $C_{10}H_{12}N_2O_3S$	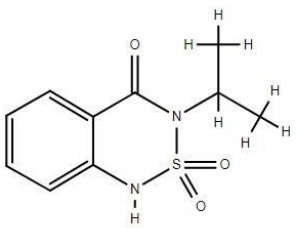
Molecular weight (g/mol)	240.28 g/mol

2.2 Apparatus and Procedures

In this procedure, an electrochemical cell consists of a 600 mL reactor, and 400 mL of the sample was used as is during the electrooxidation treatment, with 5.0 and 10.0 mM of Na2SO4 added as a supporting electrolyte. The BDD electrodes were connected to a digital power supply Sarton 3262.3 model (0-300 V and 0-4 A). During the experiment, a magnetic stirrer was used to maintain a steady stirring speed of 300 rpm. The electrochemical oxidation reactions were carried out at atmospheric pressure and room temperature and the duration of electro-oxidation process was 80 min. To estimate the COD reduction efficiency, samples were taken at regular intervals. All the experiments were performed in duplicate. A constant current density of 5, 10 15, and 20 mA/cm2 were applied in all experiments.

2.3 Boron doped diamond electrodes set up

The boron-doped diamond electrode was provided by CSEM. Two BDD electrodes were used in electrolysis with DC power supplies (an anode and cathode) with the width of 3.7 cm, length of 5 cm and the distance between two electrodes as 0.5 cm. The supporting electrolyte (Na2SO4) was employed at 5.0 mM and 10.0 mM concentrations. Along the experimental period of 80-minute, the samples were taken at 20-minute intervals for analysis.

2.4 Analytical techniques

Materials were collected and measured without any filtration throughout the experiments. Chemical oxygen demand data were evaluated using the TS2789 (water quality-Determination of COD) standard All samples titrated with ferric acid ammonium sulphate (FAS) which was standardized before each measurement to decide how much potassium dichromate was consumed.

COD removal percentages of taken samples were calculated as follows:

$$\boldsymbol{COD\ removal} = \frac{(CODo - CODt)}{CODo} * 100 \qquad (1)$$

Where CODo indicate the initial concentration and CODt indicate the concentration at given time

of the pesticide removal and treatment process and calculated in mg/L.

Remaining pollutants of bentazone concentration were measured with the UV-visible spectrophotometer at λmax= 230.

3. Results and Discussion

Despite the fact that the electro-oxidation approach has its own set of advantages and limitations, the current study seeks to determine the level of pesticide removal in wastewater using this method. Several variables in this approach were optimized, including current densities, time duration, support electrolyte concentration, and energy consumption.

3.1 COD removal capacity

The initial pH of the model solution effluent has been found to be an essential element determining the electrochemical process performance (Lepki et al., 2018). To evaluate its effect during the electrochemical treatment process, the sample pH was kept at its range.

The feasibility of using BDD in an electro-oxidation treatment process to remove bentazone pesticide and this by estimation of COD levels in the treated sample. The current density is seen to be the important factor because it controls the reactive oxygen species amounts in addition to other electro-generated oxidants that have the ability of chemical destruction. Pesticide removal has been studied in terms of applied current density and support electrolytes. Figures 1 and 2 show that current density is the most important factor affecting bentazone removal performance. This seen significantly at the 10, 15, and 20 mA/cm2. This can be described by taking into account the formation of the highly reactive hydroxyl radical, which is directly influenced by current density and other oxidizing species including peroxydisulfate (if Na_2SO_4 is applied as in this article) can also be competitively produced with reactive oxygen (Lin et al., 2013).

3.2 Supporting electrolyte

The removal efficiency of bentazone and COD was directly influenced by the addition of support electrolytes as shown in figure (3). In looking at figure 3 and scrutinizing it, it was noticed that COD removal rates were nearly 79% and 82.5 % for 5.0 mM and 10.0 mM Na2SO4, respectively. please check the results in correct way.

Table 2. COD removal and degradation cost of bentazone at 5 mM electrolyte concentration

Applied current (mA/cm^2)	Electrolysis Time (min)	COD removal (%)	Energy Consumption (kWh/m^3)	Cumulative energy consumption (KWh/m^3)	Energy cost (dollar $/m^3$)
5	80	77.29	2.38	9.58	58.25
10	80	81.03	5.74	23.01	140.51
15	80	83.98	10.63	42.12	260.50
20	80	86.01	16.72	68.54	409.679

Table 3. COD removal and degradation cost of bentazone at 10 mM electrolyte concentration

Applied current (mA/cm^2)	Electrolysis Time (min)	COD removal (%)	Energy Consumption (kWh/m^3)	Cumulative energy consumption (KWh/m^3)	Energy cost (dollar $/m^3$)
5	80	80.91	1.47	5.98	35.98
10	80	85.36	4.15	16.65	101.57
15	80	88.10	8.05	32.62	197.27
20	80	91.18	14.23	57.63	348.74

3.3 Energy consumption

In an electro-oxidation technique, the main economic parameter is an energy consumption E (kWh/m3) (Errami et al.,2014). The energy consumption parameter is calculated from the equation below:

$$Energy\ Consumption\ (E) = \frac{I*V*t}{\mathrm{Vol}*1000} \qquad (2)$$

Where I, V and t stand for electrical current intensity (I), average voltage of the EC system (V), and reaction time.

The technical feasibility of electrochemical oxidation is normally measured in terms of the percentage of pollutants removed; however, the economic feasibility is measured in terms of energy consumption and supporting electrolyte

dosage effect of on energy consumptions were investigated and tabulated in table 2 and 3. Because the support electrolytes and current density have an inverse relationship, increasing the Na2SO4 concentration decreases the energy consumption value. At 5mM Na2SO4 supporting electrolyte concentrations and 20mA/cm2 the maximum energy consumption of 68.54 kWh/m3 was observed. (Figure 4).

3.4 Energy Cost

The energy cost (dollar /m^3) for the removal of pesticides for each process was calculated by applying the following equation:

$$cumulative\ energy\ consumption\ \frac{KWh}{m^3}\ Unit\ price\left(\frac{dollar}{KWh}\right) \quad (3)$$

However, at the optimal current density of 20 mA/cm^2, the energy cost for the highest removal efficiency by electro-oxidation treatment was (348,74 dollar/m^3). (Table 2&3).

3.5 Toxicity

Toxicity assays based on V. fisheri bioluminescence which are employed as part of more rigorous environmental evaluations or for routine screening and primary evaluation of the bentazone pesticide model solution. To determine toxicity during treatment, the luminescence test was chosen as a sensitive and repeatable screening process. To evaluate the toxicity variation, percentage inhibition data taken from optimum experimental conditions were converted to a relative toxicity index (RTI). The results represented as the RTI values versus a reaction time are illustrated in Figure (6). Any decrease in RTI values during the electro-oxidation process reflects a decrease in concentration of hazardous compounds concentration. Initial toxicity EC50 (5min) was reduced by 81% after 80 minutes of the treatment by EOP. Whereas, the EC50 (15mins) values was declined by 94% for 80 minutes of electrolysis. According to category given by (Yavuz & Koparal, 2006), The EOP was found to have the potential to reduce toxicity to a minor level. This occurred along with COD reduced.

4. CONCLUSION

The electro-oxidation treatment process can efficiently remove pesticides and COD by using boron doped diamond electrode. The studies demonstrated the importance of choosing the best electrolysis parameter in order to achieve best removal rates, which are necessary for any electro-oxidation process application. The current work aimed to evaluate the electro-oxidation technique validity in the treatment of bentazone in model wastewater. The effect of current density and concentration of supporting electrolyte were evaluated on removal efficiency and COD. The current density and concentration of supporting electrolytes had an effect on the removal of bentazone pesticides in aqueous solution. The results of bentazone degradation by electro-oxidation method using BDD indicated that this process gave highest removal efficiency and COD at optimum experimental conditions. At 20mA/cm2 and 10mM supporting electrolyte, the best removal efficiency was 91,18 %. Energy consumption and cost of process at the best obtained result were 57,63 kWh/m^3 and 348,74 Krş/m^3 respectively.

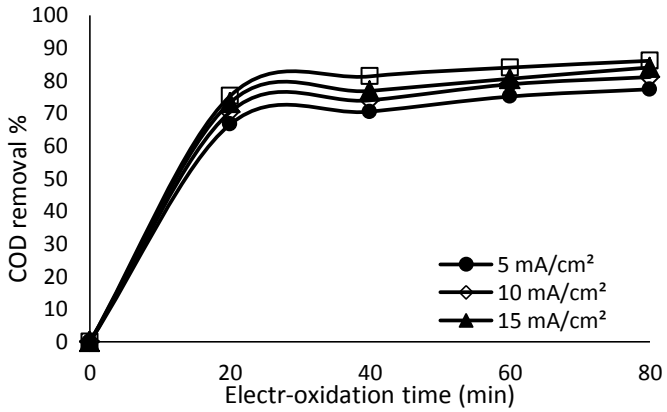

Figure 1. *Variation of COD removal over the time depending on current density (EO, Co= 300 mg/L bentazone, 5mM Na_2SO_4, pH= 6.43)*

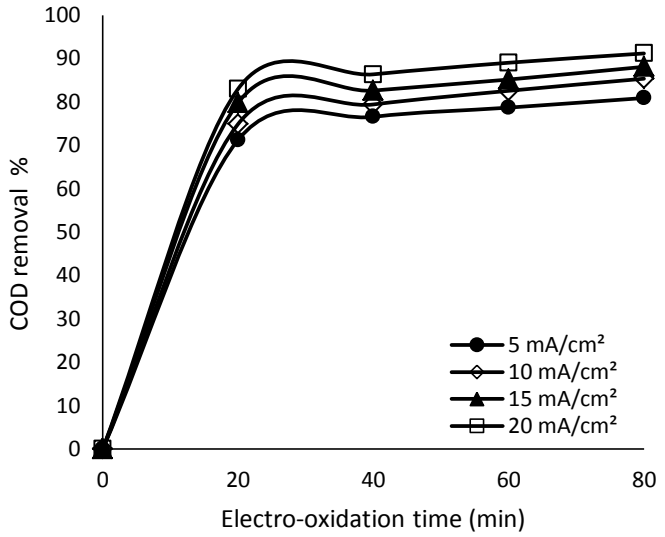

Figure 2. *Variation of COD removal over the time depending on current density (EO, Co= 300 mg/L bentazone, 10mM Na_2SO_4, pH= 6.31)*

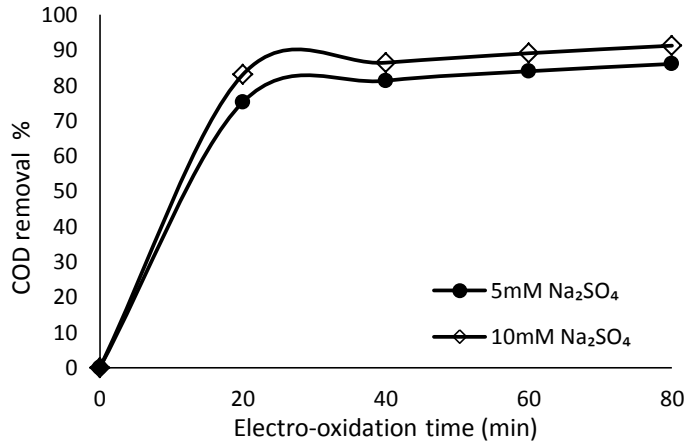

Figure 3. *Variation of COD removal over the time depending on support electrolyte concentration (EO, Co= 300 mg/L bentazone, 20 mA/cm^2)*

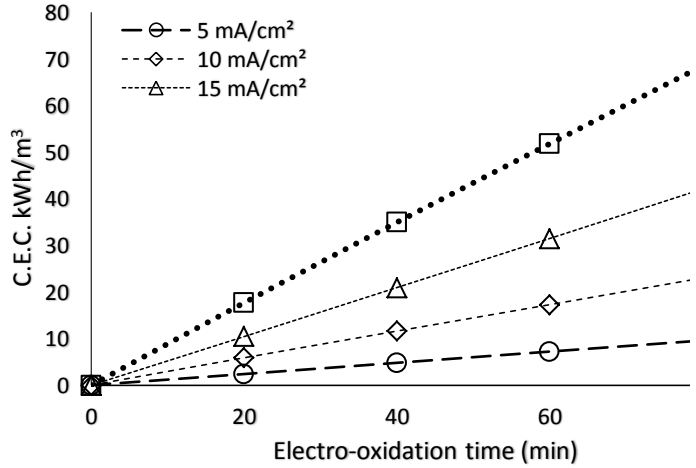

Figure 4. *Variation of energy consumption over the time depending on current density (EO, Co= 300 mg/L bentazone, 5mM Na_2SO_4, pH= 6.43)*

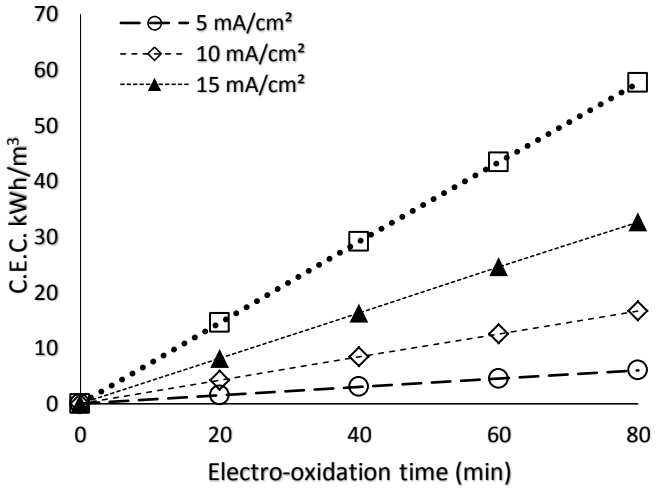

Figure 5. *Variation of energy consumption over the time depending on current density (EO, Co= 300 mg/L bentazone, 10 mM Na_2SO_4, pH= 6.31)*

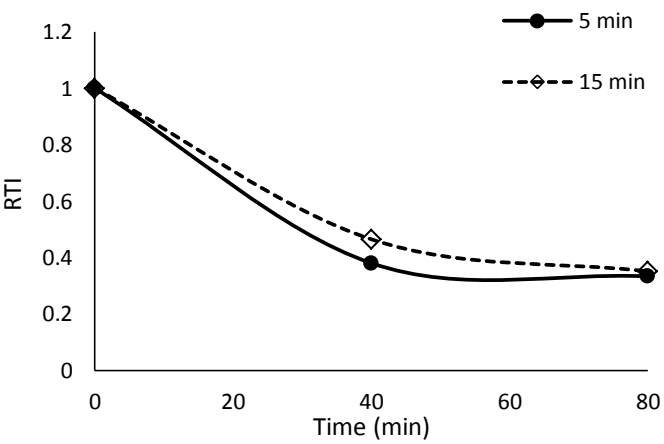

Figure 6. *Variation of 5th and 15th mins toxicity of bentazone by electro-oxidation with the time.*

References

Babu, B. R., Meera, K. M. S., & Venkatesan, P. (2011). Removal of pesticides from wastewater by electrochemical methods–A comparative approach. Methods, 12(16), 3-3.

Chiron, S., Fernandez-Alba, A., Rodriguez, A., & Garcia-Calvo, E. (2000). Pesticide chemical oxidation: state-of-the-art. *Water Research*, *34*(2), 366-377.

Errami, M., Salghi, R., Abidi, N., Bazzi, L., Hammouti, B., Chakir, A., ... & Al-Deyab, S. S. (2011). Electro-oxidation of bupirimate: a comparative study of SnO2 and boron doped diamond anodes. Int. J. Electrochem. Sci, 6, 4927-4938.

Errami, M., Salghi, R., Ebenso, E. E., Messali, M., Al-Deyab, S. S., & Hammouti, B. (2014). Anodic destruction of abamectin acaricide solution by BDD-anodic oxidation. Int. J. Electrochem. Sci, 9, 5467-5478

García, O., Isarain-Chávez, E., Garcia-Segura, S., Brillas, E., & Peralta-Hernández, J. M. (2013). Degradation of 2, 4-dichlorophenoxyacetic acid by electro-oxidation and electro-Fenton/BDD processes using a pre-pilot plant. Electrocatalysis, 4(4), 224-234.

Kapałka, A., Fóti, G., & Comninellis, C. (2010). Basic principles of the electrochemical mineralization of organic pollutants for wastewater treatment. In *Electrochemistry for the Environment* (pp. 1-23). Springer New York.

Lebik-Elhadi, H., Frontistis, Z., Ait-Amar, H., Amrani, S., & Mantzavinos, D. (2018). Electrochemical oxidation of pesticide thiamethoxam on boron doped diamond anode: Role of operating parameters and matrix effect. Process Safety and Environmental Protection, 116, 535-541.

Lin, H., Wu, J. and Zhang, H., 2013. Degradation of bisphenol A in aqueous solution by a novel electro/Fe3+/peroxydisulfate process. Separation and Purification Technology, 117, pp.18-23.

McBeath, S. T., Wilkinson, D. P., & Graham, N. J. (2019). Application of boron-doped diamond electrodes for the anodic oxidation of pesticide micropollutants in a water treatment process: a critical review. Environmental Science: Water Research & Technology, 5(12), 2090-2107.

Othman, M. A. (2018). Removal of pesticides from aqueous solution by electrochemical methods.

Panizza, M., & Cerisola, G. (2009). Direct and mediated anodic oxidation of organic pollutants. *Chemical reviews*, *109*(12), 6541-6569.

Silva, R. G. D., Aquino Neto, S., & Andrade, A. R. D. (2011). Electrochemical degradation of reactive dyes at different DSA® compositions. *Journal of the Brazilian Chemical Society*, *22*(1), 126-133.

Sivri, S., Ustun, G. E., & Aygun, A. (2020). Electro-oxidation of nonylphenol ethoxylate-10 (NP10E) in a continuous reactor by BDD anodes: optimisation of operating conditions. International Journal of Environmental Analytical Chemistry, 1-14.

Soriano, Á., Gorri, D., Biegler, L. T., & Urtiaga, A. (2019). An optimization model for the treatment of perfluorocarboxylic acids considering membrane preconcentration and BDD electrooxidation. Water research, 164, 114954.

Yavuz, Y., & Koparal, A. S. (2006). Electrochemical oxidation of phenol in a parallel plate reactor using ruthenium mixed metal oxide electrode. Journal of hazardous materials, 136(2), 296-302.